UNIVERSITY OF SOUTHAMPTON

THE EFFECT OF MOLECULAR STRUCTURE ON THE MESOGENIC PROPERTIES OF LIQUID CRYSTALLINE MATERIALS

by Steven Patrick Perkins

A dissertation submitted in partial fulfilment of
the requirements of the degree of Doctor of Philosophy
at the University of Southampton

Department of Chemistry

July1999

UNIVERSITY OF SOUTHAMPTON

ABSTRACT

FACULTY OF SCIENCE

CHEMISTRY

Doctor of Philosophy

THE EFFECT OF MOLECULAR STRUCTURE ON THE MESOGENIC PROPERTIES OF LIQUID CRYSTALLINE MATERIALS

By Steven Patrick Perkins

This Thesis presents the results of investigations into the mesogenic properties of a number of different types of liquid crystalline materials. The first Chapter presents an introduction into the different mesophases formed by liquid crystalline materials, the structure-property relationship between molecular structure and mesophase behaviour, together with various characterisation techniques. In Chapter Two we present the characterisation of an homologous series of the disc-like pentakis(phenylethynyl)phenyloxyalkanes (the so-called superdiscs) and in particular their phase diagrams of mixtures with the inductor molecule 2,4,7-trinitrofluorenone (TNF). Following on from this, Chapter Three describes the results from deuterium NMR spectroscopy studies of one member of this series, the decyl homologue, and its equimolar mixture with TNF. In particular we concentrate on the nature of the monotropic Col_1 phase and the unusual orientational ordering of the alkyl chain.

Chapter Four moves on to study the effect subtle changes in molecular structure have on the phases formed by calamitic liquid crystal dimers. We have prepared and characterised a number of non-symmetric dimers where the cyanophenyl group is linked to either a cyanobiphenyl or cyanoterphenyl moiety. The substitution of the cyano group in the cyanophenyl moiety is varied i.e either ortho- or meta-substituted and phase behaviour and transitional properties are compared with the para-substituted materials.

In Chapter Five we develop a method of assessing the biaxiality of molecules based on the angle between two linked mesogenic units. The method is then tested against a number of bent and linear materials to assess the validity of the approach. Using this method we have prepared a number of V-shaped molecules based on the biphenyl moiety in an attempt to observe a thermotropic biaxial nematic phase. Finally we attempt to determine the biaxiality, if any, of the nematic and smectic phases of specifically deuteriated CB7CB-d_2. An alternative approach to preparing thermotropic biaxial nematogens is to link disc-like and rod-like mesogenic units. In Chapter Six we describe the mesogenic behaviour of some disc-rod dimers based on the Superdisc molecules, as discussed in Chapter 2, as the rod-like unit is varied.

Finally, Chapter Seven presents the procedures used to synthesise the materials discussed in this Thesis, together with their characterisation.

ACKNOWLEDGEMENTS

I would like to thank my supervisor, Professor Geoffrey Luckhurst, for all the help, advice and encouragement over the years (and there has been a number of them!!), and for making sure this Thesis makes sense. I would also like to thank Dr. George Attard for his help and advice and for correcting me for when I was probably talking rubbish!

Thanks Fiona!!!! You've listened to my gibberish for many years and generally kept me sane! Cheers for all the beers, and dinners (although I generally end up cooking them), and all the nights down the pub, and for proof reading this Thesis.

A big thanks to the *original* 'Southampton Posse'; Mark F, Steve N., Rob W., Simon K. and Mark P., as well as myself. You made the first year of my Ph.D very hazy! (and all of the subsequent ones). Extra thanks to Simon, a long suffering housemate over the years.

Thanks to all the other people I've worked with over the years for making the lab fun, especially Mark Wilson, Sean, Pete Le Mas, Chris, Marcus, Nick, Big John, Jung, Dinali, Jon, Doina, Flavio, Stephane, and anyone I've missed out. Thanks to Tim Timimi and Mark Tearle for doing the NMR experiments for me.

Thanks to all the others outside of the lab; there's too many of you to name individually so I'll do it in groups, you all know who you are...
All the French contingent who have improved my English over the years.
Everyone I know in electrochemistry for all the Friday nights.
And numerous people I have shared houses with over the years (at the moment Matt, Jon and Sefora).

Finally, huge thanks to the Perkins Clan for, amongst other things, washing my clothes and feeding me food (Mum), dragging me down the pub (Dad), driving us back from the pub (Darren), crashing his car, ha ha! (Andrew) and letting me finish first (Mark).

CONTENTS

CHAPTER ONE

INTRODUCTION TO LIQUID CRYSTALS

1.1 Introduction

It is commonly taught that there are just three states of matter; solid, liquid and gas. There is, however, a fourth state that exists between solids and liquids, known as the liquid crystalline state. The discovery of this state is generally attributed to Friedrich Reinitzer [1], an Austrian botanist, who, while studying cholesteryl benzoate noted that it appeared to have two melting points – the melting point of the crystal at 145^{O}C and the transition to a clear liquid at 179^{O}C. This intermediate phase was investigated by Otto Lehmann [2], who showed it to have both the optical properties of a crystal, that is it was birefringent, and the fluid properties of a liquid. With these properties in mind the term 'liquid crystal' or , more correctly, mesophase, from the Greek *meso-* meaning intermediate was coined to describe this fascinating state of matter.

Compounds, or mesogens, which form this mesophase can be divided into two broad classes. One of these being lyotropic liquid crystals. These materials usually have a polar head group attached to an alkyl chain and as such are amphiphiles. The phases formed by these mesogens when dissolved in a solvent are a result of the molecular associations of these amphiphiles and the self-organisation of the aggregates in systems of two or more components. These give rise to materials as diverse as soaps and potential anti-cancer drugs [3]. This Thesis will not deal with these systems any further. The other class of compounds are thermotropic liquid crystals which form phases that are based on specific arrangements of the molecules and whose phase transitions are caused by a change in temperature, hence the term thermotropic, and, to a lesser extent, a pressure dependence. In recent years various developments [4,5] have meant that the two classifications now overlap to a considerable degree.

The most important factor necessary for molecules to form thermotropic mesophases is their molecular shape. The larger the deviation the molecular shape

has from a spherical symmetry or, in other words, the greater the degree of shape anisotropy the more likely the molecule is to form a mesophase. This concept leads to a further categorisation according to the geometric shape of the constituent molecules. If the molecule is rod-shaped (see figure 1.1a) the liquid crystal is termed calamitic and if the molecule is disc-shaped (see figure 1.1b) the liquid crystal is termed discotic. Discotic mesogens are less common, the first being discovered only about 20 years ago [6] and number around 1000 examples, compared with upwards of 50000 examples of calamitic mesogens.

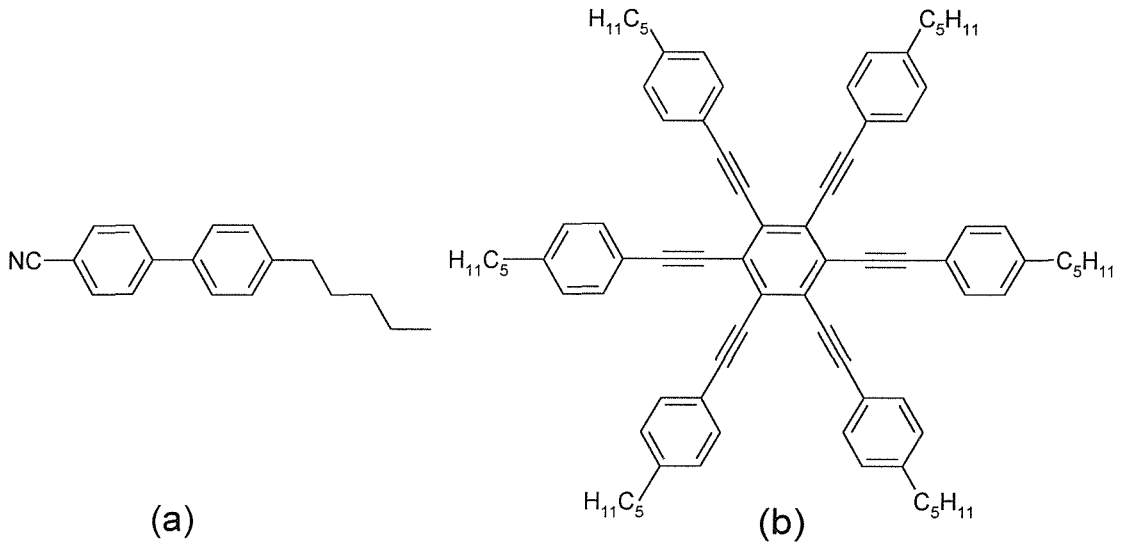

Figure 1.1 : Examples of (a) a calamitic liquid crystal and (b) a discotic liquid crystal.

1.2 Liquid Crystal Mesophases

Normally when a non-mesogenic crystal is heated there is a first order transition to an isotropic liquid with no long range orientational or positional order. The temperature at which this process occurs is known as the melting point. However, upon heating a crystalline mesogenic material, due to the anisotropic nature of the molecules, the material can break down to form different phases possessing differing degrees of both orientational and positional order until an isotropic liquid is again formed. For calamitic mesogens the molecular order present during this heating process can be divided into two general groups, the nematic phase, which includes the chiral nematic or cholesteric phase, and the smectic phases, including chiral smectic phases. Discotic materials also form various mesophases, some very similar to the calamitic phases, and others based on columnar arrangements. The

transition from mesophase to mesophase is completely reversible, as for any other thermodynamic phase transition, however sometimes, due to a degree of supercooling a mesophase may only be seen on cooling and not heating. These phases are called *monotropic* whereas mesophases seen on both heating and cooling are called *enantiotropic*. It should also be noted that different materials can, and do, exhibit different phase sequences. The following sections describes the various phases formed by both calamitic and discotic mesogens.

1.3 The Nematic Phases

The nematic phases are the most disordered of all the calamitic phases and include the nematic phase (N) and the chiral nematic phase (N*).

1.3.1 The Nematic Phase (N)

This phase possesses only one degree of long range orientational order and there is no correlation between the positions of the centres of mass at long range. The molecular long axes have a tendency to lie parallel to a common axis termed the director, and denoted by the unit vector, $\hat{n}$. In the absence of any external constraints the director axis will vary continuously and randomly throughout the phase, except at defects. A schematic illustration of the molecular organisation in the nematic phase is shown in figure 1.2. The symmetry about the director is uniaxial although it has been suggested that a nematic phase with a biaxial symmetry should exist [7]; this will be dealt with later in the Thesis. The nematic phase can show strong pretransitional effects. Close to the phase transition to a more ordered mesophase [8], areas of layered structure, similar to the smectic A (§1.4.1) or smectic C (§1.4.2) phases can be observed [9]. Such regions are the result of an increases in the translational order and are known as cybotactic groups [10].

1.3.2 The Chiral Nematic Phase (N*)

The chiral nematic or cholesteric phase is a helical phase formed by either a chiral compound or by the addition of a chiral compound to a uniaxial nematic phase. Instead of the director being arranged randomly throughout the phase, it is rotated through a constant angle on passing through the phase, thus forming a helix, as shown in figure 1.3. The pitch length is described as the distance needed for the

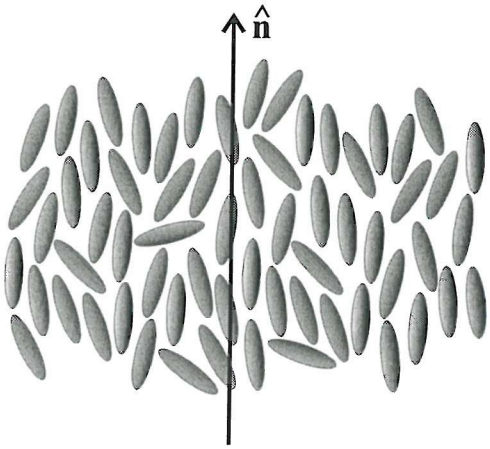

Figure 1.2 : A schematic representation of the nematic phase.

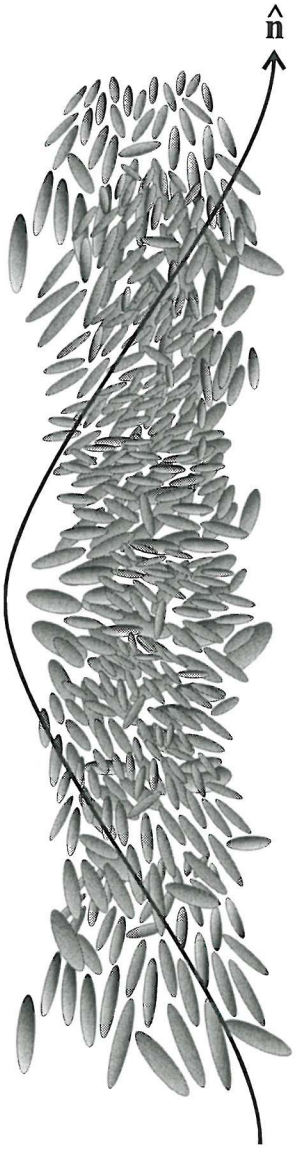

Figure 1.3 : A schematic representation of the chiral nematic phase.

director to rotate through 360° about the axis, Z, and is dependent on the constituent molecules and also temperature. The absolute chirality of the molecules will dictate the sense of the helix.

1.4 The Smectic Phases

The smectic phases have, in addition to long range orientational order, varying degrees of translational order. Those phases where the translational order is reflected by the tendency for the molecules to lie in layers are the true smectic phases and include the SmA, SmC, SmF, SmI and SmB phases.

1.4.1 The Smectic A Phase (SmA)

This phase was first described by Friedel in 1922 [11]. It has a long range orientational ordering as in the nematic phase, but the molecules tend to form themselves into a layered structure. Within the layers there is no translational order and as such the layers are liquid-like and can be considered a true two dimensional liquid. The layers are free to slide over each other and the diffusion of molecules between the layers occurs readily, although not as readily as movement within the layers. The molecules lie approximately parallel to each other with the director perpendicular to the layer. There is also free rotation about the molecular long axes. A schematic representation of the molecular organisation in this phase is shown in figure 1.4. The phase is uniaxial. This phase can also exhibit a number of modifications tending to depend on whether the molecules possess strongly polar groups or not. For example monolayer, bilayer, interdigitated and intercalated structures may be formed.

1.4.2 The Smectic C Phase (SmC)

This phase is structurally very similar to the smectic A phase, with the molecules generally lying parallel, but the director is now tilted at an angle with respect to the layer normal. This is known as the tilt angle. The molecular organisation in this phase is shown in figure 1.5. Again there is no translational order within the layers and, although there is a long range correlation of the tilt directors within the layers, there are however only short range correlations between the layers and a hindered movement of molecules between the layers. The tilt angle can remain constant with varying temperature, for example when the phase is preceded by a nematic

phase, or vary, for example during the change from a smectic A to smectic C phase. Again this phase can exhibit a number of modifications similar to the smectic A phase. Due to the presence of the tilt angle this phase is biaxial.

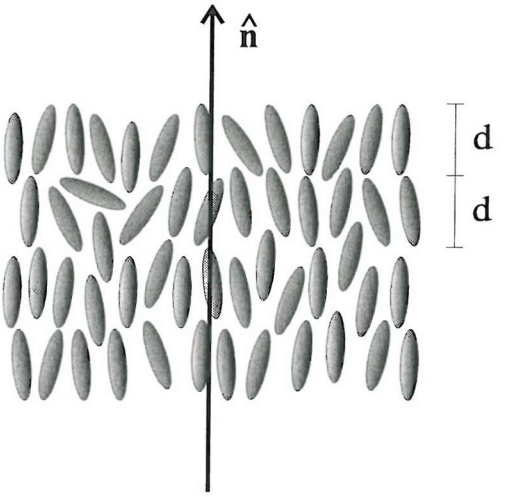

Figure 1.4 : A schematic representation of the smectic A phase.

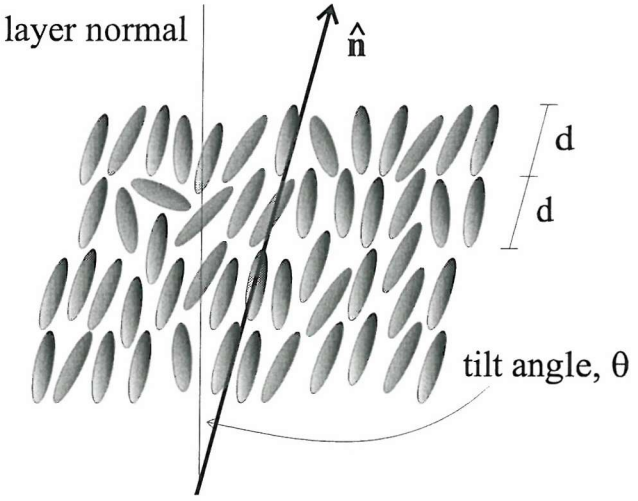

Figure 1.5 : A schematic representation of the smectic C phase.

1.4.3 The Smectic B Phase (SmB)

Due to the initial confusion over its structure, the smectic B phase is also known as the hexatic B phase. As the alternative name suggests, this phase has, within a given smectic layer, a hexagonal ordering, although the hexagonal lattices only have repeat positional order over *ca.* 150 – 600Å, as shown in figure 1.6. This type of order is known as bond orientational order. Unlike the smectic C phase the

director is not tilted with respect to the layer normal, but is perpendicular to the layers, as with the smectic A phase. The positional order is greater than that for either the smectic A or smectic C phase although there are no positional correlations between the layers. The molecules move rapidly about their molecular long axes, however studies have shown [12] that the molecules lie too closely packed for free rotation to occur and so rotate co-operatively within the layer. Finally, for compounds containing a very polar terminal group, such as a cyano group, a bilayer structure has been observed [13], as is seen for other smectic phases.

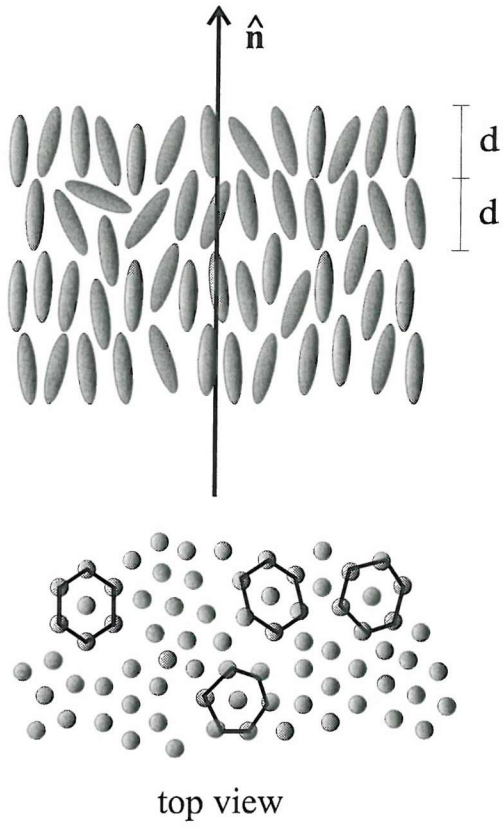

Figure 1.6 : A schematic representation of the smectic B phase.

1.4.4 The Smectic F and I Phases (SmF and SmI)

The smectic F phase, discovered in 1971 [14], and the smectic I phase, discovered in 1978 and reported in 1982 [15], are both very similar in nature and are both related to the smectic B phase. The two consist of layers of hexagonal close packed molecules having only bond orientational order within the layers, as with the smectic B phase, but the director is now tilted with respect to the layer normal and

can be considered a tilted analogue of the smectic B phase. Within the phase there are no long range correlations of the molecular centres of mass and no long range interlayer correlations exist. What distinguishes the two phases is the direction which the director's tilt makes with the hexagonal net. For the smectic F the tilt direction is towards the edge of the net, whereas for the smectic I the director tilts towards the apex of the net, as illustrated in figure 1.7.

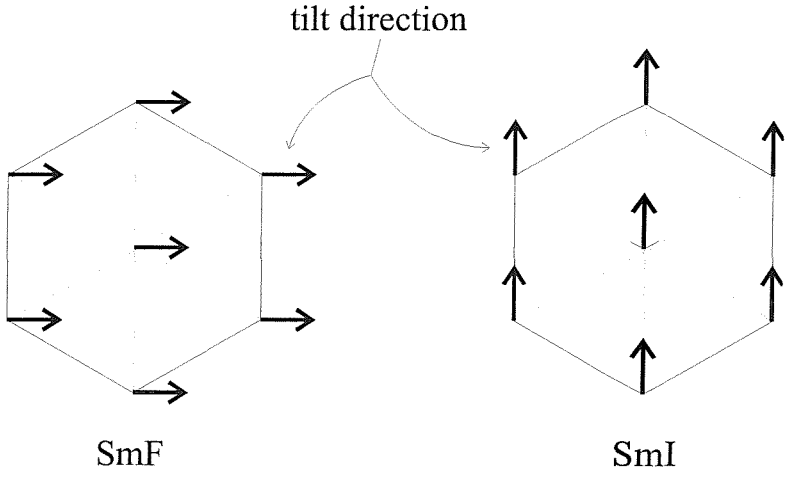

Figure 1.7 : Showing the direction of tilt in the smectic F and smectic I phases.

1.4.5 Chiral Smectic Phases (SmC*, SmF* and SmI*)

Just as the nematic phase has a chiral equivalent for optically active molecules the smectic phases can also exhibit chiral phases. Within these phases the tilted directors of the layers form a helix through the phase, i.e. the tilt direction spirals with respect to the layer normal, with the pitch length being dependent on both the tilt angle and the chirality of the constituent molecules.

1.5 The Crystal Phases

These phases were first identified as smectic phases on the basis of microscopic observations, but are in fact anisotropic soft crystals characterised by very low yield stresses. All of these crystal phases are characterised by a long range three dimensional ordering and do not lack the positional correlation between layer planes as the smectic phases do. They include the crystal B, E, G, H, J and K phases. Again the letters indicate the chronological sequence of discovery.

1.5.1 The Crystal B Phase (B)

The crystal B phase is the crystal analogue of the smectic B phase with the molecules having a hexagonal closed packed arrangement, but there are now long range layer correlations between the molecules. The correlation's between the positions of molecules in adjacent layers gives rise to a variety of possible packing arrangements as in conventional crystallography [16]. If the underlying layer's hexagonal net is twisted through 60°, mono-, bi- and tri-layers can be constructed.

1.5.2 The Crystal G and J Phases (G,J)

Just as the smectic F and I phases may be considered the tilted analogues of the smectic B phase, the crystal G and J phases may be considered the tilted analogues of the crystal B phase. Again, the difference between the two phases is a result of the director tilt with respect to the hexagonal net. The crystal G phase has the director tilt towards the edge of the hexagonal net and the crystal J phase has the tilt towards the apex.

1.5.3 The Crystal E Phase (E)

The crystal E phase is simply a crystal B phase where there is correlation of the short molecular axes. This correlation causes a contraction of one of the six-fold axes of the hexagonal net to give an orthorhombic arrangement. To accommodate this contraction the molecules form themselves into a 'herring-bone' arrangement, as shown in figure 1.8. The molecules continue to move rapidly, although now, due to the constrained nature of the phase the rotations are less than 180°, instead the molecules partake in a highly correlated flapping motion. Despite the fact the director is not tilted, the phase is biaxial in nature due to this orthorhombic unit cell.

1.5.4 The Crystal H and K Phases (H,K)

The crystal H and K phases are the tilted analogues of the crystal E phase, and as such are related to the crystal G and J phases by a contraction of the hexagonal net to a monoclinic unit cell. The crystal H phase has the director tilting towards the edge of the pseudo-hexagonal net and the crystal K phase has the director tilting towards the apex of the net as in figure 1.7. Again molecular motion is restricted to a highly correlated flapping motion of the short molecular axes.

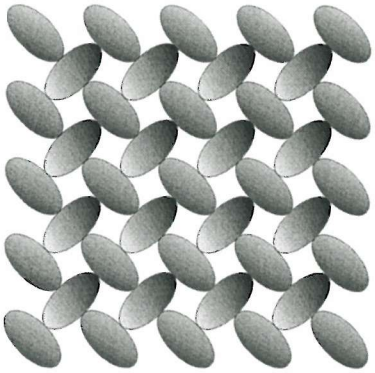

Figure 1.8 : Schematic representation of the packing of the molecules in the crystal E phase.

1.5.5 Chiral Crystal Phases

Unlike the smectic phases, crystal G, J, H and K phases formed by chiral molecules show either very low or no optical activity. This is presumably a result of the crystal forces suppressing the helical arrangement of the director.

1.6 The Discotic Phases

Mesogens formed from disc-like molecules also exhibit a number of different liquid crystalline phases in the same way calamitic mesogens do. The phases are divided into two distinct morphologies, nematic and columnar.

1.6.1 The Discotic Nematic Phase (N)

This phase, as with calamitic mesogens, is the least ordered of the discotic phases. Within the phase the disc-like molecules have a tendency to lie parallel, with their short axes – the disc normal – lying parallel to the director. There is orientational but no positional long range order. The molecular ordering can be envisioned as looking like a plate of pennies, as illustrated in figure 1.9. The entropy change (§1.9) for the N_D – I transition is smaller than that for the corresponding calamitic change which presumably indicates a reduced degree of orientational order in this phase. A chiral phase has also been reported for chiral molecules [17].

1.6.2 The Columnar Nematic Phase (N_C)

The columnar nematic phase has been reported for binary mixtures of charge transfer complexes, such as 2,4,7-trinitro-9-fluorenone, and large electron rich multiyne discotic molecules [18] (see figure 1.1b). It is believed that a quadrupolar

interaction between the different molecules leads to alternate stacking of each molecule into short columns which subsequently behave as large rod-like mesogens, with long range orientational but short range positional order. Figure 1.10 illustrates two ways in which the molecules could stack in the nematic phase. Figure 1.10a shows an extreme case, however more recent studies [19] have suggested the columnar structure is not so rigid, as shown in figure 1.10b. The measured length of each stack of molecules tends to be of around 10 – 15 molecules leading to a length to breadth ratio of about 3:1. This figure is generally taken to be what is required for a molecule to exhibit liquid crystallinity.

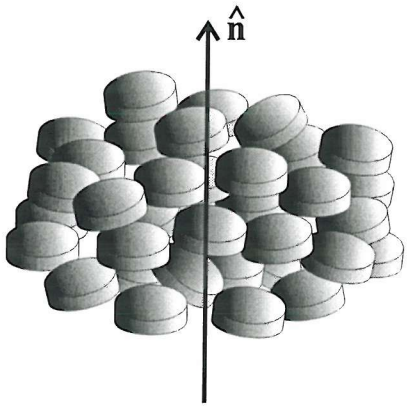

Figure 1.9 : A schematic representation of the discotic nematic phase.

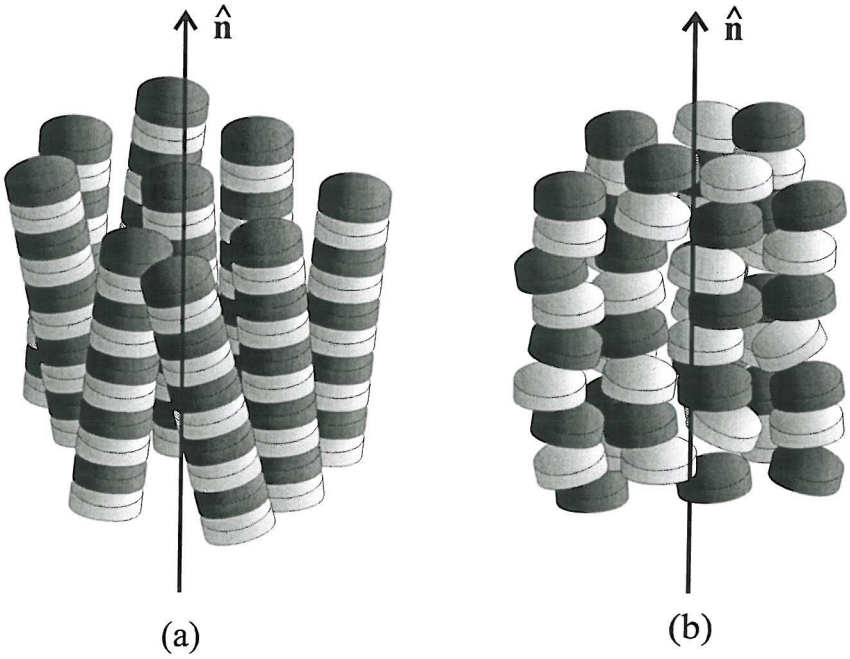

Figure 1.10 : Two representations of a columnar nematic phase.

1.6.3 The Discotic Columnar Phases (Col_{ho}, Col_{hd}, $Col_{ob,d}$ and Col_{rd})

The discotic columnar phases are characterised by stacked columns of molecules in a similar way to the columnar nematic phase although a charge transfer complex need not be formed and the stacking continues for much greater distances, with some of the phases being almost crystalline. The various phases are classified depending on the symmetry of the two-dimensional unit cell formed by the columns.

The hexagonal phase (Col_h) has, as the name suggests, a hexagonal arrangement of the columns akin to the smectic B phase. The columns themselves can have either translationally ordered or disordered packing which leads to a further classification – an ordered hexagonal phase D_{ho}, the most ordered of the discotic phases, or a disordered hexagonal phase D_{hd} as shown in figure 1.11. There is, however, some doubt as to whether there is true translational order within the columns.

The oblique phase ($Col_{ob,d}$) is comprised of columns in which the molecules are tilted with respect to the column axis and hence the phase is biaxial in nature. The columns are arranged on an oblique hexagonal array and only a disordered phase so far been reported, as illustrated in figure 1.11.

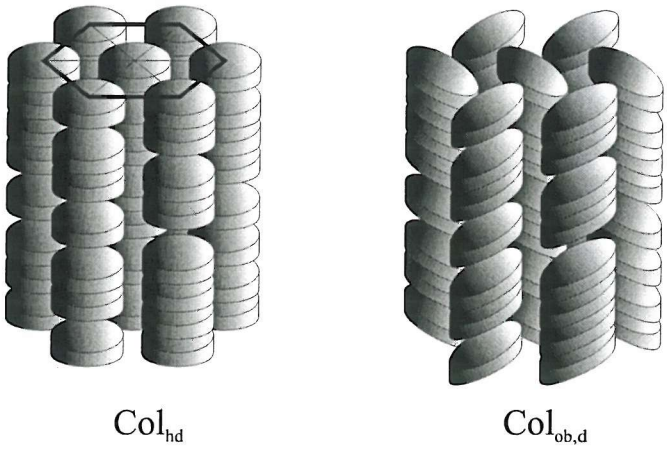

Figure 1.11 : A schematic representation of the disordered hexagonal phase (Col_{hd}) and the disorder oblique phase ($Col_{ob,d}$).

The rectangular phases (Col_{rd}) are the most complex of all the discotic phases. Once again the molecules are tilted with respect to the column axis and again only

disordered phases have been seen. The phase can be sub-divided dependent on the symmetry of the rectangular arrangement, see figure1.12, and are classified by their space group, that is $P2_1/a$, P2/a, and C2/m.

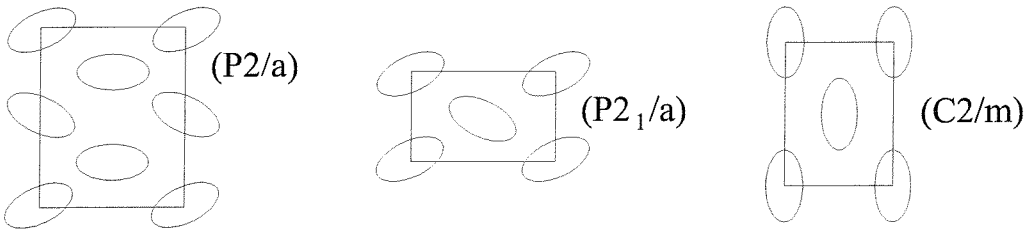

Figure 1.12 : The various symmetries that can be adopted by the rectangular discotic phases.

1.7 The Characterisation Of Liquid Crystalline Phases

There is now a battery of techniques which are used and need to be used to characterise the different phases which liquid crystals form. The three standard experimental techniques are polarising optical microscopy, differential scanning calorimetry, more commonly termed 'DSC', and X-ray diffraction. Polarising microscopy is usually the first technique employed as it can quickly provide information needed to assign the different phases, through the various characteristic textures the mesogens form, and in addition gives the transition temperatures of the phase changes. DSC is used to confirm the transition temperatures and can provide information about changes in the order, enthalpy and entropy of the phases. X-ray diffraction can be used to determine the structure and molecular arrangement of the phases. Other techniques such as deuterium NMR spectroscopy can provide detailed information about the degree of orientational order of the phase and information about director dynamics. This technique will be dealt with in detail in Chapter 3. As a compliment to this ESR spectroscopy can provide other information about the degree of order. The following sections will attempt to explain a number of these techniques in greater detail.

1.8 Polarising Microscopy

The polarising microscope is the same as any common microscope except that the sample is placed between a pair of crossed polarisers. When there is no sample present no light emerges because the light from the first polariser is not transmitted

by the second. In addition when an isotropic liquid is present as the sample there is no change because the plane of polarised light is unchanged as it travels through the sample. Liquid crystals are however birefringent, that is they have an isotropic refractive index – for uniaxial phases there is a principle component parallel to the director and the other is perpendicular to the director. The plane polarised light passing through the liquid crystal will be affected by the two refractive indices and emerge as elliptically polarised light. This light is, in general, continually rotating and is, thus, parallel to the polarising axis of the second polariser twice during each cycle. Therefore, the introduction of a liquid crystal between crossed polarisers causes the field of view to appear bright and will depend on the wavelength.

The macroscopic ordering of the director present in the different liquid crystal phases interacts with polarised light in different ways and gives rise to patterns, or textures, characteristic of the phase. Using a heating stage the sample can be heated or cooled in a controlled way, to within a tenth of a degree, and the phases can be identified with experience. Textures obtained on cooling from the isotropic liquid or nematic phase are known as natural textures, whereas textures obtained from any other texture or during heating are termed paramorphotic as the texture inherits some of the features of the preceding phase. We now give a description of the textures formed by the majority of mesophases, although more detailed descriptions can be found in a number of books [20,21].

1.8.1 The Nematic Phase

There are three distinct textures formed by this phase; the threaded, the schlieren and the homeotropic texture. The threaded texture is composed of flexible filaments floating freely in the fluid. It is from this texture that the nematic phase acquires its name. The schlieren texture, which can been seen in figure 1.13, is the most common and consists of point singularities which usually possess both two and four point brushes. The homeotropic texture is produced by surface alignment of the director along the direction of the incident light beam and appears optically isotropic and so dark. All the textures are highly mobile and, apart from the homeotropic, brightly coloured. Also when the sample is subjected to mechanical stress flashes may be observed as the director orientation is changed.

1.8.2 The Chiral Nematic Phase

Due to the helical nature of this phase the textures formed are markedly different from the normal nematic phase. Again the phase exhibits three distinct textures; the focal conic texture (§1.8.3), which when sheared gives rise to the Grandjean texture and the fingerprint texture. The Grandjean texture consists of thick bright disclinations that float over a coloured background. The colour of the background gives an indication of the pitch of the helix and the helical axis of this texture is perpendicular to the glass slide. The fingerprint texture is formed if the helical axis is parallel to the glass slide. Both are shown in figure 1.14.

1.8.3 The Smectic A Phase

The smectic A phase exhibits two natural textures; the focal conic fan and the homeotropic texture. As with the nematic phase the homeotropic texture is optically isotropic, due to the perpendicular arrangement of the director with respect to the glass slide, and appears dark. The focal conic fan texture develops on cooling from either the isotropic or nematic phase in the form of batonnetes which consist of growing focal conic domains which eventually coalesce, forming the texture, shown in figure 1.15. If the phase separates as streaks or droplets then this is an indication that the sample is impure. For the characterisation of subsequent tilted phases a homeotropic alignment of the smectic A phase is desirable. This can be achieved in a number of ways either by using very clean glass slides or by treating the slides chemically with a surfactant. For the characterisation of subsequent orthogonal phases a focal conic texture is advantageous.

1.8.4 The Smectic C Phase

The smectic C phase exhibits two natural textures, the schlieren and focal conic fan textures, and one paramorphotic texture, the focal conic fan texture. The natural focal conic fan texture is very rarely formed and is similar to the focal conic smectic A texture. On the hand the schlieren texture is far more common. It appears initially to be identical to the nematic schlieren texture but can be distinguished in two distinct ways. First, whereas the nematic schlieren texture exhibits both two and four point singularities, the smectic C schlieren texture generally exhibits only four point singularities. Second, when mechanical stress is

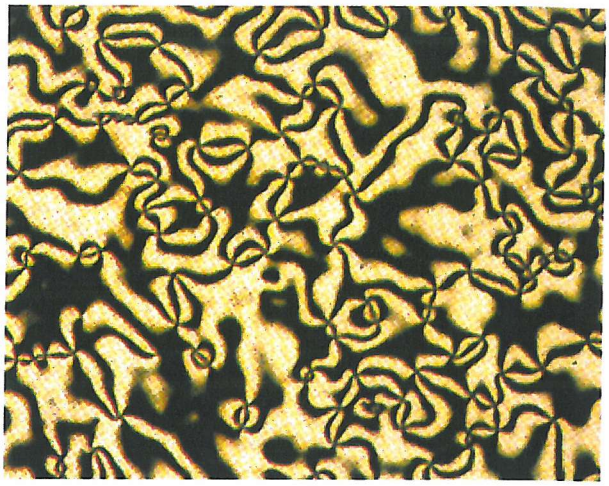

Figure 1.13 : Typical Schlieren texture exhibited by a nematic phase.

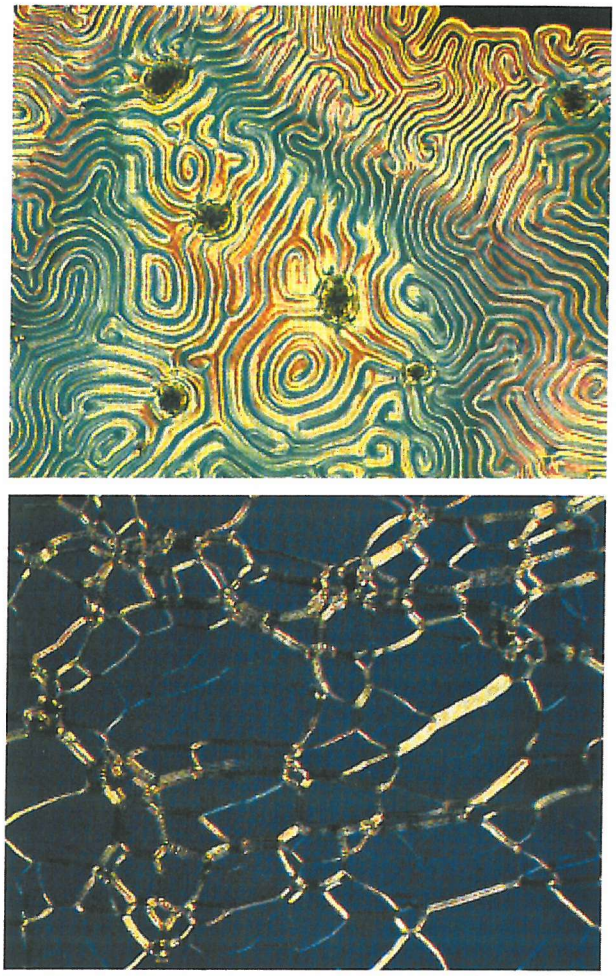

Figure 1.14 : Typical fingerprint texture (top) and Grandjean texture (bottom) exhibited by chiral nematic phases.

applied to the nematic schlieren texture it flashes whereas the smectic C schlieren texture does not. This is due to the higher viscosity of the more ordered smectic C phase. The schlieren texture may also appear to have a sanded nature due to the singularities and brushes being small. The paramorphotic focal conic fan texture is similar in appearance to the focal conic smectic A texture except that the texture is typically broken and may be sanded, as shown in figure 1.16.

1.8.5 The Smectic B Phase

The smectic B phase shows two natural textures, the homeotropic and the mosaic texture, and one paramorphotic texture, the focal conic fan texture. The homeotropic texture can also be formed paramorphotically and is identical in nature to the other homeotropic textures. The mosaic texture separates from the nematic or isotropic phase in the form of platelets, discs or oblong sheets which may have a uniquely identifiable 'H' shape. The paramorphotic focal conic fan texture is similar to the smectic A focal conic texture except that the backs of the fans appear smoother than the smectic A texture. Also, if the preceding phase is a smectic A then at the transition between the phases bars appear across the backs of the fans. This is also true upon heating the smectic B into the smectic A phase.

1.8.6 The Smectic F and I Phases

Natural textures for both the smectic F and smectic I phases are rare although it appears that both exhibit a mosaic texture. As with the natural textures the paramorphotic texture exhibited by these two phases are very difficult to distinguish from each other if observed as isolated cases, although it is easy to characterise either phase as being distinct from the other phases because of the very characteristic mosaic-schlieren texture. Upon cooling from the homeotropic smectic A or schlieren smectic C phase it is just possible to distinguish between the smectic F and smectic I phase. If the texture has a largely mosaic appearance it is probably a smectic F whereas if the texture is largely schlieren in character and hard to focus it is likely to be a smectic I phase. A focal conic fan texture also exists for the smectic F phase; it is comprised of broken fans with a characteristic 'L' shaped pattern on the backs of the fans.

Figure 1.15 : A typical focal conic texture exhibited by the smectic A phase.

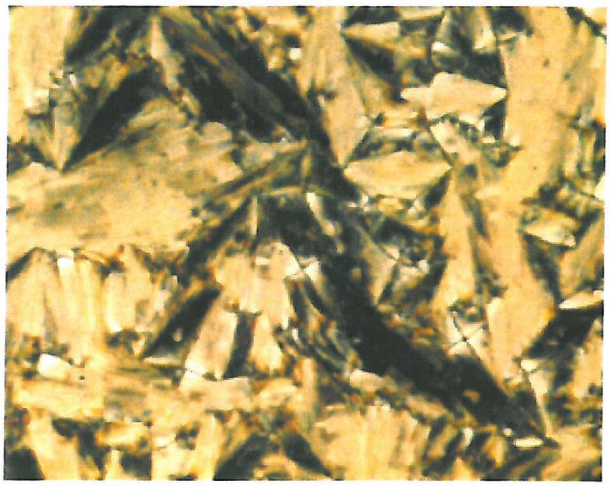

Figure 1.16 : A typical broken focal conic texture exhibited by the smectic C phase.

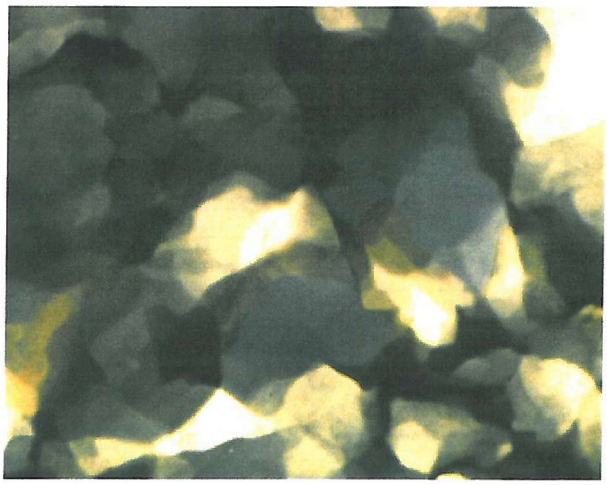

Figure 1.17 : A typical platelet texture exhibited by the crystal E phase.

1.8.7 The Crystal G and J Phases

These two phases have been found, at present, to show exactly the same textures. The natural textures, although rare, show large splinter shaped regions or lancets separating from the isotropic fluid, that join to form a mosaic texture composed of rectangular platelets. There are also a number of paramorphotic textures that are dependent on the nature of the preceding phase. The patchwork or broken fan texture is normally obtained on cooling from the smectic A, C or F phases. If the preceding smectic C phase is schlieren then a mosaic texture will be formed. The broken arced fan texture is obtained on cooling from the smectic B phase.

1.8.8 The Crystal E Phase

The crystal E phase shows both natural and paramorphotic textures. The natural texture separates from the isotropic liquid as a droplet that grows rapidly on cooling, forming an undulating, mosaic type texture. Paramorphotically there are three different textures, the focal conic fan, the mosaic and the platelet texture. In the focal conic texture the backs of the fans have concentric lines or arcs in a similar way to the broken arced fan texture of the smectic G and J phases, although unlike these textures the arcs are unbroken and very clear. The mosaic texture, normally obtained on cooling the smectic B phase, consists of mosaic platelets that are crossed with parallel lines. The platelet texture, which is characteristic of the crystal E phase, is normally obtained from the homeotropic smectic A phase, and consists of platelets that are often blue-grey to yellow in colour and appear to be transparent so that ghost-like images of platelets can be seen through the surface platelets. An example of this texture is shown in figure 1.17.

1.8.9 The Crystal H and K Phases

The crystal H and K phases show no natural textures but do exhibit a number of paramorphotic textures divided into focal conic fan and mosaic textures. The focal conic textures are generally no aid to characterisation whereas the mosaic textures are more informative. The mosaic textures range from small, well defined platelets to large areas having either a grainy or zig-zag appearance.

1.8.10 The Discotic Nematic Phase

This phase exhibits a schlieren texture and is visually identical to the calamitic nematic schlieren texture.

1.8.11 The Columnar Nematic Phase

This phase also exhibits a schlieren texture and is visually identical to all non-columnar nematic phases.

1.8.12 The Discotic Columnar Phases

On slow cooling from the isotropic liquid the texture of the Col_{ho} phase appears as flower-like hexagons which on further cooling coalesce into birefringent and homeotropic domains, as shown in figure 1.18. When cooled from the schlieren texture of a nematic phase a focal conic fan texture is observed that is reminiscent of the smectic A texture. The natural Col_{hd} texture, however, shows no mosaic structure and instead consists of either focal conic or fan shaped domains. Of the rectangular phases the C2/m symmetry has a mosaic texture similar to that of the G phase. For the other symmetries and the oblique phase there are no typical textures, indeed fingerprint, broken fan-shaped and striated textures have all been observed.

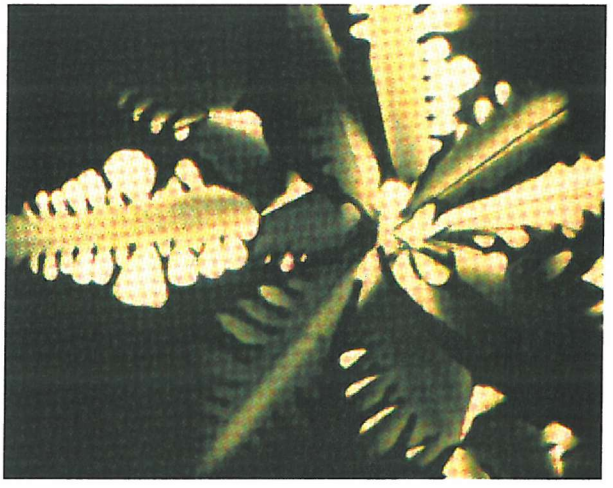

Figure 1.18 :Typical texture exhibited by the Col_{ho} phase cooled from the isotropic liquid [21].

1.9 Differential Scanning Calorimetry

Differential scanning calorimetry, or DSC, is an invaluable tool for characterising the transitions between liquid crystal and other phases. The technique relies on the fact that during a first order phase transition energy is required to disorder the system whilst at the transition temperature, in other words, a latent heat. This notion can be derived from the definition of the Gibbs free energy difference between the two phases

$$\Delta G = \Delta H - T\Delta S . \qquad (1)$$

At the transition the Gibbs free energy difference is zero and the first derivative, the entropy, $\Delta S = -(\partial \Delta G / \partial T)_P$, is non-zero, as is the enthalpy change or the latent heat required to disorder the system – and the second derivative, the heat capacity difference, $\Delta C_p = -T(\partial^2 G / \partial T^2)_P$, is infinite, also indicating that heat energy is absorbed during the phase transition. These criteria define a first order transition and the vast majority of transitions are first order in nature. A nematic to isotropic transition is weakly first order, i.e. there is a small change in entropy and enthalpy at the transition reflecting the relative translational disorder of the nematic phase, whereas the crystal to isotropic transition is strongly first order reflecting, this time, the highly ordered translational nature of the crystal structure. As a guide the entropy change, $\Delta S / R$, quoted as such to give a dimensionless value, of the nematic – isotropic transition is approximately 0.5 and the entropy change of the crystal to isotropic phase transition is much larger at 5 – 10.

Second order transitions, on the other hand, are continuous with respect to their first derivative properties, having zero enthalpies and entropies of transition, and a finite change in the heat capacity. A smectic A to smectic C transition can be second order indicating only a tilting of the directors during the transition. A glass transition is also second order.

Experimentally, a calorimeter consists of two samples, one, some form of reference (usually an empty aluminium pan) and the other the substance under examination (contained in an identical pan). These samples are placed in identical coupled heaters and heated, or cooled, at a constant rate. During a phase transition energy is required to initiate the change and therefore one of the heaters requires

more energy than the other to keep the two samples at an identical temperature. Conversely, during cooling one of the heaters requires less energy than the other during a phase transition. What is measured by the DSC is the difference between the heat input into the sample and the heat input into the reference pan, that is, ∂q. This is recorded with respect to temperature or time, $(\partial q / \partial T)_P$ i.e. the heat capacity.

On a DSC trace a first order transition appears as a peak for a transition requiring an input of energy and a dip for a transition requiring a removal of energy, whereas a second order transition appears as a step in the baseline. The temperatures of transition are calculated from the lead edge of the peak or, arbitrarily, the mid point of the step, as shown in figure 1.19.

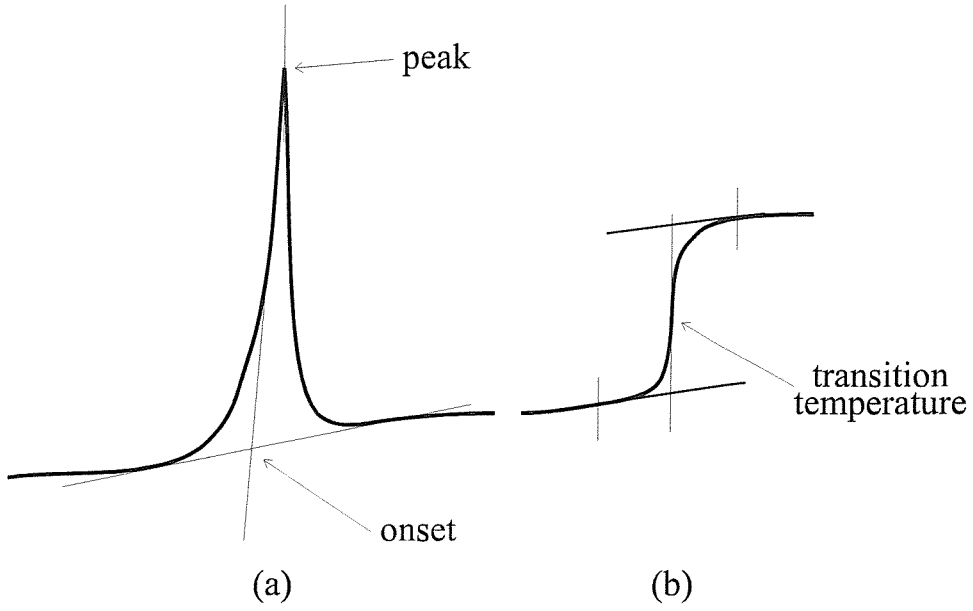

Figure 1.19 : First order (a) and second order (b) transitions as seen on a DSC trace.

The area under the peak is proportional to the transitional enthalpy and from this the transition entropy can be calculated from

$$\frac{\Delta S}{R} = \frac{\Delta H \cdot M_W}{T_t \cdot R}, \qquad (2)$$

where ΔH is the transitional enthalpy (J g^{-1}), M_W is the molecular weight of the sample (g mol^{-1}), T_t is the transition temperature (K) and R is the universal gas constant (J K^{-1} mol^{-1}).

1.10 X-ray Diffraction

X-ray diffraction is a technique that enables the local order in liquid crystal phases to be determined together with information about the periodic distances within the structure. These patterns arise from the interference between the diffracted x-ray waves. Constructive interference arises from waves whose amplitudes are in-phase and combine to enhance each other. On the otherhand, destructive interference results from waves whose amplitudes are out-of-phase and cancel each other. The phases of the waves, which are reflected by a common source are directly related to their path lengths. As can be seen in figure 1.20 the difference in the path length of the two rays reflected from the different layers of the molecules is equal to $AB + BC$. AB and BC are equal to each other and also to $d\sin\theta$. The x-rays are in phase when $2d\sin\theta$ is an integer number of wavelengths. Therefore bright reflections, or constructive interference, occurs when

$$n\lambda = 2d\sin\theta, \qquad (3)$$

where n is an integer, λ is the wavelength of the incident x-rays, θ is the angle of the diffracted x-rays and d is the periodicity. This relationship is known as Bragg's Law and by knowing the wavelength of the x-rays, 2θ can be obtained from the experiment and so, for a first order reflection where $n = 1$, the periodicity, d, can be measured.

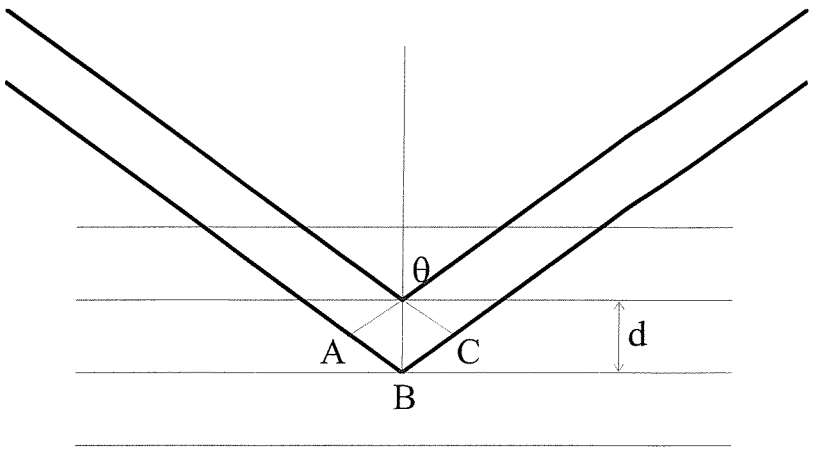

Figure 1.20 : Schematic diagram shown the reflections from crystal layers in a sample.

The diffraction patterns of aligned liquid crystalline samples usually consist of diffuse outer arcs which are known as the wide angle diffraction. These arcs correspond to the side-by-side molecular distances and result from interference

scattering between molecules side-by-side. There will also be an inner pair of sharper arcs, seen for nematic phases, or even spots, seen when in a smectic phase. This is known as the small angle diffraction. This distance corresponds to the layer spacing in smectic phases or the long molecular length in nematic phases. It should be noted that for unaligned samples the arcs and spots will appear as diffuse rings indicating the liquid-like non alignment of the sample. An idealised diagram of an x-ray diffraction pattern of a smectic C phase aligned perpendicular to the incident x-rays is shown in figure 1.21. As can be seen in the diagram the inner spots appear at an angle to the meridian (Q_{par}). This angle, θ, gives the tilt of the molecules in each layer. With proper alignment of the bulk phase a hexagonal arrangement of the spots can be seen for hexagonal phases.

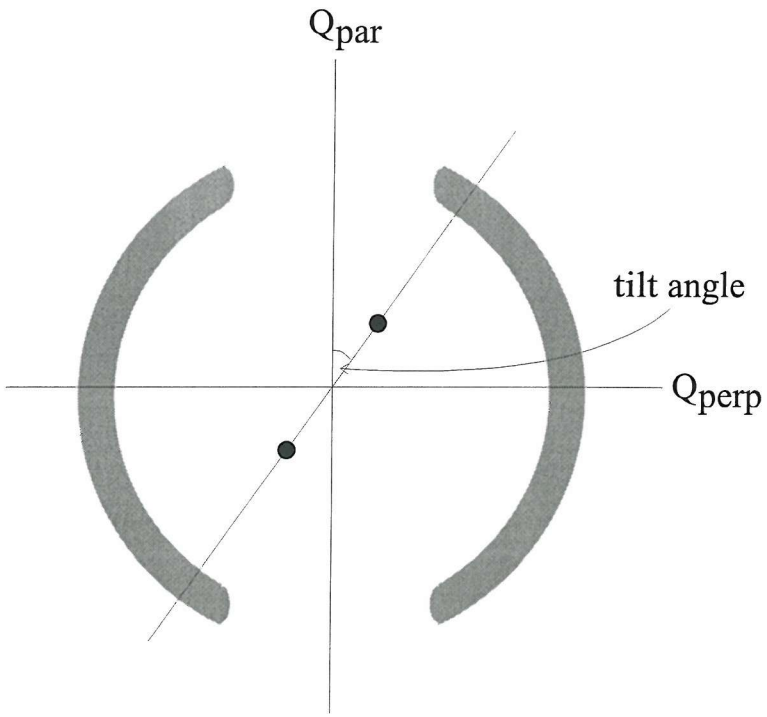

Figure 1.21 : A schematic representation of typical x-ray pattern obtained from an aligned smectic C phase with the director perpendicular to the x-ray beam.

1.11 Quantifying Order – The Order Parameter

Until now we have only been dealing with the order in mesophases in a qualitative way. It seems sensible that it should be possible to quantify the order present in the phases, and indeed this is true. As stated earlier (§1.3.1) there is a molecular director, $\hat{n}$, a unit vector that represents the preferred orientation of the molecules

within a phase. Due to the fluid nature of liquid crystal phases any single molecule will lie at an angle, β, with respect to the director, as shown in figure 1.22. It makes sense to quantify complete order, i.e. $\beta = 0°$, as '1' and complete disorder, i.e. when the molecule adopts all orientations equally, as '0'. Also the phase should be considered apolar, i.e. $\hat{n} = -\hat{n}$, as the director makes no distinction between which way up the molecules lie. Conveniently when $\beta = 0^O$, $\cos^2 \beta = 1$, however the sum of $\cos^2 \beta$ over all orientations is 1/3.

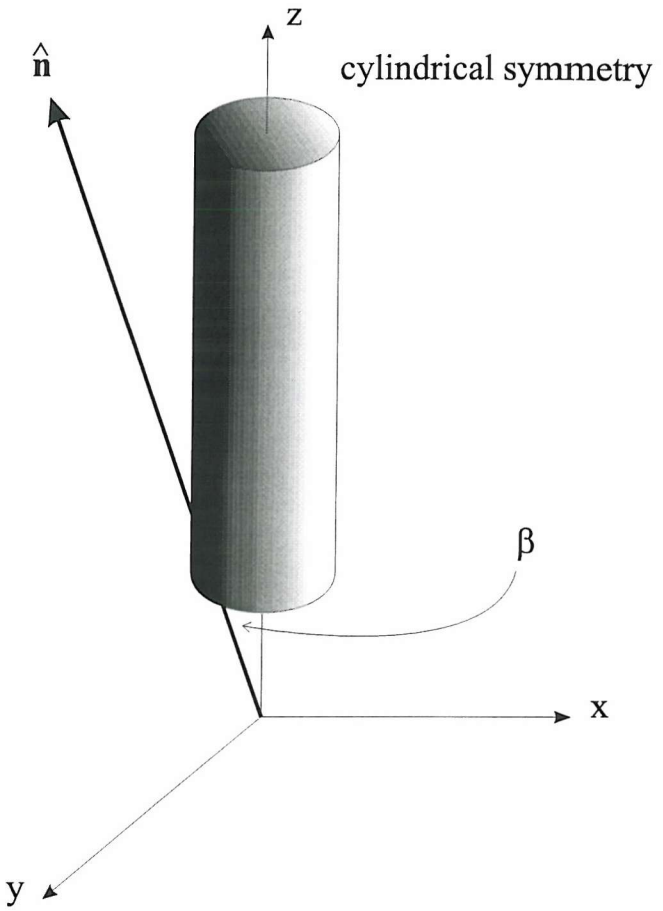

Figure 1.22: A schematic representation of a single rod-like molecule in a liquid crystal phase.

With some rearranging it is possible to obtain what is required, i.e. complete order, or '1' when $\beta = 0°$, and complete disorder, or '0' when β can take all values equally, and we end with

$$S = \tfrac{1}{2}\overline{(3\cos^2 \beta - 1)}, \qquad (4)$$

where S is called the second rank orientational order parameter.

It may seem initially naïve to suppose that we can assume the orientational order, which is the defining characteristic of a liquid crystal, can be described by an expression that is derived only from two such extreme cases, however this description works extremely well. This is not so surprising when considering the case of an aligned sample, i.e. when the director is uniform throughout the sample. The singlet orientational distribution function, $f(\beta)$, as shown in figure 1.23, gives the probability of finding a molecule at an angle, β, to the director in volume element $d\cos\beta$. Although very difficult to determine experimentally, this function can be expressed as a sum of the even ordered Legendre polynomials, in other words

$$f(\beta) = \sum_{L=0}^{\infty} f_L \, P_L(\cos\beta); \text{ for L even} \qquad (5)$$

The Legendre functions are orthogonal, and using this relationship the expansion coefficients f_L are shown to be

$$f_L = \frac{(2L+1)}{2}\overline{P_L}. \qquad (6)$$

Substituting into equation (5) we get

$$f(\beta) = \sum_{L=0}^{\infty} \frac{(2L+1)}{2}\overline{P_L} \, P_L(\cos\beta); \text{ for L even} \qquad (7)$$

where $P_L(\cos\beta)$ are the Legendre polynomials whose first few terms are

$$P_0(\cos\beta) = 1,$$
$$P_2(\cos\beta) = \tfrac{3}{2}\cos^2\beta - \tfrac{1}{2},$$
$$P_4(\cos\beta) = \tfrac{35}{8}\cos^4\beta - \tfrac{30}{8}\cos^2\beta + \tfrac{5}{8},$$
$$P_6(\cos\beta) = \tfrac{231}{16}\cos^6\beta - \tfrac{315}{16}\cos^4\beta + \tfrac{105}{16}\cos^2\beta - \tfrac{5}{16}.$$

As can be seen $\overline{P_2}$ takes exactly the same form as that described for S, the order parameter. Since $\overline{P_2}$ can be determined experimentally using techniques such as deuterium NMR(Chapter 3) and ESR and as this is usually the largest of the order parameters the degree of order in a mesophase is normally taken to be equal to this order parameter. The higher order Legendre functions can be determined using neutron diffraction [22] and so a more accurate measure of $f(\beta)$ can be determined.

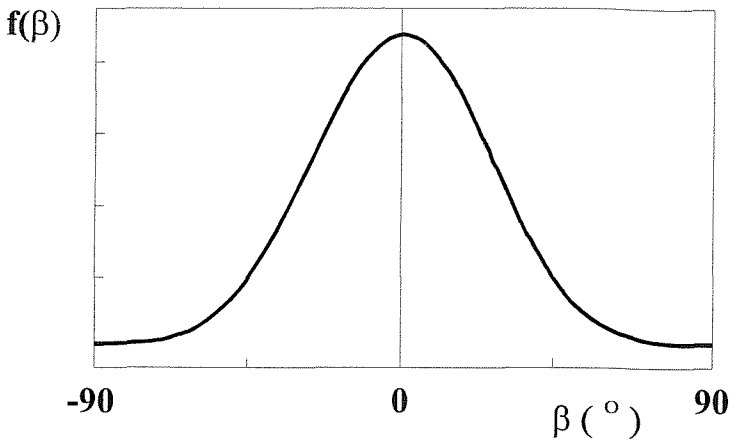

Figure 1.23 : The singlet orientational distribution function.

For a typical liquid crystal at the nematic to isotropic transition S normally takes a value between about 0.3 and 0.4, but for more ordered phases such as a crystal E or Col_{ho} phase the order parameter could be as high as 0.9.

1.12 Structure-property Relationships in Liquid Crystals

It was only 20 years after Reinitzer's 'discovery' of liquid crystallinity that Vorländer [23] presented a rule that related the structure of a molecule to its liquid crystallinity, namely the more linear a molecule is, the greater the chance of liquid crystalline behaviour. Even today the rule still proves to be a valuable guide, although the relationship is a complex one. Even subtle changes in the molecular architecture can alter the mesophase behaviour enormously. In the following section we will consider the connection between the structure and the phase behaviour of liquid crystalline materials.

1.12.1 Monomeric Liquid Crystals

The classic approach to the design of mesogenic materials is to have a semi-rigid core to which are attached, terminally, either one or two other groups:

The anisotropy of this rigid core enhances the liquid crystal to isotropic transition temperature and usually consists of aromatic rings joined via some linking unit. This unit normally contains multiple bonds in which the rotation is restricted thus

preserving the rigidity and elongation of the core which is a major driving force in the formation of liquid crystal phases. The multiple bonds also serve to increase the degree of conjugation in the core and, in turn, enhance the polarisability anisotropy of the molecule which also aids in the formation of liquid crystalline phases. The effect of increasing the molecular length on the transition temperature can be seen in figure 1.24

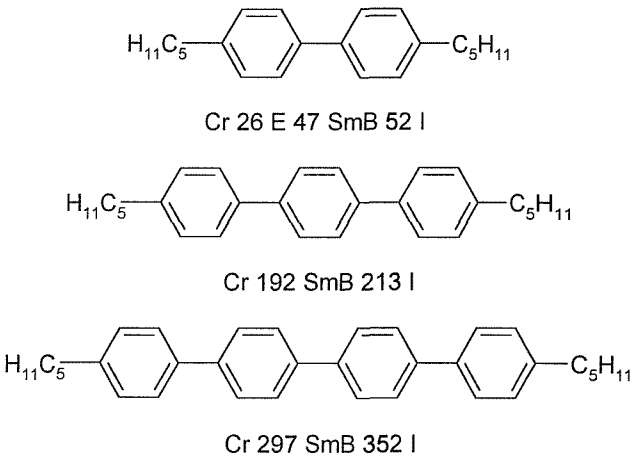

Figure 1.24 : Effect on transition temperature of extending anisotropy of the mesogenic core [9].

The abilities of these linking groups to promote mesophase stability has been investigated [24] and the order was generally found to be:

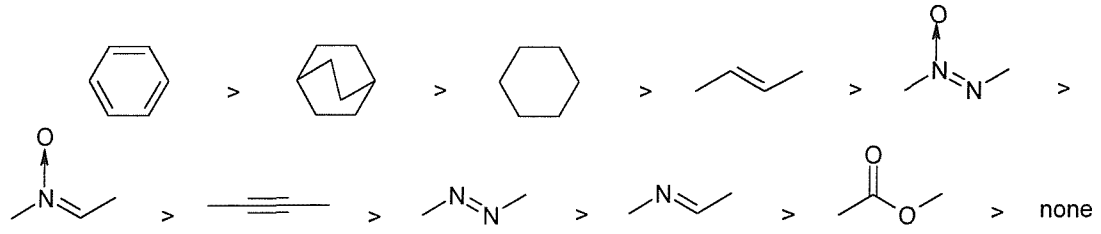

The position of the benzene ring first in the list indicates the importance linearity has on the stability of mesophases as well as the unsaturation and conjugation increasing the polarisability anisotropy and so enhancing the stability. It is interesting to note the high position the bicyclo[2.2.2]octane and cyclohexane group occupy. This serves to indicate that shape anisotropy and rigidity are important factors in mesophase formation. In fact it is possible to form liquid

crystal phases without the need for any degree of unsaturation, for example the molecule

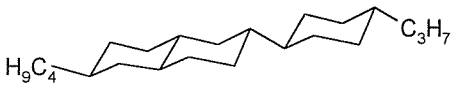

Cr 53°C N 111°C I

has a linear geometry and low polarisability anisotropy [25]. More surprisingly, the molecule

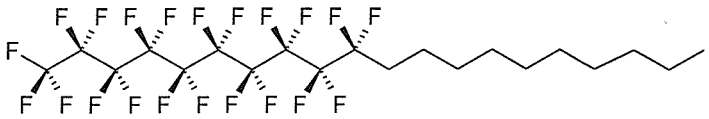

shows a smectic B phase [26] without having any rigid ring system at all. This is, in fact, due to the rigid nature of the perfluorinated chain.

There is normally either one or two terminal substituents attached to the semi-rigid core. Not surprisingly the choice of these groups is also important in determining mesophase behaviour. The relative efficiency of a number of these terminal groups to increase the nematic to isotropic transition temperature of a mesogen has also been investigated [24]. The order is generally found to be:

$$Ph > NHCOCH_3 > CN > OCH_3 > NO_2 > Cl > Br > N(CH_3)_2 > CH_3 > F > H$$

This ordering can be rationalised in terms of the substituents effect on the polarisability and ability to interact with the cores conjugated system as well as the effect on the shape anisotropy. The dipole associated with the group may also play an important role in determining the stability of the mesophase. This possibility is explored in Chapter 4.

It is usual, and necessary, for one of the terminal substituents to be an alkyl or alkoxy chain, and these groups have received the greatest attention – homologous series of compounds being constructed and studied. The flexible chain serves to reduce the melting point of the molecule and thus reveals an underlying mesophase or extends or affects mesophase stability. The compounds shown in figure 1.25 illustrate this idea.

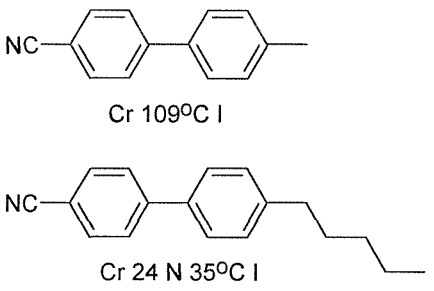

Figure 1.25 :The effect of extending the terminal chain length on transition temperatures [27].

If the phase transition temperatures of an homologous series are plotted against the number of carbon atoms in the terminal alkyl chain it is often found that an odd-even alternation occurs for the nematic – isotropic transition temperature. This is illustrated for a series of 4-alkyl-4'-cyanobiphenyls in figure 1.26.

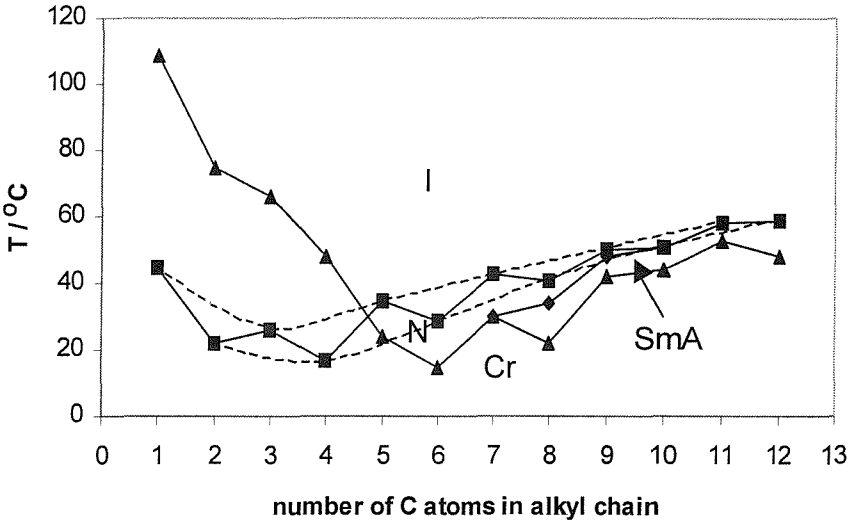

Figure 1.26 : Transition temperatures for a series of 4-*n*-alkyl-4'-cyanobiphenyls [27].
▲ Cr – SmA, N or I, ■ N –I, ◆ SmA – N or I. Dotted lines show the curves the clearing tempertures for the odd and even members lie on.

This odd-even effect can be explained by considering the conformational distribution of an alkyl chain. Any conformation that increases the molecular anisotropy, or more simply, the length-to-breadth ratio, of a molecule will enhance the stability of the mesophase and thus increase the transition temperature. Conversely, any conformation that reduces the length-to-breadth ratio will destabilise the mesophase and result in a lower transition temperature. For

molecules containing an odd number of carbon atoms in the alkyl chain, the number of conformations resulting in an increase in the molecular anisotropy is greater than for an alkyl chain in which there are an even number of carbon atoms. This can be more clearly illustrated by considering the all-trans configuration of the alkyl chain. Adding a carbon atom to give an odd number extends the length of the molecule, whereas adding a carbon atom to give an even number extends not only the length, slightly, but also the breadth. This leads to the transition temperatures lying on two smooth curves – the odd being at a higher temperature than the even. Also as the chain length increases the transitional entropy attenuates. This can be attributed to the large increase in the number of conformers available for longer chain lengths. This reduces the distributional bias in the conformations for the nematic phase and thus reduces the difference in molecular shape of the odd and even members.

If one of the terminal groups is now an alkoxy chain as opposed to an alkyl chain it is found that the clearing temperature of an analogous material is increased by between 30° and 40°C. More strikingly, it is noticed that the odd-even trend is reversed. When the molecular structure of the alkoxy substituted material is considered it becomes apparent why this is – the first atom in the chain is an oxygen atom therefore causing the first methylene unit to lie at an angle to the long molecular axis rather than along it, as occurs for an alkyl chain. The increase in the clearing temperature was generally attributed to the ability the oxygen atom has in interacting with the conjugated aromatic system thereby increasing the polarisability anisotropy. However, it has been recently argued that the relative geometries of the ether and methylene linking units play a large part in the difference in transition temperatures [28]. The more acute the linking unit the more the alkyl chain extends laterally thereby reducing the length-to-breadth ratio of the molecule and lowering the clearing point, hence an ether link, with a larger angle than a methylene link, will increase the transition temperature. This also leads to a reduction in the odd-even alternation of the clearing temperatures with increasing chain length. The larger bond angle of the ether link means the difference in the length-to-breadth ratios between the even homologue and the odd homologue is now smaller thereby resulting in a smaller odd-even effect.

It is also found that increasing the terminal chain length promotes the formation of smectic phases, as shown in figure 1.26. This ultimately leads to the eradication of nematic properties. This behaviour is considered a result of microphase separation where unlike parts of the molecule, i.e. aromatic-aliphatic, interact less favourably than like parts. This causes the molecules to adopt a layered, that is smectic, structure where the aliphatic regions have more conformational freedom hence the entropy is larger and more favourable.

1.12.2 Dimeric Liquid Crystals

A dimeric liquid crystal is one in which two mesogenic units are linked via a flexible spacer. The two mesogenic units can either be identical, and are termed symmetric dimers, or they can be different, and are termed non-symmetric. The flexible spacer is usually aliphatic although siloxane and oligooxyethylene chains can be used.

The first examples of dimeric materials were synthesised by Vorländer in the late 1920's [29] and were found to be liquid crystalline; they were of the form

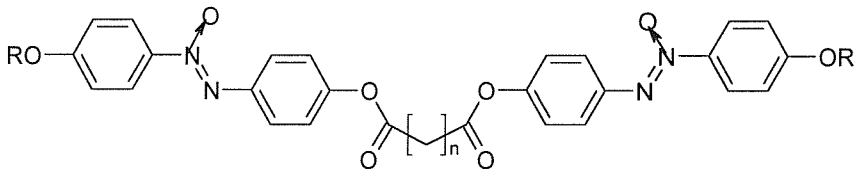

However, dimeric systems such as these did not receive any significant attention until the 1980's when it became apparent from their properties that dimers were good models for main chain liquid crystal polymers [30]. These polymeric materials incorporate mesogenic units into the polymer chain and as such suffer from a number of problems being complex, polydisperse and often difficult to purify. The dimers on the other hand can be easily synthesised and purified and so aiding both experimental and theoretical studies.

The transitional properties of dimeric liquid crystals have been found to depend strongly on both the length and parity of the flexible spacer chain as well as the nature of the link between the chains and the mesogenic groups. The nematic – isotropic transition temperature and entropy change, shown in figures 1.27 and 1.28, for a series of α,ω- bis(4'-cyanobiphenyl-4-yloxy)alkanes [31] illustrate this.

It can be seen that the odd-even effect for dimers is far larger than in monomeric systems. The even dimers tend to have significantly higher transition temperatures than the odd dimers. Also the odd dimers have a transitional entropy comparable to the corresponding monomeric materials whereas the entropy change for the even dimers is typically three times larger.

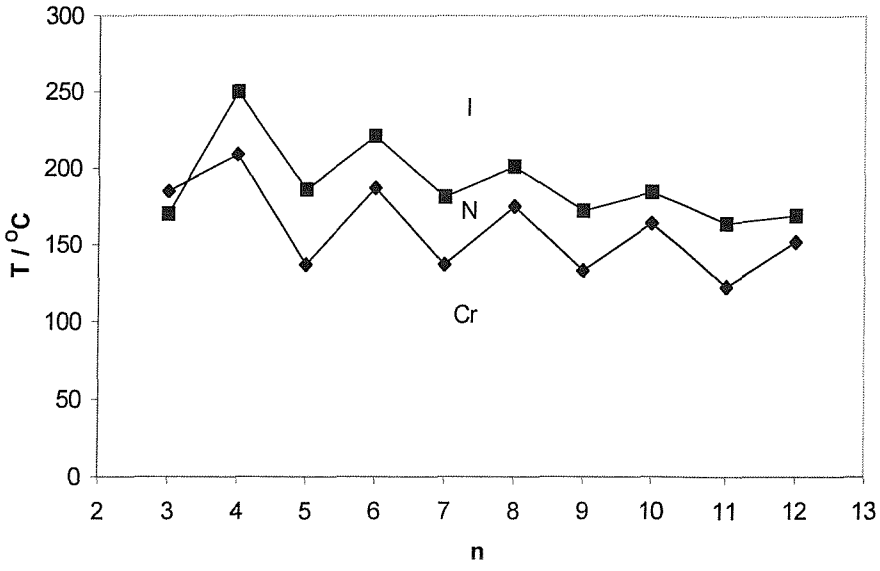

Figure 1.27 : The transition temperatures for the α,ω-bis(4'-cyanobiphenyl-4-yloxy) as the number of carbon atoms, n, in the chain is increased. ◆ Cr – N or I, ■ N – I.

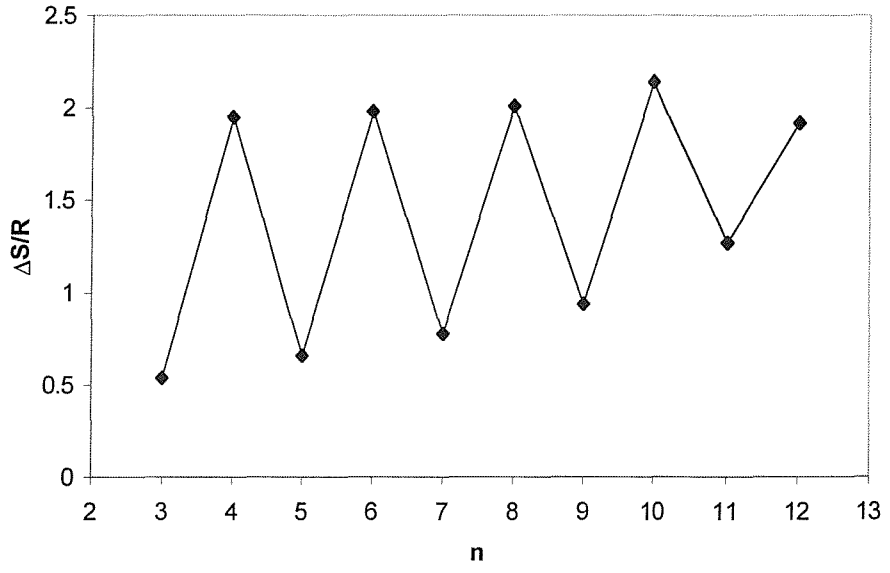

Figure 1.28 : Entropy change for the α,ω-bis(4'-cyanobiphenyl-4-yloxy) alkanes at the N – 1 phase transition on changing the number of carbon atoms, n, in the chain.

It is obvious from figure 1.29 that for an all-*trans* configuration of the chain the molecular shape of the even dimer has a greater length-to-breadth ratio than for a dimer with an odd number of methylene links and, more importantly, the odd dimers are bent. If we consider a liquid crystal dimer as binary mixture of bent and linear molecules, and ignore the alkyl chain, we can begin to understand the characteristic properties of these materials. For a linear conformer the mesogenic groups are parallel, whilst for the bent conformer the mesogenic groups are at an angle of 109.5°, the tetrahedral angle, to each other. To convert the bent conformers to linear ones we need to add *gauche* defects to the alkyl chain thereby increasing the energy. The lowest energy state for an even dimer is the all-*trans* conformation where the mesogenic groups are parallel and therefore we have a linear conformer. For the odd dimers the lowest energy state is, again, the all-*trans* conformation, however this leads to a bent conformer. For the molecule to exist in a linear form we need to add a number of *gauche* links to the alkyl chain. This is energetically unfavourable and so, for the odd dimers, there are many more bent conformers than linear ones. In the isotropic phase about 50% of the conformers are linear for the even dimer and so the nematic – isotropic transition temperature is high compared to the odd dimers. There are still bent conformers present, however, and these reduce the transition temperature by diluting the effect of the linear conformers. On cooling from the isotropic phase into the nematic phase the bent conformers present for the even dimer are converted to linear conformers. Although there is an energy penalty due to this conformational change, the gain in orientational energy offsets this energy penalty. The increase in the concentration of the linear conformers increases the effective nematic – isotropic transition temperature and also increases the order in the system, thereby increasing the transitional entropy. For the odd dimer the majority of conformers are bent. The conformational energy required to convert these to the linear form is no longer compensated by the gain in orientational order, and therefore there is no increase in the nematic – isotropic transition temperature or in the order of the system resulting in lower transition temperatures and entropies.

Also it has been found that as the chain length increases the alternation in the nematic – isotropic transition temperature attenuates although, contrary to observations for monomeric materials, the alternation in the transitional entropies

remains essentially unattenuated, although for chain lengths with twenty or more methylene units the entropies slowly begin to attenuate [32].

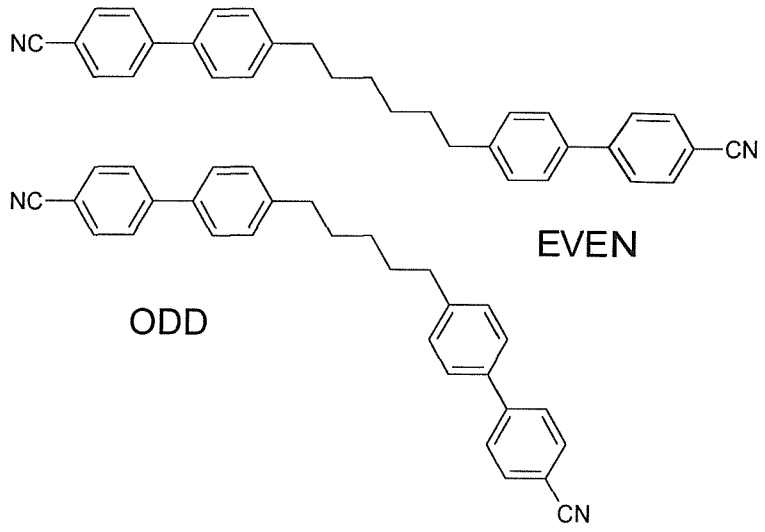

Figure 1.29 : The linear and bent conformations of even membered and odd membered cyanobiphenyl dimers, respectively.

As with the monomeric materials the nematic to isotropic transition temperature is sensitive to the choice of atom linking the mesogenic unit to the flexible chain. For example the clearing temperature of the ether linked cyanobiphenyl dimers shown in figure 1.27 are higher than the corresponding methylene linked dimers, shown in figure 1.29, although the difference in temperature between the odd and even dimers is less. The higher transition temperatures for the ether linked dimers are, again, due to the geometry of the linking atom. The larger angle of the oxygen atom means that for an odd number of methylene units the deviation from a linear geometry is smaller than the deviation caused by methylene linking groups and hence the difference between the conformers of the odd and even dimers is less.

Dimeric compounds have also been prepared where both the terminal and spacer chain lengths can be varied such as [33].

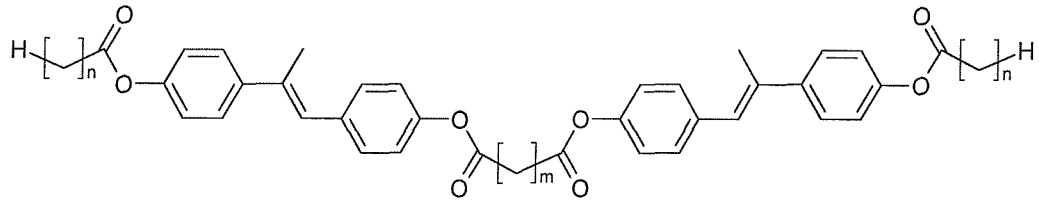

The results indicate that the dominant influence on the clearing temperature is due to the parity of the spacer chain with the parity of the terminal chains having little effect on the transition temperature. Increasing the terminal chain length increased the formation of smectic phases, as found for monomeric mesogens. However, increasing the spacer chain length promoted nematic phase behaviour which is contrary to general observations. Similar trends have also been seen for the following Schiff's base dimers studied by Date *et al.* [34]

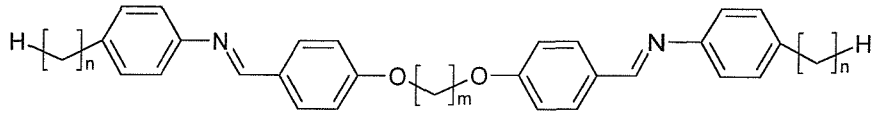

Until now only symmetric dimers have been discussed, however non-symmetric dimers exist where the two mesogenic groups are different. A well studied class of non-symmetric dimers are the α-(4-cyanobiphenyl-4'-yloxy)-ω-(4-alkylanilinebenzylidene-4'-oxy)alkanes [35] shown below.

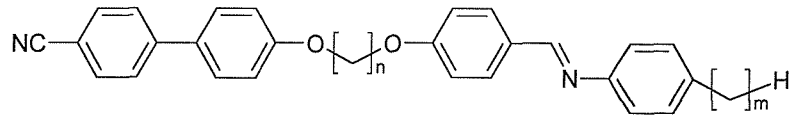

It was found that these materials were highly smectogenic, displaying a number of different smectic phases. The most striking feature of these dimers, though, was the existence of either an intercalated smectic phase, where the layer spacing is about 0.5 times the molecular length, or an interdigitated smectic phase, where the layer spacing is between about 1.4 and 1.6 times the molecular length, the difference between these two smectic modifications being shown in figure 1.30. It was found that for dimers with a long linking chain and short terminal chain intercalated phases were formed, and dimers with a short linking chain and long terminal chain interdigitated phases were formed. Intercalated phases are formed for the former because of the microphase separation caused by specific interactions between the different mesogenic units and the ability of the short terminal chains to fit in the gap caused by the long linking chain (figure 1.30b). If the terminal chain is longer than the linking chain the space between the molecules is not enough to accommodate the long terminal chain and therefore an interdigitated structure is formed where different mesogenic units still lie next to each other but only at one end of the dimer, as shown in figure 1.30a. Again, as with the

symmetric dimers, there is a large alternation in clearing temperature on increasing the linking spacer chain length and little, if no, alternation in clearing point on increasing the terminal chain length.

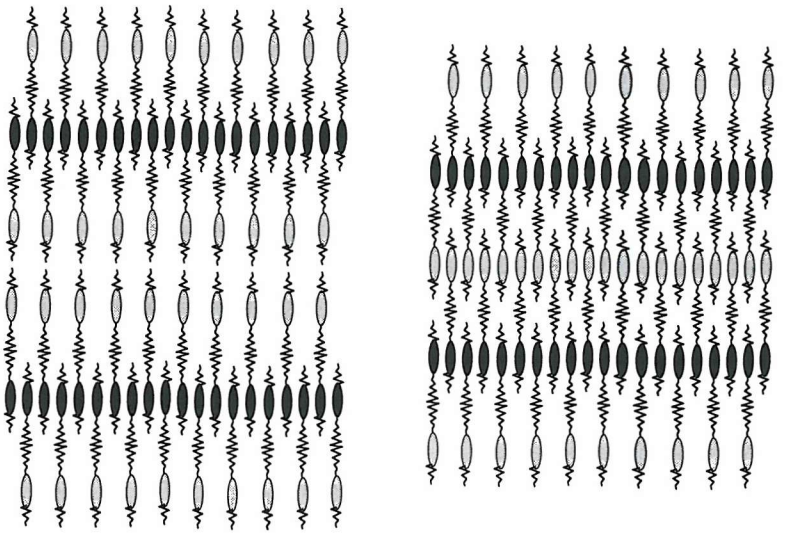

Figure 1.30 : Representation of an (a) intedigitated and (b) intercalated smectic A phase.

1.12.3 Discotic Liquid Crystals

Generally speaking discotic liquid crystals possess flat, or nearly flat cores with six or eight long chain substituents at the perimeter; the first examples were synthesised by Chandrasekhar *et al.* in 1977 [36] and were hexaesters of benzene. Like these examples the cores are normally aromatic, such as benzene, naphthalene or triphenylene, or partially unsaturated such as truxene, shown in figure 1.31 Generally, the larger the core diameter the greater the shape anisotropy and therefore the more likely a mesophase will be formed [37,38]. For example, the truxene core, with six nonyl ester groups ($-OCO(CH_2)_8CH_3$) attached has a clearing temperature of 280°C and a mesomorphic range of 212°C [39] whereas the corresponding triphenylene has a clearing temperature of only 126°C and a smaller mesomorphic range of only 51°C [40]. It should also be noted that the core of the molecule need not necessarily be flat to form discotic phases, examples of molecules where the core is either conical or pyramidal exist that form discotic phases [41,42].

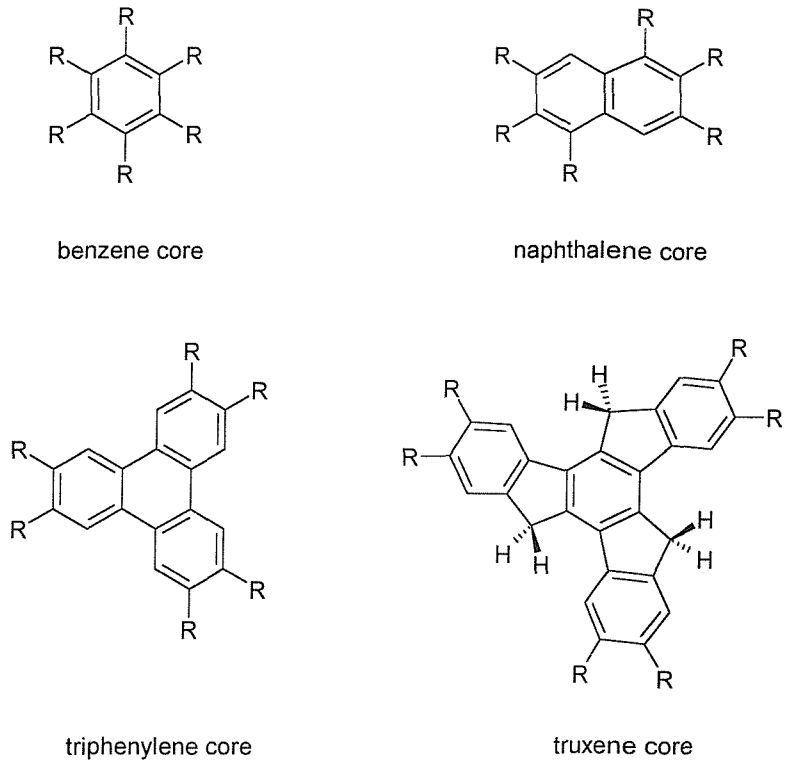

Figure 1.31 : Examples of the disc-shaped cores used to produce discotic mesogens.

As with calamitic mesogenic materials the use of flexible alkyl chains, substituted around the aromatic core, serve to reduce the melting points of the molecules and thus aiding the formation of liquid crystal phases. The general trend, as the chain length is increased, is for the transition temperatures to decrease and the probability of columnar phases forming to decrease also, as shown for the naphthalene derivative in figure 1.32 and the truxene derivative in figure 1.33. This observation can be rationalised by considering the packing of the molecules in a columnar phase. To form, for example, an hexagonal columnar phase (Col_h) the columns of molecules have to be arranged in a closely packed hexagonal net. Long alkyl chains protruding from the 'rim' of a disc in one of the columns will disrupt the close packing of the nearest neighbouring columns. Eventually this disruption will become energetically unfavourable and so only nematic phases will be formed where this close proximity of the neighbouring molecules no longer occurs.

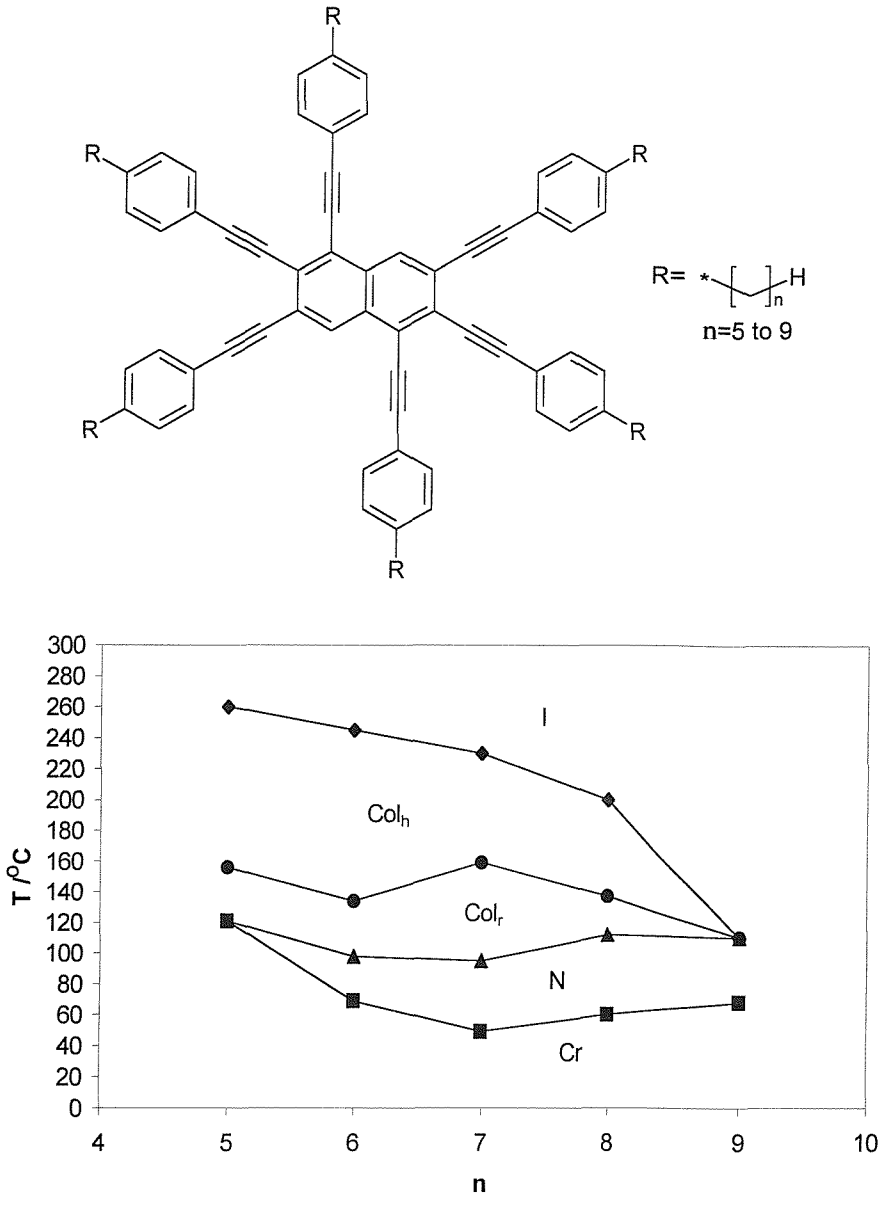

Figure 1.32 : The influence on mesophase behaviour of increasing the number of carbon atoms, n, in the peripheral alkyl chains of the naphthalene derivative (above) [43]. ■ Cr – N, ▲ N – Col_r, ● Col_r – Col_h, ◆ Col_h – I.

It is, however, interesting to note that there appears to be little or no odd-even alternation in the clearing temperature upon increasing the peripheral chain length. This is because the driving force for the formation of columnar phases is not influenced by the length or parity of the peripheral chains, unlike for the formation of nematic phases. The lack of an odd-even effect on changing the length and parity of terminal alkyl chains is also seen for smectic – isotropic transitions. This point can be illustrated by comparing the clearing temperatures of the naphthalene

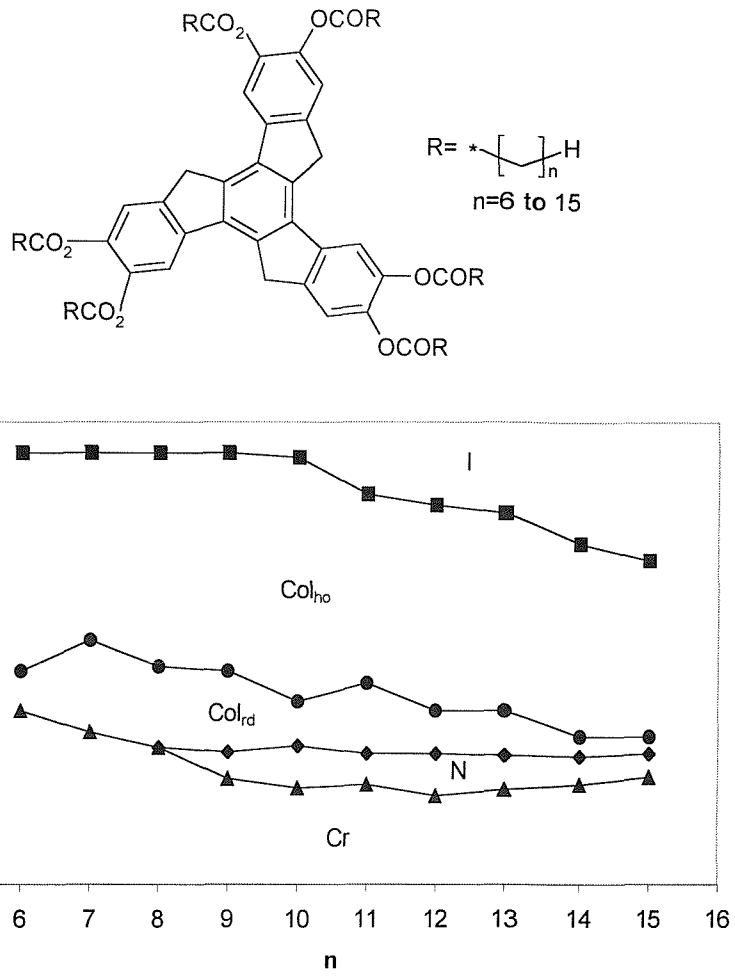

Figure 1.33 : The influence on mesophase behaviour of increasing the number of carbon atoms, n, in the peripheral alkyl chains of the truxene derivative (above) [44].
■ Cr – N, ▲N – Col_{rd}, ● Col_{rd} – Col_{ho}, ◆ Col_{ho} – I.

and truxene derivatives with the mesophase – isotropic transition temperatures of an homologous series of N,N',N''-1,3,5-benzene tricarboxamides [45] of the form

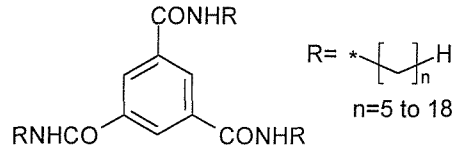

as shown in figure 1.34.

The mesophases of the benzene tricarboxamides are considered to have a highly disordered columnar structure, although the columnar structure has not been unambiguously confirmed, and it is tempting to consider the phase as having a columnar nematic type structure.

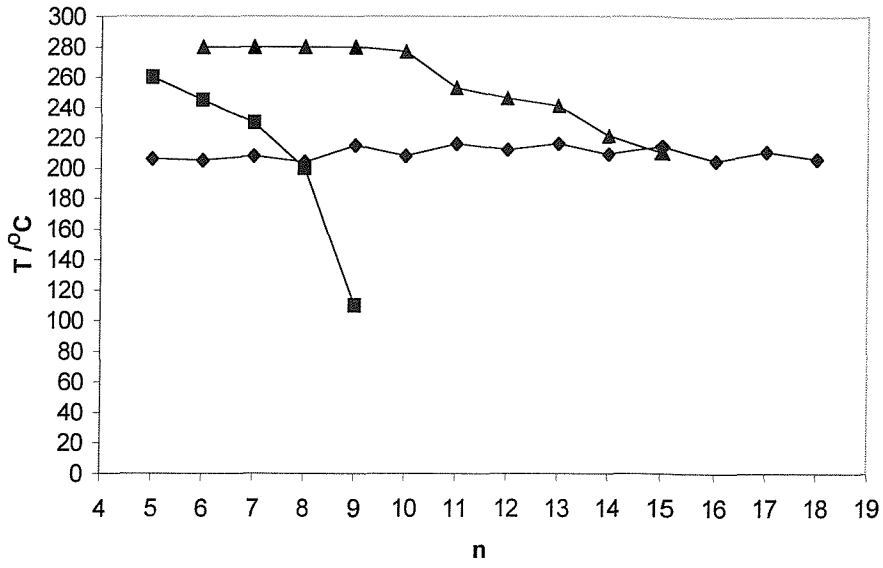

Figure 1.34 : Comparison of the transiton temperatures of a series of naphthalene Derivatives [43] (■), truxene derivatives [44] (▲) and benzene tricarboxamide derivatives [45] (●), on changing the number of carbon atoms, n, in the peripheral alkyl chains.

It is also possible, with the addition of electron deficient molecules such and 2,4,7-trinitrofluorenone, to induce nematic and columnar phases in some of these large electron-rich disc-like materials.

1.13 Summary

As this Introduction has shown, there are a wealth of factors that can influence the behaviour of mesophases. Chapter 2 of this Thesis investigates the use of electron-deficient materials to induce discotic mesophases in larger electron-rich disc-like molecules. We then explore in more detail, in Chapter 3, the nature of these mesophases using deuterium NMR spectroscopy. As small changes to the molecular structure can have a large effect on mesophase behaviour Chapter 4 explores the effect minor changes in the molecular structure can have on highly mesogenic materials, in particular the cyanobiphenyl and cyanoterphenyl moieties. In Chapter 5 we consider possibility of the existence of thermotropic biaxial nematic phases and the types of materials that may form this elusive phase. In particular we attempt to quantify the biaxiality of mesogenic materials by considering the angle at which two mesogenic moieties are linked together. Finally, we studied a possible thermotropic biaxial nematic mesogen using

deuterium NMR spectroscopy. An alternative approach to the preparation of thermotropic biaxial nematic materials is to link a disc-like moiety to a rod-like moiety via a flexible alkyl chain. Therefore in Chapter 6 a number of disc-rod dimers, based on the large electron-rich disc-like materials studied in Chapter 2, were synthesised and investigated.

1.14 References

[1] Reinitzer, F., *Mh.Chem*, **9**, 421, (1888).

[2] Lehmann, O., *Vernhandl d.Deutschen Phys.Ges., Sitzung v*, **12**, 163, (1900).

[3] Wan, J.W. *PhD. Thesis, University of Southampton*, (1997).

[4] Bazuin, C.G., Guillon, D., Skoulios, A., and Nicoud, J.F., *Liq. Cryst.*, **1**, 188, (1986).

[5] Fuller, S, Shinde, N.N., Tiddy, G.J.T., Attard, G.S. and Howell, O., *Langmuir*, **12**, 1117, (1996).

[6] Chandrasekhar, S., *Liq. Cryst.*, **14**, 3, (1993).

[7] Fan, S.M., Fletcher, I.D., Gundogen, B., Heaton, N.J., Kothe, G., Luckhurst, G.R. and Praefcke, K., *Chem. Phys. Lett.*, **204**, 517, (1993).

[8] Attard, G.S., and Luckhurst, G.R., *Liq. Cryst.*, **2**, 441, (1987).

[9] Leadbetter, A.J. (Chapter 1), Toyne, K.J. (Chapter 2), *Thermotropic Liquid Crystals*, Ed. Gray, G.W., John Wiley & Sons, Chichester (1987).

[10] IUPAC Recommendations

[11] Friedel, G., *Ann Physique (9)*, **18**, 273, (1922).

[12] Levelut, A.M., and Lambert, M., *Compt. Rend. Acad. Sci. (Paris)*, **272**, 1018, (1971).

[13] Barbarin, F., Dugay, M., Piovesan, A., Fadel, H., Guillon, D., and Skoulious, A., *Liq. Cryst.*, **2**, 815, (1987).

[14] Demus, D., Diele, S., Klapperstück, M., Link, V., and Zaschke, H., *Mol. Cryst. Liq. Cryst.*, **15**, 161, (1971).

[15] Richter, L., Demus, D., and Sackmann, H., *Mol. Cryst. Liq. Cryst.*, **80**, 195, (1982).

[16] Leadbetter, A.J., Frost, J., Gaughan, J.P., and Mazid, M.A., *J.Phys. (Paris)*, **40**, C3-185, (1979).

[17] Destrade, C., Tinh, N.H., Malthete, J. and Jacques, J., *Phys. Lett., Ser. A*, **79**, 189, (1980).

[18] Praefcke, K., Singer, D., Kohne, B., Ebert, M., Liebmann, A., and Wendorff, J.H., *Liq. Cryst.*, **10**, 147, (1991).

[19] Singer, D., Liebmann, A., Praefcke, K., and Wendorff, J.H., *Liq. Cryst.*, **14**, 785, (1993).

[20] Demus, D. and Richter, L., *Textures of Liquid Crystals*, Verlag Chemie: Weinheim, New York, (1978).

[21] Gray, G.W. and Goodby, J.W., *Smectic Liquid Crystals: Textures and Structures*; Leonard Hill: London, Glasgow, (1984).

[22] Date, R.W., Hamley, I.W., Luckhurst, G.R., Seddon, J.M. and Richardson, R.M., *Mol. Phys.*, **76**, 951, (1992).

[23] Vorländer, D., *Chemische Kristallographie der Füssigkeiten* (Akademische Verlagsgesellschaft), (1924).

[24] Gray, G.W., *The Molecular Physics of Liquid Crystals*, edited by G.R.Luckhurst and G.W.Gray (Academic Press), Chapter 1., (1979).

[25] Petrzilka, M., and Schleich, K., *Helv. Chim. Acta*, **116**, 1242, (1982).

[26] Mahler, W., Guillon, D., and Skoulios, A., *Mol. Cryst. Liq. Cryst. Lett.*, **2**, 111, (1985).

[27] Data Sheet supplied by Merck Ltd, UK.

[28] Emerson, A.P.J., and Luckhurst, G.R., *Liq. Cryst.*, **10**, 861, (1992).

[29] Vorländer, D., *Z. Phys. Chem.*, **126**, 449, (1927).

[30] Griffin, A.C., and Britt, T.R., *J. Am. Chem. Soc.*, **103**, 4957, (1981).

[31] Emsley, J.W., Luckhurst, G.R., Shilstone, G.N., and Sage, I., *Mol. Cryst. Liq. Cryst. Lett.*, **102**, 223, (1984).

[32] Farrand, F.J., *PhD Thesis, University of Southampton*, (1998).

[33] Centore, R., Roviello, A. and Sirigu., *Liq. Cryst.*, **3**, 11, (1988).

[34] Date, R.W., Imrie, C.T., Luckhurst, G.R. and Seddon, J.W., *Liq. Cryst.*, **12**, 203, (1992).

[35] Attard, G.S., Date, R.W., Imrie, C.T., Luckhurst, G.R., Roskilly, S.J., Seddon, J.M., and Taylor, L., *Liq. Cryst.*, **16**, 529, (1994).

[36] Chandrasekhar, S., Sadashiva, B.K. and Suresh, K.A., *Pramana*, **9**, 471 (1977).

[37] Kohne, B., and Praefcke, K., *Chimea*, **41**, 196, (1987).

[38] Praefcke, K., Kohne, B., Gutbier, K., Johnen, M., and Singer, D., *Liq. Cryst.*, **5**, 233, (1989).

[39] Tinh, N.H., Foucher, P., Destrade, C., Levelut, A.M. and Malthete, J., *Mol. Cryst. Liq. Cryst.*, **111**, 277, (1984).

[40] Destrade, C., Mondon, M.C. and Malthete, J., *J. Phys. Colloq. C3*, **40**, 17, (1979).

[41] Malthête, J., and Collet, A., *Nouv. J. Chim.*, **9**, 151, (1985).

[42] Zimmerman, H., Poupko, R., Luz, L., and Billard, J., *Z. Naturf* A, **40**, 149, (1985).

[43] Praefcke, K., Kohne, B., Gutbier, K., Johnen, N., Singer, D., *Liq. Cryst.*, **5**, 233, (1989).

[44] Tihn, N.H., Foucher, P., Destrade, C., Levelut, A.M., Malthete, J., *Mol. Cryst. Liq. Cryst.*, **111**, 277, (1984).

[45] Matsunaga, Y., Miyajima, N., Nakayasu, Y., Sakai, S. and Yonenaga, M., *Bull. Chem. Soc. Jpn.*, **61**, 207, (1988).

CHAPTER TWO

CHEMICAL INDUCTION OF DISCOTIC MESOPHASES

2.1 Introduction

One remarkable property of liquid crystals is the miscibility displayed by different materials possessing the same liquid crystal phase. Indeed, this property has been used to assign newly discovered phases [1]. Even if the two materials are quite different with respect to their molecular architecture, as long as the respective phases have the same symmetry, there is a high probability they will still be miscible. We should now consider what occurs when two mesogenic materials are mixed. As happens with non-mesogenic materials that are miscible, the melting points of the two materials are reduced until, at a certain composition, a minimum is reached, known as the eutectic point where the materials pass from a uniform liquid to crystal with no biphasic behaviour, as shown in figure 2.1. If the two materials are, for example, nematic, then we also see a reduction in the melting points. As well as this, we also see a linear dependence, to a good approximation, in the nematic to isotropic transition temperature; this is given by

$$T_{NI}^{mix} = xT_{NI}^{A} + (1-x)T_{NI}^{B}, \qquad (1)$$

where x is the mole fraction of component A.

As can be seen from figure 2.1 this dependence has the effect of widening the nematic range which is important when developing materials for liquid crystal displays (LCDs). Sometimes, though, the interactions between the two mesogens will actually raise the clearing temperature above the value expected for the mixture and form a chemically induced phase, for instance mixtures between 4,4'-diheptylazobenzene and 4-*n*-pentyl-4'-cyanobiphenyl (5CB) [2]. Chemical induction has also been defined, by some authors, as cases where although the clearing temperature is not moved, the phase is 'upgraded' to one possessing a

higher symmetry or more order, for example from a nematic to a smectic A phase, both cases are illustrated in figure 2.2

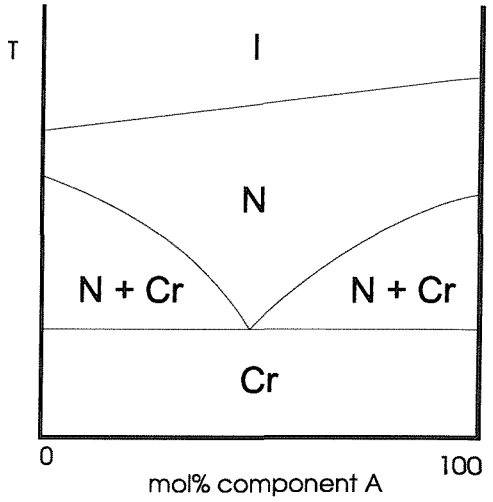

Figure 2.1 : The effect on transition temperatures upon mixing two nematogens.

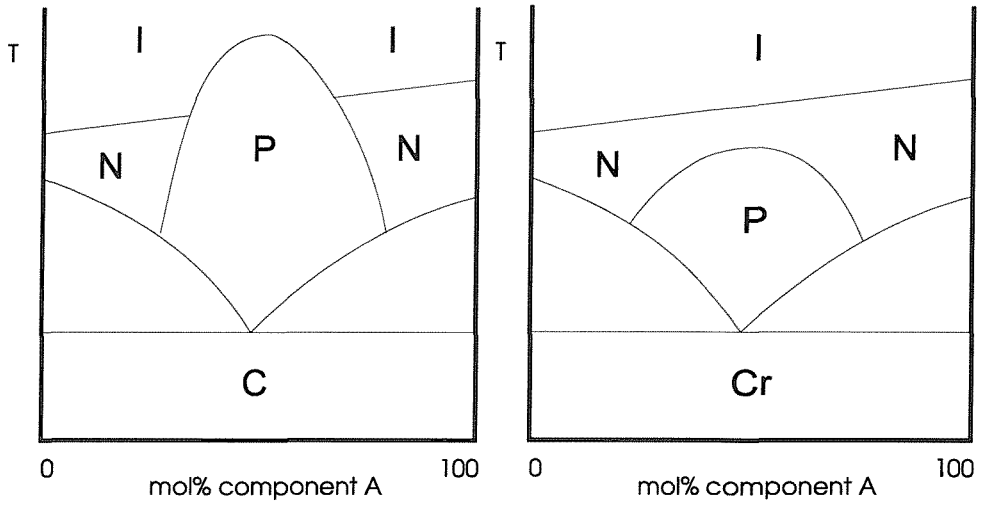

Figure 2.2 : Phase induction by mixing two nematogens.

An example of this type of upgrading of phases is the formation of a smectic A phase from mixtures of nematic, biforked compounds and 4,4'-dialkoxyazoxybenzene [3]. The smectic A phase results from the so-called space-filling effect, where the smaller component fits in the gaps made by the larger, biforked component, as shown in figure 2.3

Other examples of phase induction involving two mesogens include 4,4'-diacylbiphenyl and N,N'-dialkyl-4,4'-diaminobiphenyl derivatives [4] – the smectic A phase being caused by hydrogen-bonding between the molecules – and

mixtures of a biphenyl alkyl diamide and a dicyano-ester [5], which has been attributed to the formation of a charge transfer-complex, a description of which will be given later in this Introduction.

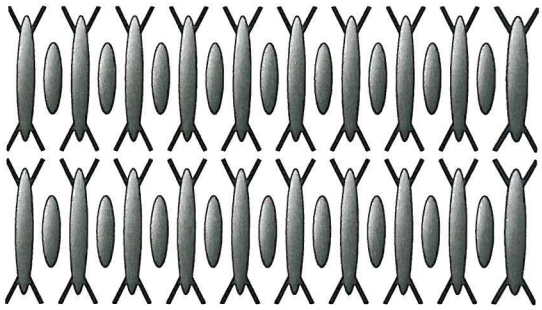

Figure 2.3 : Schematic representation of the 'space-filling' effect.

The possibilities when one of the compounds is liquid crystalline and the other is not are equally intriguing. In the simplest case, when the non-mesogen is added to the mesogenic material the mesophase will eventually be lost. If we extrapolate this to 100% of the non-mesogenic material it is possible to discover its so-called virtual transition temperature, as shown in figure 2.4. This is the temperature at which there would be a hypothetical nematic to isotropic transition of the non-mesogenic material, had the melting point not hidden this transition. This assumes the nematic – isotropic transition temperature of the mixture is linear, that is it obeys equation (1).

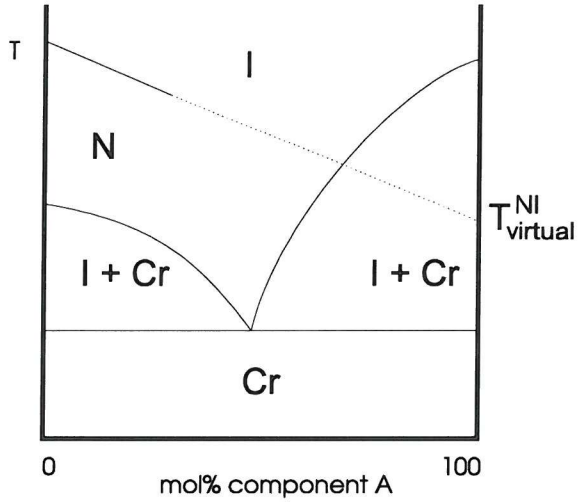

Figure 2.4 : Determining the virtual transition temperature of non-mesogenic component B.

However, it is possible that some non-mesogens will stabilise the existing liquid crystalline phase of the mesogenic material and induce new phases, a hypothetical example is given in figure 2.5. Again, this can often be attributed to the space-

filling effect where smaller non-mesogenic molecules occupy the voids caused by the inefficient packing of laterally substituted or 'swallow tailed' molecules [6]. Phase induction may also be caused by hydrogen bonding, intriguing examples being given in references [7,8], and by the formation of charge-transfer complexes [9]. (The charge-transfer induction of discotic mesophases will be discussed later in this Introduction).

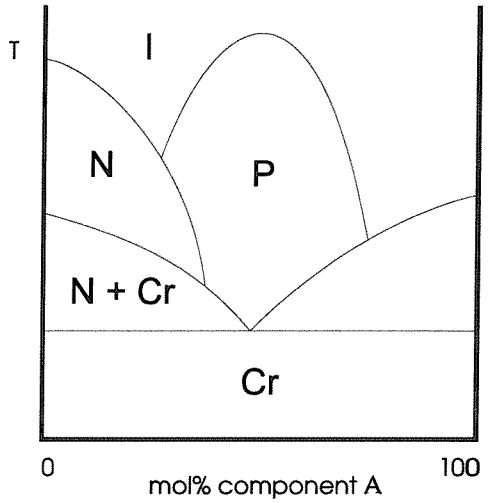

Figure 2.5 : Phase induction by non-mesogenic component B.

This leads us to the question of whether it is possible that mixing two non-mesogenic materials will lead to the induction of liquid crystalline phases. As stated previously in this Introduction, when two miscible non-mesogenic materials are mixed the melting points will be reduced until a minimum is reached at the eutectic point, as shown in figure 2.6. Sometimes this depression in the melting point will reveal a hidden mesophase near the eutectic point. In this instance, as the phase is only revealed because of the reduction in the melting point arising from the physical interactions within the system, it is not said to be chemically induced. Chemical induction is defined to occur when the two materials interact to form a stable mesophase above the anticipated melting point, as illustrated in figure 2.7.

In all of the cases of mesophase induction mentioned here, the induced phase, whether it is nematic, smectic or columnar, is essentially indistinguishable from phases formed by pure liquid crystals. The orientational and translational order appear not to differ. Other physical properties, though, such as the electrical

conductivity, viscosity and colour of the mixtures may vary enormously. For this reason chemically-induced liquid crystal phases have been studied in great detail.

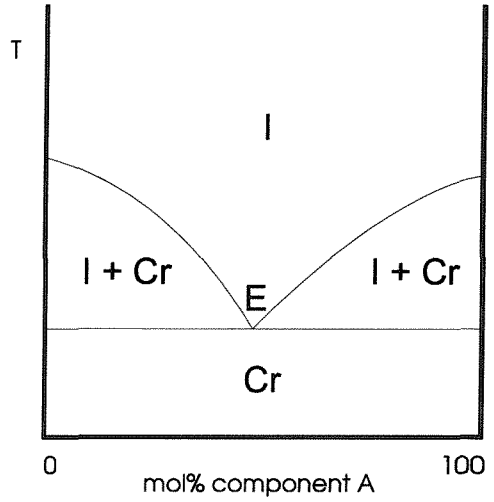

Figure 2.6 : A mixture of two non-mesogenic materials, showing the eutectic point, E.

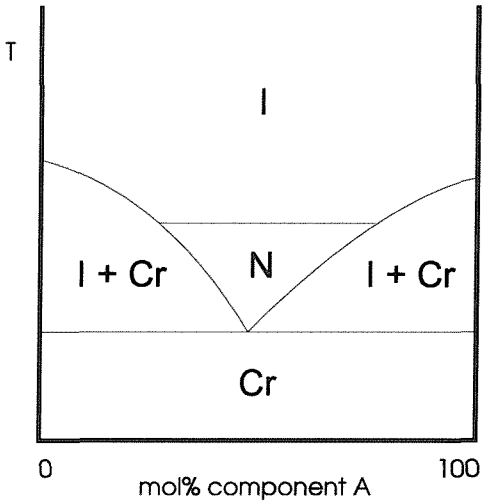

Figure 2.7 : A hidden mesophase revealed due to the reduction in melting point for a mixture of two non-mesogenic materials

In recent years there has been considerable interest in liquid crystal phase induction in mixtures of non-mesogens or materials with small mesophase ranges. Much of this has been directed towards the study of discotic materials, particularly large, electron-rich molecules. One of the first examples being the so-called charge transfer induced phases formed by highly conjugated, electron-rich multiyne aromatics and the electron deficient, high electron affinity, trinitrofluorenone, (TNF), [10] as shown in figure 2.8.

Formation of these charge-transfer induced mesophases by discotic non-mesogens is by no means unique, for there are examples of larger disc [11] and core [12]

sizes, the induction of chiral discotic phases [13] and even the induction of phases in polymeric systems [14,15]. An important feature involving these charge transfer induced phases of discotic systems is the novel structure of the nematic phase that is said to be formed. The nematic columnar (N_C) phase, as discussed in the Introduction (§1.6.2), seems to be formed exclusively by these charge transfer induced systems [10]. The phase is formed from columns of alternating electron donor and acceptor molecules, as shown in figure 2.9. It should be noted that the characteristics of this phase are identical to the nematic discotic (N_D) phase apart from the X-ray diffraction pattern, and indeed this is the only way the phase can be conclusively assigned, as the textures are similar, although the entropy change at the clearing point is often larger for the nematic columnar phase.

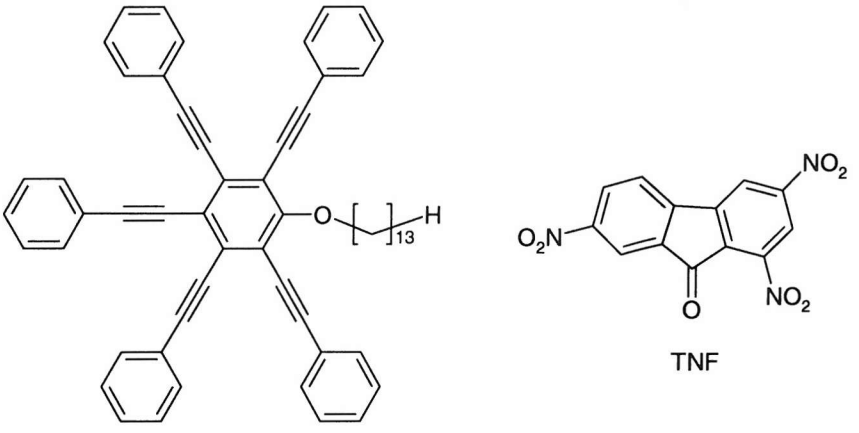

Figure 2.8 : Structures of pentakis(phenylethynyl)phenyloxytridecane and 2,4,7-trinitrofluorenone (TNF).

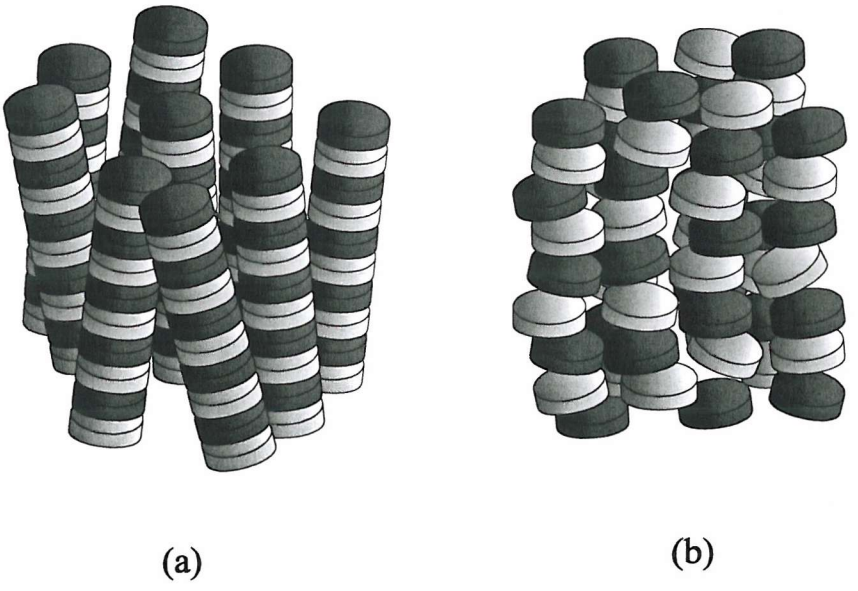

Figure 2.9 : Two different representations of a nematic columnar phase. The light discs represent the TNF, the dark discs represent the electron-rich disc-like molecule.

These large, electron-rich molecules are important not only because of their interesting behaviour with electron acceptors, such as TNF, but also because when substituted with a long alkyl chain or linked via a flexible spacer they have been reported to exhibit a biaxial nematic phase [16,17]. The nature of biaxial nematogens and discotic dimers will be dealt with elsewhere in this Thesis (see Chapters 5 & 6). It should be noted, also, that these large electron-rich discotic molecules can, and do, form mesophases without the need for chemical induction. Substitution of flexible alkyl chains in the para-position of the peripheral phenyl rings yield materials that form a nematic phase, as shown below.

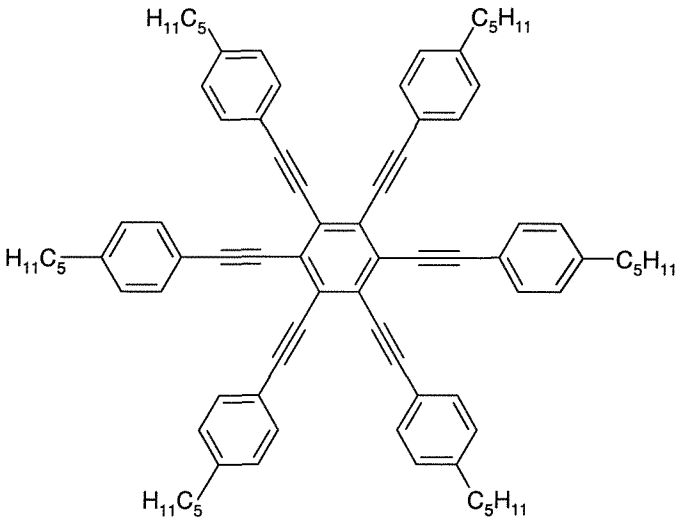

It has been shown that depending on the relative amounts of donor and acceptor compounds in the binary mixtures of some [1,2,3,5,6-pentakis(phenylethynyl)phenyl-4-oxy]alkanes more ordered discotic phases, such as the discotic hexagonal ordered (Col_{ho}) phase can be formed, and also it appears that the discotic hexagonal ordered phase is extinguished for long chain lengths [10]. To fully investigate the phase behaviour of these materials when mixed with TNF, and to investigate this assertion that the D_{ho} phase will persist for only short chain lengths, the homologous series shown in figure 2.10 was synthesised and the phase behaviour studied. It should be noted that two members of the series, the C9 and C13 homologues, have been prepared previously [10].

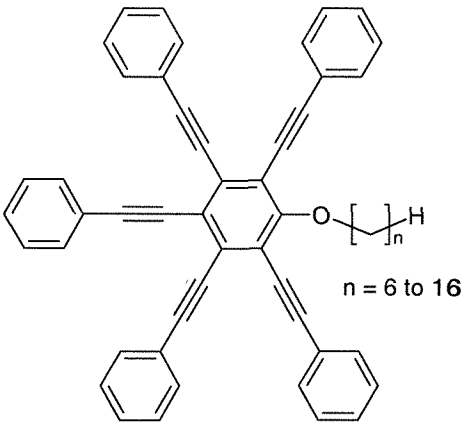

Figure 2.10 : Structure of the materials synthesised and studied in this Chapter.

2.2. Results and Discussion

2.2.1 Phase Behaviour of C6SD and TNF

The phase behaviour of a mixture of 1,2,3,5,6-pentakis(phenylethynyl)phenyl-4-oxyhexane (C6SD) (**2a**) (refer to Chapter 7 for numbering of compounds prepared) and 2,4,7-trinitrofluorenone (TNF) is shown in figure 2.11 and the transitional properties of an equimolar mixture are given in table 2.2. The behaviour observed upon both heating and cooling are presented on the same diagram for comparison, and this convention is used for all subsequent phase diagrams. Neither of the materials exhibit liquid crystalline phases when pure, with the melting point of TNF being 176°C and the melting point of pure C6SD being given in table 2.1. The thermodynamic properties of this, and subsequent phase diagrams presented in this Chapter were determined using a combination of optical microscopy and differential scanning calorimetry (DSC). Mixtures containing a known concentration of TNF, and contact preparations, were used to determine the nature of the phases formed and their transitional behaviour.

As can be seen, for mixtures of less than *ca.* 25mol% or greater than *ca.* 65mol% TNF there is no mesophase formed, however for mixtures with concentrations of TNF between these values one enantiotropic phase is induced with the mesophase range being on average, for the median concentrations, about 65°C. From optical microscopy observations this phase has been assigned as a hexagonal columnar

phase due to the characteristic growth of flower-like hexagons separating from the isotropic liquid, which slowly merge, upon further cooling, into birefringent and homeotropic domains. This is characteristic of the ordered hexagonal columnar phase (Col_{ho}), and has been confirmed by X-ray diffraction [10]. An example of the texture is shown in figure 2.12.

Material	Mpt /°C
C6SD	219
C8SD	125
C9SD	128
C10SD	118
C11SD	111
C12SD	108
C13SD	109
C14SD	98
C15SD	95
C16SD	91

Table 2.1 : The melting points of the pure materials

It can also be seen that upon cooling there appears to be a significant amount of supercooling, with the mesophase emerging, on average, around 7°C lower than the clearing point. Also, the mixtures crystallise on average 30°C lower than the melting points over the whole of the induced phase region. More significantly, though, is the appearance of a second, monotropic mesophase. This is observed for mixtures containing between about 48 and 60mol% TNF. The nature of this phase remains unknown and we refer to it as the Col_I phase, although the nature of this will be discussed later in this Chapter. The optical texture of this phase is similar to the Col_{ho} phase but more sanded in appearance, and is shown in figure 2.13. Although we were unable to obtain an entropy change at the Col_{ho} – I transition, the entropy change at the Col_{ho} – Col_I transition is only weakly first order, being 0.25, whereas a typical Col_{ho} – I transitional entropy is ~1.5, which suggests that the difference in order of these two phases is only small – again this will be discussed later in the Chapter.

	Heating		Cooling	
	T /°C	ΔS/R	T /°C	ΔS/R
Cr	•	•	•	•
	160.5	2.26	133.3	1.04
Col_1	•	•	•	•
			153.7	0.25
Col_{ho}	•	•	•	•
	213.0	*	208.9	*
I	•	•	•	•

* transitional entropy unobtainable

Table 2.2 : The transitional properties of an equimolar mixture of C6SD and TNF.

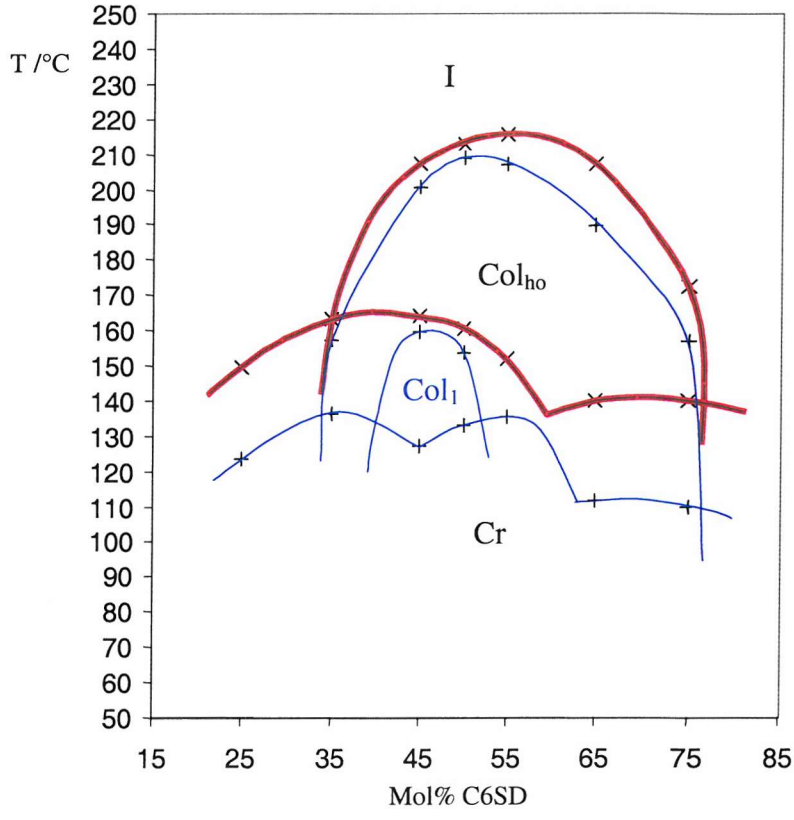

Figure 2.11 : Phase diagram for a mixture of C6SD and TNF. Red lines indicate heating, blue lines indicate cooling.

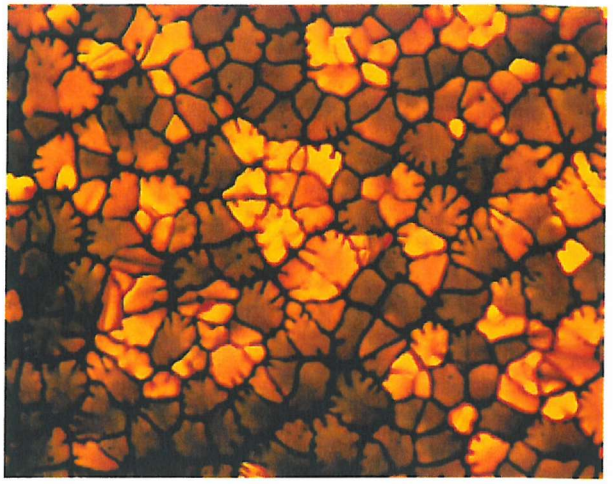

Figure 2.12 : The optical texture exhibited by the Col_{ho} phase of an equimolar mixture of C6SD and TNF on cooling at 190°C (magnification x100).

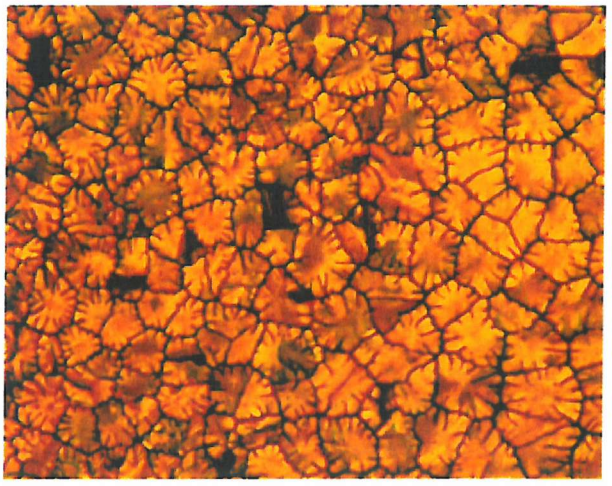

Figure 2.13 : The optical texture exhibited by the Col_{1} phase of an equimolar mixture of C6SD and TNF on cooling at 140°C (magnification x100).

2.2.2 Phase Behaviour of C8SD and TNF

The phase behaviour of 1,2,3,5,6-pentakis(phenylethynyl)phenyl-4-oxyoctane (C8SD) (**2b**) and TNF is shown in figure 2.14, and the transition properties for an equimolar mixture are given in table 2.3. Pure C8SD is not liquid crystalline and, not surprisingly, a mesophase is induced when mixed with TNF in concentrations of between around 25 and 75mol% TNF. The mesophase was identified as an ordered hexagonal columnar phase from the texture observed under a polarising microscope, with flower-like hexagons separating from the isotropic liquid over a range of about 5°C. The clearing point of an equimolar mixture is somewhat lower than with the C6 homologue, in this case occurring at 182°C, whereas the

	Heating		Cooling	
	T /°C	ΔS/R	T /°C	ΔS/R
Cr	•	•	•	•
	119.3	3.88	91.8	1.48
Col_I	•	•	•	•
			110.4	0.51
Col_{ho}	•	•	•	•
	181.7	1.54	163.2	0.85
I	•	•	•	•

Table 2.3 : The transitional properties of an equimolar mixture of C8SD and TNF.

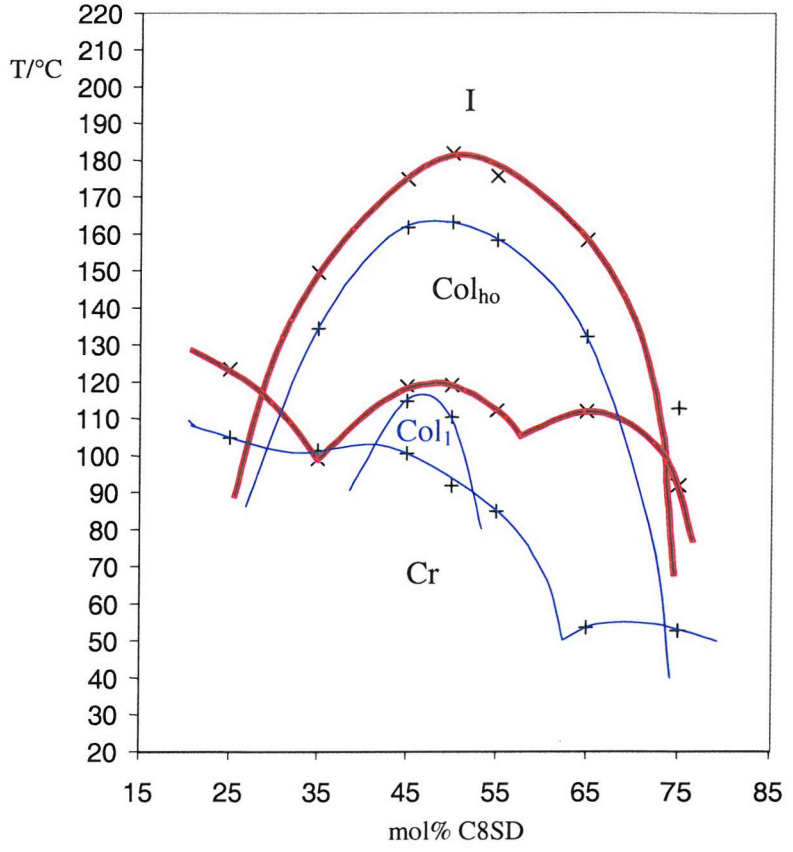

Figure 2.14 : Phase diagram for a mixture of C8SD and TNF. Red lines indicate heating, blue lines indicate cooling.

average phase range, for intermediate TNF concentrations, remains similar at about 65°C as does the entropy change, ΔS/R of 1.54, being typical for this type of transition.

Once more there is considerable supercooling, especially for mixtures containing lower concentrations of TNF; this is particularly strong for mixtures containing around 35mol% TNF, with crystallisation occurring about 60°C below the melting point. Also, the transition from the isotropic liquid to the mesophase occurs about 10°C lower on cooling than the corresponding transition on heating. As with the C6 homologue there is a transition to a monotropic columnar phase for concentrations of TNF between *ca.* 48 and 60mol%. The optical texture of this phase is identical to that seen for C6SD and is therefore assigned as the Col_I phase.

2.2.3 Phase Behaviour of C9SD and TNF

The phase behaviour of 1,2,3,5,6-pentakis(phenylethynyl)phenyl-4-oxynonane (C9SD) (**2c**) and TNF is shown in figure 2.15, and the transition properties of an equimolar mixture listed in table 2.4. C9SD exhibits induced mesophase behaviour for mixtures with concentrations of TNF between *ca.* 25 and 70mol%. Unlike the hexyl and octyl homologues it can be seen that, upon heating, at higher concentrations of TNF (around 55 to 70mol%) there is the emergence of a columnar nematic phase (N_C). This phase was identified as a nematic phase by the characteristic schlieren texture observed under the polarising microscope, shown in figure 2.16. The phase is highly mobile and flashes when subjected to mechanical stress. This phase has been shown by Praefcke *et al.* to be columnar in nature by X-ray diffraction [10]. ΔS/R for this columnar nematic phase to isotropic transition is 0.21 which, although being lower than for most calamitic nematic to isotopic transitions, is higher than for discotic molecules of a similar structure to those forming a nematic phases (N_D) [18]. Also, the mesophase range is beginning to decrease when compared to the C6 and C8 homologues, with the average temperature range over intermediate TNF concentrations being about 55°C.

	Heating		Cooling	
	T /°C	ΔS/R	T /°C	ΔS/R
Cr	•	•	•	•
	119.2	3.39	62.2	2.07
Col_1	•	•	•	•
			99.4	0.42
Col_{ho}	•	•	•	•
	159.1	1.14	135.0	0.28
N	•	•	•	•
			154.2	*
I	•	•	•	•

* transitional entropy unobtainable

Table 2.4 : The transitional properties of an equimolar mixture of C9SD and TNF.

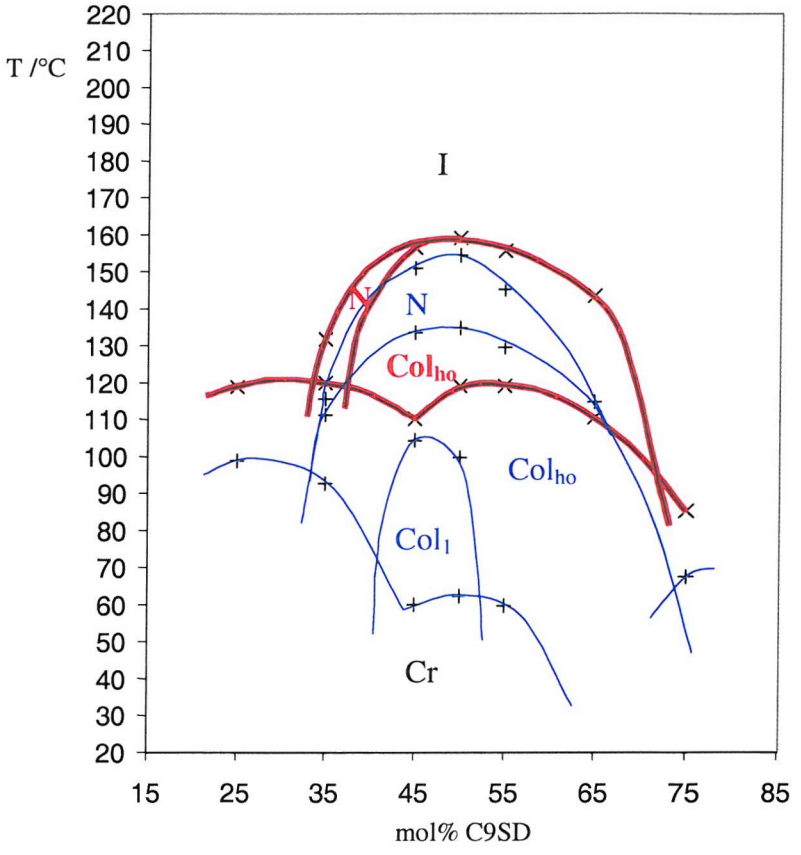

Figure 2.11 : Phase diagram for a mixture of C9SD and TNF. Red lines indicate heating, blue lines indicate cooling.

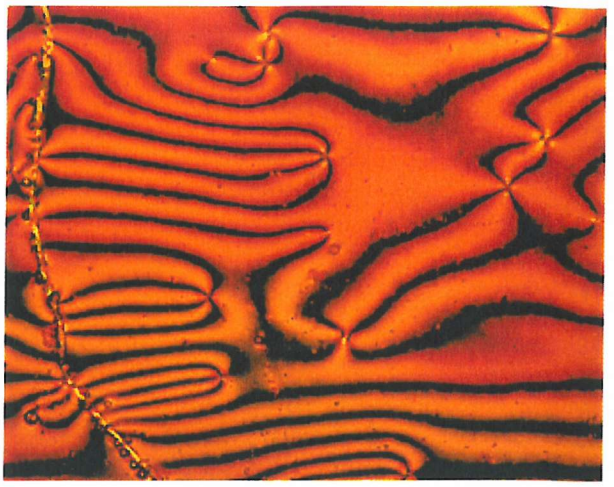

Figure 2.16 : The optical texture exhibited by the nematic phase of an equimolar mixture of C9SD and TNF on cooling at 150°C (magnification x100).

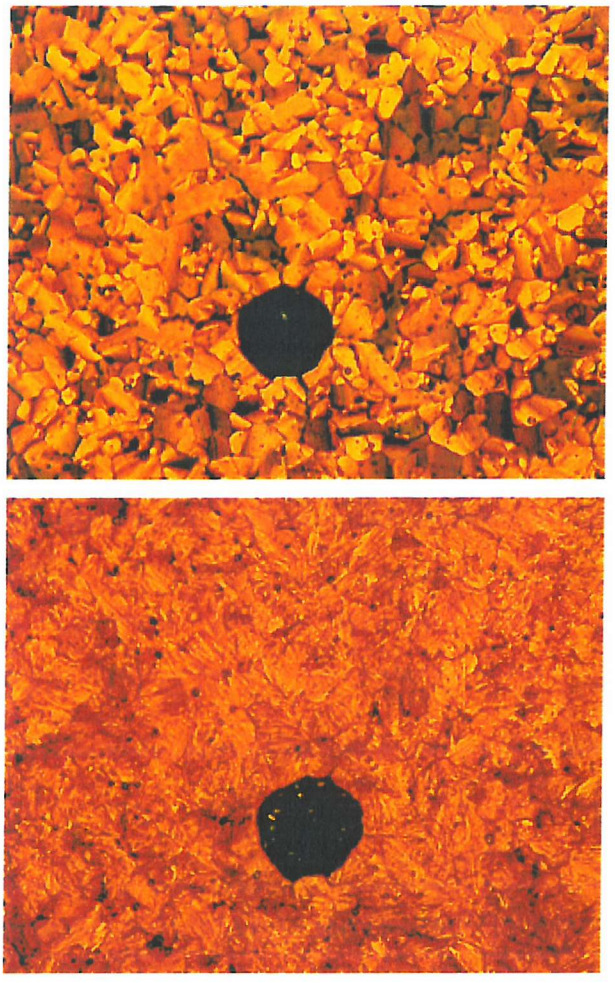

Figure 2.17 : The optical textures exhibited by the Col_{ho} phase (top) and the Col_1 phase of an equimolar mixture of C6SD and TNF on cooling at 120°C and 90°C (mag x100).

When considering the data obtained from the DSC traces at lower temperatures and concentrations of TNF, only the phase identified as Col_{ho} is seen on heating, with a direct transition from this phase to the isotropic liquid occurring for concentrations of between *ca.* 25 to 55mol% TNF. However, upon cooling, over the concentration range of between 35 and 60mol% TNF, there is first a transition from the isotropic liquid to the nematic columnar phase, and then from this to the Col_{ho} phase. This surprising behaviour can be explained when the mixtures are viewed under the polarising microscope. For mixtures of about 45 to 55mol% TNF the transition from the Col_{ho} phase to the isotropic phase appears to be accompanied by the transition from the Col_{ho} – N_C and subsequently to the isotropic phase over a very small temperature range of about 1°C. When this transition is observed by DSC it is not surprising that the two peaks for these transitions will coalesce, because the Col_{ho} phase transition occurs over a range of about 4 or 5°C. Even slowing the scan rate fails to separate the two transitions. When cooling these mixtures, however, there is the initial formation of the highly mobile N_C phase and then this slowly undergoes a transition into the highly ordered Col_{ho} phase. The temperature range over which these transitions occur is large enough for the two peaks to be resolved on the DSC trace thereby giving rise to these unusual features on heating and cooling.

Once more it is apparent that there is a large degree of supercooling, leading not only to the reduction in the N_C – Col_{ho} transition temperature, but also to the reduction of the crystallisation point. This reveals the monotropic Col_1 phase again for mixtures containing between *ca.* 48 to 60mol% TNF. The texture of this phase is different to that seen for the C6 and C8 homologues, being a sort of diffuse focal conic, as the preceeding Col_{ho} phase this time exhibits a focal conic texture more typical of a Col_{hd} mesophase [19], both textures (Col_{ho} and Col_1) are shown in figure 16. There again appears to be a large amount of supercooling for mixtures containing about 35mol% TNF, with the Col_{ho} phase persisting to below 40°C.

2.2.4 Phase Behaviour of C10SD and TNF

The phase behaviour of 1,2,3,5,6-pentakis(phenylethynyl)phenyl-4-oxydecane (C10SD) (**2d**) and TNF is shown in figure 2.18, and the transition properties of an equimolar mixture given in table 2.5. It can be seen that for mixtures with TNF

	Heating		Cooling	
	T /°C	ΔS/R	T /°C	ΔS/R
Cr	•	•	•	•
	128.5	4.94	71.9	3.26
Col_1	•	•	•	•
			91.4	0.39
Col_{ho}	•	•	•	•
			126.9	0.18
N	•	•	•	•
	159.9	0.27	157.0	0.31
I	•	•	•	•

Table 2.5 : The transitional properties of an equimolar mixture of C10SD and TNF.

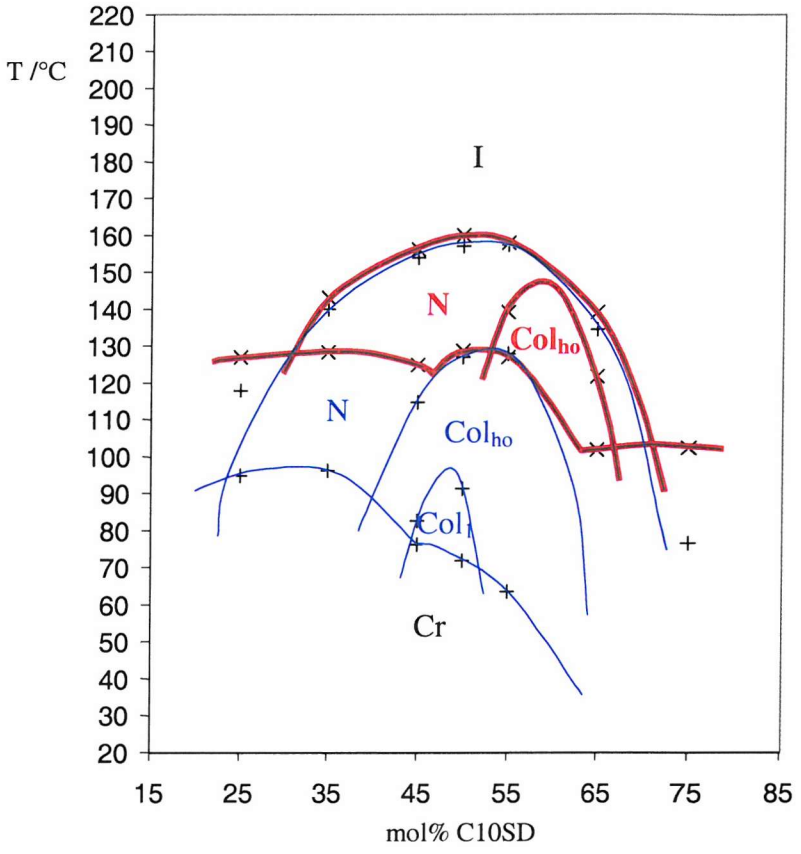

Figure 2.18 : Phase diagram for a mixture of C10SD and TNF. Red lines indicate heating, blue lines indicate cooling.

concentrations of between about 25 and 70mol% two mesophases are formed on heating. As with the nonyl homologue, these are considered to be the columnar nematic phase and the ordered hexagonal columnar phase, with the N_C phase now stable over the majority of the induced phase region and the Col_{ho} phase occurring only for TNF concentrations of between *ca.* 33 and 47mol% and below a temperature of about 145°C. The mesophase range is also beginning to decrease significantly with the average phase range now being only about 40°C. Apart from the melting transition, the Col_{ho} – N_C and the N_C – I transitions are both weakly first order, with the transitional entropy $\Delta S/R$ being 0.21 and 0.31, respectively.

Upon cooling, it can be seen that there is still significant supercooling, especially for mixtures with TNF concentrations of around 35mol% with the material not crystallising even at 40°C. Because of this supercooling the extent to which the Col_{ho} phase exists is increased, occurring for TNF concentrations of between *ca.* 35 and 60mol%. Again there is the formation of the Col_1 phase, although due to the smaller region when the Col_{ho} phase is stable, this phase now exists over a slightly smaller TNF concentration range, i.e. between about 47 and 55mol%.

Again, because of the highly ordered nature of the Col_{ho} phase there are regions of the phase diagram that exhibit significantly different phase behaviour on heating and cooling. For example, for mixtures containing about 30mol% TNF the nematic range, on heating, is only about 4°C, whereas on cooling it is approximately 30°C. The slow rearrangement of the nematic phase into the highly ordered Col_{ho} phase that may account for the unusual behaviour seen for the C9 homologue would also explain the behaviour seen here.

2.2.5 Phase Behaviour of C11SD and TNF

The phase behaviour of 1,2,3,5,6-pentakis(phenylethynyl)phenyl-4-oxyundecane (C11SD) (**2e**) and TNF is shown in figure 2.19, and the transition properties of an equimolar mixture listed in table 2.6. As can be seen, for concentrations of TNF between about 25 and 70mol% there is still the induction of two mesophases, the N_C phase and the Col_{ho} phase, although the latter phase is now almost completely extinguished, occurring only when the TNF concentration is between

	Heating		Cooling	
	T /°C	ΔS/R	T /°C	ΔS/R
Cr	•	•	•	•
	127.0	5.95	76.2	2.03
Col_{ho}	•	•	•	•
			82.6	1.92
N	•	•	•	•
	154.9	0.29	151.8	0.32
I	•	•	•	•

Table 2.6 : The transitional properties of an equimolar mixture of C11SD and TNF.

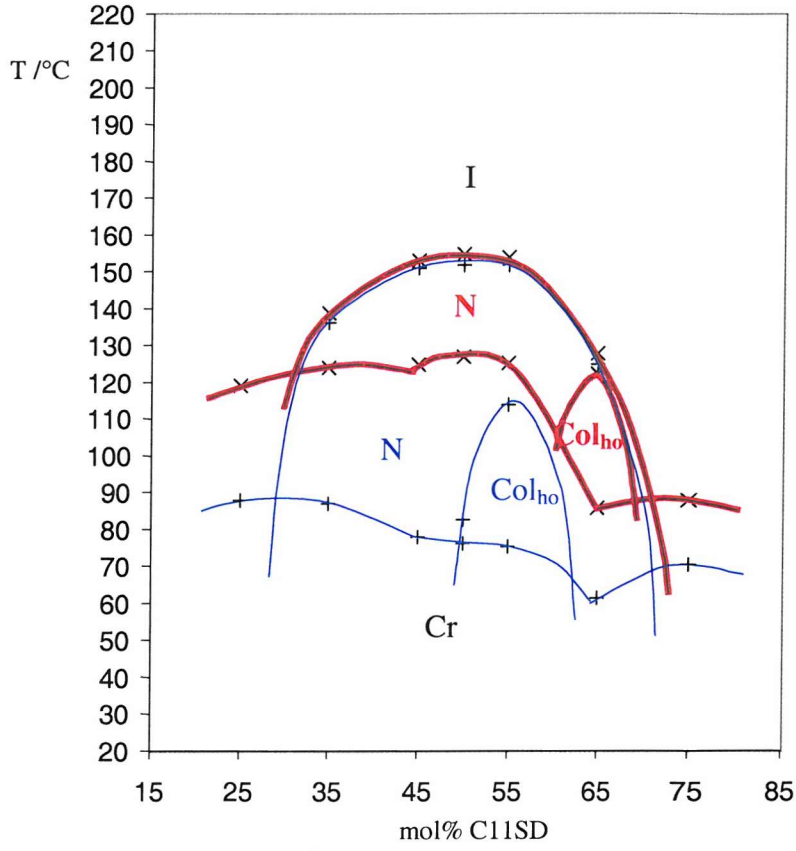

Figure 2.19 : Phase diagram for a mixture of C11SD and TNF. Red lines indicate heating, blue lines indicate cooling.

30% and 40mol%, with the N_C phase dominating the region of mesophase stability. In addition the average mesophase range continues to fall, now being less than 30°C.

Upon cooling we still see a large degree of supercooling, for some mixtures this is almost 50°C, however we do not see the extensive supercooling found for mixtures containing around 35mol% TNF as for the previous homologues. Also, it should be noted that the monotropic Col_I phase is no longer formed as found for the earlier members of the series. It would appear that this phase only occurs when cooled from the Col_{ho} phase and then for only certain concentrations of TNF. For this C11 homologue the Col_{ho} phase is not stable for TNF concentrations higher than about 50mol% and therefore the Col_I phase is unable to form.

2.2.6 Phase Behaviour of C12SD and TNF

The phase behaviour of 1,2,3,5,6-pentakis(phenylethynyl)phenyl-4-oxydodecane (C12SD) (**2f**) and TNF is shown in figure 2.20, and the transition properties of an equimolar mixture given in table 2.7. It is readily apparent from the phase diagram that there is now only one mesophase present over the whole of the thermodynamically stable induced region, from about 25mol% TNF to about 70mol% TNF. This is a nematic phase, identified by the characteristic schlieren texture observed under the polarising microscope. The entropy change at the nematic – isotropic transition for an equimolar mixture, being 0.23, is approximately equal to the entropy change for the N_C – I transition found for the nonyl, decyl and undecyl homologues and so it is sensible to assume that this nematic phase is of the columnar type, and not a conventional N phase, however X-ray diffraction would be needed to definitely confirm this assignment. The average phase range over intermediate TNF concentrations is similar to the C11 homologue, being around 30°C, whereas the clearing temperature for the equimolar mixture is lower at 140°C .

There is still some degree of supercooling, however this is not as great as the previous examples with the mixtures crystallising, on average about 35°C lower than the corresponding melting points. Also, this supercooling, like the C11 homologue, does not reveal any hidden monotropic phases, which again seems to

suggest that the Col_1 phase will only form if cooled from a preceding Col_{ho} phase, although this does not necessarily offer conclusive proof, as will become apparent.

	Heating		Cooling	
	T /°C	ΔS/R	T /°C	ΔS/R
Cr	•	•	•	•
	113.2	4.54	81.2	1.95
N	•	•	•	•
	140.5	0.23	133.8	0.25
I	•	•	•	•

Table 2.7 : The transitional properties of an equimolar mixture of C12SD and TNF.

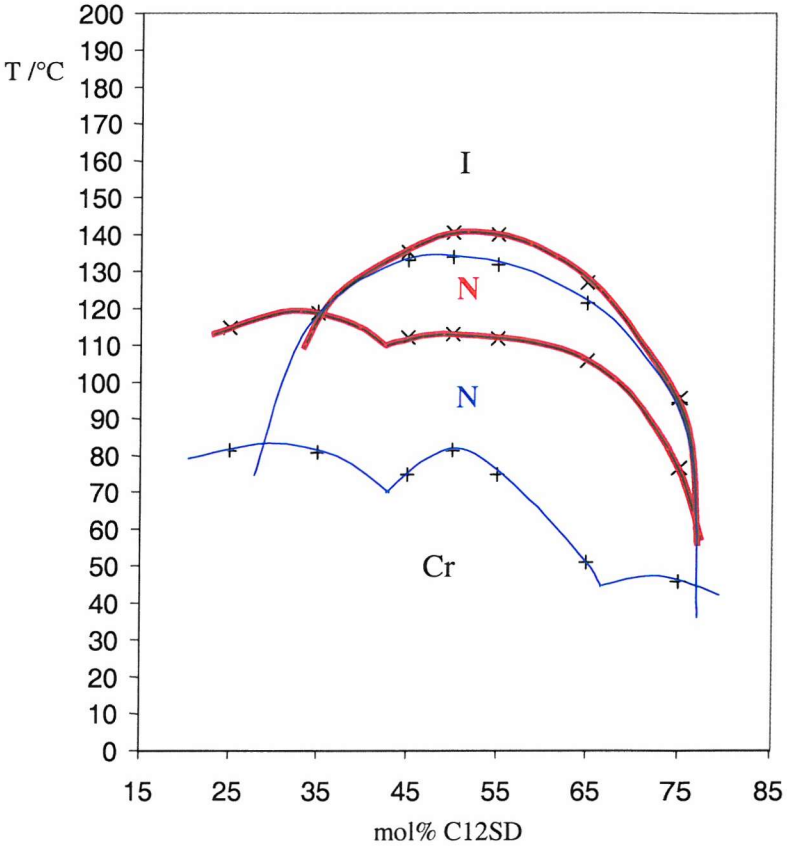

Figure 2.20 : Phase diagram for a mixture of C12SD and TNF. Red lines indicate heating, blue lines indicate cooling.

2.2.7 Phase behaviour of C13SD and TNF

The phase behaviour of 1,2,3,5,6-pentakis(phenylethynyl)phenyl-4-oxytridecane (C13SD) (**2g**) and TNF is shown in figure 2.21, and the transition properties of an equimolar mixture given in table 2.8. It can be seen from the phase diagram that over a TNF concentration of 25 to 65mol% a columnar nematic phase is formed. The average phase range for intermediate TNF concentrations is again about 30°C, however the clearing point of the equimolar mixture at 146°C is higher than for the C12 homologue. What is most apparent though, is that for TNF concentrations of about 55mol% and temperatures of less than 120°C another phase is formed. This appears on the DSC trace as a strong first order transition from the crystal to this phase, which we term here the Col_2 phase, and then a weak first order transition from this phase to the columnar nematic phase. When these transitions are viewed under the polarising microscope the crystal phase appears to brighten first, and then the texture changes to a schlieren texture indicative of the N_C phase.

When cooled, there is the first transition from the isotropic to the columnar nematic phase and then, for TNF concentrations of between *ca.* 45 and 57mol%, a transition to the Col_2 phase, and subsequently crystallisation. The entropy changes for the Col_2 – N_C phase transition and the Col_2 – Cr phase transition are of a similar size, being 1.13 and 1.89 respectively, for the equimolar mixture. When viewed under the microscope, a schlieren texture is first seen for the N_C phase and then the phase appears to crystallise at the N_C – Col_2 phase transition, but this phase then appears to crystallise again at the Col_2 – Cr phase transition, although the growth of this texture occurs more slowly than the previous one. The course of these transitions can be seen in figure 2.22. With this evidence from the optical microscopy it is tempting to suggest that the Col_2 phase is in fact an alternate crystal phase, however this will be discussed later in this Chapter.

Once again there is a large degree of supercooling, especially for mixtures containing around 35mol% TNF.

	Heating		Cooling	
	T /°C	ΔS/R	T /°C	ΔS/R
Cr	•	•	•	•
	114.7	5.44	89.8	1.89
Col_2	•	•	•	•
			98.9	1.13
N	•	•	•	•
	146.0	0.28	142.6	0.26
I	•	•	•	•

Table 2.8 : The transitional properties of an equimolar mixture of C13SD and TNF.

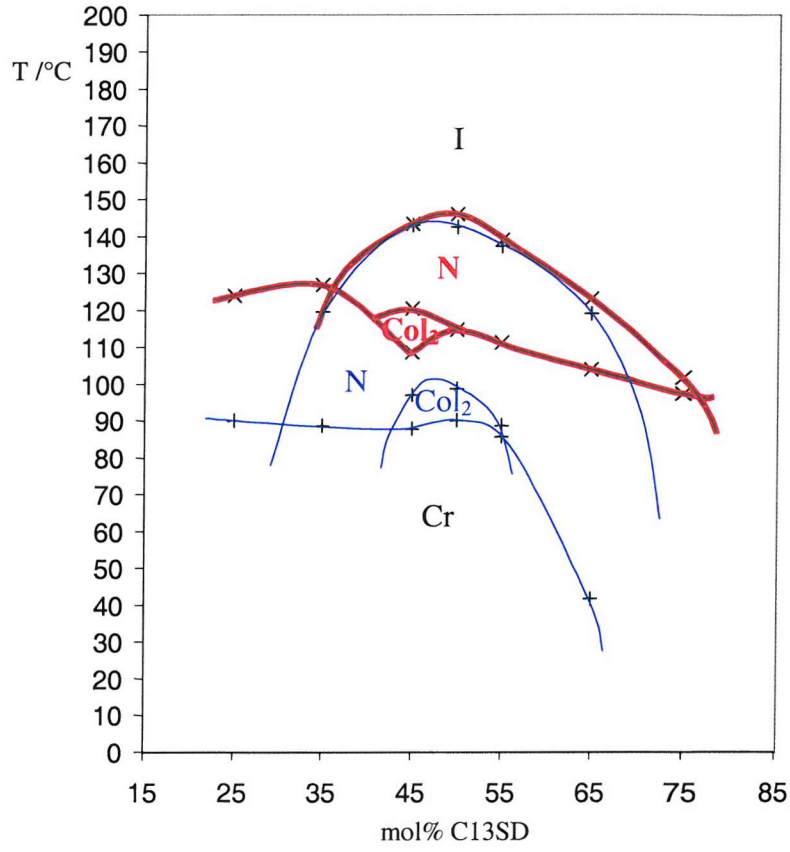

Figure 2.21 : Phase diagram for a mixture of C13SD and TNF. Heavy lines indicate heating, light lines indicate cooling.

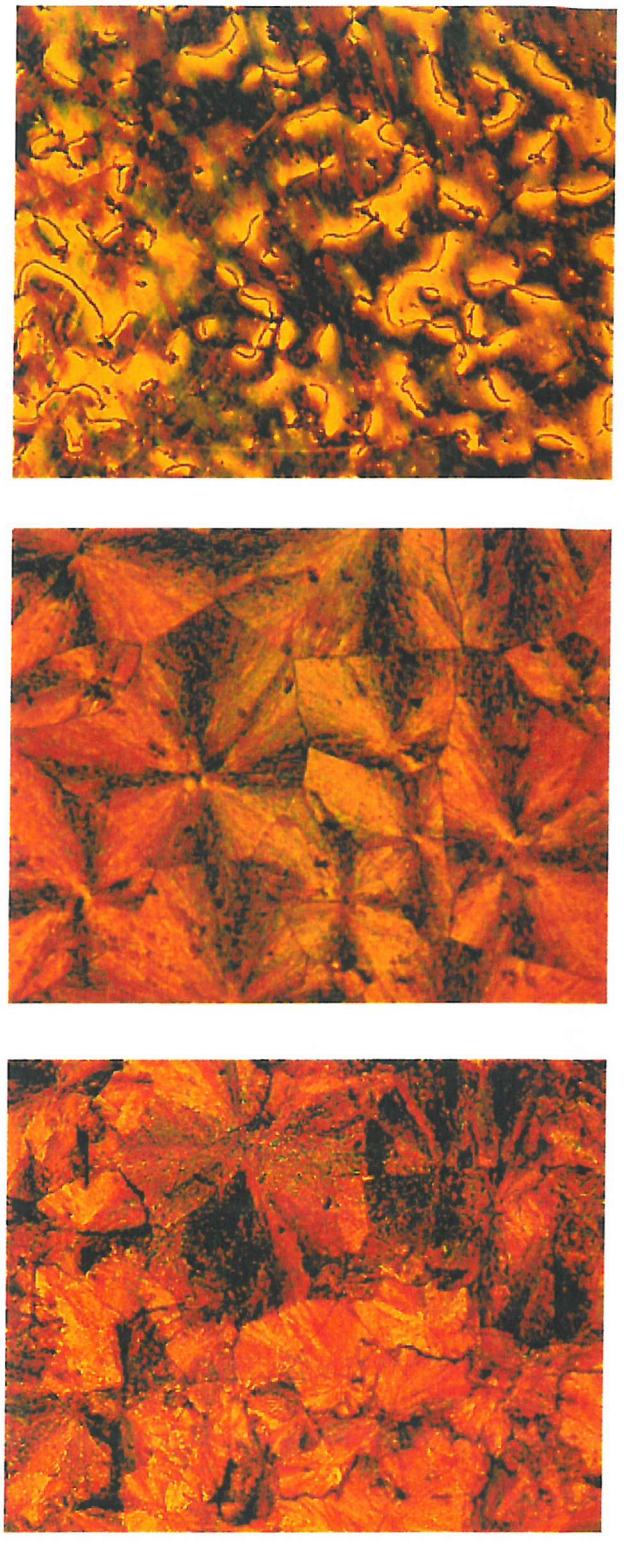

Figure 2.22 : The optical textures exhibited by the nematic phase (top) at 130°C the Col_2 phase (middle) at 95°C and the crystal phase (bottom) at 70°C of an equimolar mixture of C13SD and TNF on cooling (magnification x100).

2.2.8 Phase Behaviour of C14SD and TNF

The phase behaviour of 1,2,3,5,6-pentakis(phenylethynyl)phenyl-4-oxytetradecane (C14SD) (**2h**) and TNF is shown in figure 2.23, and the transition properties of an equimolar mixture given in table 2.9. As was the case for the C13 homologue, it can be seen that, upon heating, for mixtures with between *ca.* 25 and 65mol% TNF there is the induction of a columnar nematic phase, as well as the formation of the Col_2 phase for TNF concentrations of between about 45 and 57mol%, and temperatures below 122°C. The optical textures observed on heating are the same as those for C13SD, with the crystal phase appearing to brighten, and then a transition to a schlieren texture. For the equimolar mixture the entropy change, $\Delta S/R$, at the Col_2 – Cr phase transition is 2.83, whilst at the Col_2 – N_C phase transition it is extremely weak, being only 0.12.

The behaviour observed when cooling the mixtures is very similar to that observed on cooling mixtures of C13SD and TNF, there being a transition to the N_C phase from the isotropic liquid, and then for mixtures of *ca.* 45 to 57mol% TNF a transition to the Col_2 phase and then subsequent crystallisation. The optical textures seen on cooling an equimolar mixture are the same as those shown in figure 2.22. Also, like the C13 homologue, $\Delta S/R$ for the two transitions, N_C – Col_2 and Cr –Col_2, are different to those seen for the same transition on heating, being 1.25 and 1.76 respectively. It can also be seen that the extent to which the phases supercool is beginning to diminish slightly, although once again for mixtures containing around 35mol% TNF there is still quite extensive supercooling when compared to that seen for other mixture compositions.

2.2.9 Phase Behaviour of C15SD and TNF

The phase behaviour of 1,2,3,5,6-pentakis(phenylethynyl)phenyl-4-oxypentadecane (C15SD) (**2i**) and TNF is shown in figure 2.24, and the transition properties of an equimolar mixture listed in table 2.10. It is apparent that the phase behaviour for mixtures of this material upon heating is essentially identical to both the C13 and C14 homologues, with the presence of a columnar nematic phase for TNF concentrations of between about 30 and 65mol%. There is also the appearance of the Col_2 phase for mixtures containing about 45 to 57mol%

	Heating		Cooling	
	T /°C	ΔS/R	T /°C	ΔS/R
Cr	•	•	•	•
	111.2	2.83	87.0	1.76
Col_2	•	•	•	•
	119.7	0.12	100.5	1.25
N	•	•	•	•
	141.4	0.27	138.3	0.29
I	•	•	•	•

Table 2.9 : The transitional properties of an equimolar mixture of C14SD and TNF.

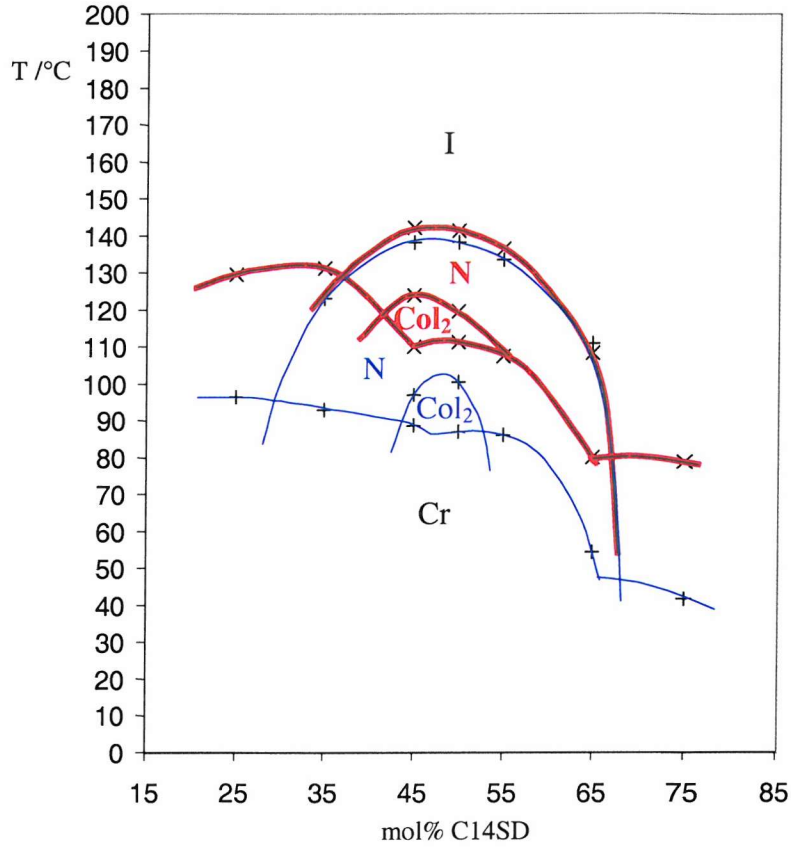

Figure 2.23 : Phase diagram for a mixture of C14SD and TNF. Heavy lines indicate heating, light lines indicate cooling.

	Heating		Cooling	
	T /°C	ΔS/R	T /°C	ΔS/R
Cr	•	•	•	•
	110.6	3.00	90.7	2.02
Col_2	•	•	•	•
	117.5	0.04	102.6	1.16
N	•	•	•	•
	132.0	0.17	129.6	0.27
I	•	•	•	•

Table 2.10 : The transitional properties of an equimolar mixture of C15SD and TNF.

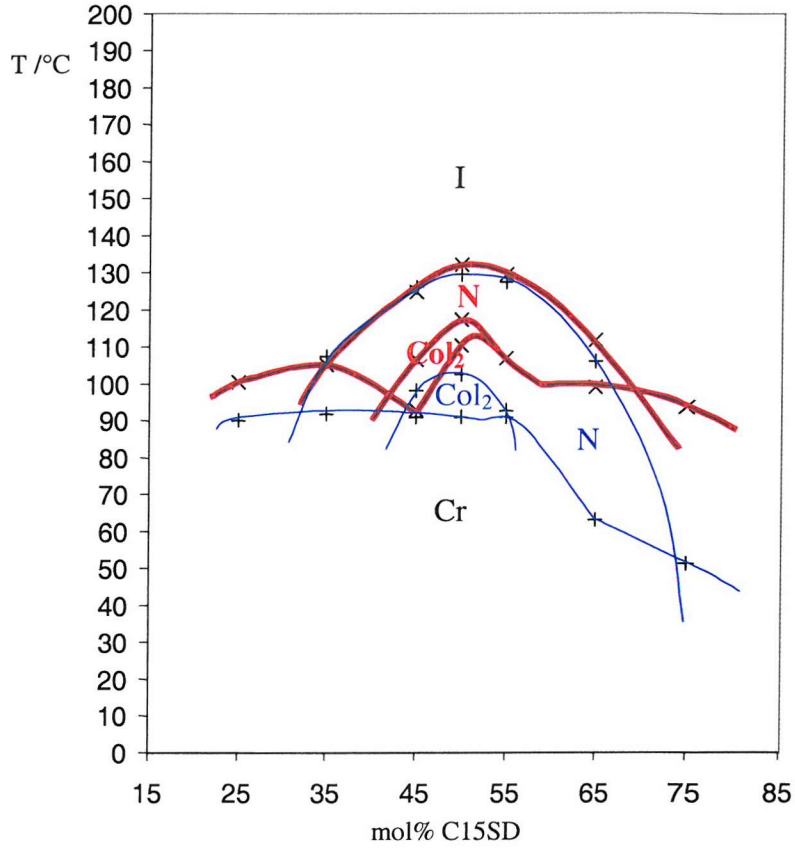

Figure 2.24 : Phase diagram for a mixture of C15SD and TNF. Heavy lines indicate heating, light lines indicate cooling.

TNF and for temperatures less than about 119°C. The optical textures of these phases are similar to those seen for the C13 and C14 homologues as are the entropy changes for an equimolar mixture, with the N_C – I phase transition being typical for this type of transition, the Cr – Col_2 phase transition being strongly first order and the Col_2 – N_C phase transition being only weakly first order. It should also be noted that the average phase range for intermediate concentrations of TNF is now only about 25°C whereas the for the hexyl analogue it was about 65°C and the clearing point for the equimolar mixture has also fallen from 213°C for equimolar C6SD – TNF to 132°C for this material.

Upon cooling we see also the presence of a columnar nematic phase and for lower temperatures and intermediate TNF concentrations, 45 to 57mol%, the existence of the Col_2 phase. The optical textures observed are identical to those shown in figure 2.22 and as was seen for the C13 and C14 homologues the entropy changes for the N_C – Col_2 and Col_2 – Cr phase transitions are significantly different to those found on heating. Also, the extent of supercooling is now considerably diminished when compared to earlier members of the series, although there is still quite a large degree of supercooling for mixtures with low TNF concentrations.

2.2.10 Phase Behaviour of C16SD and TNF

The phase behaviour of 1,2,3,5,6-pentakis(phenylethynyl)phenyl-4-oxyhexadecane (C16SD) (**2j**) and TNF is shown in figure 2.25, and the transition properties of an equimolar mixture given in table 2.11. It can be seen that when mixtures of between *ca.* 30 and 65mol% TNF are heated there is, in general, a transition from the crystal phase to the columnar nematic phase and then a transition to the isotropic liquid. There is, however, as with the previous three homologues, for mixtures containing between around 45 and 57mol% TNF a transition from the crystal phase to the Col_2 phase first, and then a transition to the N_C phase. Once more the optical textures observed are the same as those seen for the C13, C14 and C15 homologues, and the entropy changes at the phase transitions are also of a similar order to the previous examples, $\Delta S/R$ being 0.13 and 3.05, respectively for the N_C – Col_2 and Col_2 – Cr phase transitions, on heating.

	Heating		Cooling	
	T /°C	ΔS/R	T /°C	ΔS/R
Cr	•	•	•	•
	101.2	3.05	87.1	2.45
Col_2	•	•	•	•
	110.9	0.13	101.6	0.90
N	•	•	•	•
	123.8	0.07	117.4	0.12
I	•	•	•	•

Table 2.11 : The transitional properties of an equimolar mixture of C16SD and TNF.

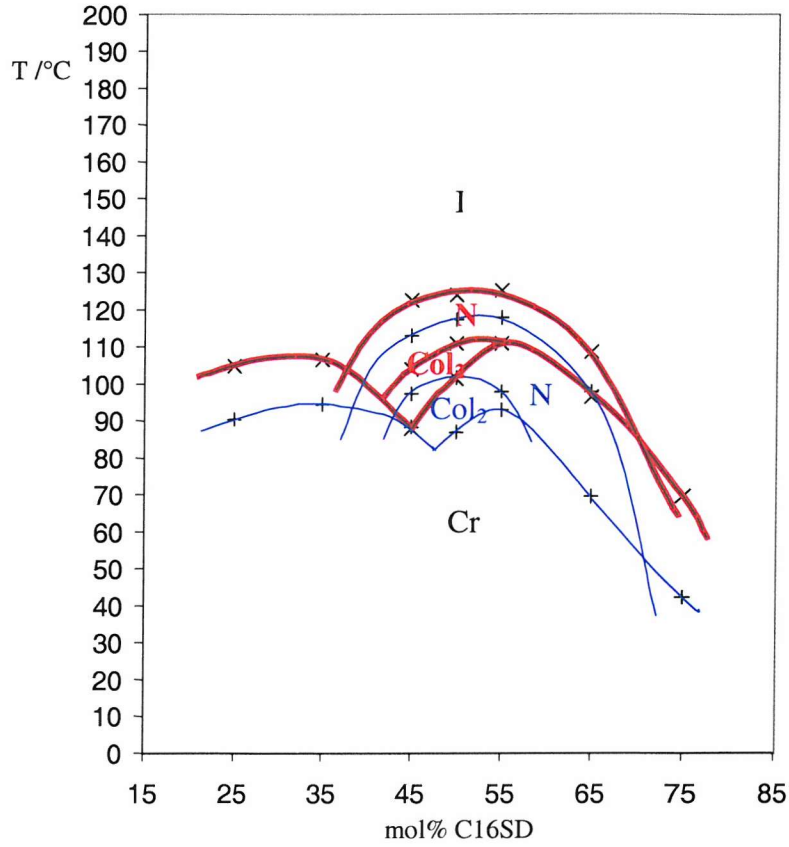

Figure 2.25 : Phase diagram for a mixture of C16SD and TNF. Heavy lines indicate heating, light lines indicate cooling.

The behaviour on cooling is practically identical to that found on heating, however the temperatures at which the transitions occur are now about 5 or 6°C lower. Unlike the previous homologues, where there is significant supercooling resulting in the phase ranges of the cooling scans being much larger than when the mixtures are heated, the C16SD phase range on cooling and heating are almost identical. However, as the alkyl chain length has been increasing as we ascend the homologous series the difference between the two phase ranges, on heating and cooling, has decreased. Therefore, it would seem sensible to suggest that as the chain lengths are increased supercooling becomes less favourable.

2.2.11 Discussion

It is obvious from the previous results that for all members of the series we see a phase induction upon the addition of TNF. The change in colour from a pale yellow to deep red-orange when the TNF is added to the 'Superdisc' materials would seem to indicate that the formation of a charge-transfer complex is the driving force for the mesophase formation. However, work carried out with other inductor molecules, such as octafluoronaphthalene [20], seems to suggest that the complex is stabilised by electrostatic quadrupolar interactions and that the charge-transfer only gives rise to the colour change. Nevertheless, it is obvious that the formation of a complex between the 'Superdisc' materials and TNF, leading to ordered stacks of molecules, gives rise to the liquid-crystal phases observed.

With such a large amount of data being presented for the whole series of compounds it would seem sensible to compare, initially, the behaviour of just the equimolar mixtures for all members of this homologous series, the C*n*SD's. The transition temperatures and phase behaviour for the series are presented graphically in figure 2.26.

Because the behaviour observed for these mixtures, when cooled, is somewhat different to that seen when heating, the heating and cooling data are presented separately.

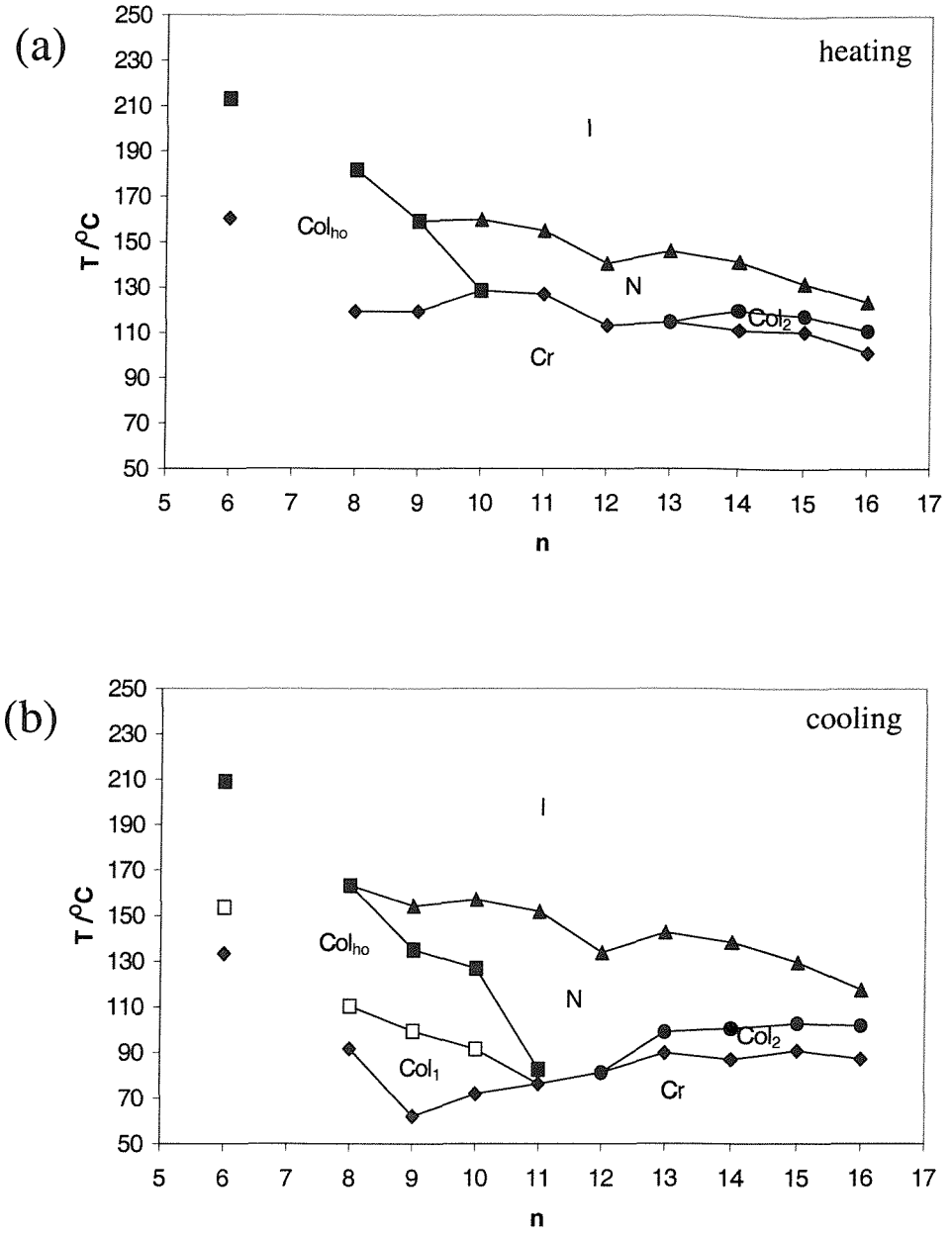

Figure 2.26 : The transitional properties of equimolar mixtures of the C*n*SD's and TNF as the number of carbon atoms, n, in the alkyl chain is changed, (a) heating, (b) cooling. ■ Col_{ho} – I or N, ▲ N – I, ● Col_2 – N, ◆ Cr – Col_{ho}, Col_1, Col_2 or N, □ Col_1 – Col_{ho}.

As can be seen from figure 2.26(a), as the chain length is increased, for the C6, C8 and C9 homologues, there appears to be a steady but rapid decrease in the clearing temperature, however the absence of any information for the heptyl analogue makes it difficult to substantiate this conclusively. For the C10 to C16 homologues there is still a steady decrease in clearing temperatures, apart from the C12 homologue which has a clearing temperature lower than both the C11 and C13

homologues, however it appears the decline in temperature is now somewhat less rapid than with the C6 to C9 homologues. This slowdown in the decline occurs at same point where the phases exhibited by these equimolar mixtures change from the Col_{ho} phase to the N_C phase. This change in the rate of decline may be explained in terms of the molecular packing within the respective phases. Within the Col_{ho} phase there is close side-by-side packing of the columns which make up the hexagonal net, and therefore any protrusion of the alkyl chain outside of the circumference of the rigid discotic core will serve to disrupt this side-by-side packing. The effect the alkyl chain has on the packing of the columns depends on the orientation of the chain with respect to the discotic core. Assuming the chain adopts an all-*trans* conformation there are two possible orientations for the alkyl chain, one, in figure 2.27(a), where the dihedral angle between the aromatic ring and alkyl chain is 90°, and, for figure 2.27(b), where the dihedral angle is 180°, or indeed 0°. As can be seen, when the dihedral angle is 180°, although the chain lies in the plane of the disc there is a large degree of steric hindrance due to the neighbouring phenyl ring. This hindrance causes the ring to twist out of the plane of the disc, by about 35°. (The torsional twist angles of the peripheral phenyl rings were obtained from an energy minimised structure modelled by Tearle [20] and were taken to be 0° for the ring para- to the ether-link, 44° for the rings meta- to the ether-link and 15° for the rings ortho- to the ether-link. These values were set in the model before the steric energy of the structure was minimised using the MM2 force field in the CambrigeSoft Chem3D Pro modelling package). When the dihedral is set to 90° there is no longer any steric hindrance due to the neighbouring phenyl rings and although the alkyl chain now protrudes from the bottom of the disc this would seem to be a more likely conformer. It has been suggested [20], and as will be described in the next Chapter, that, based on deuterium NMR studies of chain ordering, the dihedral angle may actually lie somewhere between 50° and 70°, although this will still result in the chain protruding from the bottom of the disc. Figure 2.27(a) also shows that for chain lengths of 5 carbon atoms or less the chain does not protrude from the circumference of the disc and that chains with 6 and 7 carbon atoms only just extend from the disc.

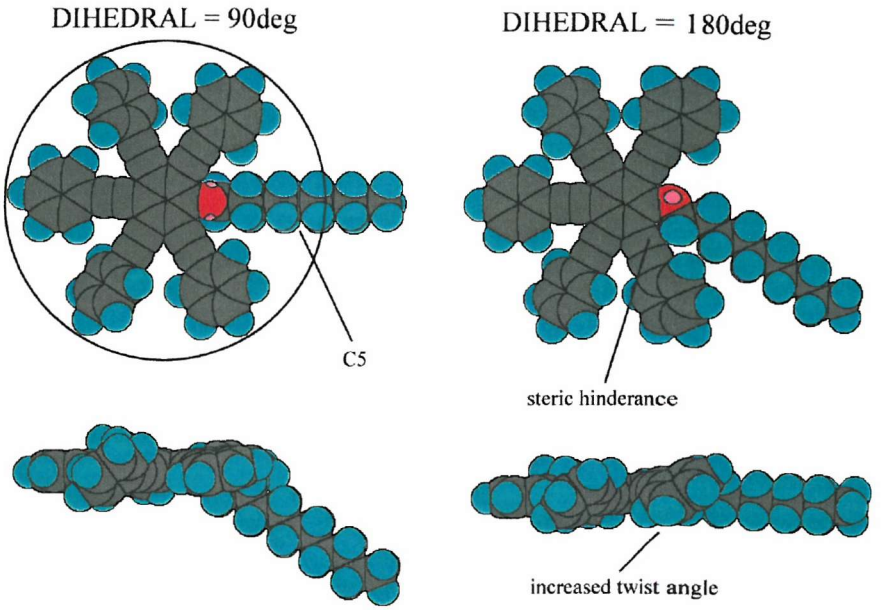

Figure 2.27 : Two possible orientations the alkyl chain can adopt in the C*n*SD materials, showing the steric hindrance a dihedral angle of 180° has on the peripheral phenyls rings.

As the chain length increases, the disruption to this close packing increases and within the Col_{ho} phase this serves to reduce the clearing temperatures significantly. However, in the N_C phase the side-by-side packing is now no longer so rigid, as the disorder within the phase is now greater. The increase in alkyl chain length will now no longer affect the packing of the molecules to such a large extent as there is more room to accommodate the extra methylene group in the chain within a nematic phase than for the Col_{ho} phase. Therefore it would be expected that the decrease in the nematic – isotropic transition temperature upon increasing the chain length will now be smaller.

This disruption to the side-by-side packing of the columns also explains why the Col_{ho} phase is seen for short chain lengths and the N_C phase is seen for longer chain lengths. As the chain length is increased a point is reached where it becomes energetically favourable for the molecules to adopt a columnar nematic arrangement as it becomes more and more difficult to try and accommodate the chains in the close packed hexagonal arrangement. This also suggests that the disruption causes the columns to adopt shorter stacks in the nematic phase, and as

stated in the Introduction (§1.6.2) the columns in are taken to consist of between 10 and 15 molecules.

It is also apparent from figure 2.26(a) that there is no discernible odd-even alternation in the clearing temperature upon increasing the alkyl chain length. Generally, for multiply substituted discotic materials, such as the hexakis(4-*n*-alkylphenylethynyl) naphthalenes [21] or the hexaesters of truxene [22] (see §1.12.3) there is little or no alternation in the clearing temperatures on increasing the length of the alkyl chain. This is because the there is usually a transition from an ordered columnar phase to the isotropic phase and we would not expect an odd-even alternation. However, for the 'Superdisc' materials where the number of carbon atoms in the alkyl chain is greater than nine there is a transition from a nematic phase to the isotropic phase. For these materials it may have been expected that there would be a small odd-even alternation in the clearing temperature upon increasing the alkyl chain length, analogous to the monomeric calamitic liquid crystals. The lack of odd-even alternation may be due to the fact that the macroscopic ordering of the molecules, i.e. their tendency to arrange themselves into a columnar structure in both the N_C and Col_{ho} phases, will effectively remove any difference there is between the conformations of the odd and even chains. For example, in a stack of disc and TNF molecules there are a number of alkyl chains present, and these may adopt any position around the periphery of the column, as shown in figure 2.28. On the addition of another methylene unit to the alkyl chains, for there to be any significant difference between the odd and even conformers, a large majority of the alkyl chains will have to adopt the same conformation, which would seem unlikely, particularly in the N_C phase.

It can be seen that for those members of the series with alkyl chains greater than 12 carbon atoms there is the emergence of the Col_2 phase at lower temperatures; the nature of this phase will be discussed later in the Chapter.

Figure 2.28 : Possible positions adopted by the alkyl chains around the periphery of stack of disc and TNF molecules, accounting for the lack of odd-even effect seen in nematic – isotropic transition temperature on increasing the alkyl chain length.

If the behaviour found on cooling the equimolar mixtures, shown in figure 2.26(b) is now examined we see the same steady drop in the isotropic – columnar nematic phase transition as the alkyl chain length is increased, although again the C12 seems to have an anomalously low transition temperature. However, it can be seen that there is now a transition from the isotropic to the Col_{ho} phase for only the C6 and C8 homologues, with the C9 homologue now having a transition to the N_C phase first. This unusual behaviour is due to some supercooling occuring at the Col_{ho} – I transition, and is explained more fully earlier in the Results section (§2.2.3). Again there appears to be no apparent odd-even alternation in the isotropic – N_C phase transition temperature upon increasing the length of the alkyl chain, although there is no reason to expect that there would be, for the same reasons which we have discussed previously.

As was seen in the phase diagrams, for those members of the series with alkyl chains containing less than 11 carbon atoms, there is, on cooling the Col_{ho} phase, the formation of the Col_1 phase. It is more apparent from the plot of the phase behaviour for the equimolar mixtures that the Col_1 phase only emerges when there is a preceding Col_{ho} phase and that the stability of this phase diminishes as the N_C phase becomes more prominent. Thus we find that the C12 homologue only exhibits an N_C phase. For those members of the series with more than 12 carbon atoms in the alkyl chain there is, as was found when the samples were heated, the

presence of the Col_2 phase. It has been argued [20] that the formation of the Col_1 phase may be a consequence of either the rearrangement of the packing of the TNF molecules within the stacks, or even the TNF crystallising out in the phase. If the same is true of the Col_2 phase it is interesting to note that this phase is enantiotropic whereas the Col_1 phase is monotropic. However, X-ray diffraction studies need to be carried out on these materials in order to conclusively identify such phases.

It is also readily apparent that there is a large degree of supercooling of the phases, however, this appears to diminish rapidly as the chain length is increased and the N_C phase becomes prominent. It should not be too surprising that supercooling occurs for those homologues that exhibit a Col_{ho} (and Col_1) phase, as this phase is already highly ordered and it is not unusual for the molecular motion in highly ordered phases to 'freeze out'. For example, for calamitic systems exhibiting a crystal E phase it is not uncommon for this phase to crystallise slowly over a number of hours after cooling to room temperature, due to the high viscosity of the preceding phase making it difficult for the highly ordered crystalline phase to form (see Chapter 4). However, it is interesting that the C9 homologue shows, for the equimolar mixture, the largest amount of supercooling, i.e. has the largest phase range, with the material crystallising at approximately 60°C. It would seem that this behaviour is not only unique to these monomeric systems. Coincidentally, studies carried out by Fletcher [23] on these large disc-like units attached to either rod-like units or disc-like units seem to show that the C9 homologues again supercool by the largest amount, with the lowest crystallisation points, over the whole homologous series.

Let us now consider the entropies of transition for equimolar mixtures of the these materials at the clearing temperature. Figure 2.29 shows the entropies for both heating and cooling the samples for comparison.

Unfortunately, the entropy values for some of the Col_{ho} – I transitions were unobtainable for some of the shorter chain members of the series. However, it can be seen that for those values obtained the entropy change is consistent with a Col_{ho} – I transition, for the C8 homologue $\Delta S/R$ is 1.54, and for the C9 homologue it is

1.14. For example, the pure hexakis(alkyloxy) triphenylenes have entropy values for the Col_{ho} – I transition of *ca.* 1, with the value for the decyloxy substituted material being as low as 0.16 [24.

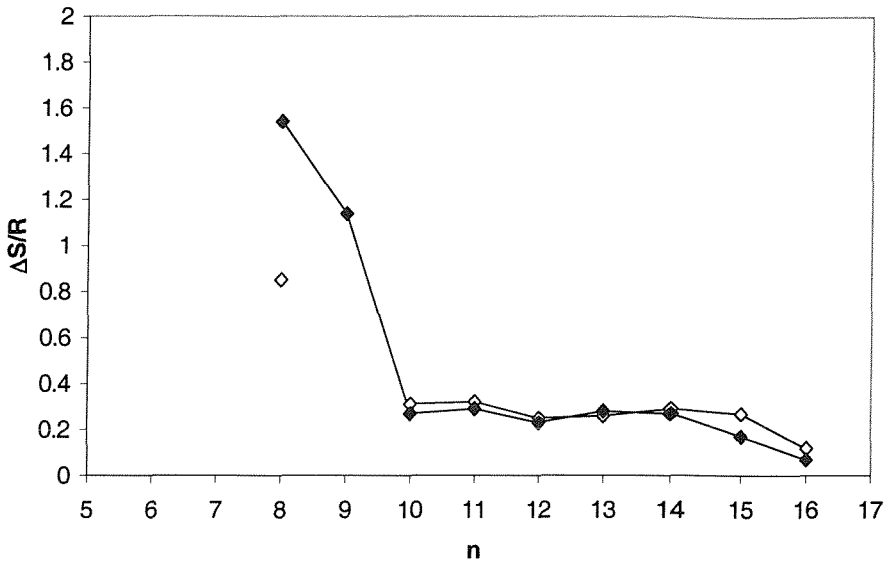

Figure 2.29 : The entropy change at the Col_{ho} or N – I transition as the number of carbon atoms, n, in the alkyl chain is increased. ◆ heating, ◇ cooling.

The entropy values for members of the series with ten or more carbon atoms in the alkyl chain, i.e. those having a transition from an N_C phase to the isotropic phase, exhibit values consistent with a columnar nematic phase. As was observed for the N_C – I transition temperatures of the equimolar mixtures there appears to be no obvious odd-even alternation in the transitional entropies upon increasing the alkyl chain length. However, it can be seen that for C15SD and C16SD the transitional entropy begins to fall, becoming only 0.07 for the C16 homologue. Interestingly this value is now more consistent with a nematic discotic (N) – isotropic transition than a columnar nematic to isotropic phase transition [18]. From the optical texture alone it is impossible to determine the structure of the nematic phase, however there has been speculation that other examples of these large multiyne discotic materials may form a conventional nematic phase as opposed to an N_C phase when mixed with TNF. For example Fletcher [23] prepared dimeric materials consisting of a 'Superdisc' joined via an ether linked alkyl spacer to a cyanobiphenyl moiety. It was suggested that those materials containing between 6 and 12 carbon atoms in the flexible spacer exhibited a conventional nematic phase when mixed with

equimolar amounts of TNF. These dimers where, now, the phenyl rings of the discotic moiety were substituted with pentyl chains in the para-position were also prepared and it was found that those materials containing between 6 and 10 carbon atoms in the spacer chain exhibit a monotropic nematic phase when mixed with TNF. In all of these examples the assignment that the nematic phase was of the discotic type and not the columnar kind was based solely on the magnitude of the transitional entropy. However, to determine conclusively the structure of the nematic phase requires the use of X-ray diffraction.

It could be argued that the cyanobiphenyl group disrupts the packing of the columns to such an extent that the N_C phase cannot form, and this perturbing effect is also observed for monomeric discotic systems. For example the C10 'Superdisc' homologue with pentyl chains substituted in the para-position on the phenyl rings exhibits a nematic discotic phase in the pure state and when complexed with TNF does not show an N_C phase, as C10SD does, only a Col_{ho} phase over intermediate concentrations, whilst the overall stabilisation is small [20]. It was suggested that the peripheral pentyl chains have, to some degree, hampered the formation of a stable columnar structure. The extent to which peripheral substitution with alkyl chain disrupts the side-by-side packing of these materials is not trivial. For example, C16SD in the pure state does not show any mesophases, with the material melting to the isotropic liquid at 91°C, however with substitution of just methyl groups around the perimeter of the disc the melting point increases to 162.3°C with the formation of a nematic discotic phase and then a transition to the isotropic liquid at 192.5°C [13]. For the C16SD/TNF mixture, the hexadecyl chains may now be long enough to begin to destabilise the columnar packing of the mesophase, and as with the 'Superdisc'-cyanobiphenyl dimers [23], cause the formation of an N_D phase. However this seems unlikely as it is the formation of a complex between the 'Superdisc' molecule and TNF that induces a mesophase, as both pure materials are non-mesogenic. Although the stabilisation of the complex may not be charge-transfer in nature, the colour change indicates that a charge-transfer interaction does occur, and that to cause the most favourable overlap of molecular orbitals to allow 'charge' to transfer from one site to the other, the molecules stack into short columns, alternating 'Superdisc' – TNF – 'Superdisc' and so on. For a nematic discotic phase this stacking does not occur and therefore

we might not expect to see a charge-transfer interaction. It seems likely, then, that the low value obtained for the transitional entropy of the $N_C - I$ transition may be due to increased disorder between the columns, caused by the long alkyl chains, rather than disorder between the packing of the molecules themselves within the columns.

The identity of the Col_2 phase that appears at lower temperatures for those homologues with 13 or more carbon atoms in the alkyl chain has not yet been determined. It is unlikely to be a nematic discotic phase as the optical texture appears to be that of a crystal in nature, and not a schlieren texture as would be expected for a nematic phase, and it does not flash when subjected to mechanical stress. Also, it is unlikely to be either a hexagonal or rectangular columnar phase as the long alkyl chains discourage the close packing needed to form these phases. Therefore, this phase is probably either an alternate crystal structure or, like the Col_1 phase, a consequence of one of the components in the mixture crystallising out. However, to determine fully the nature of this phase further studies using X-ray diffraction or deuterium NMR are needed.

Let us now consider some of the features seen in the phase diagrams themselves. The most prominent feature in the majority of the phase diagrams is the apparent disparity in transition temperatures seen at the clearing points. For pure mesogenic materials the temperature at which there is a transition from the isotropic to the mesophase is usually within about 1 or 2°C of the temperature at which the mesophase to isotropic transition occurs, i.e. there is little supercooling. However, for some of these discotic materials there is a difference between the two temperatures of up to approximately 15°C. This is especially noticeable for the C8 and C9 homologues, and also for the C16 homologue, and to a lesser extent the C6 homologue. For the shorter chain homologues this may be explained as a consequence of the Col_{ho} phase emerging from the isotropic fluid. As this phase is quite highly ordered it emerges from the isotropic phase relatively slowly, as is readily apparent when observed under the polarising microscope – flower-like hexagons separating from the isotropic liquid and slowly coalescing upon further cooling. When this transition is seen on the DSC trace it appears as a broad hump, as shown in figure 2.30. It can be seen that it is difficult to determine the limits of

the transition as well as where the peak occurs, especially for the heating scans. As the transition temperatures were taken from the DSC traces it is likely that this problem may well account for a difference seen in the transition temperatures for heating and cooling, however this does not account for the large differences seen for C8SD/TNF and C9SD/TNF. One possible explanation for this large difference is the fact that, although there is an interaction occurring between the 'Superdisc' and the TNF, the mesophases are actually quite mobile, especially in the N_C phase. This view is supported by the fact explored in the next Chapter that at the Col_{ho} to N_C transition it would appear that some of the TNF molecules are squeezed out of the columns, whilst there is some molecular reorganisation, and gradually reincorporated into the columns again in the new phase – this phenomenon will be discussed more fully in the next Chapter. With this extra mobility comes the problem of biphasic regions at the phase transitions, especially for mixtures containing non-equimolar amounts of TNF. Indeed, mixtures containing more than about 60mol% TNF tend to be thermodynamically unstable, with phase separation beginning to occur, however this is not shown on the phase diagrams.

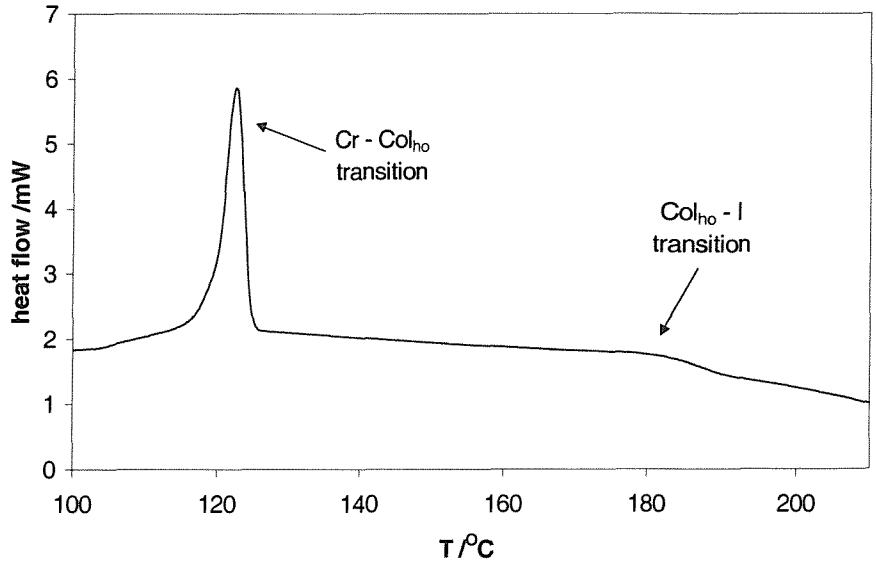

Figure 2.30 : Example of a DSC trace of C8SD on heating showing the broad peak of the Col_{ho} – I transition.

2.3 Conclusions

In this Chapter we have described the preparation of an homologous series of the large disc-like, electron-rich pentakis(phenylethynyl)phenyloxyalkanes (CnSD) based on the materials initially studied by Praefcke *et al.* [10]. We have varied the number of carbon atoms in the alkyl chain from 6 to 16 atoms. No members of this series exhibit mesophases in the pure state, however it is possible to induce mesophases with the addition of 2,4,7-trinitrofluorenone (TNF). As the molar ratios of the TNF with the CnSD's are varied, the nature of the mesophases change. We have therefore, investigated the phase behaviour of these disc-like mesogens as the amount of TNF is varied.

It has been found that the nature of the mesophase is not only dependent on the length of the alkyl chain but also on the concentration of the TNF in the mixtures. For TNF concentrations of less than 25mol% or greater than 75mol% no mesophases are observed. For concentrations between these two limits a nematic phase, as well as a number of columnar phases, are observed. For alkyl chain lengths of less than nine carbon atoms only an ordered columnar hexagonal phase (Col_{ho}) is observed. However, as the chain length is increased the disruption to the neighbouring columns increases and we see the emergence of a nematic phase. This phase emerges on the phase diagrams at low TNF concentrations and moves across as the chain length is increased until, for C12SD, the Col_{ho} phase is completely extinguished and only a columnar nematic phase is observed over the whole TNF concentration range.

For those mixtures that exhibit a Col_{ho} upon cooling we have observed another mesophase, for TNF concentrations of between approximately 45 and 60mol%; this has been labelled the Col_1 phase. The optical texture of this phase appears similar to the preceding phase but has a more sanded appearence. It has been speculated that this phase is in fact a consequence of the TNF crystallising, and this speculation is dealt with in the next Chapter. Also, for those materials with 13 or more carbon atoms in the alkyl chain we see the appearance of an enantiotropic mesophase at low temperatures and intermediate TNF concentrations, which we have labelled the Col_2 phase. From the optical textures it is likely be that this phase

is an alternate crystal form, although X-ray diffraction studies need to be carried out in order to confirm this, as well as the nature of the Col_1 phase.

Although it can be seen that the driving force for mesophase formation is the addition of TNF to the pure Superdisc materials, we have found that the alkyl chain length affects the packing of the resultant columns. This disruption to the packing dictates the nature of the mesophases formed. In the following Chapter we undertake a more detailed investigation into the conformation of the alkyl chain in equimolar mixtures of C10SD and TNF and also gain an insight into the nature of the Col_1 phase.

2.4 References

[1] Demus, D., Diele, S., Grande, S. and Sackmann, H., *Adv. Liq. Cryst.*, **6**, 1, (1983).

[2] Szabon, J. and Diele, S., *Cryst. Res. Technol.*, **17**, 1315, (1982).

[3] Pelzl, G., Humke, S., Diele, S. and Demus, D., *Liq. Cryst.*, **3**, 1047, (1988).

[4] Kolbe, A. and Pelzl, G., *Adv. Molec. Relax. Interact. Proc.*, **24**, 251, (1982).

[5] Demus, D., Hauser, A., Pelzl, G., Böttger, U. and Schönburg, S., *Cryst. Res. Technol.*, **20**, 381, (1985).

[6] Diele, S., *Ber. Bunsenges. Phys. Chem.*, **97**, 1326, (1993).

[7] Kresse, H., Szulzewsky, I., Diele, S., Paschke, R., *Mol. Cryst. Liq. Cryst.*, **283**, 13, (1994).

[8] Brienne, M.J., Gabard, J., Lehn, J.M. and Stibov, J., *J. Chem. Soc., Chem. Commun.*, **1989**, 1868, (1989).

[9] Neumann, B., Joachimi, D., Tschierske, C., *Liq. Cryst.*, **22**, 509, (1997).

[10] Praefcke, K., Singer, D., Kohne, B., Ebert, M., Liebmann, A. and Wendorff, J.H., *Liq. Cryst.*, **10**, 147, (1991).

[11] Bengs. H., Karthaus, O., Ringsdorf, H., Baehr, C., Ebert, M. and Wendorff, J.H., *Liq.Cryst.*, **10**, 161, (1991).

[12] Zamir, S., Singer, D., Spielberg, N., Wachtel, E.J., Zimmermann, H., Poupko, R. and Luz, Z., *Liq. Cryst.*, **21**, 39, (1996).

[13] Praefcke, K., Singer, D. and Eckert, A., *Liq. Cryst.*, **16**, 53, (1994).

[14] Janietz, D., *Liq. Cryst.*, **20**, 459, (1996).

[15] Ringsdorf, H., Wustefeld, R., Zerta, C., Ebert, M. and Wendorff, J., *Angew. Chem.*, **101**, 934, (1989).

[16] Praefcke, K., Kohne, B., Gündogan, B., Singer, D., Demus, D., Diele, D., Pelzl, G. and Bakowsky, U., *Molec. Cryst. Liq. Cryst.*, **198**, 393, (1991).

[17] Praefcke, K., Kohne, B., Singer, D., Demus, D., Pelzl, G. and Diele, S., *Liq. Cryst.*, **7**, 589, (1990).

[18] Praefcke, K., Kohne, B., and Singer, D., *Angew. Chem. Int. Ed. Eng.*, **29**, 177, (1990).

[19] Destrade, C., Foucher, P., Gasparoux, H., Tinh, N.H., Levelut, A.M., and Malthete, J., *Mol. Cryst. Liq. Cryst.*, **106**, 121, (1984).

[20] Tearle, W.M., *Ph.D Thesis, University of Southampton*, (1995).

[21] Preafcke, K., Kohne, B., Gutbier, K., Johnen, N. and Singer, D., *Liq. Cryst.*, **5**, 233, (1989).

[22] Tinh, N.H., Foucher, P.,Destrade, C., Levelut, A-M. and Malthete, J., *Mol. Cryst. Liq. Cryst.*, **111**, 277, (1984).

[23] Fletcher, I.D., *Ph.D Thesis, University of Southampton*, (1993).

[24] Destrade, C., Mondon, M.C., Malthete, J., *J. Phys. Colloq.*, **C3**, 17, (1979).

CHAPTER THREE

AN NMR STUDY OF CHEMICALLY INDUCED DISCOTIC MESOPHASES

3.1 Introduction

In the previous Chapter the homologous series of 'Superdiscs', the C*n*SD's, with the structure

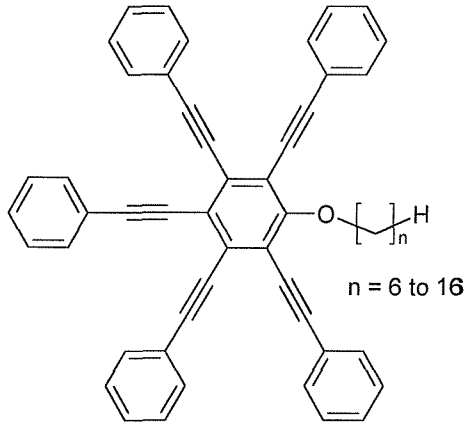

were studied. It was found that when there are between 6 and 10 carbon atoms in the alkyl chain, cooling mixtures containing approximately 50mol% TNF (2,4,7-trinitrofluorenone), as well as the more common N_C and Col_{ho} phases, before crystallisation, there emerges an unusual phase, the Col_1 phase. Whilst the identification of this phase could not be made by optical microscopy alone, deuterium NMR studies on fully and specifically deuteriated materials have allowed certain conclusions to be drawn about its nature. In addition to this, during some of these studies, it emerged that there appeared to be an unusual orientational ordering within the chain of the disc-like molecule and some of these results are also presented here. The work described in this Chapter was carried out in collaboration with Dr. Mark Tearle and a more detailed discussion of this is also presented elsewhere [1]. For the purposes of these studies the decyl homologue, C10SD, (also known as D102 [1]) was chosen, as this material exhibited the richest mesomorphic behaviour when mixed with an equimolar amount of TNF, namely Cr-N_C-I on heating, and I-N_C-Col_{ho}-Col_1-Cr on cooling. However, before

we present the results it is helpful to cover some of the basic aspects of NMR spectroscopy on liquid crystal systems. In essence, deuterium NMR spectroscopy allows us to probe the orientational order within a liquid crystal phase. This can be achieved by studying pure systems through the specific deuteriation of liquid crystalline molecules or by dissolving a deuteriated solute in a liquid crystalline solvent. It is also possible to study director distributions and dynamics using deuterium NMR spectroscopy.

3.2 Deuterium NMR of Liquid Crystals

Most nuclei possess an intrinsic angular momentum, known as the spin, the magnitude of which is $[I(I+1)]^{\frac{1}{2}}\hbar$ where $\hbar = h/2\pi$ (h is the Planck constant) and I is the spin quantum number and can take values of $n/2$ where n is an integer. The angular momentum, $\boldsymbol{I}$, of a spin-I nucleus has $2I + 1$ projections onto an arbitrarily chosen axis such that the z-component, say, is quantised

$$I_z|m\rangle = m\hbar|m\rangle, \qquad (1)$$

where m is the magnetic quantum number and has $2I + 1$ values between $+I$ and $-I$ i.e. $m = I, I-1, I-2, \ldots -I+1, -I$.

The magnetic moment of a nucleus is related to its spin angular momentum by

$$\mu = \gamma \boldsymbol{I}, \qquad (2)$$

where μ is the magnetic moment and γ is the isotope specific gyromagnetic ratio. In the absence of a magnetic field all $2I + 1$ orientations of a spin-I nucleus are degenerate. However, upon the application of a magnetic field this degeneracy is removed and the energy of the magnetic moment is available from the spin hamiltonian

$$H = -\mu \cdot \boldsymbol{B}, \qquad (3)$$

where $\boldsymbol{B}$ is the magnetic flux density. Now, if we choose the axis system such that the z-axis is parallel to the magnetic field direction, equation (3) becomes

$$H = -\mu_z B_z, \qquad (4)$$

and equally

$$\mu_z = \gamma I_z; \qquad (5)$$

it follows from equation (1) that

$$E_m = -m\hbar\gamma B_z \,. \qquad (6)$$

The selection rule for NMR is that $\Delta m = \pm 1$ and so the resonance conditions will be

$$\Delta E = h\nu = \hbar\gamma B_z, \qquad (7)$$

where $\nu = \frac{\gamma B_z}{2\pi}$ and is known as the Larmor frequency.

Equation (3) is in fact the Zeeman interaction, described by Zeeman in 1896, and forms part of the full static spin Hamiltonian for a molecule comprising more than one magnetic nucleus and is given by

$$H = H_Z + H_J + H_D + H_Q \,, \qquad (8)$$

where H_Z is the Zeeman interaction, H_J is the indirect spin-spin coupling, H_D is the direct dipolar coupling and H_Q is the quadrupolar interaction.

The chemical shift, which arises because a specific nucleus in a molecule experiences a slightly different field depending on the chemical environment of the nucleus, and maybe even the spin-spin coupling can yield information relating to the orientational order of the molecule. However, it is more usual to use the direct dipolar and quadrupolar interactions to obtain this information. Both the direct dipolar and quadrupolar interactions have second rank tensorial properties and can thus yield the second rank order parameters.

3.2.1 The Direct Dipolar Interaction

The formal expression of the components of the direct dipolar coupling between a pair of nuclei is

$$D_{ij}^{\alpha\beta} = \frac{3\mu_0\gamma_i\gamma_j h}{32\pi^2 r_{ij}^3}\left(3\cos\theta_\alpha\cos\theta_\beta - \delta_{\alpha\beta}\right) \qquad (9)$$

where μ_0 is the permitivity of free space, γ_i and γ_j are the gyromagnetic ratios of the i^{th} and j^{th} nuclei respectively, $\boldsymbol{r}_{ij}$ is the internuclear separation and θ_α and θ_β are the angles between the α-axis and the β-axis and the vector r_{ij} respectively. In a uniaxial phase, i.e. that formed by a typical nematic mesogen, the only component of the dipole-dipole interaction that is experimentally important is that along the magnetic field. If the director for the material aligns parallel to the magnetic field,

that is it possesses a positive magnetic susceptibility i.e. $\Delta\tilde{\chi} > 0$, and whose molecular motion is frozen, we find

$$D_{ij}^{zz} = \frac{3\mu_0\gamma_i\gamma_j h}{32\pi^2 r_{ij}^3}\left(3\cos^2\theta_z - 1\right) \qquad (10)$$

However, since the molecular motion in a mesophase is not frozen the dipolar interaction in equation (10) must be averaged over the orientations adopted. This gives the average dipolar interaction as

$$\tilde{D}_{ij}^{zz} = \frac{3\mu_0\gamma_i\gamma_j h}{16\pi^2\left\langle r_{ij}^3\right\rangle}S_{ij} \qquad (11)$$

where $S_{ij} = \frac{\overline{\left(3\cos^2\theta_{ij} - 1\right)}}{2}$ and is the order parameter of the internucleus vector connecting the i and j nuclei, where θ_{ij} is the angle between the director and the internuclear vector. If we know the average internuclear distance r_{ij} it is usually possible to obtain the order parameter for the internuclear axis.

Whilst this may seem an ideal method for determining the order parameter, for a liquid crystal there may be, in practice, a large number of dipolar interactions involving numerous protons that are significant and this leads to highly complex spectra that are very difficult, or even impossible to analyse. However, by specifically deuteriating the liquid crystalline material, and decoupling the deuterons from the protons, the proton spectrum is simplified and its analysis is usually possible. Alternatively 'probe molecules' containing only a few nuclear spins can be dissolved in the liquid crystal and can provide indirect information about the ordering of the liquid crystalline phase. A second advantage with selectively deuteriated materials is that a deuterium nucleus has a spin of 1 (i.e. I = 1), and thus possesses an electric quadrupole moment. This leads to an extremely simplified deuterium NMR spectrum for a liquid crystal, with the resulting quadrupolar splittings yielding the orientational order parameters. This leads us to consider the nuclear quadrupolar interaction.

3.2.2 The Quadrupolar Interaction

Any nucleus with a spin greater than ½ does not have a spherically symmetric distribution of charge, and as such possesses an electric quadrupole moment that

can interact with electric field gradients at the nucleus generated from electron distribution in the molecular orbitals. The energy of the spin states of an $I = 1$ nuclei, assuming a cylindrically symmetric field gradient at the nucleus, can be shown to be

$$E_m/h = -m\gamma B_0/2\pi + \frac{3e^2qQ}{4h}\left(3m^2-2\right).\frac{\left(3\cos^2\theta-1\right)}{2}, \qquad (12)$$

where the first term is the familiar Zeeman interaction, which is clearly dependent on the magnetic field strength. The second part of the expression is the quadrupolar interaction which is independent of the field and for deuterons is usually of the order of around 100 – 200 kHz. Here θ is the angle between the magnetic field and the assumed symmetry axis of the electric field gradient tensor and the expression e^2qQ/h is the quadrupolar coupling constant and is usually written as q_{CD}. For deuterium attached to carbon q_{CD} is usually between about 150 and 200 kHz, and although this value is dependent on the type of bond, it is not significantly affected by the rest of the molecule. Therefore in this Thesis the value of 183 kHz is used for aromatic C-D bonds [2] and 168 kHz for aliphatic C-D bonds [3].

There are three energy levels available for deuterium, corresponding to $m = -1, 0, +1$, and as the only allowed transitions are $\Delta m = \pm 1$ this gives rise to two transitions for a deuteron, thus

$$\nu_1 = \gamma B_0/2\pi - \tfrac{3}{4}q_{CD}\,(3\cos^2\theta - 1)/2$$

$$\nu_2 = \gamma B_0/2\pi + \tfrac{3}{4}q_{CD}\,(3\cos^2\theta - 1)/2 \qquad (13)$$

and therefore two lines would be expected in the spectrum with a frequency separation

$$\Delta\nu = (\tfrac{3}{2})q_{CD}, \qquad (14)$$

centred on the Zeeman frequency, $\gamma B_0/2\pi$.

Since we are dealing with liquid crystalline phases we need to take account of the reorientational motion which 'averages' the quadrupolar splitting and so we should consider the orientational average. This leads to the quadrupolar splitting of any deuteron in a uniaxial liquid crystalline phase as being

$$\Delta\tilde{\nu} = \frac{3}{2}\frac{\left(3\cos^2\varphi-1\right)}{2}\frac{\overline{\left(3\cos^2\beta-1\right)}}{2}q_{CD}, \qquad (15)$$

where φ is the angle between the director and the magnetic field and β is the angle between the C-D bond and the director. In this and the previous Chapter the materials studied are discotic and, as with most disc-shaped molecules, align with their director perpendicular to the magnetic field because $\Delta\tilde{\chi} < 0$. This serves to simplify the expression in equation (15) and gives

$$\Delta\tilde{\nu} = -\frac{3}{4} q_{CD} \frac{\overline{\left(3\cos^2\theta - 1\right)}}{2} \qquad (16)$$

which is written as

$$\Delta\tilde{\nu} = -\tfrac{3}{4} q_{CD} S_{CD} . \qquad (17)$$

In order to relate S_{CD} to the molecular order parameters it is necessary to determine the molecular geometry for the system studied. Fortunately for the discotic materials investigated here it is relatively straightforward to relate S_{CD} to S_{zz}, the order parameter along the molecular symmetry axis. Assuming the C-D bonds are in the molecular plane and the disc containing the C-D bonds are free to rotate about an axis orthogonal to this plane, i.e. the C-D bonds are orthogonal to the symmetry axis of the disc then

$$S_{zz} = \frac{8\Delta\tilde{\nu}}{3q_{CD}} \qquad (18)$$

This situation is only true for deuterons in the para-position in the phenyl rings for C10SD because, as was seen for the energy minimised structures in the previous Chapter, the phenyl rings are twisted out of the plane of the disc. However, for a 50mol% mixture with TNF, the TNF molecule is assumed to lie in a plane parallel with the C10SD molecule, i.e. in a stack, and therefore any deuterons present in TNF will lie in the molecular plane. Therefore we can still use equation (18) to determine the order parameter, S_{zz}. For the alkyl chain, however, this is not the case as the chain does not lie in the plane of the disc and also adopts many conformations. Also, although hard to define since the chain is not rigid, the molecular biaxiality of the chain is not low, i.e. $S_{zz} \neq S_{xx} \neq S_{yy}$. In this case the expressions relating the quadrupolar interaction to the order parameters are more complex. To determine a value for the major order parameter, S_{zz}, for the chain deuteriated C10SD-d_{21} a small amount of deuteriated TNF-d_5 was added to the sample as it has been shown that TNF and C10SD have similar order parameters [1].

3.2.3 The NMR Experiment

Deuterium NMR studies were carried out on equimolar mixtures of C10SD and TNF-d_5, chain deuteriated C10SD-d_{21} and TNF, and specifically deuteriated α-C10SD-d_2 (**6**) (the site of specific deuteration is indicated in figure 3.1) and TNF-d_5. The samples were prepared identically to that outlined by Dr W.M.Tearle [1]. For each experiment the Quadours pulse sequence was used, however more details on this can be obtained from the Thesis by W.M.Tearle [1].

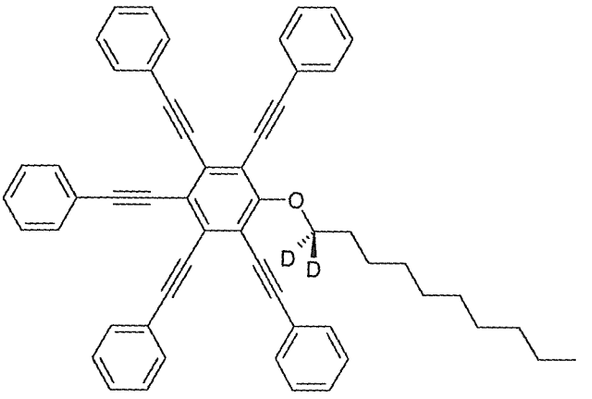

Figure 3.1 : The deuteriated C10SD (6) used in the NMR experiment (§3.3.3)

3.3 Results and Discussion

3.3.1 NMR Results of C10SD and TNF-d_5

Spectra were accumulated every 2 – 3°C on cooling from the isotropic phase until a signal was no longer detectable. A delay of about 800 seconds was allowed between each temperature to allow for thermal equilibrium to be reached. Figure 3.2 shows the deuterium NMR spectra of the equimolar mixture at two different temperatures. As can be seen, for any one liquid crystal phase the spectra consists of essentially a single quadrupolar doublet. As the five deuterons in TNF-d_5 are non-equivalent, the fact that only one quadrupolar doublet is seen is an indication that the TNF molecules are only able to rotate about an axis that is perpendicular to the plane of the molecule. Also this rotation is fast on the timescale of the NMR experiment thus averaging out the different signals from the non-equivalent deuterons, i.e. the biaxiality is low with $S_{xx} \approx S_{yy}$.

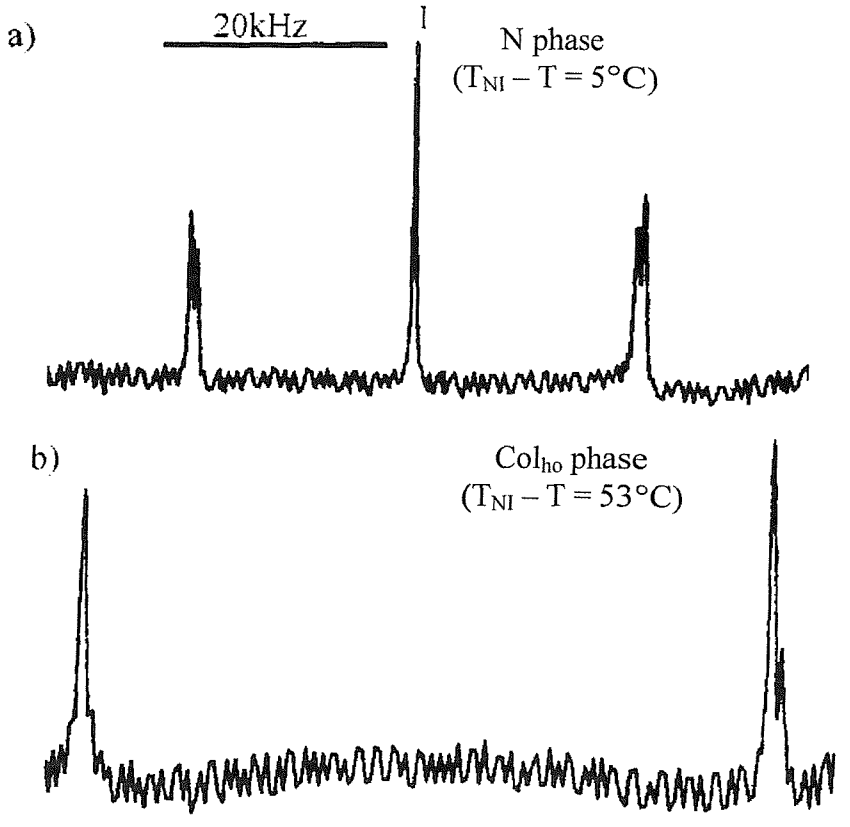

Figure 3.2 : Deuterium NMR spectra of an equimolar mixture of C10SD and TNF-d_5. (a) the nematic phase and (b) the Col_{ho} phase.

The first spectrum to show an aligned mesophase occurs at about 162°C, T_{NI}, and has a quadrupolar splitting of 25.4 kHz, and consists of a sharp pair of peaks as well as a peak due to a residual amount of isotropic still being present. With continued cooling in the N_C phase the quadrupolar splitting increases significantly until it reaches a maximum, at $T_{NI} - T = 28°C$, of 50.1 kHz just before the onset of the Col_{ho} phase. At this phase transition, where $T_{NI} - T = 30°C$, a second set of peaks appear in the spectrum with a larger quadrupolar splitting than the inner peaks due to the N_C phase. This splitting being about 58.5 kHz compared to about 50.3 kHz, and corresponds to the Col_{ho} phase. Over the next 4 or 5°C the outer pair of peaks, from the Col_{ho} phase, increase in intensity while the inner pair of peaks, from the N_C phase, diminish. This jump in the quadrupolar splitting at the phase transition, as shown in figure 3.3, corresponds to a larger order parameter in the more ordered Col_{ho} phase, and being discontinuous indicates that the transition is first order, as stated in the previous Chapter. Also, it was noticed that immediately after the phase transition a low intensity isotropic peak appeared at the centre of

the spectrum which persisted for a further 10°C. Although this peak amounts to only a small percentage of the total signal it could suggest that there may be some molecular reorganisation at the phase transition with some of the TNF being pushed out from the stacks and forming small pockets of isotropic TNF which is gradually reincorporated into the columns.

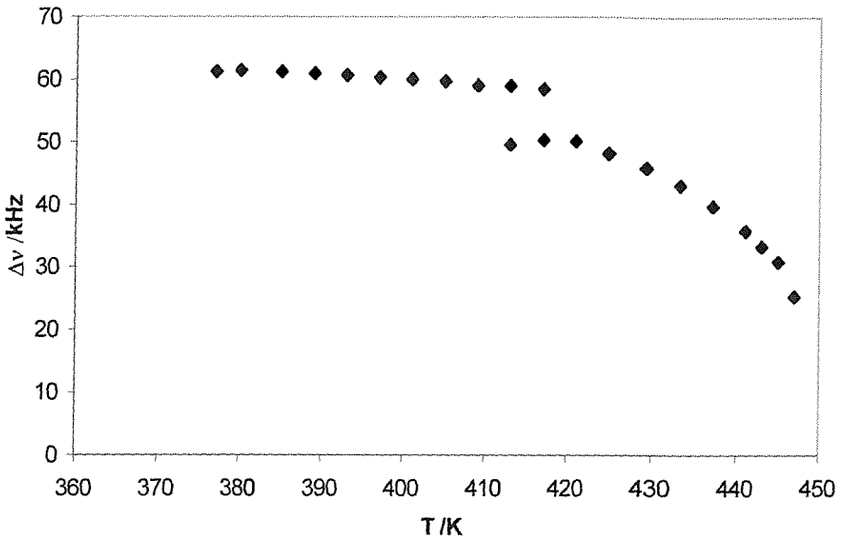

Figure 3.3 : The quadrupolar splitting for an equimolar mixture of C10SD and TNF-d_5.

Unlike the N_C phase the temperature dependence of the quadrupolar splitting in the Col_{ho} phase is much smaller. Whereas the quadrupolar splitting basically doubles from T_{NI} to the N_C – Col_{ho} phase transition, within the Col_{ho} phase the splitting only increases from about 58.5 kHz at $T_{NI} - T = 30°C$ to about 61.4 kHz at $T_{NI} - T = 70°C$ when the signal from TNF-d_5 is lost. It is interesting to note that no signal was observed from the TNF-d_5 in the Col_1 phase, whereas for mixtures where the C10SD is specifically deuteriated, as will become apparent, there is a detectable signal in the Col_1 phase. The implications of this will be discussed later in this Chapter.

Using equation (18) and assuming a value for q_{CD} of 183 kHz [4] the major orientational order parameter, S_{zz}, is found to be 0.37 at T_{NI}, rising to 0.73 in the N_C phase and 0.85 in the Col_{ho} phase at the N_C – Col_{ho} phase transition, and ultimately reaching a maximum in the Col_{ho} phase of 0.89 at $T_{NI} - T = 70°C$.

3.2.2 NMR Results of Chain Deuteriated C10SD-d_{21} and TNF

Spectra were accumulated, on cooling from the isotropic phase, every 1 – 2°C until the equimolar mixture crystallised and a signal was no longer detectable. Figure 3.4 shows the deuterium NMR spectrum of an equimolar mixture of chain deuteriated C10SD-d_{21} and TNF in the nematic columnar phase. It can be seen that the ten different deuteron sites give rise to up to eight pairs of peaks. Also the quadrupolar splitting are significantly smaller than those from deuteriated TNF with a maximum splitting of about 9.6 kHz at T_{NI} (162°C) rising to 13.9 kHz just before the onset of the Col_{ho} phase at $T_{NI} - T = 20°C$ compared with a maximum splitting of 50.1 kHz in the N_C phase for deuteriated TNF. The size of these splittings suggest that the alkyl chain is quite disordered. Alternatively the chain may have an unfavourable geometry in that, as the quadrupolar splitting is given by equation (15), if the angle between the C-D bond and the magnetic field approaches the 'magic angle' of 54.7° the quadrupolar splitting will approach zero. However the values seem consistent with the behaviour seen for another series of discotic materials, the chain deuteriated hexaalkyloxytriphenylenes (THEn) [5]. Although the spectra are relatively complex it should be possible to make some assignment of the splittings to the different groups in the alkyl chain. The methyl group should be readily identifiable by integration of the peaks as it possesses three deuterons whilst the other methylene groups have only two deuterons. Also, it is expected that it will also have the smallest quadrupolar splitting [5], as this should have the lowest order of all the alkyl groups, being situated at the end of a flexible alkyl chain. Figure 3.4(a) shows all distinct peaks labelled from *a* through to *h* and, although precise integration is difficult for some of the overlapping peaks, the peaks *a*, *b*, *c*, *d*, *e* and *g* have an intensity corresponding to two deuterons and are therefore distinct sites along the alkyl chain, whereas the peaks *f* and *h* would seem to correspond to more than one site along the alkyl chain. Also, it is noticeable that the peak *h* and its partner *h'*, which should be identical, are in fact slightly different with peak *h'* being almost a doublet whereas *h* is essentially a single peak with a small shoulder. The integration shows that both these peaks correspond to five deuterons and therefore it would seem sensible to assign three of the deuterons as coming from the methyl group and consequently the other two deuterons must correspond to one of the methylene groups. The unusual splitting of peaks *h* and *h'* suggest that the deuterons for one of these groups have a

distinctly different chemical shift from the rest of the chain. The midpoint of the quadrupolar splitting of the shoulder of peak *h* and the smaller doublet of peak *h'* is shifted to the left relative to the midpoints of the other quadrupolar splittings by about 150 Hz. As the frequency of the spectrometer was 30.7 MHz this corresponds to a chemical shift of about 4.9 ppm. The only deuterons expected to show such a large chemical shift are ArO-CD_2-R deuterons as is evident from the isotropic proton NMR spectrum (see §7.1 for the proton NMR chemical shift). It is usual to expect the deuterons closest to the mesogenic core to have the highest order, and hence the greatest splitting, in an alkyl chain, with a decrease in the splitting when moving along the chain from the core to the methyl group at the end, which is expected to have the smallest splitting. Although it has been shown that this is not necessarily always the case [6] the fact that the ArO-CD_2-R deuterons appear to have the smallest splitting is rather surprising.

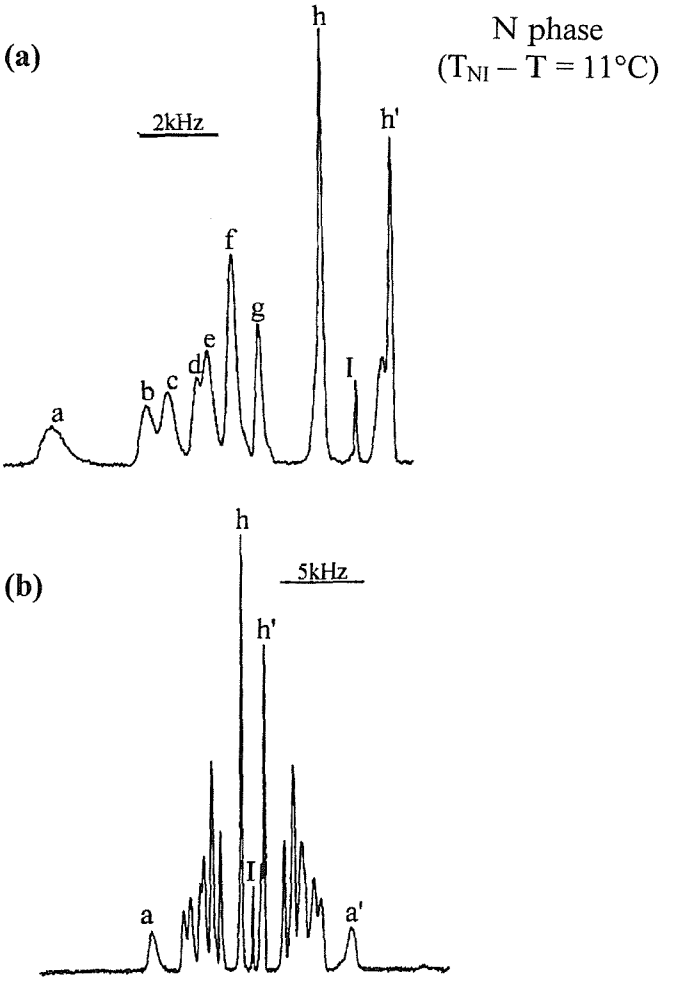

Figure 3.4 : The deuterium NMR spectrum of an equimolar mixture of chain deuteriated C10SD-d_{21} and TNF in the N phase. (a) is expanded region of whole spectrum (b).

As with the C10SD/TNF-d_5 mixture the quadrupolar splittings are significantly temperature dependent, with the outer peaks, *a* and *a'*, having the largest dependence – rising from 9.6 kHz at T_{NI} to 13.9 kHz at the N_C – Col_{ho} phase transition.

If we now consider the NMR spectrum at the N_C – Col_{ho} transition (141°C, T_{NI} – T = 21°C) we find that over the next 3 or 4°C the N_C phase coexists with the Col_{ho} phase and as a consequence up to 11 different quadrupolar splittings are observable. When this biphasic regime has disappeared we find there are now 9 different splittings observeable and that the largest splitting, *a* – *a'*, has increased discontinuously from 13.8 kHz to 15.8 kHz, indicating the first order nature of this phase transition. Unlike the N_C phase, the splittings in the Col_{ho} phase are only slightly temperature dependent with the largest splitting increasing to only 16.8 kHz at T_{NI} – T = 70°C (92°C) – the Col_{ho} to Col_I phase transition. The fact that there are now nine different quadrupolar splittings instead of the eight seen in the N_C phase suggests that one of the two overlapping signals has resolved itself into two separate signals. Integration of peak *f* indicates that this still corresponds to four deuterons and therefore comes from more than one site on the alkyl chain, so it seems sensible to assume that the peak *h* from the previous spectrum (figure 3.4) has been resolved. Indeed integration of the peak marked *h* in figure 3.5 shows that this corresponds to two deuterons and the new peak, *i*, integrates to three deuterons. Therefore, it seems that the quadrupolar splitting for the ArO-CD_2-R deuterons has increased above that of the methyl group at the end of the chain, and inspection of the chemical shift of this peak, which is about 150 Hz or ~4.9 ppm again, makes this a reasonable assumption. The quadrupolar splittings are shown in figure 3.6.

Upon continued cooling the system undergoes a transition from the Col_{ho} phase to the Col_I phase at a temperature of 91°C or T_{NI} – T = 71°C, as noted in Chapter 2. As with the N_C – Col_{ho} transition there is a discontinuous jump in the quadrupolar splitting of the outer peaks (*a* and *a'*), going from 16.8 kHz to 17.2 kHz, which rises to 17.4 kHz before crystallisation at 89°C. The spectrum in figure 3.7 shows that all the peaks have become considerably broader than the previous phase which may be due to a slowing down of the molecular motion in this phase

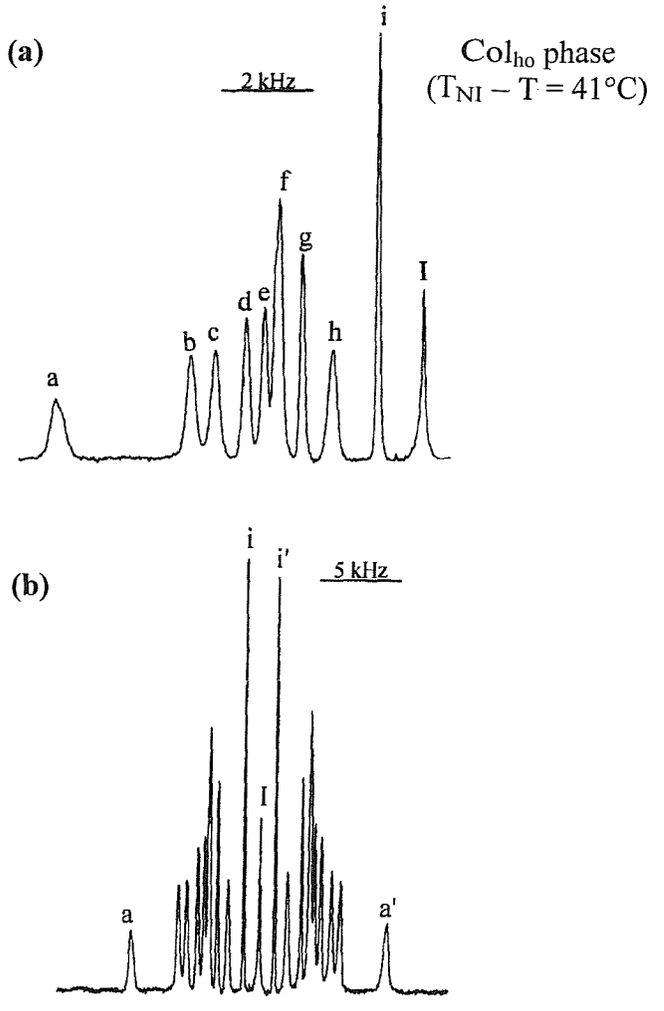

Figure 3.5 : The deuterium NMR spectrum of an equimolar mixture of chain deuteriated C10SD-d_{21} and TNF in the Col_{ho} phase. (a) is expanded region of whole spectrum (b).

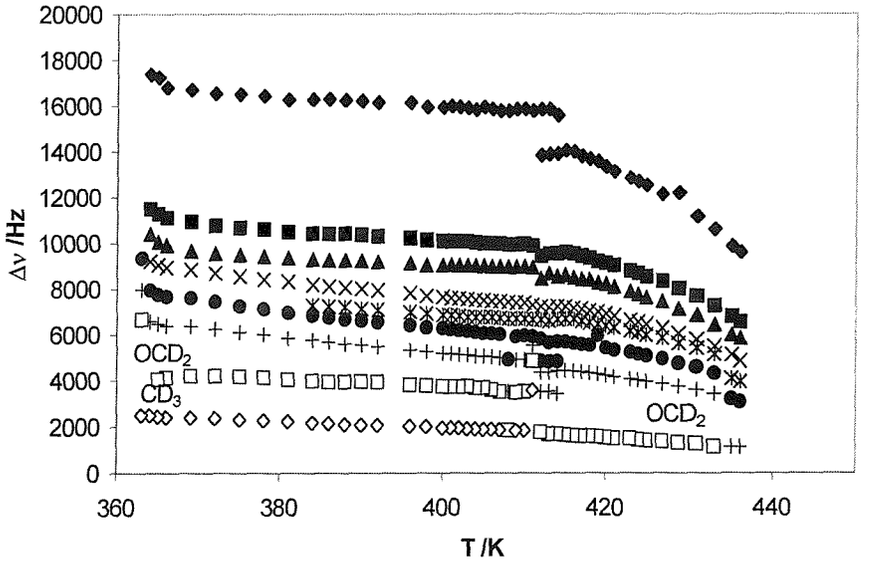

Figure 3.6 : The quadrupolar splitting for an equimolar mixture of chain deuteriated C10SD-d_{21} and TNF, showing the OCD_2 (□) and CD_3 (◇) splittings.

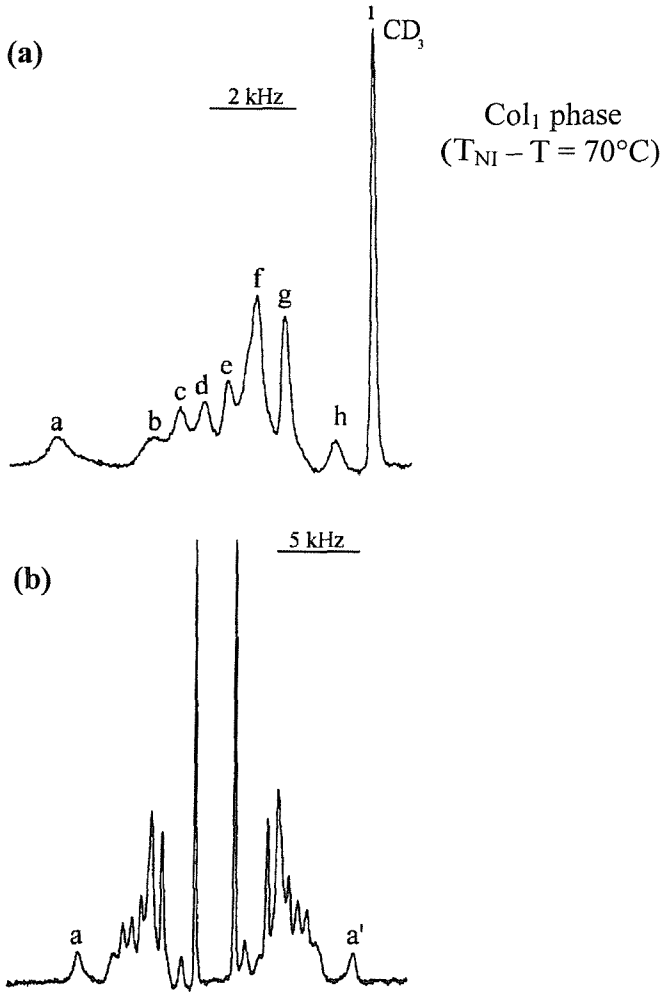

Figure 3.7 : The deuterium NMR spectrum of an equimolar mixture of chain deuteriated C10SD-d_{21} and TNF in the Col_1 phase. (a) is expanded region of whole spectrum (b).

or because the director is becoming less well aligned. Although it is possible to pick out nine different pairs of peaks, it is difficult to determine which one is due to the ArO-CD_2-R deuterons although it is assumed that the relative splittings will not change. Also, it is interesting to note that whereas a signal is detectable in the Col_1 phase for chain deuteriated C10SD-d_{21} no signal was detectable for TNF-d_5, as was noted in the previous section (§3.3.1). The reasons why this dramatic difference might occur will be considered later in this Chapter.

3.3.3 NMR Results of α-C10SD-d_2 and TNF

Because of the totally unexpected assignment of a relatively small quadrupolar splitting to the α-deuterons (ArO-CD_2-R) we sought to confirm that this is indeed correct. Spectra of an equimolar mixture of α-C10SD-d_2 and TNF were

accumulated every 2 – 3°C from the isotropic phase until no signal was observable at crystallisation. In order to ensure that the experiment was comparable to the previous experiments TNF-d_5 was used in the equimolar mixtures. This also allowed us to get a measure of the order parameter, S_{zz}. The much larger quadrupolar splitting of the TNF-d_5 compared to the α-C10SD-d_2 can be seen in figure 3.8. As was expected the quadrupolar splitting is small and showed a strong temperature dependence in the N_C phase, with the splitting rising from only 470 Hz at T_{NI} (162°C) to 1910 Hz at $T_{NI} - T = 30°C$ (132°C) at the $N_C - Col_{ho}$ phase transition. At this transition there is a discontinuous rise in the splitting, changing to 3500 Hz and subsequently rising to 4230 Hz, where there is a first order transition at $T_{NI} - T = 74°C$ (88°C) to the Col_I phase, where the splitting is approximately 5820 Hz.

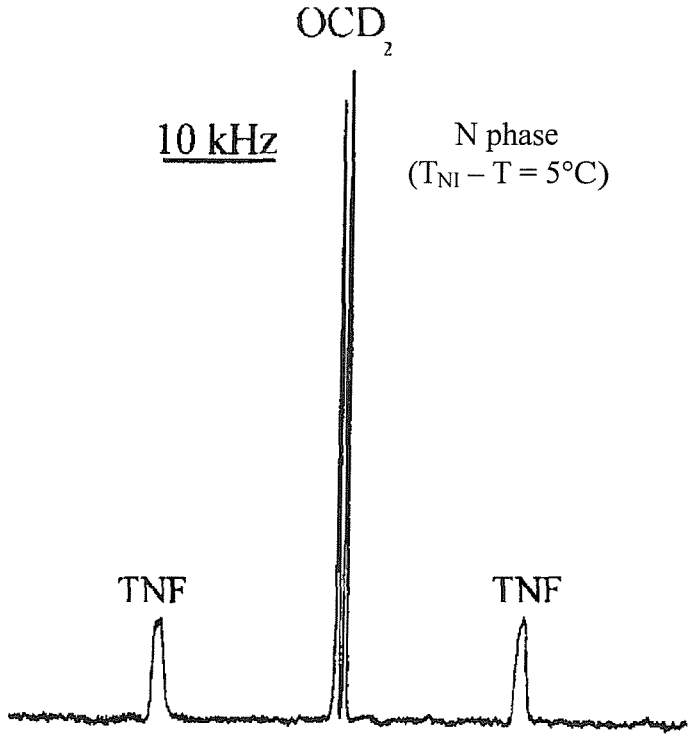

Figure 3.8 : Deuterium NMR spectra of an equimolar mixture of α-C10SD-d_2 and TNF-d_5.

Figure 3.9 shows the quadrupolar splittings for both the α-C10SD-d_2 and the ArO-CD_2-R deuterons of the chain deuteriated C10SD-d_{21}. The match in the Col_{ho} phase is good which indicates that the assignment of the α-deuterons in the chain deuteriated case is correct, however it does not appear to be so good in the N_C phase. As the temperature approaches T_{NI} the agreement becomes worse, with the

α-C10SD-d_2 deuterons having a smaller splitting than that measured for the chain deuteriated C10SD-d_{21}. However this is not that surprising, as the measurement of the quadrupolar splitting from the chain deuteriated C10SD-d_{21} is not easy because of the neighbouring methyl deuteron peaks obscuring the peaks whose quadrupolar splitting is being measured, whereas for the specifically deuteriated material this clearly is not a problem.

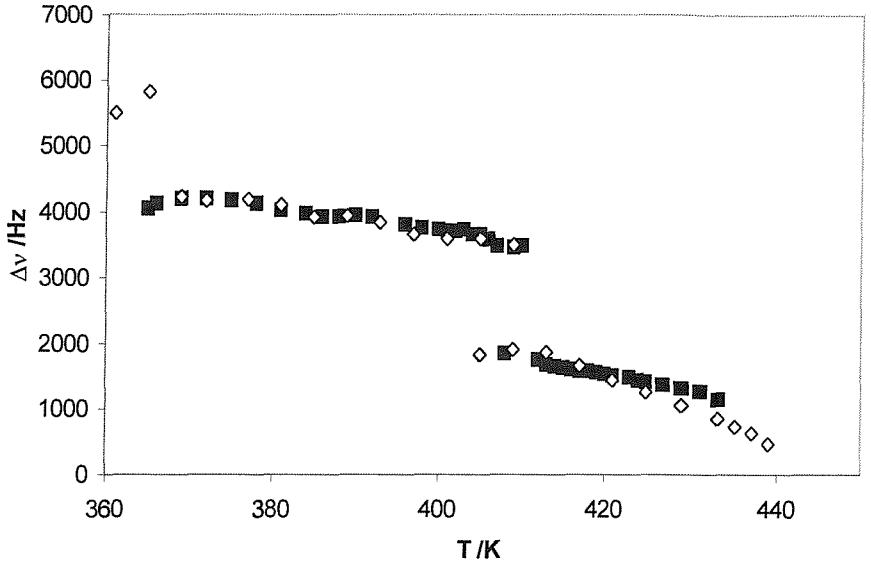

Figure 3.9 : The quadrupolar splitting for an equimolar mixture of α-C10SD-d_2 (◇) and TNF, compared with the ArO-CD_2-R splitting (■) from an equimolar mixture of chain deuteriated C10SD-d_{21}.

From these results we can conclude that the assignment of the ArO-CD_2-R deuterons is correct, and that these have the lowest orientational order parameter $|S_{CD}|$ of the all the deuterons in the alkyl chain in the N_C phase, and the second lowest in the Col_{ho} phase. In the next section we will consider very briefly an explanation as to why this is the case, based on the conformation adopted by the alkyl chain. The assignment of the ArO-CD_2-R deuterons is more difficult in the Col_1 phase because of the poor resolution caused by the larger line widths.

3.3.4 The Modelling of the Alkyl Chain in the C10SD/TNF System

In an attempt to explain the unusually small quadrupolar splitting, the dihedral angle made by the alkyl chain to the molecular plane of the discotic core was modelled using a modelling program based on the Emsley-Luckhurst-Stockley (ELS) theory [7] written by Dr. Roskilly [8] and Dr. Emerson [9]. C10SD was also

minimised using Biosym's Discover and InsightII molecular mechanics packages to obtain a reasonable starting point for the ELS calculations. This section will essentially describe only the results obtained by this approach and for a more in-depth study the following references should be consulted [1].

For calamitic liquid crystals the core is usually, to a good approximation, taken to be axially symmetric about the principle axis, z, and therefore the dihedral angle made with the C-C_{ar}-O-C_α atoms does not need to be considered, as the orientational order parameter along the chain has no dependence on this dihedral angle because of the symmetry. However, in discotic liquid crystals this no longer the case, as shown in figure 3.10, and the value of this dihedral angle should affect the value of $|S_{CD}|$ calculated. For the THEn [5] homologues it has been shown experimentally that the O-C_α bond lies in a plane perpendicular to the molecular plane of the discotic core i.e. the dihedral angle is 90° [5,10]. It was with this value that the ELS theory was shown to be successful in matching the order parameters of the chain [11].

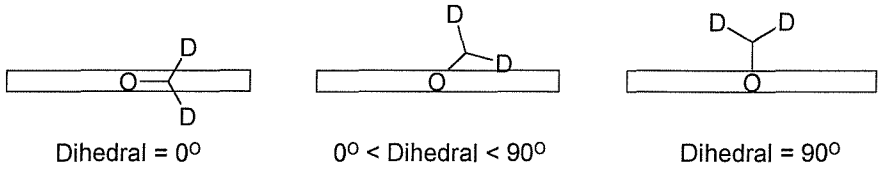

Figure 3.10 : The effect the dihedral angle has on the orientation of a C-D bond with respect to the core of the disc.

By modelling C10SD using Discover, the minimised structure showed the dihedral angle to be 90°, however, when this value was used in the ELS theory modelling program, the match of the observed order parameter profile of the chain was not a good fit when compared with the order parameter profile of the chain determined using the T_1 relaxation times of the chain [1]. By assuming the dihedral angle C-C_{ar}-O-C_α to be somewhere between 50° and 70° the unusual alternation of $|S_{CD}|$ with the α-deuterons having the smallest quadrupolar splitting and the β-deuterons having the largest and so on, as shown by the relaxation experiments, can be accounted for. Although it is unreasonable to expect the dihedral angle to have a fixed value, and indeed it was found that the best fits to the experimental data came

when a weighted average of dihedral angles was used, the ELS theory suggested that the best fit came when the dihedral angle had an average value of 58°. Therefore, we can say that is actually the geometry of the chain that leads to the unusually small quadrupolar splitting and not a consequence of the α-deuterons being more disordered than the rest of the chain. Also, the value of this dihedral angle may have a consequence on the packing of the disc-rod dimers studied in Chapter 6.

3.3.5 The Nature of the Col_1 Phase

The nature of the Col_1 phase remains uncharacterised by X-ray diffraction, however the NMR results allow us to speculate on its possible structure. The first thing to note about this phase is that it is monotropic and, as shown in the previous Chapter, only forms on cooling those homologues where there is a Col_{ho} phase formed for concentrations of TNF greater than around 50mol%, and appears to be more stable at higher TNF concentrations, up to around 60mol%. This would suggest that the phase is stable when there is a small molar excess of TNF present in the mixture, but becomes thermodynamically unstable when the excess of TNF becomes too great. Secondly, the Col_{ho} - Col_1 transition is first order, but with small entropies of transtion, $\Delta S/R$ being around 0.4. This would make it unlikely that the phase is a columnar rectangular phase, as this transition has been considered to be second order [12]. However, it has also been shown that the Col_{ho} - Col_{hd} phase transition should be first order [13,14,15] but optical texture of these systems are not consistent with this possibility.

More unusually, though, is the inability for the TNF-d_5 to give any signal in the Col_1 phase, when deuteriated C10SD does in fact show a quadrupolar splitting in this phase. This would suggest that the molecular motion of the TNF has slowed down considerably, while the averaging process for the deuterons in C10SD are still rotating quite quickly. As there is no appearance of a small isotropic peak at the Col_{ho} - Col_1 phase transition, while there is at the N_C - Col_{ho}, due the squeezing out of TNF from the columns during the molecular rearrangement, it seems that the Col_{ho} and Col_1 phase are structurally similar, as the phase does not require a major molecular reorganisation.

Therefore it would seem that the Col_1 phase is probably hexagonal in nature, but possessing more orientational order than the Col_{ho} phase, where the molecular motion of the columns is somewhat different.

3.4 Conclusions

In order to understand the nature of the Col_1 phase exhibited by equimolar mixtures of the 'Superdiscs', (C*n*SD), where *n* is between 6 and 10 carbon atoms, and TNF, deuterium NMR spectroscopic studies have been carried out on a number of deuteriated materials. In particular the studies have looked at equimolar mixtures of C10SD and TNF-d_5, chain deuteriated C10SD-d_{21} and TNF, and the specifically deuteriated C10SD-d_2 and TNF.

In the process of the investigations of an equimolar mixture of chain deuteriated C10SD-d_{21} and TNF it appeared that, in the nematic phase, the α-deuterons had the lowest order of all the deuterons in the chain, and the second lowest orientational order in the Col_{ho}. As it is expected that the deuterons nearest the mesogenic core should have the highest order of all the chain deuterons we prepared C10SD-d_2 specifically deuteriated at the α-position, to confirm our assignment of the chain deuteriated material. Our assignment was indeed correct and in an attempt to explain this unusual result we modelled the conformation the chain makes with the plane of the discotic core, and in particular the dihedral angle made by the chain to the molecular plane of the discotic core. We have found that by taking the dihedral angle C-C_{ar}-O-C_α to be somewhere between 50° and 70° we can match the order parameter profile of the chain and explain the anomalously low order seen for the α-deuterons. This shows that alkyl chain does not lie within the plane of the disc, but it does not lie totally out of the plane of the disc because of steric interactions.

The studies of an equimolar mixture of α-C10SD-d_2 and TNF-d_5 have shown that in the Col_1 phase that whilst there is a signal from the α-C10SD-d_2 deuterons, there is no signal observed from the TNF deuterons. This would suggest that the molecular motion of the TNF molecules has slowed down considerably. It is suggested that the phase is probably hexagonal in nature, however to confirm this we would need to carry out some X-ray scattering experiments.

3.5 References

[1] Tearle, W.M., *Ph.D Thesis, University of Souhampton*, (1995).

[2] Duer, M.J., *J. Chem. Soc. Faraday Trans.*, **89**, 823, (1993).

[3] Veracini, C.A., '*Nuclear Magnetic Resonance of Liquid Crystals*', Ed. Emsley, J.W., Reidel, Dordrecht, (1985).

[4] Duer, M.J., *J. Chem. Soc., Faraday Trans.*, **89**, 823, (1993).

[5] Goldfarb, D., Luz, Z. and Zimmermann, H., *J. Chem. Phys.*, **78**, 7065, (1983).

[6] Emsley, J.W., Foord, E.K., Gandy, P.J.F., Turner, D.L. and Zimmermann, H., *Liq. Cryst.*, **17**, 303, (1994).

[7] Emsley, J.W., Luckhurst, G.R. and Stockley, C.P., *Mol.Phys.*, **44**, 565, (1981).

[8] Roskilly, S., *Ph.D. Thesis, University of Southampton*, (1994).

[9] Emerson, A.P.J., *Ph.D. Thesis, University of Southampton*, (1991).

[10] Cotrait, M., Marsau, P., Pesquer, M. and Volpilhac, V., *J. Phys. (Paris)*, **43**, 355, (1982)

[11] Cheng, G.Q. and Dong, R.Y., *J. Chem. Phys.*, **89**, 3308, (1989).

[12] Destrade, C., Foucher, P., Gasparoux, H., Tihn, N.H., Levelut, A.M. and Malthete, J., *Mol. Cryst. Liq. Cryst.*, **106**, 121, (1984).

[13] Kohne, B., Poules, W. and Praefcke, K., *Chem. Ziet.*, **108**, 113, (1984).

[14] Fontes, E., Heiney, P.A. and de Jeu, W.H., *Phys. Rev. Lett.*, **61**, 1202, (1988).

[15] Gramsbergen, E.F., Hoving, H.J., de Jeu, W.H., Praefcke, K. and Kohne, B., *Liq. Cryst.*, **1**, 397, (1986).

CHAPTER FOUR

LIQUID CRYSTALS WITH NON-MESOGENIC TERMINAL GROUPS

4.1 Introduction

We have already established in the Introduction (§1.12.1) that for an homologous series of liquid crystalline materials, in which the flexible alkyl chain is varied, there is an odd-even effect in the thermodynamic properties at the nematic to isotropic transition. This effect is especially pronounced for a series of dimeric liquid crystals [1] and is attributed, in the first instance, to the movement on and off axis of one of the mesogenic units with respect to the other. There are, however, other examples of materials in which there is a similarly large alternation in the clearing temperature. These materials usually consist of a mesogenic unit to which is attached a flexible alkyl chain terminated not by a methyl group, as for conventional monomeric materials, but a larger, bulky group, often a phenyl ring [2]. As can be seen, if the bulky terminal group is itself a mesogenic unit then we have a conventional dimeric liquid crystal, otherwise these materials are structurally intermediate between monomers and dimers.

Gray *et al.* [3,4,5] have carried out detailed investigations of the phenyl and ω-phenylalkyl 4-(4'-substituted-benzylideneamino)cinnamates, that is

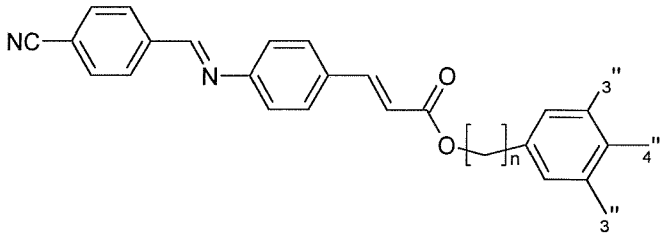

These materials showed a very pronounced alternation in the nematic to isotropic transition temperature upon increasing the length of the alkyl chain as well as an apparent attenuation of the transition temperatures. This is illustrated for the ω-phenylalkyl 4-(4'-cyanobenzylidineamino)cinnamates in figure 4.1 and is clearly similar to that seen for dimers.

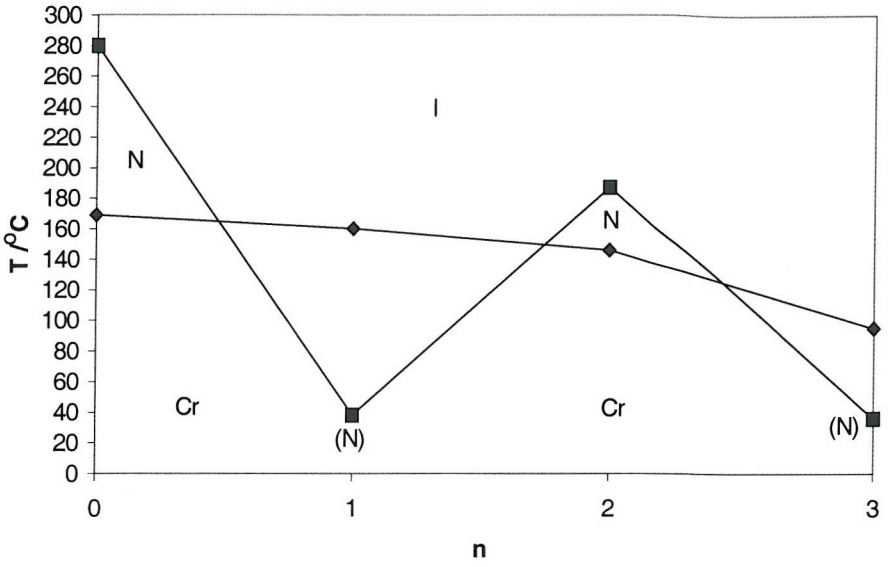

Figure 4.1 : Transition temperatures for a series of ω-phenylalkyl 4-(4'-cyanobenzylidineamino)cinnamates [4], as the number of carbon atoms, n, in the alkyl chain is increased, ■ N – I, ◆ Cr – N or I.

This behaviour was attributed to the possibility that the terminal phenyl ring moves in and out of line with the molecular long axis of the rest of the molecule as the number of atoms in the chain alternates from odd to even [4]. Thus, it can be seen in figure 4.2 molecules with an even number of atoms in the flexible chain are essentially linear, even with the introduction of gauche links. However,

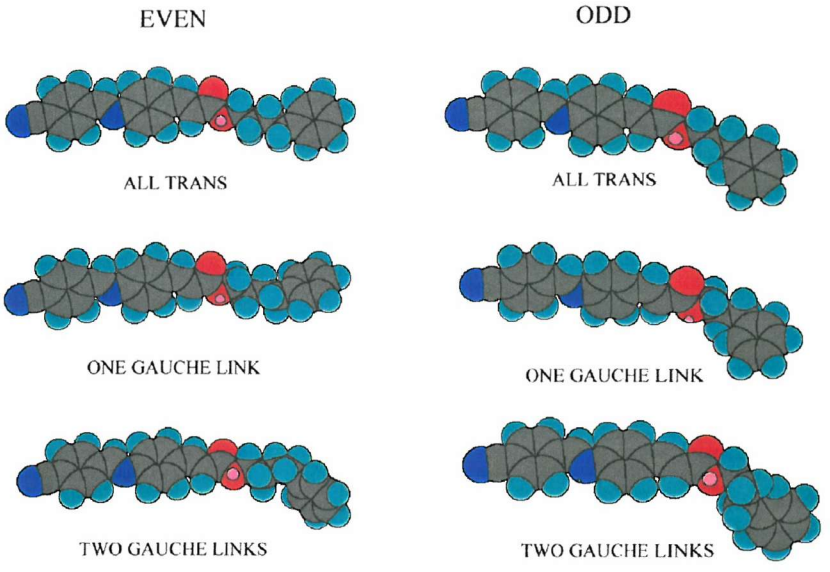

Figure 4.2 : Comparison of the conformations of the odd and even members of the ω-phenylalkyl 4-(4'-cyanobenzylidineamino)cinnamates.

molecules with an odd number of atoms in the chain tend to take on a bent conformation, with some conformers being almost L-shaped in appearance.

To test the idea that the large alternation in the clearing temperatures was due to the movement of the smaller terminal group on and off the long axis of the rest of the molecule Gray *et al.* [4,5] synthesised esters containing 4''-chloro, 4''-methyl, 3''-chloro and 3''-methyl substituents on the terminal phenyl ring (the positions are shown in figure 4.1). It was found that for molecules with an even number of atoms in the chain, substitution in the 4''-position enhanced the stability of the nematic phase, or in other words, increased the nematic to isotropic transition temperature. This is consistent with an increase in the length-to-breadth ratio of the molecule caused by the methyl or chloro terminal substituent. For chains with an odd number of atoms, substitution in the 4''-position diminishes the stability of the nematic phase, in comparison with the unsubstituted molecule. Here, the length-to-breadth ratio of the molecule is decreased because the methyl or chloro substituents broaden the molecule as the phenyl ring already lies off the long molecular axis. Both these views are analogous to the all-*trans* conformations of the analogues shown in figure 4.2.

For substitution in the 3''-position it was noted [4] that if there is rotation about the O-ring or CH_2-ring bonds then there are two extreme positions that can be adopted by the 3''-substituents when the ring is co-planar with the rest of the molecule, for both even and odd chain lengths. The nematic – isotropic transition is lowered in temperature for even chain lengths as the methyl or chloro substituent has the effect of broadening the molecule irrespective of which 3''-position the substituent adopts, as shown in figure 4.3. When the chain has an odd number of atoms the situation is not so clear cut. It was found [4] that in three of the examples the stability of the nematic phase was diminished, whereas in one case the stability was actually increased. From figure 4.3 it can be seen that one substitution in one 3''-position will have a different effect from the other; one will increase the length-to-breadth ratio of the molecule, so increasing the stability of the nematic phase, whereas the other position will decrease the length to breadth ratio, reducing the phase stability. This lack of consistency in the position adopted by the 3''-substituent independent of the substituent and length of the odd chain led Gray to

comment that there appears to be no free rotation about the CH_2-ring bond occurring in the nematic phase.

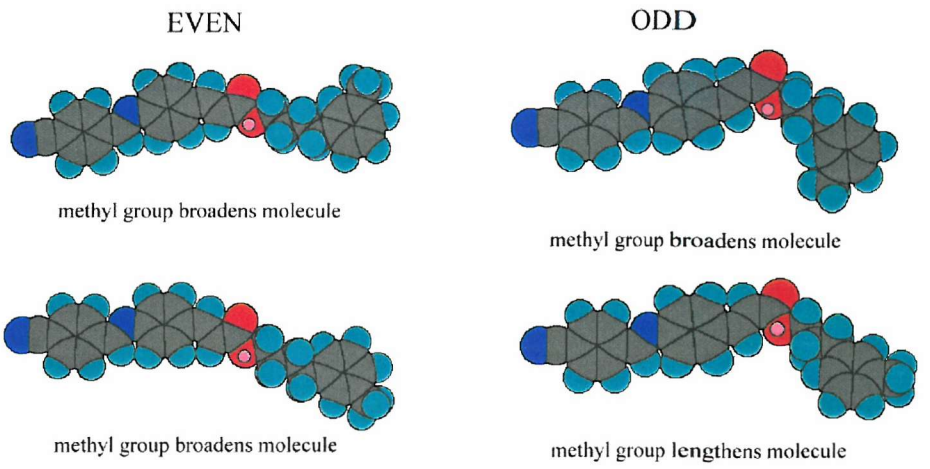

Figure 4.3 : Showing the effect substitution in the 3''-position has on the length to breadth ratio of a molecule

Although we have seen that these materials, which are structurally intermediate between monomers and dimers, mimic dimers in the large alternation of the clearing temperature, of the order of 200°C, upon varying the parity of the spacer, it has not been established whether there is a similarly large alternation in the entropy change at the nematic – isotropic transition. However, work by Ennulat and Brown [6] reported both the transition temperatures and entropies for a series of cholesteryl ω-phenylalkanoates. As can be seen in figure 4.4 there is a large alternation in the chiral nematic – isotropic transition temperature on varying the length of the alkyl chain. The alternation appears to attenuate with increasing chain length which is analogous to the behaviour of dimeric materials. The transitional entropies, shown in figure 4.5, also display a large odd-even alternation of around 1.7, which again mimics the behaviour of dimeric compounds. It should also be noted that the even members have a higher entropy change than the corresponding cholesteryl alkanoates, which strengthens the argument that these materials are intermediate between monomers and dimers.

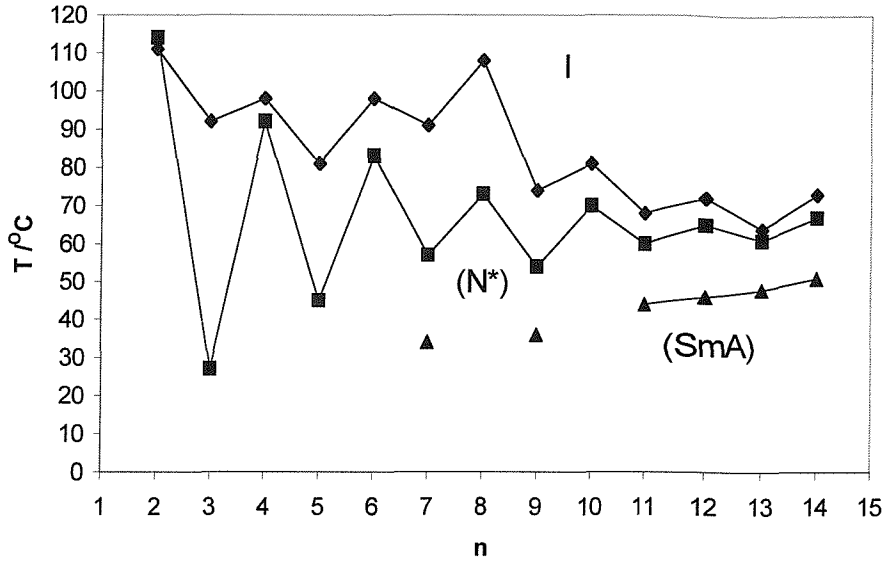

Figure 4.4 : Transition temperatures for a series of cholesteryl ω-phenylalkanoates as the number of carbon atoms, n, in the alkyl chain is increased [6].
◆ Cr – I, ■ N* – I, ▲ SmA – N*.

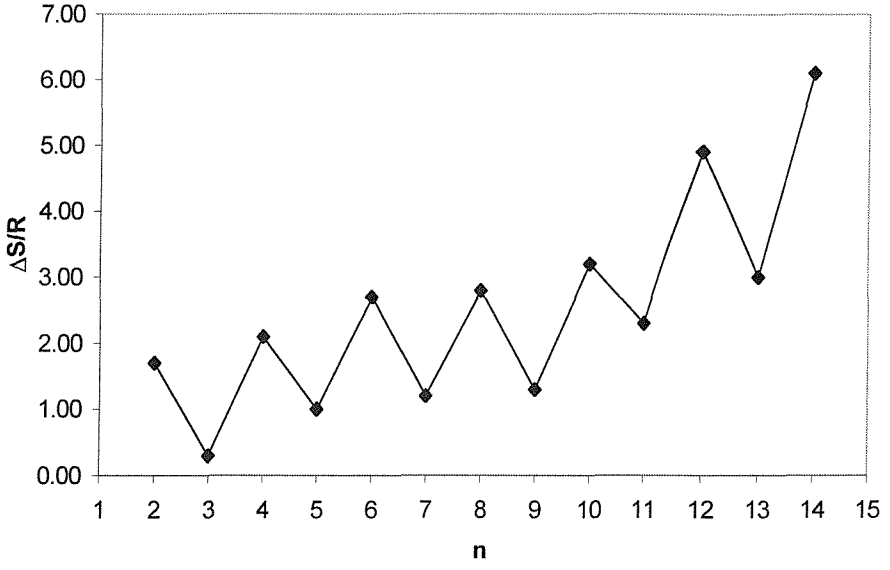

Figure 4.5 : Entropies associated with the chiral nematic – isotropic transition for a series of cholesteryl ω-phenylalkanoates as the number of carbon atoms, n, is increased [6].

In an attempt to assess the effect that small terminal non-mesogenic groups have on the mesophase stability of these intermediate group of compounds Imrie [7] prepared a series of compounds of the form:

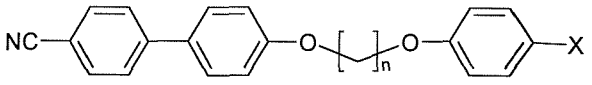

X = H : n = 2 to 6
X = CN, CHO, Ph : n = 3 to 6

These materials were chosen because they represent intermediate structures between the α,ω-bis(4'-cyanobiphenyl-4-yloxy)alkanes [1] and the 4-*n*-alkyloxy-4'-cyanobiphenyls [8], and thus easy comparisons could be made as both these series have been well studied.

It was found that all four series had properties intermediate between that of the monomer and dimer, as shown in figure 4.6.

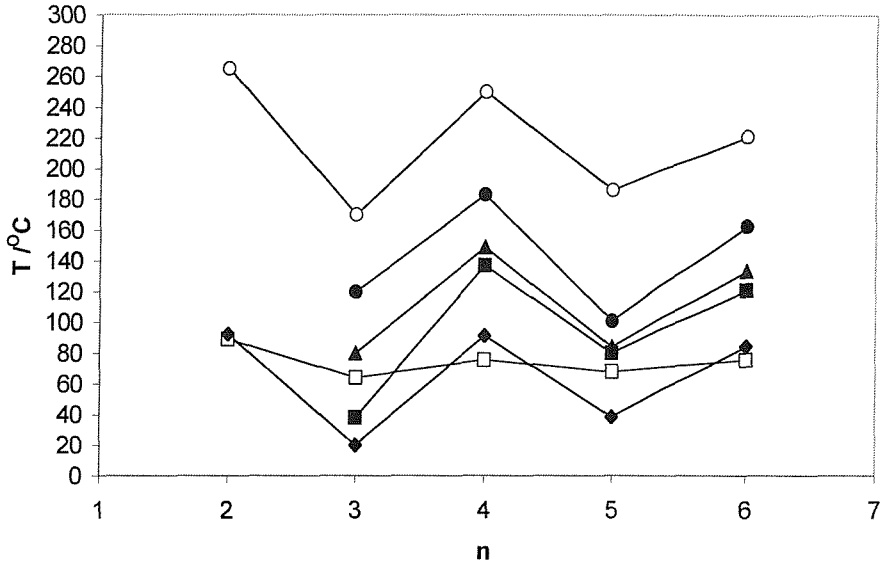

Figure 4.6 : The nematic – isotropic transition temperatures for the series compounds studied by Imrie [7] as the number of carbon atoms, n, in the alkyl chain is increased. X = H (◆), CN (▲), CHO (■) and Ph (●), in comparison with the nOCB's (□) And the CBOnOCB's (○).

Apart from the obvious dependence of the nematic – isotropic transition temperatures on the length of the alkyl chain, it is apparent from figure 4.6 that the efficiency of the 4-substituent in increasing the thermal stability of the nematic

phase for both the odd and even membered compounds is:

$$PhCN > Ph > CN > CHO > H$$

This is in accord with that generally observed for terminal substituents in monomeric liquid crystals [9]. It may be assumed, therefore, that the chloro-substituent, as seen in Gray's materials, occupies a position lower in the list than the CHO group, with the methyl group being lower than the chloro group, but both being higher in the list than the proton. The increase for both the odd and even members is in conflict with the findings by Gray for the 4''-substituted-ω-phenylalkyl 4-(4'-cyanobenzylideneamino)cinnamates [4,5] where the 4''-substituent was found to lower the nematic to isotropic transition temperature for odd members. It was argued that this was due to the size and polarisability of the terminal substituent. The methyl and chloro substituents are small and only conjugate weakly with the phenyl ring, whereas the PhCN, Ph, CN, and CHO groups are readily polarisable and interact strongly with the phenyl ring thus making a larger contribution to the anisotropic properties of the molecule, such as the anisotropy in the polarisability. For the methyl and chloro substituents the increase in the molecular volume outweighs the interaction of the terminal group with the molecular field and therefore there is destabilisation of the nematic phase for the odd members. However, the interaction of the readily polarisable Ph, CN and CHO groups with the molecular field more than offsets the increase in molecular volume thereby increasing the thermal stability of the nematic phases for both the odd and even members.

To explore further the idea that the substitution of easily polarisable groups onto the non-mesogenic moiety of these intermediate materials can, in fact, have a large bearing on the mesogenic properties we have synthesised several series of compounds in which the position of a cyano group is varied around the phenyl ring of the non-mesogenic moiety thus:-

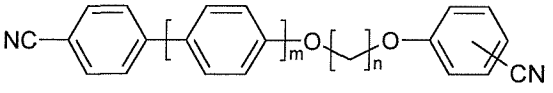

m = 1 or 2, n= 3 to 12

This particular set of compounds was chosen for a number of reasons. First, the α-(4-cyanobiphenyl-4'-yloxy)-ω-(*x*-cyanophen-4-yloxy)alkanes (CBOnO*x*CP's) (**15, 16**), where the *x* denotes the substitution of the cyano group around the phenyl ring, can be directly compared to the α-(4-cyanobiphenyl-4'-yloxy)-ω-(4-cyanophenyloxy)alkanes prepared by Imrie [7]. Also a comparison can be made with the materials prepared by Gray [4,5] in which there is a methyl or chloro group substituted in the 3''-position of the ω-phenylalkyl 4-(4'-substituted-benzylideneamino)cinnamates. Finally, these particular materials are intermediate between that of the nOCB's [8] and the BCBO-n's / CBOnOCB's [1].

The α-(4-cyanoterphenyl-4''-yloxy)-ω-(*x*-cyanophen-4-yloxy)alkanes (CTOnO*x*CP's) (**19,20**) were chosen for a number of reasons. The low stability of the nematic phase exhibited by the α-(4-cyanobiphenyl-4'-yloxy)-ω-(4-cyanophen-4-yloxy)alkanes prepared by Imrie [7] – the even members having a nematic range of only a few degrees, and the odd members showing substantial monotropic behaviour – suggests that the related CBOnO*x*CP's may also exhibit a similarly poor nematic phase stability and thus prove difficult to study. For the terphenyl materials this problem should be avoided. Studies on the 4-*n*-alkyl-4''-cyanoterphenyls (nCT's) [10] and the 4-*n*-alkyloxy-4''-cyanoterphenyls (nOCT's) [11] show these materials to have large nematic ranges of around 100°C. It would be expected, therefore, that the CTOnO*x*CP's should also have relatively large mesophase ranges making characterisation easier. Also, it would be interesting to see if the small size of the cyanophenyl group affects the behaviour of the significantly larger cyanoterphenyl moiety less than the somewhat smaller cyanobiphenyl moiety. Finally, comparisons of these intermediate materials can be made not only with the nOCT's, the α-(4-cyanoterphenyl-4''-oxy)-ω-(4-cyanophenyloxy)alkanes (CTOnO4CP's) and the α,ω-bis(4-cyanoterphenyl-4''-oxy)alkanes (n-BCTO's / CTOnOCT's), but also with the α-(4-cyanoterphenyl-4''-oxy)-ω-(4-cyanobiphenyl-4'-oxy)alkanes (CTOnOCB's) which possess a large cyanoterphenyl moiety joined via an ether linked flexible chain to a cyanobiphenyl moiety.

4.2 Results and Discussion

4.2.1 The CBOnO2CP Series

The transitional properties of the CBOnO2CP series are given in table 4.1. These values, and all other subsequent values presented in this Chapter were determined using a combination of optical microscopy and differential scanning calorimetry (DSC). It can be seen that not all the materials prepared show a liquid crystalline phase, and those homologues that do, exhibit only a monotropic phase. This monotropic phase is a nematic phase and was assigned on the basis of the schlieren texture observed when viewed under the polarising optical microscope. In addition, the phase was highly mobile and flashed when subjected to mechanical stress. An example of the schlieren texture exhibited by the CBO4O2CP homologue is shown in figure 4.9. It is readily apparent from figure 4.7 that only the even members of the series show a monotropic nematic phase, apart from the undecyl (C11) homologue that also exhibits a monotropic nematic phase. The melting points do not show any apparent regular dependence on the length of the flexible spacer apart from a steady decrease as the chain length is increased. Since only the even homologues, and the C11 homologue, exhibit a liquid crystalline phase it is not possible to determine whether there is any odd-even effect in the nematic – isotropic transition temperatures, although the transition temperature of the C11 homologue seems to indicate that there may only be an small odd-even dependence. Despite this, it is clear that there is very little difference between the transition temperatures for those members that exhibit a nematic phase, there being no greater than 11°C difference between the lowest transition temperature (C8, 57°C) and the highest transition temperature (C4, 68°C).

A solution to the problem of determining whether any of the odd members of this series show any mesogenic behaviour is to cool small droplets of the material on a microscope slide in the absence of a cover slip and observe any transitions that take place. The lack of the cover slip may aid supercooling and therefore a mesophase may be seen at a lower temperature than the crystallisation point, when observed under the optical microscope. Unfortunately, the cooling of droplets of the odd members did not reveal any mesophases as the materials crystallised before any mesophase transition was observed.

Table 4.1 : Transition temperatures of the CBOnO2CP series

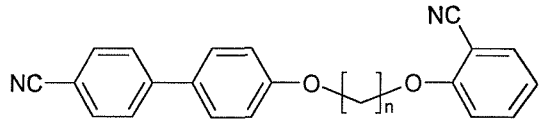

	Transition temperatures / °C				
n	Cr		N		I
3	•	159	•		•
4	•	112	(•	68)	•
5	•	115	•		•
6	•	102	(•	58)	•
7	•	92	•		•
8	•	96	(•	58)	•
9	•	80	•		•
10	•	75	(•	63)	•
11	•	72	(•	53)	•
12	•	67	(•	58)	•

Parentheses denote a monotropic transition.

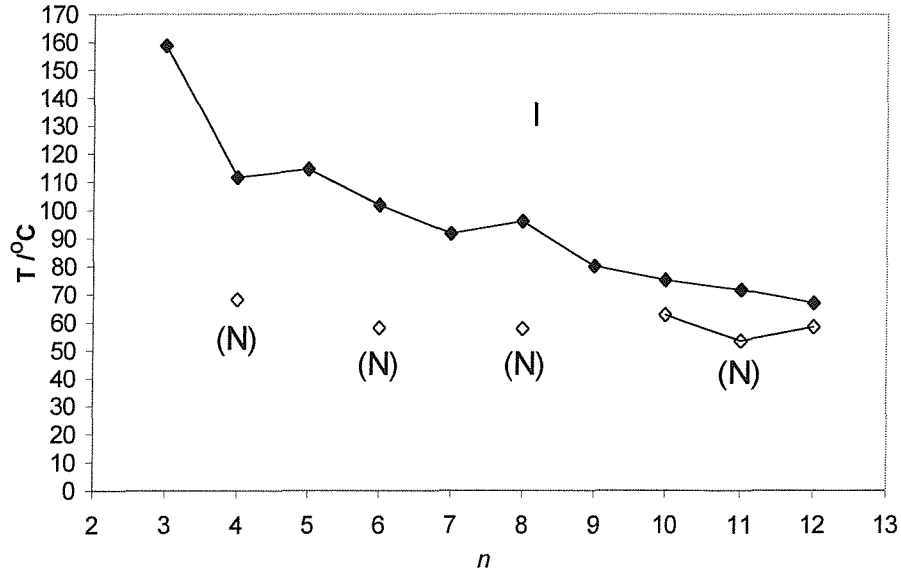

Figure 4.7 : Transition temperatures of the CBOnO2CP series as the number of carbon atoms, n, in the alkyl chain is increased. ◆ Cr – I, ◇ N – I.

Table 4.2 : Transition entropies for the CBOnO2CP series

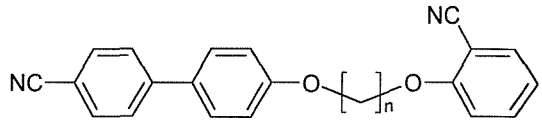

	Transition entropies, ΔS/R				
n	Cr		N		I
3	•	10.26	•		•
4	•	7.57	(•	0.23)	•
5	•	10.95	•		•
6	•	11.22	(•	0.53)	•
7	•	12.81	•		•
8	•	11.85	(•	*)	•
9	•	15.74	•		•
10	•	8.80	(•	0.55)	•
11	•	14.79	(•	0.28)	•
12	•	15.22	(•	0.96)	•

Parentheses denote a monotropic transition

* transition entropy unobtainable

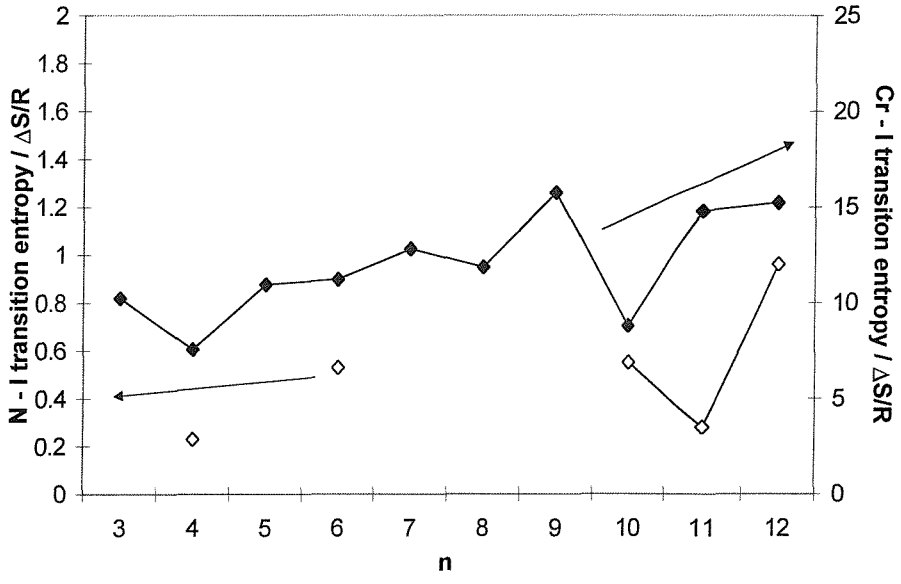

Figure 4.8 : Transitional entropies of the CBOnO2CP series as the number of carbon atoms, n, in the alkyl chain is increased. ◆ Cr – I, ◇ N – I.

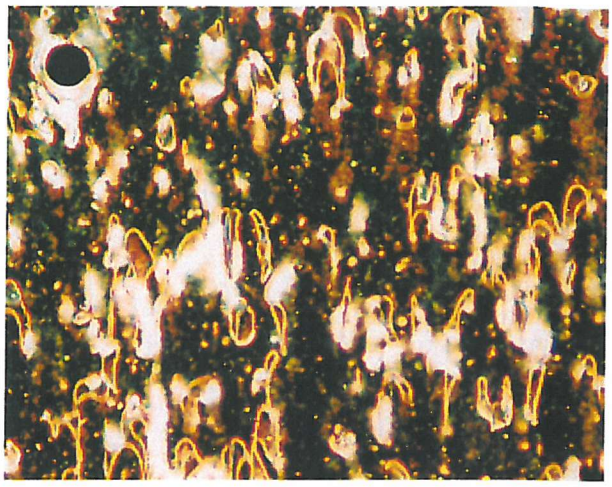

Figure 4.9 : Nematic texture exhibited by CBO4O2CP at 55°C (magnification x100).

Figure 4.10 : Glassy texture exhibited by CBO4O2CP at 25°C (magnification x100).

For the materials containing 4 or 6 carbon atoms in the spacer chain, it becomes evident that they do not crystallise immediately even on cooling to room temperature. This is indicated by the lack of a peak below the monotropic transition temperature during the cooling scan on the DSC trace. When viewed under the optical microscope the schlieren texture becomes brighter and lines appear across the viewing area; this can be seen for the CBO4O2CP homologue in figure 4.10. The phase also becomes extremely viscous. It may be argued that this is in fact a transition to a nematic glass, although the expected second order glass transition is not seen on the DSC trace, however glass transitions are not always easily seen by DSC. The lifetimes of these glassy phases vary, with slow crystallisation occurring within a matter of hours, or the glass sometimes persisting

for a day or two. Also, when these glassy phases are heated the materials crystallise first and then melt into the isotropic phase.

Figure 4.8 shows the dependence of the entropy associated with both the crystal – isotropic transition and the nematic – isotropic transition on the length of the flexible alkyl chain spacer. Unfortunately the data for the nematic – isotropic transition is somewhat sparse since only the even members show any mesophase behaviour, and this is compounded by the fact that an entropy value for the C8 homologue could not be ascertained from the DSC trace. Despite this, there appears to be a slow rise in the entropies as the chain length is increased. This is consistent with the steady rise seen for the even members of the α,ω-bis (4'-cyanobiphenyl-4-yloxy)alkanes (CBOnOCB's) [1]. As for the entropy associated with melting, there seems to be no regular dependence on the spacer length, although we could argue that the entropies appear to be lower for the even members of the series.

4.2.2 The CBOnO3CP Series

The transitional properties of the CBOnO3CP are listed in table 4.3, and are plotted in figure 4.11. As we found for the CBOnO2CP series the materials do not exhibit enantiotropic phases only monotropic phases, and of these only odd members, with the exception of the C3 homologue, show this monotropic phase. In addition the C12 homologue exhibits a monotropic phase. This phase is, again, assigned as a nematic, due to the highly mobile schlieren texture seen when viewed under the optical microscope. It is interesting to note that for this series of compounds the odd members are monotropic as opposed to the even members as seen for the CBOnO2CP series, the reasons for this will be discussed later in this Chapter.

The melting points for this series show an interesting dependence on length of the alkyl spacer chain. For those five members with the shortest spacer chain length, from the C3 to the C7 homologues, there is steady decrease in temperature of almost 80°C, and then a strong parity dependence, with the odd members having a melting point around 35°C higher than the even members, which may indicate a

Table 4.3 : Transition temperatures of the CBOnO3CP series

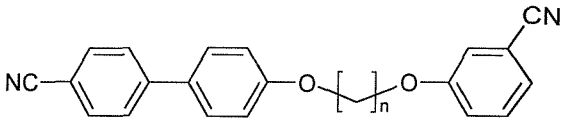

	Transition temperatures / °C				
N	Cr		N		I
3	•	143	•		•
4	•	119	•		•
5	•	101	(•	42)	•
6	•	93	•		•
7	•	70	(•	59)	•
8	•	106	•		•
9	•	80	(•	52)	•
10	•	112	(•	70*)	•
11	•	76	(•	61)	•
12	•	91	(•	62)	•

Parentheses denote a monotropic transition.

* transition temperature obtained from cooling isolated droplets

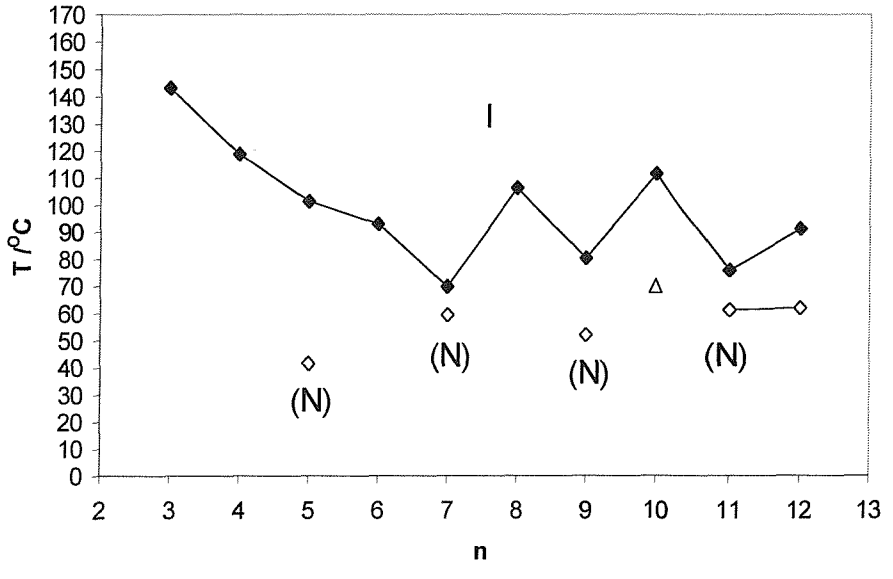

Figure 4.11 : Transition temperatures of the CBOnO3CP series as the number of carbon atoms, n, in the alkyl chain is increased. ◆ Cr – I, ◇ N – I.

Table 4.4 : Transition entropies of the CBOnO3CP series

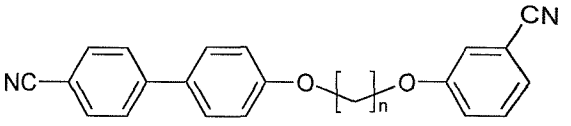

	Transition entropies, ΔS/R				
N	Cr		N		I
3	•	12.56	•		•
4	•	10.68	•		•
5	•	12.63	(•	0.40)	•
6	•	12.94	•		•
7	•	7.87	(•	0.39)	•
8	•	18.03	•		•
9	•	*	(•	0.38)	•
10	•	19.18	(•	*)	•
11	•	14.23	(•	0.53)	•
12	•	19.90	(•	0.79)	•

Parentheses denote a monotropic transition

* transition entropy unobtainable

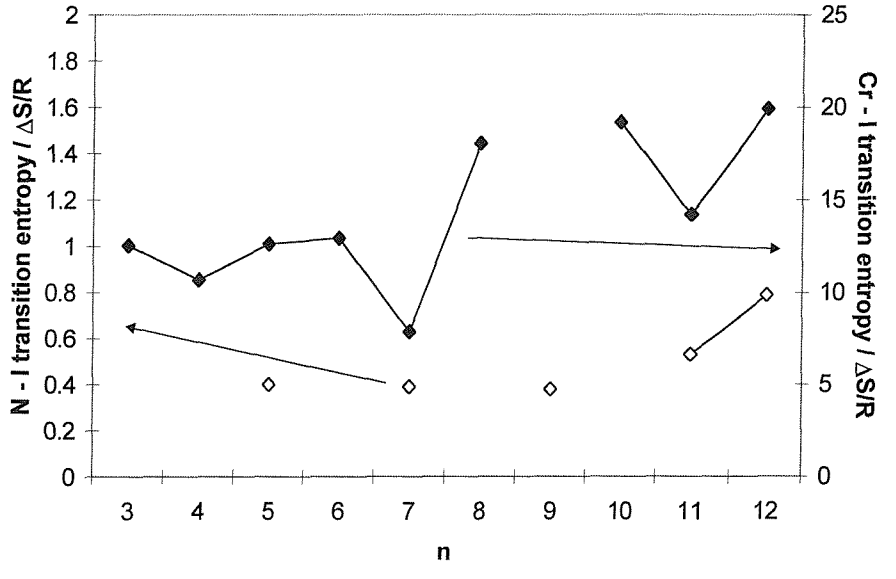

Figure 4.12 : Transitional entropies of the CBOnO3CP series as the number of carbon atoms, n, in the alkyl chain is increased. ◆ Cr – I, ◇ N – I.

change in way the materials pack in the crystal for longer chain lengths. As only the odd members, apart from the C3 homologue, show a liquid crystalline phase it is again not possible to establish whether there is any significant odd – even effect in nematic to isotropic transition temperatures. Although the C12 homologue exhibits a mesophase this provides very little extra information for determining the extent of any odd – even dependence however the cooling of droplets of the non-mesogenic members of the series did, this time, prove to be useful. The C10 member showed a nematic phase at about 70°C, which then crystallised about 1°C lower. This extra transition is included in figure 4.11. As can be clearly seen, this transition, and all of the other nematic to isotropic transitions, show very little variation in temperature with spacer length.

As we found for the CBOnO2CP series, those members possessing a short spacer chain and exhibiting a monotropic nematic phase, formed, on cooling, a highly viscous , almost glassy nematic phase. Similarly, the C5 and C7 homologue of this series also exhibit this highly viscous nematic phase. This was identified, again, by the dramatic increase in the viscosity of the phase and the slight brightening of the schlieren texture, although, again, no glass transition was seen on the DSC trace.

Figure 4.12 gives the entropies associated with both the crystal – isotropic and the nematic – isotropic transitions. It is readily apparent that the entropy change at the nematic – isotropic transition appears to be almost the same for each of the odd members, $\Delta S/R$ being around 0.4. This is in contrast to the behaviour seen for the CBOnOCB series, where there is a steady rise in the transitional entropies for the odd members, starting at 0.54 for the C3 homologue and rising to 1.27 for the C11 homologue, and the even members have a higher transitional entropy than the odd members. This behaviour is seen for the C12 homologue of the CBOnO3CP series. The melting point entropies appear to show no regular features upon increasing the spacer chain length.

4.2.3 Summary of the CBOnO*x*CP Series

If we compare the behaviour of the transition temperatures of the CBOnO2CP and the CBOnO3CP series, shown together with the CBOnO4CP series in figures 4.13 and 4.14 there are a number of interesting features.

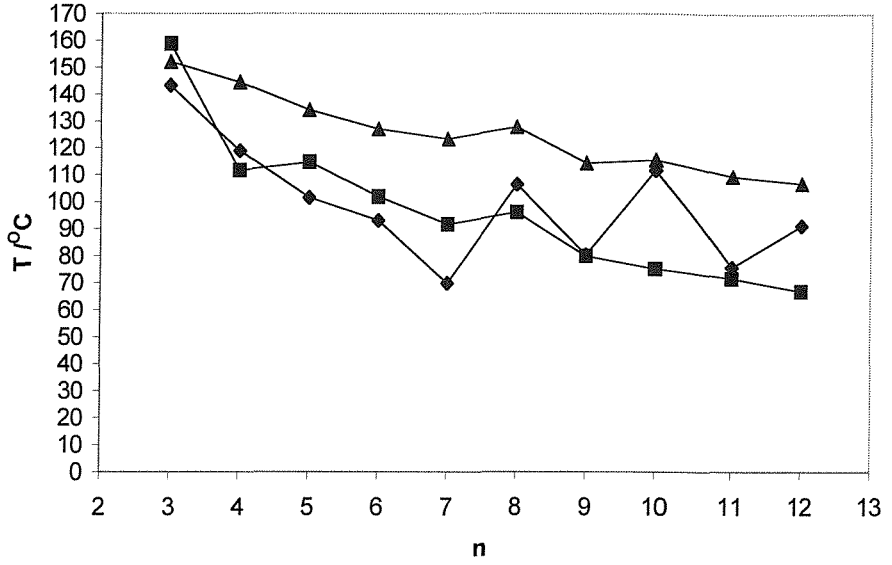

Figure 4.13 : Transition temperatures for the melting transition as the number of carbon atoms, n, in the alkyl chain is increased [11].
■ CBOnO2CP's, ◆ CBOnO3CP's, ▲ CBOnO4CP's.

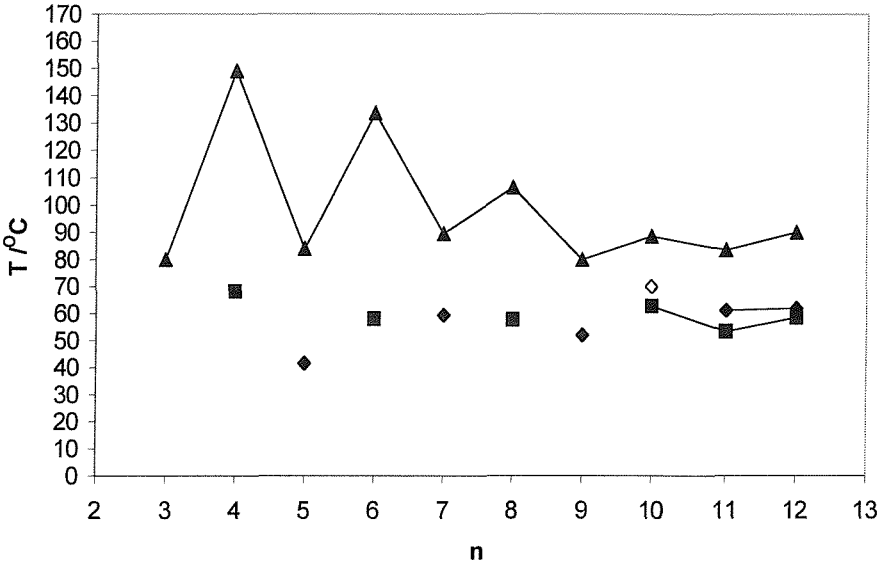

Figure 4.14 : Transition temperatures for the N – I transition as the number of carbon atoms, n, in the alkyl chain is increased [11].
■ CBOnO2CP's, ◆ CBOnO3CP's, ▲ CBOnO4CP's

First, there is the dependence of the melting points with increasing spacer chain length. As can be seen, there is, for both series, a steady decrease in temperature until the number of carbon atoms in the spacer chain becomes greater than seven, when the meta-substituted series shows a marked odd-even effect, whereas the ortho-substituted series continues to decline steadily. The para-substituted series shows an almost identical steady decrease in melting points as the ortho-substituted series. It is interesting to note that the nOCB's [8] show both an increase in the melting point temperature and an odd – even alternation opposite to that of the meta-series for chain lengths greater than seven carbon atoms, whereas the CBOnOCB's [1] show both a steady decrease and an odd – even alternation with the same trend as the meta-series for increasing chain lengths.

More interestingly, for the nematic – isotropic transition, if the ortho- and meta-substituted materials are considered together, it appears that, for increasing spacer chain lengths, this transition is linear in the length. Although it is obvious that the two series possess a different, if somewhat subtle, molecular structure, and that it is naïve to make such a comparison, this is an intriguing result. Indeed, if the transition temperatures of the compounds containing 10, 11 and 12 carbon atoms in the spacer chain of the two series are compared, then it appears that the transition temperatures of the two different compounds containing the same number of spacer chain carbons are in fact very similar. This seems to suggest that, if a mesophase was exhibited by the odd members of the ortho-series and the even members of the meta-series, then the transition temperature would be very close to that of the other series, i.e. we would expect, say, CBO9O2CP to have a nematic – isotropic transition temperature akin to that of CBO9O3CP, and likewise for any of the other materials. This seems to show that there is very little odd-even alternation in the nematic – isotropic transition temperatures, and, as can be seen in figure 4.15, when compared to either the nOCB's or the CBOnOCB's, that these materials behave more as monomers that dimers. Whether this is really the case will be discussed later in this Chapter. At this point it is interesting to note that the CBOnO4CP's, despite being structurally very similar to ortho- and meta-series, seem to behave more like the dimers than the monomers, having a large odd-even alternation in the nematic – isotropic transition temperature. Although the

transitions temperatures are somewhat lower, the relative alternation is larger than for the CBOnOCB's.

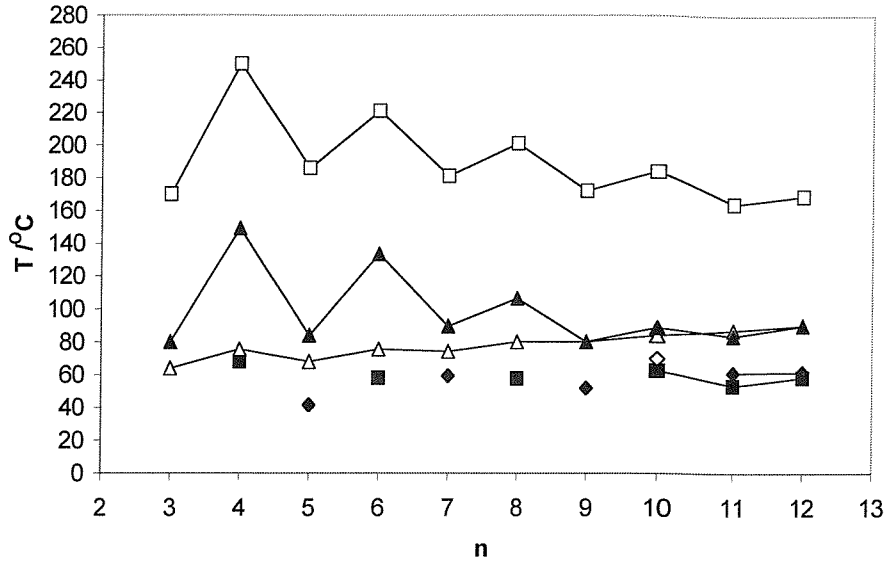

Figure 4.15 : Transition temperatures for the N – I transition as the number of carbon atoms, n, in the alkyl chain is increased.
■ CBOnO2CP's, ◆ CBOnO3CP's, ▲ CBOnO4CP's, △ nOCB's, □ CBOnOCB's.

If we now compare the entropies associated with the nematic – isotropic transition a similar phenomenon is not seen. As shown in figure 4.16 it appears this time that the ortho-series has a higher transitional entropy than the meta-series. Although when we compare these transitional entropies with the nematic – isotropic transitional entropies for the CBOnOCB's, as shown in figure 4.16, this is not a particularly surprising result. As is normally seen for an homologous series of liquid crystal dimers the even members have a significantly higher transitional entropy than the odd members. As, basically, only the even members of the CBOnO2CP's and the odd members of the CBOnO3CP's exhibit a mesophase it is not too surprising that the ortho-series appears to have higher transitional entropies. Indeed, for the longer spacer chain lengths this odd-even dependence becomes apparent, and it could be argued that the meta-series has a smaller odd-even alternation than the ortho-series. Whether this last statement holds true will be discussed later in this Chapter. Again it is interesting to note that the CBOnO4CP's appear to behave more like a true liquid crystal dimer than the other two series, having very similar transitional entropies to the CBOnOCB's for the even members of the series, especially for longer spacer chain lengths.

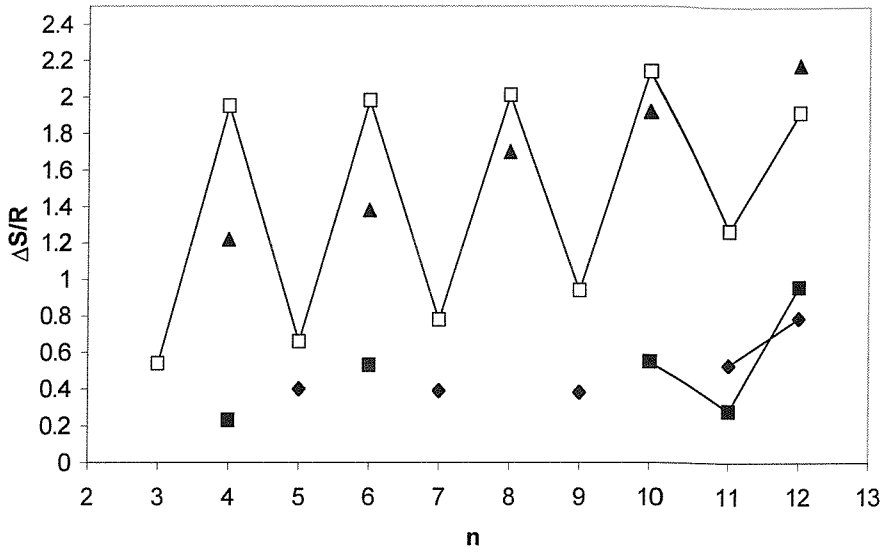

Figure 4.16 : The entropy change at the N – I transition as the number of carbon atoms, n, in the alkyl chain is increased.
■ CBOnO2CP's, ◆ CBOnO3CP's, ▲ CBOnO4CP's, □ CBOnOCB's.

4.2.4 The CTOnO2CP Series

The transitional properties of the CTOnO2CP series are presented in table 4. All the members of the series are mesogenic and exhibit enantiotropic phases, apart from the C3 homologue which has a monotropic nematic phase. The optical texture of the nematic phase, exhibited by all the members of the series, was homeotropic and therefore displayed no distinct features, although the sample flashed when subjected to mechanical stress. By shearing the phase, a schlieren texture was seen, but this quickly reverted to the homeotropic texture. For members of the series with seven or more carbon atoms in the alkyl spacer chain either a smectic A or smectic B phase is seen on cooling from the nematic phase, although the assignment of this phase is uncertain. When cooled from a nematic phase exhibiting a homeotropic texture the smectic A or smectic B phase also exhibits a homeotropic texture, but this time the phase does not flash when subjected to mechanical stress. Also, the entropies of transition (discussed later) seem to suggest that this phase is a smectic B. For members of the series with more than nine carbon atoms in the alkyl spacer chain a crystal E phase is seen on cooling from the smectic A/B phase. When cooled from the homeotropic smectic A/B phase the characteristic platelet texture is seen, shown in figure 4.19, which indicates that this is definitely a crystal E phase.

The dependence of the transition temperatures on the length of the spacer chain is shown in figure 4.17. It is immediately obvious that the nematic – isotropic transition shows an odd-even alternation upon increasing the spacer chain length, with the odd members having a lower transition temperature than the even members, and that this alternation attenuates as the chain length increases. Also, the stability of the nematic phase remains approximately constant, until the formation of the smectic A phase, at which point it slowly decreases. For spacer chain lengths of nine or more carbon atoms, when the crystal E phase appears, the smectic A/B – nematic transition temperature remains almost constant, while the stability of the smectic A/B phase appears to increase slowly as the nematic phase stability is reduced. Again, there does not seem to be a regular dependence of the melting points on the length of the spacer chain. An interesting feature seen by both DSC and optical microscopy is the lack of crystallisation upon cooling members of the series with more than seven carbon atoms in the spacer chain. Upon heating, the materials crystallise first before melting into either the smectic A/B or crystal E phase. We would expect the crystal E phase to have difficulty crystallising as this phase can be considered to be a 'soft crystal', but it is surprising that this behaviour is also seen for the smectic A/B phase of the C7 and C8 homologues.

Figure 4.18 shows the dependence of the entropies of transition with varying spacer chain length. The nematic – isotropic transitional entropies show a regular odd-even alternation, albeit quite small – varying from 0.15 to 0.28 – with the odd members having a lower value than the even members, which appears to attenuate as the spacer chain length is increased. This behaviour is in strong contrast to that seen for the clearing entropies of the CBOnOCB's [1] where the odd-even alternation appears not to attenuate. The transitional entropies for the smectic A/B – nematic transition have a high value, in the region of 3.0 to 3.5, for the C7 and C8 homologues, which suggests that the phase may indeed be a smectic B, and then show a sharp drop to very low values, around 0.15, for longer spacer chain lengths. This behaviour seems to suggest that there is a change in the nature of the smectic phase at this point. The lower transitional entropies may indicate that this smectic phase could be a smectic A and this sudden drop is accompanied by the emergence of the crystal E phase. The entropies associated with this transition

Table 4.5 : Transition temperatures of the CTOnO2CP series

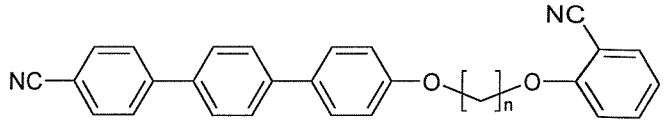

	Transition temperatures /°C									
n	Cr		E		SmA/B		N		I	
3	•	198.3	•		•		(•	178.6)	•	
4	•	178.9	•		•		•	216.6	•	
5	•	147.1	•		•		•	187.1	•	
6	•	164.1	•		•		•	201.0	•	
7	•	132.3	•		•	144.1	•	185.2	•	
8	•	116.4	•		•	141.9	•	190.3	•	
9	•	113.0	•	141.1	•	157.5	•	177.8	•	
10	•	117.9	•	135.8	•	158.7	•	179.9	•	
11	•	93.8	•	135.1	•	156.8	•	170.9	•	
12	•	98.2	•	131.9	•	158.6	•	169.2	•	

Parentheses denote a monotropic transition

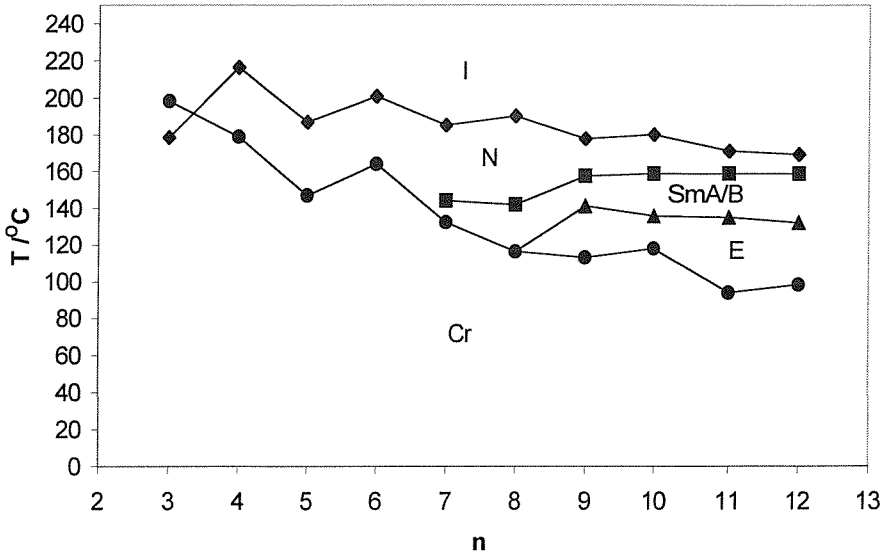

Figure 4.17 : Transition temperatures of the CTOnO2CP series as the number of carbon atoms, n, in the alkyl chain is increased.

● Cr – E, SmA/B, N or I, ▲ E – SmA/B, ■ SmA/B – N, ◆ N – I.

Table 4.6 : Transition entropies of the CTOnO2CP series

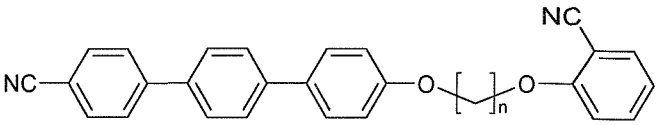

	Transition entropies, ΔS/R										
n	Cr		E		SmA/B		N		I		
3	•	12.38	•		•		•	0.18	•		
4	•	11.57	•		•		•	0.26	•		
5	•	12.78	•		•		•	0.15	•		
6	•	13.08	•		•		•	0.28	•		
7	•	*	•		•	3.24	•	0.19	•		
8	•	5.98	•		•	2.87	•	0.27	•		
9	•	1.88	•	2.69	•	0.12	•	0.21	•		
10	•	8.7	•	2.29	•	0.11	•	0.28	•		
11	•	*	•	2.28	•	0.16	•	0.21	•		
12	•	13.67	•	2.11	•	0.19	•	0.25	•		

Parentheses denote a monotropic transition

* transition entropy unobtainable

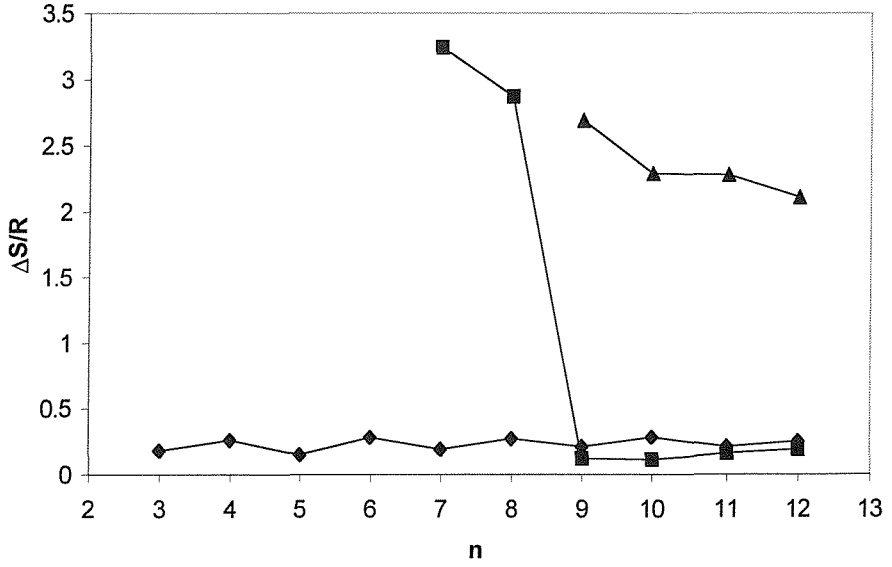

Figure 4.18 : Transitional entropies of the CTOnO2CP series as the number of carbon atoms, n, in the alkyl chain is increased.

▲ E – SmA/B, ■ SmA/B – N, ◆ N – I.

have values in the region of 2.0 to 2.5, with a steady downward trend with increasing spacer chain length. In fact there seems to be a general downward trend for this smectic A/B – nematic or crystal E – smectic A/B transition as the spacer chain is increased in length.

Figure 4.19 : The characteristic platelet texture exhibited by the E phase of CTO11O2CP on cooling from the homeotropic SmA/B phase at 120°C (magnification x100).

4.2.5 The CTOnO3CP Series

Table 4.7 shows the transitional properties of the CTOnO3CP series. As with the CTOnO2CP all members are mesogenic, although now they are all enantiotropic. All members exhibit a nematic phase on cooling from the isotropic and, as shown in figure 4.20, for those materials with six or more carbon atoms in the spacer chain, a smectic A/B phase is seen on cooling from the nematic phase. Again, the textures seen by optical microscopy for these two phases show a homeotropic alignment and therefore appear isotropic thereby hindering the identification of the smectic phase, although the nematic phase flashed when subjected to mechanical stress. On further cooling of the materials with a spacer alkyl chain greater than nine the platelet texture of the crystal E phase is seen (figure 4.19). Again, when the spacer chain length is greater than six, the materials appear reluctant to crystallise upon continued cooling.

The nematic – isotropic transition temperatures show an odd-even alternation, albeit small, upon increasing the spacer chain length and this alternation decreases as the chain length is increased. The nematic phase stability remains fairly constant, until the emergence of the smectic A phase, whereupon it rapidly

Table 4.7 : Transition temperatures of the CTOnO3CP series

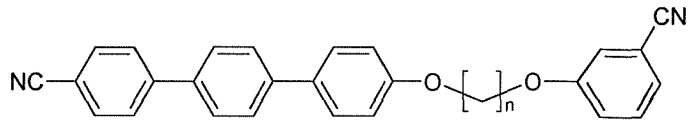

	Transition temperatures /°C									
n	Cr		E		SmA/B		N		I	
3	•	150.3	•		•		•	202.9	•	
4	•	156.3	•		•		•	212.4	•	
5	•	141.2	•		•		•	198.9	•	
6	•	116.7	•		•	128.6	•	200.3	•	
7	•	109.6	•		•	138.8	•	191.9	•	
8	•	125.7	•		•	146.6	•	188.8	•	
9	•	96.7	•	144.5	•	151.2	•	181.9	•	
10	•	119.6	•	146.2	•	161.5	•	179.9	•	
11	•	99.9	•	143.8	•	159.8	•	173.4	•	
12	•	109.4	•	143.3	•	152.9	•	161.2	•	

Parentheses denote a monotropic transition

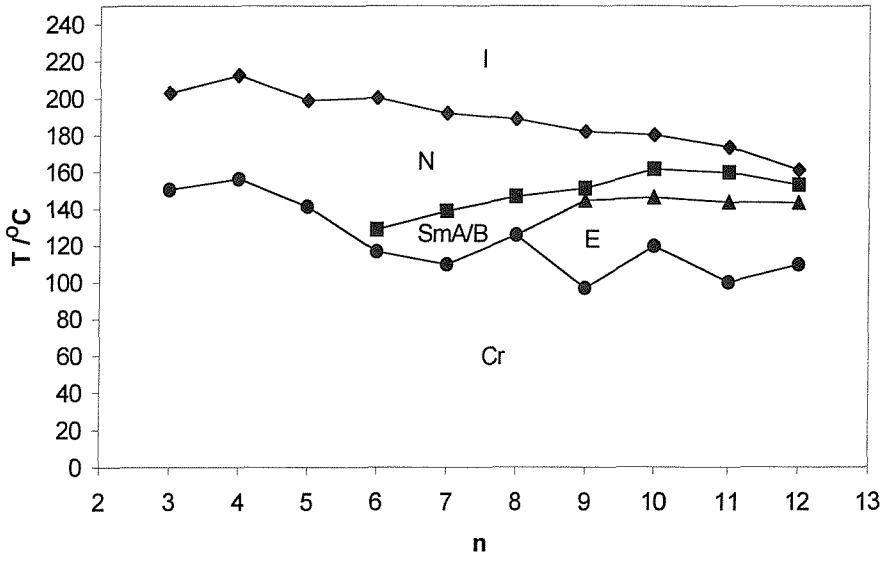

Figure 4.20 : Transition temperatures of the CTOnO3CP series as the number of carbon atoms, n, in the alkyl chain is increased.

● Cr – E, SmA/B or N, ▲ E – SmA/B, ■ SmA/B – N, ◆ N – I.

Table 4.8 : Transition entropies of the CTOnO2CP series

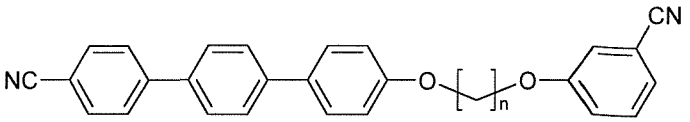

	Transition entropies, ΔS/R									
n	Cr		E		SmA/B		N		I	
3	•	12.94	•		•		•	0.29	•	
4	•	12.49	•		•		•	0.27	•	
5	•	14.05	•		•		•	0.29	•	
6	•	9.03	•		•	2.64	•	0.27	•	
7	•	5.44	•		•	2.99	•	0.28	•	
8	•	12.09	•		•	3.07	•	0.27	•	
9	•	7.96	•	2.84	•	0.03	•	0.28	•	
10	•	6.73	•	2.69	•	0.11	•	0.27	•	
11	•	9.66	•	2.53	•	0.07	•	0.27	•	
12	•	4.59	•	2.74	•	0.18	•	0.25	•	

Parentheses denote a monotropic transition

* transition entropy unobtainable

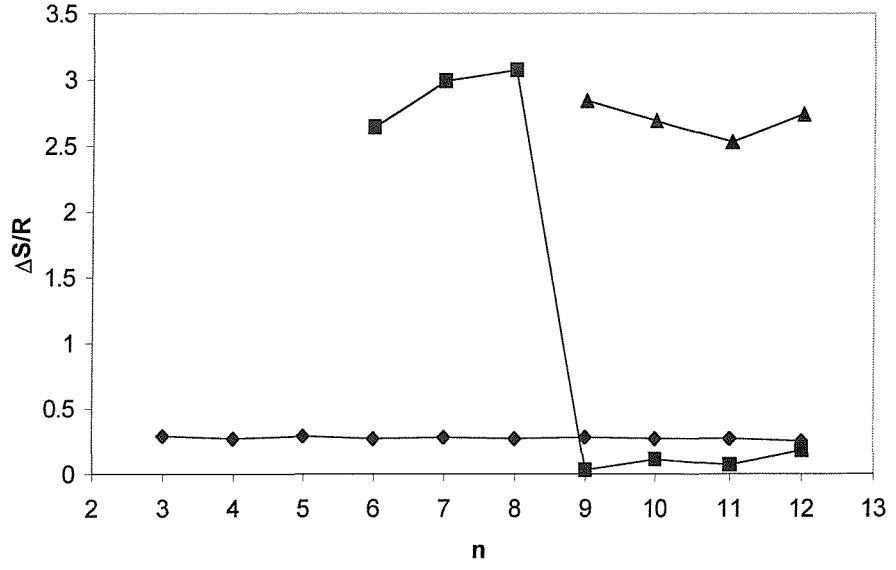

Figure 4.21 : Transitional entropies of the CTOnO3CP series as the number of carbon atoms, n, in the alkyl chain is increased.

▲ E – SmA/B, ■ SmA/B – N, ◆ N – I.

decreases until for the C12 homologue, the nematic phase range is only about 8°C. The stability of the smectic A/B phase decreases with the formation of the crystal E phase for chain lengths of nine or more carbon atoms, and appears to be diminishing as the spacer chain length is increasing. As with the ortho-series, the melting points show only an irregular dependence on the spacer chain length.

The entropies associated with the various phase transitions upon increasing the spacer chain length are shown in figure 4.21. It is immediately obvious that the clearing point entropy has an extremely small odd-even alternation, the difference between the largest and smallest entropies being only 0.04, and that this appears to attenuate as the spacer chain length is increased. What is not immediately apparent, due in part the scale on the y-axis, is that the alternation is reversed, with the odd members having a slightly higher entropy than the even members, which is in complete contrast to the behaviour seen for the CTOnO2CP series. This intriguing result is discussed later in this Chapter. The entropy associated with the smectic A/B to nematic transition is very high, which may suggest, once more, that this smectic phase may be a smectic B, and shows an increase, from 2.6 to 3.1, on going from the C6 to the C8 homologue. There is then a sharp drop to an almost second order transition, $\Delta S/R$ being only 0.03, for the C9 homologue, and then remaining around 0.1, with a small alternation until the C12 homologue. This drop is associated with the emergence of the crystal E phase and may again indicate a change in the nature of the smectic phase. The entropy of transition from the crystal E phase to the smectic A/B phase shows, in general, a reduction, from 2.8 to around 2.6, on increasing the spacer chain length.

4.2.6 Summary of the CTOnO*x*CP Series

Comparison of the CTOnO2CP's and the CTOnO3CP's with the CTOnO4CP's and other cyanoterphenyl systems show results as intriguing as the cyanobiphenyl systems studied earlier. The phase behaviour of the ortho- and meta-substituted series is shown in figure 4.22. At this point a number of general observations may be made. First, and most obviously, is the odd-even alternation in the nematic – isotropic transition temperatures. Although there is a consistent alternation for both series, with the odd members having a lower transition temperature than the even,

this alternation is substantially reduced for the meta-substituted series. Secondly, for the two series the phase ranges of the various phases appear to differ. The meta-series shows a greater nematic phase range over increasing alkyl spacer chain length, than the ortho-series, whereas the the smectic A/B phase range is greater for the ortho-series than the meta-series, especially after the emergence of the crystal E phase in the phase behaviour. Just to confound matters further, the crystal E phase appears to have a larger phase range for the meta-series than the ortho-series. Finally, and perhaps less significantly, the smectic A phase emerges at the C6 homologue for the meta-series, whereas it emerges at the C7 homologue for the ortho-series.

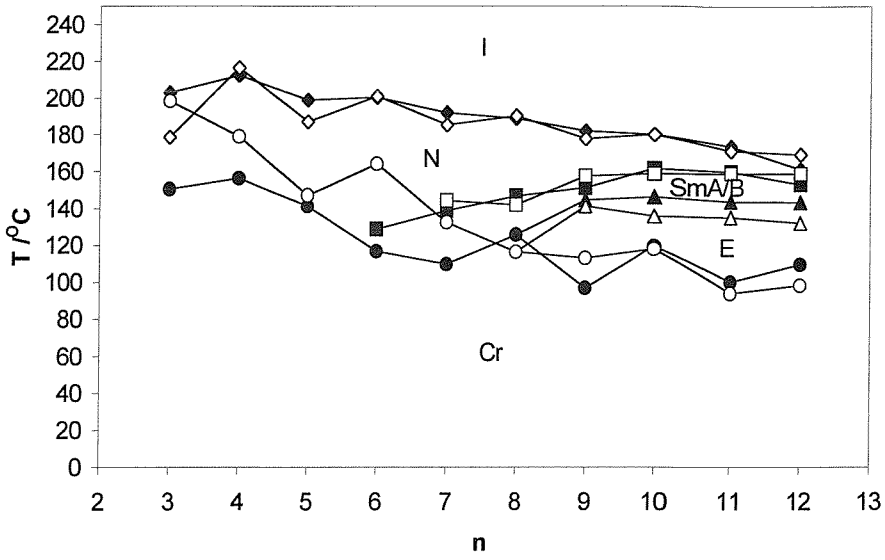

Figure 4.22 : Transition temperatures of the CTOnO2CP and CTOnO3CP series as the number of carbon atoms, n, in the alkyl chain is increased.
○ Cr – E, SmA/B, N or I, △ E – SmA/B, □ SmA/B – N, ◇ N – I. (CTOnO2CP)
● Cr – E, SmA/B, N or I, ▲ E – SmA/B, ■ SmA/B – N, ◆ N – I. (CTOnO3CP)

The fact that the differences between the phase behaviour of the two series is only slight is not that unexpected as the two series differ in only the position of a cyano group on the phenyl ring. However, when we consider the phase behaviour of the CBOnO4CP's, prepared by Wilson [11], the results are extremely surprising. All members of this series exhibit only a nematic phase, with no smectic phases appearing for spacer chain lengths up to 12 carbon atoms. Also, the clearing temperatures are of the order of 40°C higher than the clearing temperatures of the CTOnO2CP and CTOnO3CP series and the odd-even alternation with increasing

spacer chain length is larger. A comparison of the clearing temperatures of ortho- and meta-substituted materials with the para-substituted, together with those of the 4-alkyl-4''-cyanoterphenyls (nOCT's) and the α-(4''-cyanoterphenyl-4-yloxy)-ω-(4'-cyanobiphenyl-4-yloxy) alkanes (CTOnOCB's), again prepared by Wilson [11], are shown in figure 4.23. It is immediately apparent that not only do the ortho- and meta-series have a lower clearing temperature than the para-series, but also lower than the dimeric CTOnOCB's and the monomeric nOCT's. In addition, the CTOnO3CP series seems to have an odd-even alternation more akin to the monomeric materials, while the CTOnO4CP series has an odd-even alternation closer to that of the dimeric materials. The CTOnO2CP series, meanwhile, has an odd-even alternation closer to the trend exhibited by the para series.

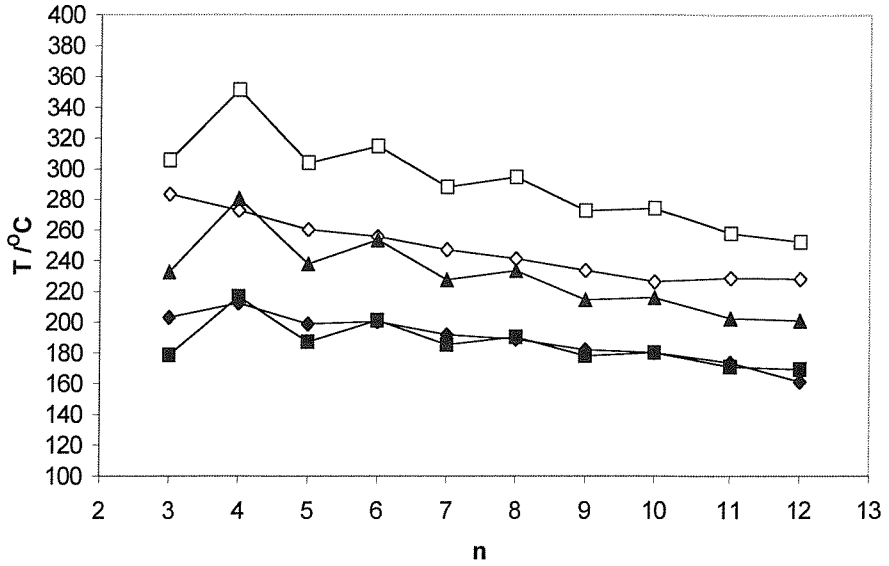

Figure 4.23 : Transition temperatures for the N – I transition as the number of carbon atoms, n, in the alkyl chain is increased.
■ CTOnO2CP's, ◆ CTOnO3CP's, ▲ CTOnO4CP's, ◇ nOCT's, □ CTOnOCB's

If we now compare the entropy change at the nematic – isotropic transition for the ortho-, meta- and para-substituted series, as shown in figure 4.24, similarly surprising results are seen. Not only is the odd-even alternation substantially larger for the para-series than the other two, but the meta-series exhibits an odd-even alternation that although extremely small is opposite to that seen for the ortho- and para-series. It is interesting to note, that whilst the even members of the CTOnO4CP's have a transitional entropy approximately three times larger than the even members of the ortho- or meta-series, the odd members have a very similar

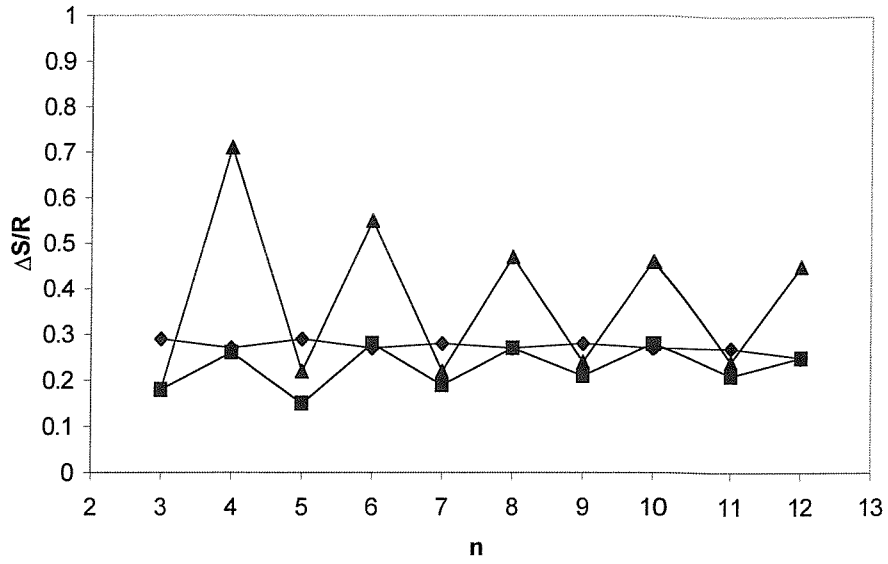

Figure 4.24 : The entropy change at the N – I transition as the number of carbon atoms, n, in the alkyl chain is increased.
■ CTOnO2CP's, ◆ CTOnO3CP's, ▲ CTOnO4CP's.

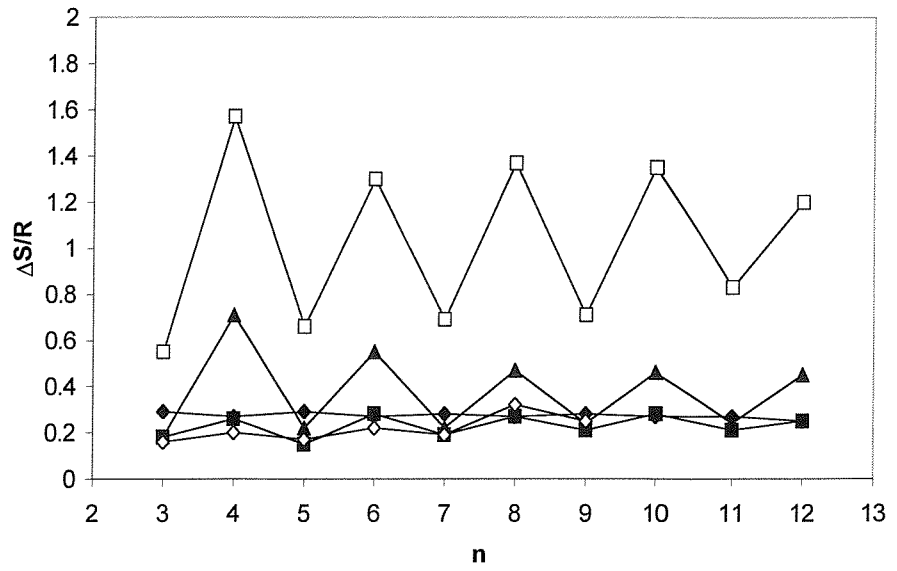

Figure 4.25 : The entropy change at the N – I transition as the number of carbon atoms, n, in the alkyl chain is increased.
■ CTOnO2CP's, ◆ CTOnO3CP's, ▲ CTOnO4CP's, △ nOCT's, □ CTOnOCB's

value to that of the odd members of the CTOnO2CP and CTOnO3CP series. Also, the even members of both the ortho- and meta-series have almost identical transitional entropies, whereas the odd-members are different, due mainly to the reversed odd-even alternation in the nematic – isotropic transition seen for the CTOnO3CP's. All three series, however, appear to show the entropies attenuating

as the spacer chain length is increased. When the behaviour of these intermediate materials are compared to monomeric, i.e. the nOCT's, and dimeric, i.e. the CTOnOCB's, systems, as shown in figure 4.25, we see, again, that the para-substituted series behave more as dimers, and the ortho- and meta-series behaving more as monomers. Although the odd-even alternation in transitional entropies for the para-substituted materials is not as large as that for the dimeric materials it is still somewhat larger than the odd-even alternation seen for the monomeric materials, and larger than the ortho- and meta-substituted materials.

4.2.7 Summary and Discussion of the Intermediate Materials – The CBOnO*x*CP's and the CTOnO*x*CP's

In order to understand the behaviour of these intermediate dimeric systems we begin by considering only the terphenyl materials, and then apply these ideas to the biphenyl materials, as it is difficult to assertain much useful information from the biphenyls because of their substantially reduced phase behaviour.

First, in all of the terphenyl systems the dominant intermolecular interaction will be the interaction between two terphenyl units, with the dipoles associated with the cyano group aligned in an antiparallel arrangement. This assumption is borne out by the results for the monomeric nOCT's studied by Wilson [11]. X-ray diffraction data showed the layer spacing in the smectic A phase exibited by these materials to be about 1.4 times the molecular length indicating an antiparallel arrangement of molecules. We would expect the interaction between the cyanophenyl units to be only weak when compared to the terphenyl-terphenyl interaction, however the cyano group on the phenyl ring should help to increase some of the anisotropic properties of the cyanophenyl moiety, as was seen in the work by Imrie [7] mentioned in the Introduction. Secondly, in order to discuss the phase behaviour seen we will concentrate primarily on the molecular geometries and the arrangement they have in the liquid crystal phase, in particular the conformations adopted by the cyanophenyl moieties in relation to the flexible chain.

Figure 4.26 shows various possible molecular arrangements for the CTOnO2CP series. The first thing to consider is the intramolecular dipolar interactions occuring for the members of this series. The values quoted in figure 4.26 for the steric

energy were calculated for 1-methyloxy-2-cyanophenyl using Chem3D Pro produced by the CambridgeSoft Corporation. The two different conformers were energy minimised using the MM2 minimisation routine and the steric energy, which is defined for this software as a single point energy computation that calculates the total steric energy for the current conformation [12], is calculated from that conformation. Comparing the steric energies of the various conformers allows us to determine the relative stabilities of these conformations. As there is a dipole associated with the oxygen atom of the ether linkage then it is sensible to imagine that due to the rotation about the C_{ring}-O bond and the interaction of the dipoles associated with the cyano group and the oxygen atom, then the preferred molecular geometry would be that shown in figure 4.26(a) and not that in figure 4.26(b). Even allowing for the possibility of the ring flipping the dominant conformation can be assumed as being structure (a).

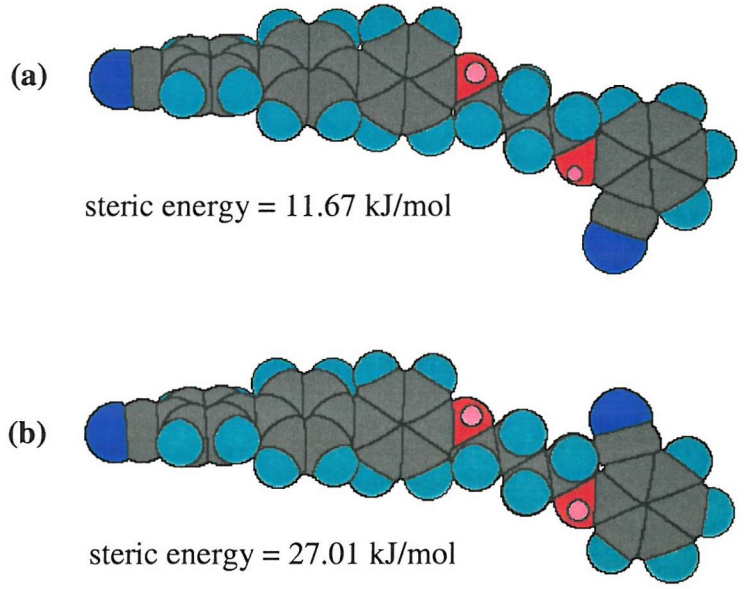

Figure 4.26 : Two possible configurations of CTO4O2CP and the calculated steric energies for the 1-methoxy-2-cyanophenyl fragment.

If we now consider the possible molecular arrangements for both the odd and even members of the series, we can imagine an ideal smectic arrangement of the molecules in an all-*trans* conformation, as shown in figure 4.27. Here the terphenyl units are considered to be aligned antiparallel, as for the monomeric nOCT's, and

there may also be some interaction between the phenyl units, although this interaction would be weak.

If the chain remains in an all-*trans* configuration and we try to invisage a possible structure for a nematic phase, where the phenyl units may now also be interacting with the terphenyl units, as shown in figure 4.27, it becomes apparent that the packing requirements are now unfavourable when compared to the packing of the smectic phase. We would expect, therefore, a high possibility of smectic phases occuring and there to be a low nematic phase stability.

If the anisotropic interactions of the polarisable cyanophenyl are considered we find that, because the anisotropy in this moiety is not parallel with the molecular long axis of the terphenyl moiety, for the all-*trans* configuration of both the odd and even members of the series, the interaction of this group with the molecular field is poor when compared to the effect the increase in molecular volume has on the nematic phase stability. This leads to a situation where these materials behave more as the monomeric terphenyl materials (nOCT's), with the spacer chain now behaving more like a terminal chain with a large "blob" on the end of it. This will lead to a lowering of the nematic – isotropic transition temperature when compared to the nOCT's and low transitional entropies. For monomeric materials with short terminal chains, generally only nematic phases are seen, with the tendency to form smectic phases occuring for longer terminal chain length, which explains why only nematic phases are seen for the shorter spacer chain lengths, with the smectic phases appearing at longer spacer chain lengths.

We can, however, think of another way of arranging the molecules in a nematic phase. By aligning the cyano group of the cyanophenyl moiety with the long molecular axis of the cyanoterphenyl moiety should allow a better interaction with the molecular field, i.e. it should make the molecule more anisotropic. To do this we need to introduce a kink into the flexible chain, as shown in figure 4.27. As this is energetically unfavourable there are more conformers where the dipoles are not aligned favourably. Therefore, at the nematic – isotropic transition there is a high proportion of conformers where there is not a favourable alignment of the dipoles and the change in the conformation of the molecules results in an energy penalty

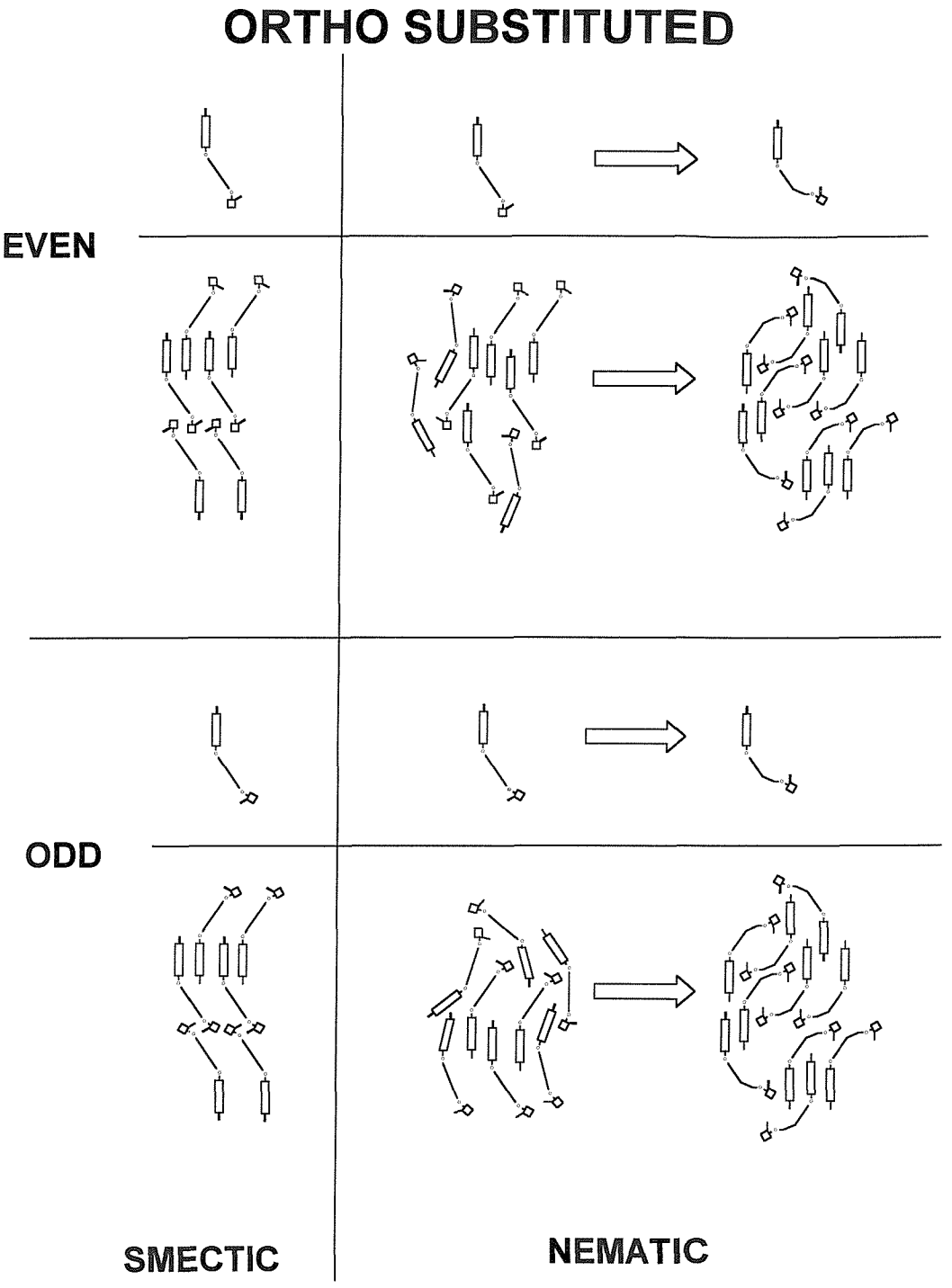

Figure 4.27 : The possible arrangements of molecules in the smectic and nematic phases showing the effect that adding a 'kink' to the alkyl chain can have on the packing of the molecules in the nematic phase (right side of figure).

which is not compensated for by the gain in orientational energy due to the favourable alignment of the dipoles. This will reduce both the nematic – isotropic transition temperature and the transitional entropies of both the odd and even members. This effect, and the effect of the bulky terminal group when there is an unfavourable alignment of the dipoles, will reduce the transition temperatures and entropies when compared to the nOCT's, but which effect dominates is unclear.

We now consider the possible molecular arrangements for the CTOnO3CP series. This time there is no preferred orientation of the cyanophenyl ring with respect to the ether linkage as the intramolecular dipoles are not close enough to have any effect, as shown in figure 4.28, since the dipole/dipole interaction is proportional to $1 / r^3$, where r is the distance between the two dipoles. For both the odd and even members of the series a number of smectic orderings, for an all-*trans* conformation of the spacer chain, depending on the orientation of the cyano group on the phenyl ring can be envisaged, as shown in figure 4.29. Once more the dominant interaction will be between the terphenyl units, with the phenyl units having only a weak interaction. This tendency towards smectic behaviour and monomer-like behaviour should lead to the formation of smectic phases for long chain lengths, which we see, and a reduced nematic – isotropic transition temperature, when compared to the nOCT monomers, as the "terminal chain" now has a bulky cyanophenyl group at the end of it, as was seen for the CTOnO2CP series.

Unlike the CTOnO2CP series, however, there will be a difference, in the nematic phase, between the odd and the even members. For the odd members, one of the orientations of the cyanophenyl moiety allows, for an all-*trans* conformation of the spacer chain, the cyano group to align with the molecular long axis of the terphenyl moiety, as shown in figure 4.29. At the nematic – isotropic transition there are a higher proportion of molecules where the dipoles have a favourable alignment than for the CTOnO2CP series and therefore the energy penalty paid to convert those molecules where there is not a favourable alignment is offset by the increase in orientational energy due to the favourable interaction of the polarisable cyanophenyl group with the molecular field. We would therefore expect to see an increase in both the nematic – isotropic transition temperatures and the associated

transitional entropies for the odd members of the CTOnO3CP's when compared to the odd members of the CTOnO2CP series, which is indeed what we see.

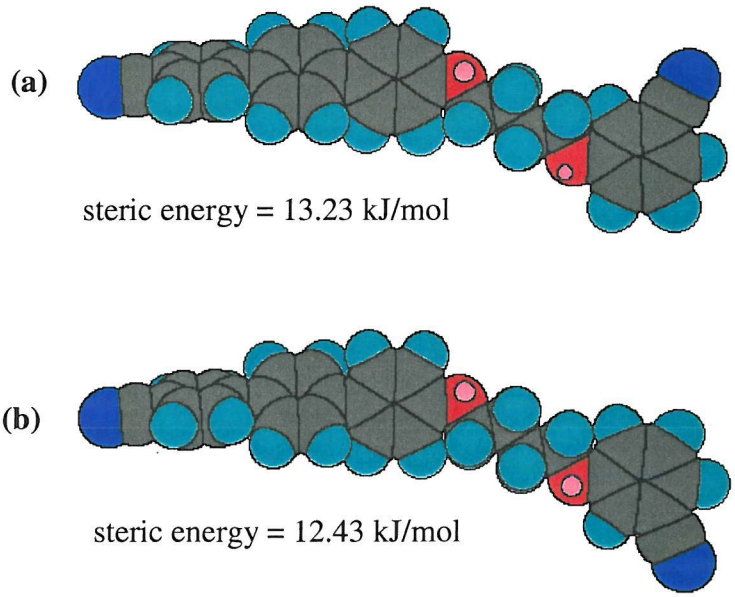

Figure 4.28 : Two possible configurations of CTO4O3CP and the calculated steric energies for the 1-methoxy-2-cyanophenyl fragment.

If we now consider the even members of the CTOnO3CP series, in the nematic phase, for an all-*trans* configuration of the spacer chain, the cyano group of the phenyl moiety does not align with the molecular long axis of the cyanoterphenyl moiety, as shown in figure 4.29. This lack of alignment of the cyano group is independent of the orientation of the cyanophenyl moiety, i.e. inducing a ring flip will not aid with the alignment of the cyano group with the molecular long axis of the cyanoterphenyl moiety. The lack of alignment is an identical situation to that seen for the CTOnO2CP series. Again, if we introduce a kink into the spacer chain, by adding several gauche links, for example, we can align the dipole of the cyanophenyl moiety with the molecular long axis of the cyanoterphenyl moiety. However, this means, at the nematic – isotropic transition, there are higher proportion of conformers that do not have a favourable alignment of dipoles. Again, the energy penalty paid by converting these conformers to a conformation where there is a favourable alignment of dipoles is not compensated for by the increase in orientational order that may arise from this favourable alignment.

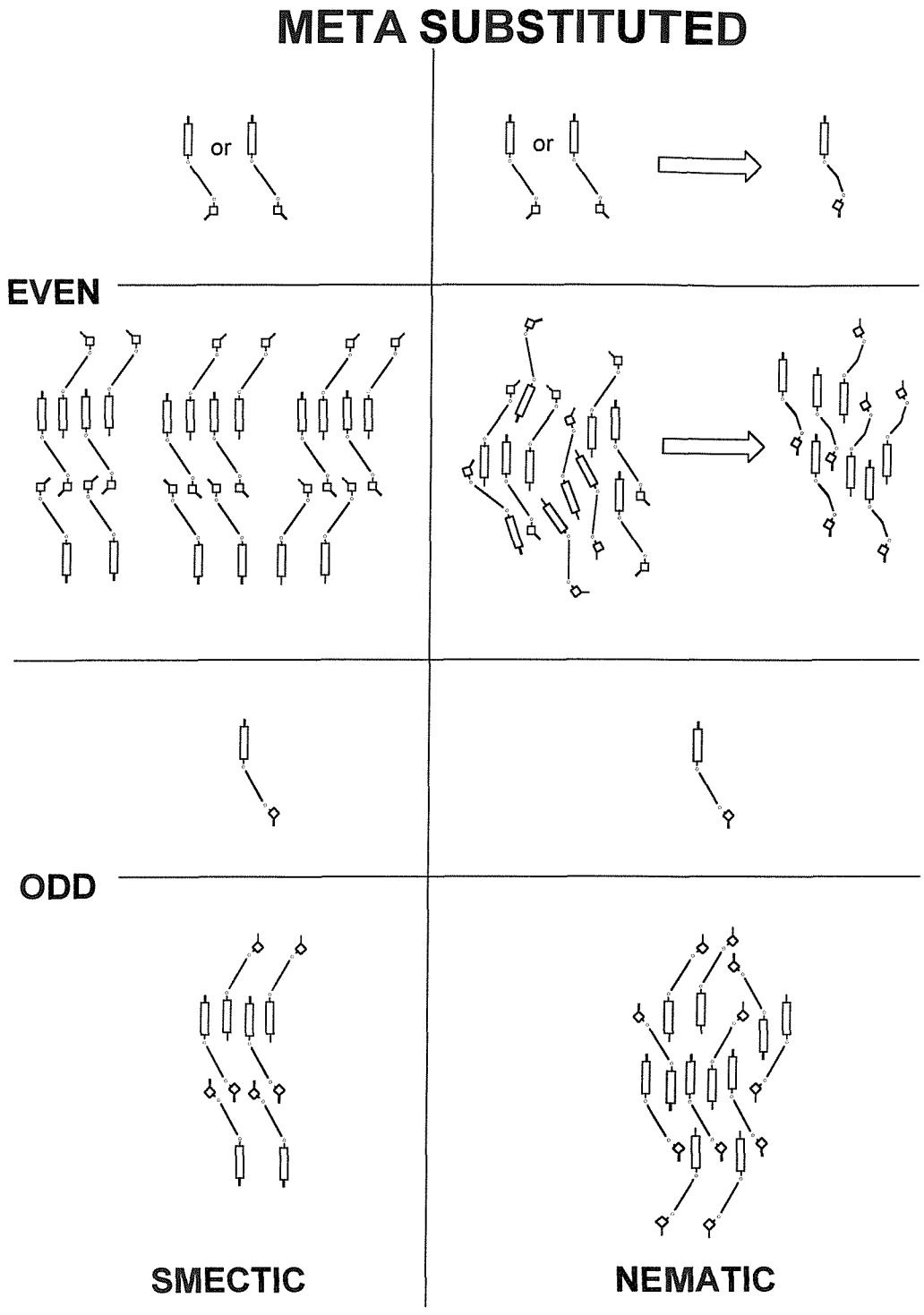

Figure 4.29 : The possible arrangements of molecules in the smectic and nematic phases showing the effect that adding a 'kink' to the alkyl chain can have on the packing of the molecules in the nematic phase (right side of figure).

Therefore we would expect there to be a reduction in both the nematic – isotropic transition temperature and the transitional entropies when compared to the odd members of the series. This should lead to the even members of the CTOnO3CP series having similar nematic – isotropic transition temperatures and entropies to the even members of the CTOnO2CP series, and indeed this is so.

By considering the previous arguments it becomes obvious why the meta-substituted materials have a much smaller, and opposite odd-even alternation in the nematic – isotropic transitional entropies than the ortho-substituted materials. The alignment of the dipole of the cyanophenyl moiety with the molecular long axis of the terphenyl moiety for the odd members of the CTOnO3CP series means the transitional entropies are higher than would be expected and leads to these materials having a slightly higher transitional entropy than the even members of the series. Had this alignment not arisen we would have expected the odd-even alternation to mimic that seen for the CTOnO2CP series. Similarly, the smaller odd-even alternation in the nematic – isotropic transition temperatures, when compared to the ortho-substituted materials, is a consequence of the alignment of the dipole of the cyanophenyl moiety with the molecular long axis of the terphenyl moiety for the odd members of the CTOnO3CP series.

If we use the same arguments as above, we can explain why only a nematic phase is seen for the CTOnO4CP series, studied by Wilson [11] and why the nematic – isotropic transition temperatures and entropies are higher than the other two series. We still have the favourable interaction between the terphenyl units, but with the para-substituted cyano group in the cyanophenyl moiety there is, especially for the even members of the series, a favourable alignment of the cyano group dipole with the molecular long axis of the terphenyl moiety. It has been suggested [11] that this interaction may stabilise the crystal packing of the material and therefore the tendency to form smectic phases is reduced. As this favourable dipolar alignment is less likely for the odd members of the series we may expect there to be the formation of smectic phases for longer chain lengths. Figure 4.30 shows the structures for a proposed smectic phase, if one was formed, for both the odd and even homologues. If the interactions between the like-like units is favourable enough then a smectic phase may be formed. In fact, if the

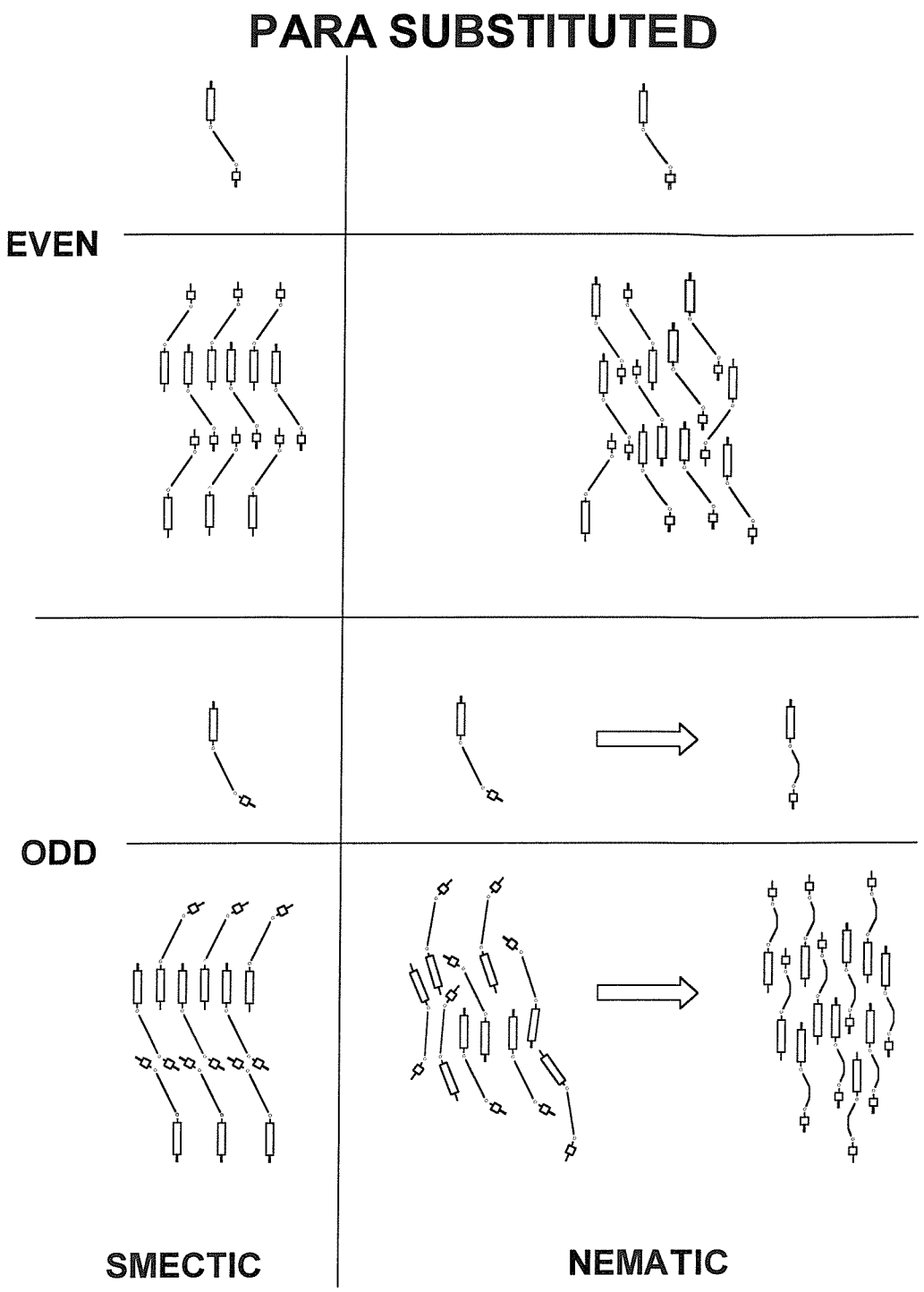

Figure 4.30 : The possible arrangements of molecules in the smectic and nematic phases showing the effect that adding a 'kink' to the alkyl chain can have on the packing of the molecules in the nematic phase (right side of figure).

cyanophenyl units are now replaced by cyanobiphenyl units, as in the CTOnOCB series, where the interaction between the cyanobiphenyls is now increased, for the C9 and C11 homologues a monotropic smectic A phase is seen.

Figure 4.30 shows an idealised picture of the nematic phase formed by both the odd and even homologues. As can be seen for the even members of the series, there is a favourable alignment of cyano group dipole with the molecular long axis of the terphenyl moiety when the chain is in an all-*trans* conformation. Therefore, we would expect there to be, at the nematic – isotropic transition, a high proportion of conformers possessing this favourable alignment. The energy required to convert those conformers with an unfavourable alignment is more than offset by the increase in orientational order and, therefore, we would expect the even members of the CTOnO4CP series to have the highest nematic – isotropic transition temperatures and entropies of all three series. For the odd members of the series there will be a higher proportion of conformers where the dipole alignment is less favourable. Therefore, due to the higher conformational energy at the nematic – isotropic transition we would expect the transition temperatures and entropies to be lower. In fact, because of the favourable dipole alignment seen for the odd members of the CTOnO3CP series the nematic – isotropic transition entropies for the para-substituted homologues are lower than for the meta-substituted homologues.

If we now consider the behaviour seen for the biphenyl systems we find that due to the reduced mesogenicity of the cyanobiphenyl moiety over the cyanoterphenyl moiety the phase behaviour is reduced to only monotropic phases being observed. Again, for the ortho- and meta-substituted series the materials behave more as monomers than dimers because of the weak interactions between the cyanophenyl groups and therefore the spacer chain becomes, once more, essentially a terminal chain with a large group on the end. As the cyanobiphenyls (nOCB's) have lower transition temperatures than the cyanoterphenyls (nOCT's) we find only monotropic phases being exhibited as the melting points become prohibitive to the formation of enantiotropic phases. For the CBOnO2CP's only the even members exhibit phases because the length to breadth ratio is greater in these materials than the odd members. Although for longer chain lengths, namely the C11 homologue,

the conformational freedom of the chain allows the dipole of the cyanophenyl moiety to be brought back in line with the long molecular axis.

For the CBOnO3CP's the converse is true. For the odd members the dipoles can now begin to be aligned coparallel without the need for a kink in the spacer chain, and therefore only the odd-members exhibit a montropic phase. Whereas for the para-substituted series, the interactions between the cyanophenyl and cyanobiphenyl are larger and therefore stablise the nematic phase because of the weak association increasing the molecular anisotropy leading to monotropic behaviour for all members of the series.

4.3 Conclusions

In this Chapter we have described the preparation and characterisation four novel homologous series of compounds each containing a cyanophenyl moiety. Two series are based on the 4-cyanobiphenyl mesogenic group and the other two are based on the 4-cyanoterphenyl mesogenic group.

For the cyanobiphenyl dimers (CBOnO*x*CP's) we have shown that mesomorphic behaviour is substantially reduced when compared to either the cyanobiphenyl monomers (nOCB's) or the cyanobiphenyl dimers (CBOnOCB's), as the non-symmetric CBOnO*x*CP dimers exhibit only monotropic phases. This is a consequence of the materials having bulky non-mesogenic units attached to the end of a flexible alkyl chain. In addition we have shown that the position of substitution of the cyano group around the cyanophenyl ring affects the mesomorphic behaviour significantly. The materials prepared by Wilson [11], where the cyano group is para-substituted to the ether link in the cyanophenyl unit (CBOnO4CP's) exhibit monotropic nematic phases as the number of carbon atoms in the alkyl spacer chain varies from 3 to 12. However, when the cyano group is ortho-substituted to the ether link (CBOnO2CP's) only those members with an even number of carbons atoms in the alkyl spacer exhibit monotropic nematic phases. It is only when the spacer chain length is greater than 10 carbon atoms that the odd members exhibit a monotropic nematic phase. Conversely, for the CBOnO3CP series, where the cyano group is meta-substituted, only the odd members of the series exhibit monotropic nematic phases. Again, as the spacer chain length increases to greater than 10 carbon atoms the even members exhibit monotropic nematic phases.

When the mesogenic moiety was changed from the cyanobiphenyl to the larger cyanoterphenyl unit the results were just as surprising. The materials prepared by Wilson [11], where the cyano group in the cyanophenyl moiety is para-substituted to the ether link (CTOnO4CP), exhibit only nematic phases for the whole series. However, for both the ortho- and meta-substituted dimers (CTOnO2CP and CTOnO3CP) the mesogenic behaviour is much more interesting. For spacer lengths from 3 to 7 carbon atoms only a nematic phase is observed. A smectic A or B phase (the identification of this phase has not yet been established) and nematic

phase is observed for spacer lengths of 8 and 9 carbon atoms. For spacer lengths of greater than 9 carbon atoms a crystal E phase is also observed at low temperatures. This behaviour is analogous to that seen for the cyanoterphenyl monomers (nOCT's).

The transitional entropies associated with the nematic – isotropic transition for these non-symmetric cyanoterphenyl dimers also showed some interesting results. For the CTOnO4CP series the transitional entropies for the even members of the series were at least 2.5 times greater than for the odd members of the series. For the CTOnO2CP series the transitional entropies for the odd members of the series were similar to those seen for the odd members of the CTOnO4CP's, however the even members had transitional entropies that were at least twice a small as the even members for the CTOnO4CP series. More surprisingly the meta-substituted dimers had transitional entropies that remained almost constant as the spacer chain length was increased, with $\Delta S/R$ for the odd members being only 0.01 greater than for the even members.

This unusual behaviour has been explained as a consequence of the electric dipole associated with the cyano group of the cyanophenyl moiety. In order to align the dipole of the cyano group with the long molecular axis of the mesogenic moiety the spacer chains have to adopt different conformations depending upon the position of the cyano group around the cyanophenyl unit and the parity of the spacer chain. This leads, in some cases, to analogous materials which have significantly different transition properties. We have shown, therefore, that very subtle changes to the molecular structure of non-symmetric liquid crystal dimers can lead to very different mesogenic behaviour.

4.4 References

[1] Emsley, J.W., Luckhurst, G.R., Shilstone, G.N. and Sage, I., *Mol. Cryst. Liq. Cryst.*, **102**, 223, (1984).

[2] Gray, G.W. and Harrison, K.J., *Mol. Cryst. Liq. Cryst.*, **13**, 37, (1971).

[3] Gray, G.W. and Harrison, K.J., *Symposia of the Faraday Soc.*, **5**, 54, (1971).

[4] Gray, G.W., *J. Phys. (Paris).*, **36**, C337, (1975).

[5] Coates, D. and Gray, G.W., *J. Phys. (Paris).*, **36**, C365, (1975).

[6] Ennulat, R.D., and Brown, A.J., *Mol. Cryst. Liq. Cryst.*, **12**, 367, (1971).

[7] Imrie, C.T., *Ph.D. Thesis, University of Southampton*, (1988).

[8] Gray, G.W., *The Molecular Physics of Liquid Crystals*, edited by G.R.Luckhurst and G.W.Gray (Academic Press), Chapter 1., (1979).

[9] Gray, G.W., *The Molecular Physics of Liquid Crystals*, edited by G.R.Luckhurst and G.W.Gray (Academic Press), Chapter 1., (1979).

[10] Leadbetter, A.J., Tucker, P.A., Gray, G.W. and Tajbakhsh, A.R., *Liq. Cryst.*, **8**, 1, (1990).

[11] Wilson, M.J., *PhD. Thesis, University of Southampton*, (1998).

[12] Help file from CambridgeSoft Chem3D.

CHAPTER FIVE

THERMOTROPIC BIAXIAL NEMATIC PHASES

5.1 Introduction

The notion of molecular biaxiality in liquid crystals has, to a large extent, been ignored when considering the phases formed by mesogenic materials. For example, the phases formed by calamitic liquid crystals are based on the common assumption that the mesogenic molecules within the materials are rigid cylindrical rods. The long molecular axis is taken to be the z-axis and the perpendicular x and y axes are taken to be equivalent, as shown in figure 5.1. Here, the only order parameter considered is that along the molecular long axis, i.e. S_{zz}, which depends only on the fluctuations in the angle this axis makes with the director. Likewise, discotic liquid crystals are usually considered to be flat circular discs where the z-axis is now perpendicular to the molecular plane , and the x and y axes are also equivalent.

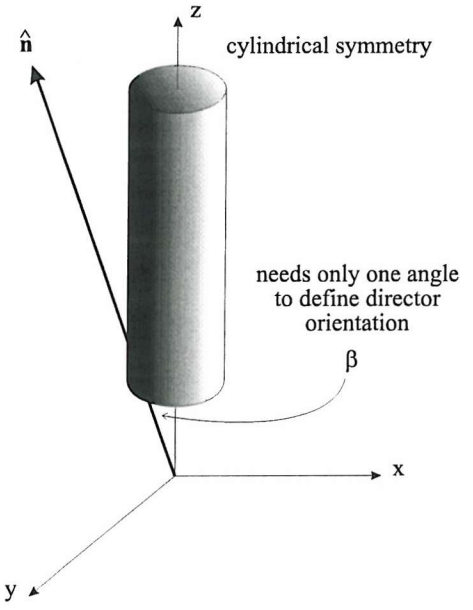

Figure 5.1 : Defining the director orientation for a uniaxial molecule.

However, if the x-axis is not equivalent to the y-axis, and the molecular long axis is still taken to be the z-axis the geometry now resembles that of a flat slab. In this case there is a major order parameter, S_{zz}, which depends on the fluctuations in the

angle this axis makes with the director, but there is also another, minor or biaxial order parameter that depends on an orientation perpendicular to the *z*-axis, as shown in figure 5.2.

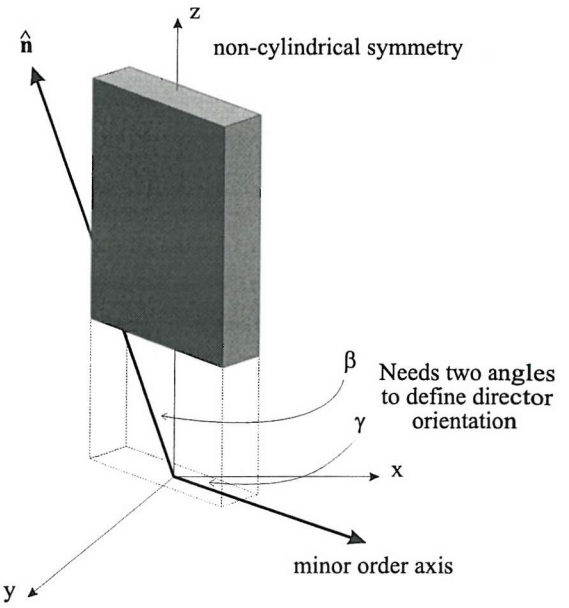

Figure 5.2 : Defining the director orientation for a biaxial molecule.

The majority of calamitic liquid crystals do not conform to the cylindrical symmetry described and the consequence of this reduction in symmetry was explored by Freiser in 1970 [1]. Taking into account the biaxiality of the molecules, the molecular field theory predicts a first-order transition from the isotropic phase to a uniaxial nematic phase, and then at a lower temperature, a second-order transition from this uniaxial phase to a biaxial nematic phase. In other words the phase sequence on cooling should be $I - N_U - N_B$. As the molecular biaxiality increases the isotropic – uniaxial nematic transition weakens and the $I - N_U$ and $N_U - N_B$ transitions approach each other until, at a maximum biaxiality, there is a direct, second-order transition from the isotropic phase to the biaxial nematic phase, called the Landau point.

Computer simulation studies of particles with a D_{2h} symmetry interacting via attractive [2] as well as repulsive [3] forces have confirmed these predictions, as have simulations carried out on equimolar mixtures of discs and rods that are constrained to specific lattice sites. The results indicate that the two interpenetrating sub-lattices of discs and rods exhibit a biaxial nematic phase [4].

In light of these predictions the question has to arise as to whether real physical examples of biaxial nematic phases exist. The answer is in fact yes, with a number of examples being observed experimentally in lyotropic systems. The first reported evidence of a biaxial nematic phase was made by Yu and Saupe in 1980 [5] in a ternary mixture of potassium laurate, 1-decanol and D_2O, the phase diagram of which is shown in figure 5.3.

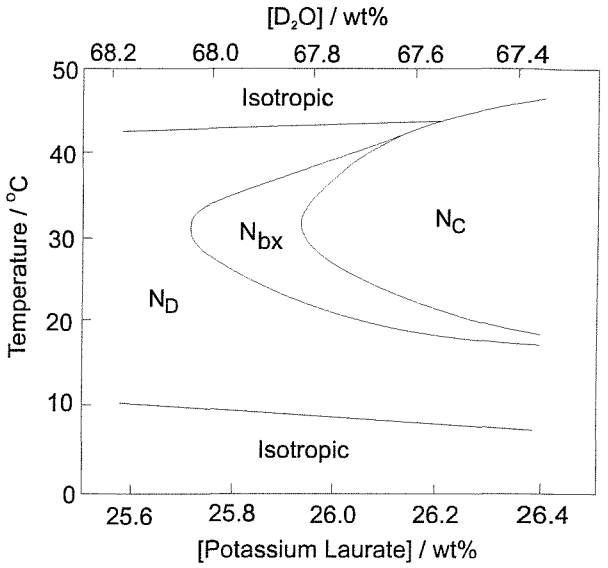

Figure 5.3 : A small region in the phase diagram of potassium laurate, 1-decanol and water, showing the existence of a biaxial nematic phase [5].

The nematic phases observed in these systems are a consequence of the aggregation of amphiphiles to form micelles whose shape and size are changed by temperature and concentration. Depending on the shape of the micelles three distinct nematic phases can occur. At lower temperatures and lower potassium laurate concentrations a disc-like micellar structure formed by bilayers of surfactant molecules, labelled N_D, is formed. At higher temperatures and higher potassium laurate concentrations the micelles take on a cylindrical shape, labelled N_C. Both these phases are optically uniaxial. However, between these two extremes there exists a nematic phase that is optically biaxial, labelled N_b, with the micelles in this case taking on an ellipsoidal shape that is intermediate between the two extreme geometries. Other systems exhibiting all three nematic phases include sodium decylsulphate/1-decanol/water [6], sodium decylsulphate/1-decanol/water/Na_2SO_4 [7], potassium laurate/decylammonium chloride/water [8,9]

and a system closely related to the system previously studied, namely sodium dodecylsulphate/1-decanol/water [10].

The search for thermotropic biaxial nematics has, however, been somewhat more difficult. As stated at the start of this Introduction virtually all molecules forming thermotropic liquid crystal phases do not conform to the cylindrical symmetry generally assumed for them and as such possess some degree of biaxiality. Therefore it should be possible, in principle, to observe biaxial nematic phases for thermotropic mesogens. However, this generally does not occur for a number of reasons. First, the inherent biaxiality of the molecule is not large enough, and second, the nematic phase cannot be preserved at sufficiently low temperatures, with the uniaxial nematic phase forming either a smectic phase or crystallising totally. Before we examine the attempts that have been made to uncover a thermotropic biaxial nematic phase we should consider the various methods of characterising suspected biaxial nematic mesogens.

5.2 Characterisation of Biaxial Nematic Liquid Crystals

The existence of lyotropic biaxial nematic phases has allowed us to determine what results we should expect to see when assessing the biaxiality of thermotropic nematogens using various characterisation techniques. The techniques discussed here will include polarising microscopy, conoscopy, x-ray diffraction and deuterium NMR spectroscopy.

5.2.1 Polarising Microscopy

As is the case with all mesogenic materials, one of the easier methods for deciding the nature of the phases formed by liquid crystals is to use polarising microscopy. The Introduction (§1.8) gave a brief overview of the different textures exhibited by different liquid crystal phases. For a normal uniaxial nematic phase a schlieren texture consisting of point disclinations which possess two and four-point brushes is usually seen and is characteristic of this phase. However, polarising microscopy studies of lyotropic biaxial nematic phases [11] have revealed that the texture observed can be somewhat different, with characteristic zig-zag disclinations running through the sample. An example of the texture that may be formed is shown in figure 5.4 [12] (It will be demonstrated later in this Chapter that the

assignment of this phase as being a thermotropic biaxial nematic was in fact incorrect. However, it would be expected that the texture exhibited by a thermotropic biaxial nematogen should be very similar). It has also been suggested that the schlieren texture formed by biaxial nematic phases consist of only two-point brushes [13], as shown in figure 5.5.

Figure 5.4: Texture exhibited by a biaxial nematic phase, showing the characteristic zig-zag disclinations.

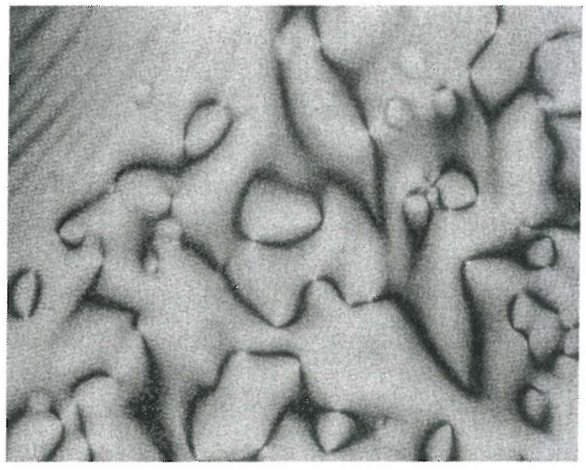

Figure 5.5 : The schlieren texture consisting of only two-point brushes that has been suggested will form for a thermotropic biaxial nematic phase.

5.2.2 Conoscopy

Despite using the same piece of equipment conoscopy differs from polarising microscopy in one important aspect. Whereas microscopy is the observation of a sample's magnified image, i.e. a sample's optical texture, using polarised light conoscopy is the observation of an interference figure of the object when a strongly convergent beam of light is passed through the sample. This allows an examination of the sample's optical character in not just one direction, i.e. that parallel to the objective, as in microscopy, but in many directions simultaneously. The simple addition of a Bertrand lens in the optical tube above the objective allows an ordinary polarising microscope to be used for conoscopy.

Figure 5.6 shows a schematic of the microscope when used for conoscopic observations. Polarised light is concentrated upon the object, X, and the divergent rays emerging pass through the objective and converge again in the upper focal plane, U, of the objective to form a real image. Each point of the image is the focal point of light which has passed in a definite direction through the sample and for this reason the image is sometimes called a directions image. To observe good interference figures the size of the microscope aperture should be as large as possible while the sample thickness should be between about 25 - 100μm. In addition for a uniaxial phase the sample should be well-aligned with the optic axis of the phase parallel to the observation direction and therefore a homeotropic alignment is required.

For uniaxial liquid crystals the interference image appears as a dark, blurred Maltese cross with concentric interference rings appearing across the image, as shown in figure 5.7(a). Due to the birefringence of an anisotropic sample any incident light ray at an angle other than 0° or 90° will be doubly refracted and the ordinary and extraordinary light waves will travel through the sample at different velocities. When they emerge from the sample, if the phase difference between the two waves is exactly an integer number of wavelengths the two waves are said to be out-of-phase and destructive interference occurs leading to darkness. Conversely, if the emerging waves have a phase difference that are multiples of half a wavelength the waves are 'in-phase' leading to constructive interference and

brightness. This interference gives rise to the light and dark rings seen in figure 5.7(a). The Maltese cross figure, also called an isogyre – meaning sites of identical vibration directions – is a consequence of the way in which the extraordinary and ordinary waves vibrate. The extraordinary waves vibrate in planes which include, for a uniaxial phase, the sample axis, whereas the ordinary waves vibrate perpendicular to these, or tangentially to the interference rings, as shown in figure 5.7(b). Where the vibration directions are parallel to the polarisers these areas appear dark and give rise to the interference figure of a cross. On rotating the microscope stage the interference figure remains the same indicating that the phase is uniaxial as the optic axis remains in line with the microscope axis.

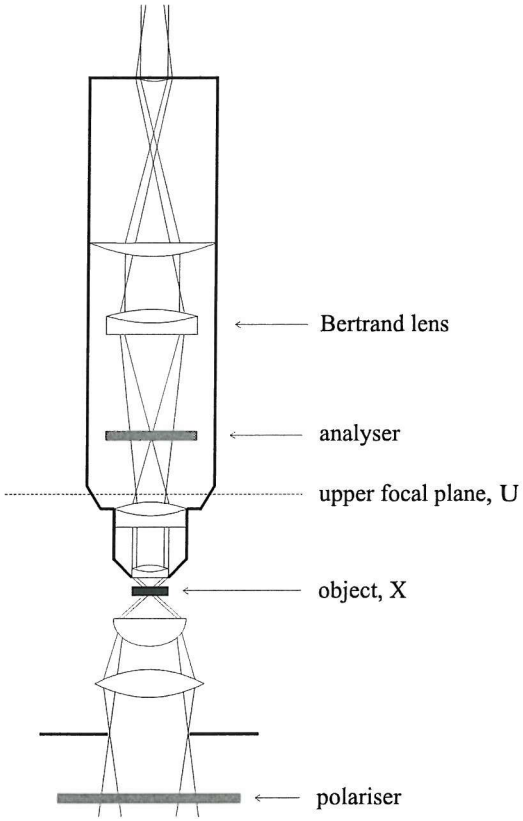

Figure 5.6 : Schematic representation of a microscope used for conoscopic studies.

When observing a biaxial phase using conoscopy an interference figure is produced in much the same way as for a uniaxial phase, however the effect of the two optic axes that biaxial phases possess must be taken into account. As with uniaxial phases a monodomain is required, however both the major axis and the minor axis must be aligned. This may be achieved by, for example, treating the microscope slides chemically to align one of the axes, and applying a magnetic or

electric field to align the other orthogonally to this. The interference figure observed for a biaxial phase is shown in figure 5.8(b). As can be seen there are two eye-like patterns, called melatopes, that are surrounded by interference rings, which mark the points of emergence of the optic axes from the sample. The inner rings are nearly circular, surrounding each melatope which, as they become larger, are initially figure-of-eight shaped and eventually become elliptical. Two isogyres pass through the centres of the melatopes and form a cross shape. When the microscope stage is rotated through 45° the cross opens up and splits into two hyperbolic brushes that are centred on the melatopes. The extent to which the brushes split gives an indication of the degree of phase biaxiality, or more strictly the biaxiality of the refractive index, with the case for maximum biaxiality shown in figure 5.8(a). If the microscope stage is rotated a further 45° the cross shape is reformed.

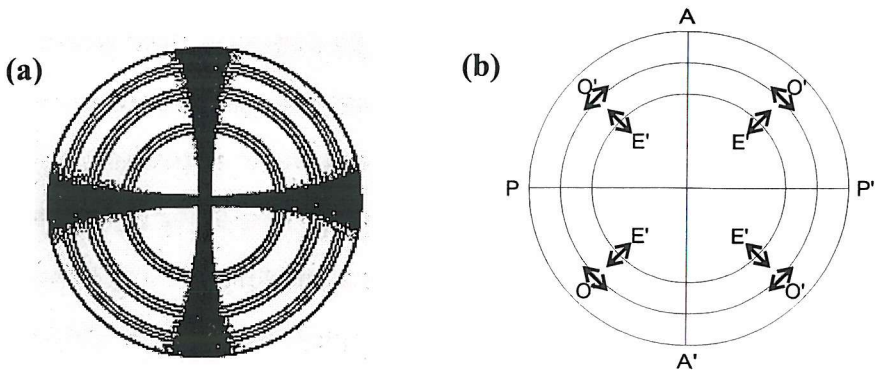

Figure 5.7 : (a) Conoscopic image for a uniaxial phase, (b) the direction of vibration of the light rays. A,A': analyser axis, P,P': polariser axis, O': ordinary rays, E': extraordinary rays.

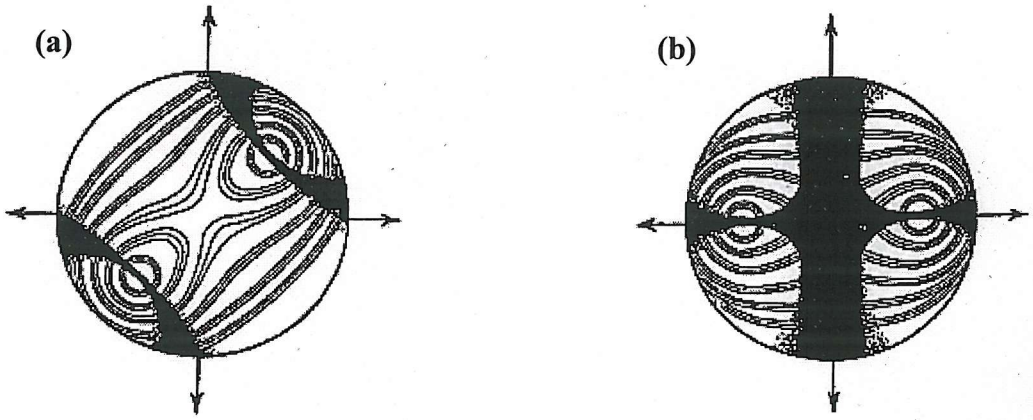

Figure 5.8 : Conoscopic images for a biaxial phase, (a) with the microscope stage rotated through 45°, (b) in the extinction position before rotation.

5.2.3 X-ray Diffraction

As discussed in the Introduction (§1.10) the diffraction pattern of an aligned uniaxial nematic phase will, with the correct orientation of the beam to the director, consist of a pair of diffuse outer arcs that correspond to the side-by-side molecular distances and a pair of smaller inner arcs that correspond to the effective molecular length of the mesogenic moiety. The presence of the single pair of wide angle arcs is an indication of cylindrical symmetry of the uniaxial mesogens as there is no preferred alignment of the minor axes. A monodomain biaxial nematic phase will give a diffraction pattern that consists of, once again, a small pair of low angle arcs, corresponding to the molecular length along the long molecular axis, *z*. However, there should be two pairs of wide angle arcs that correspond to the different molecular lengths in both the *x*- and *y*-directions, indicating the biaxial nature of the mesogens. Alternatively, if the beam is aligned along the main director we will see a diffuse ring for uniaxial mesogens, and a diffuse pair of arcs for biaxial mesogens, with a second aligning field.

5.2.4 Deuterium NMR Spectroscopy

As it is possible to examine the orientational order of a liquid crystal phase using deuterium NMR, the technique also allows us to determine the phase symmetry and director distributions of uniaxial and biaxial phases. As was stated previously (§3.2.2) the separation between the two peaks of the doublet obtained from the quadrupolar splitting in a liquid crystalline phase is simply

$$\Delta\tilde{\nu} = \tfrac{3}{2} q_{CD} S_{CD}, \qquad (1)$$

where q_{CD} is the quadrupolar coupling constant for the deuteron in the C-D bond and S_{CD} is the order parameter for the C-D bond. For liquid crystals with a positive diamagnetic susceptibility, $\Delta\tilde{\chi}$, the director will align parallel with the magnetic field. However, if the sample is rotated by an angle, β, with respect to the magnetic field the quadrupolar splitting becomes

$$\Delta\tilde{\nu}(\beta) = \Delta\tilde{\nu}(0) \cdot \frac{(3\cos^2\beta - 1)}{2}. \qquad (2)$$

Therefore on rotating the sample the splitting will decrease until, at the so-called magic angle of 54.7°, only a single line is observed. Beyond this value the peaks move apart again until at 90°, that is when the director is orthogonal to the field,

the splitting becomes equal to $-\Delta\tilde{\nu}(0)/2$, however the sign cannot be determined, or half the value of the quadrupolar splitting when the director is parallel with the magnetic field.

As mentioned previously, for a uniaxial phase the order parameter along the *z*-direction is different to that along the *x*- and *y*-directions and that the order parameters, S_{xx} and S_{yy}, along these two directions are identical. For a biaxial phase these order parameters along all three directions are different. Therefore it is possible to determine the symmetry of the phase using deuterium NMR spectroscopy as the form the spectrum will take depends on the director distributions in the different phases. If there is a non-uniform distribution of the directors we should see different quadrupolar splittings for the three principle directions. The following will give a description of the possible director distributions.

5.2.5 The 3D Powder Pattern

Figure 5.9 shows the deuterium NMR spectra for both a uniaxial phase and a biaxial phase for a three-dimensional random director distribution with respect to the field. For the uniaxial phase, figure 5.9(a), we see that the spectrum consists of an inner doublet, or horns, and a pair of outer wings. The separation of the outer wings is twice that of the inner doublet. The outer wings are due to domains in the sample in which the major axis or director, i.e. the *z*-axis is parallel to the magnetic field, and the inner doublet results from the director being perpendicular to the magnetic field. As equation (2) shows, the quadrupolar splitting when the director is perpendicular to the magnetic field is half that for when the director is parallel with the field and therefore the separation between the inner doublet is half that of the outer wings.

However, as can be seen in figure 5.9(b), the spectrum is qualitatively different for a biaxial phase. Here the quadrupolar splittings along the *x*- and *y*-axes are different and therefore the inner doublet is split into two doublets. As all director orientations are possible in a three-dimensional powder distribution, as well as those when the *z*-axis is either parallel or perpendicular to the magnetic field, the

spectrum consists of a pair of outer wings, from the order parameter along the *z*-axis, and an inner doublet that has a pair of shoulders corresponding to the quadrupolar splittings along the *x*- and *y*-axes.

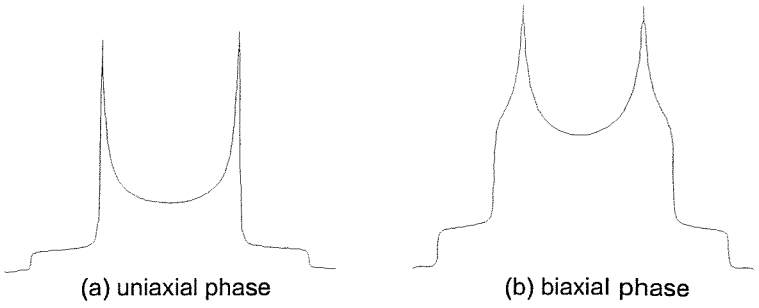

Figure 5.9 : The 3D powder spectrum exhibited by a uniaxial and biaxial phase.

5.2.6 The 2D Powder Pattern

If we now consider a situation in which the two minor directors are distributed randomly in a plane orthogonal to the magnetic field and the major director is aligned parallel to the magnetic field, for a uniaxial phase we obtain a spectrum of the form shown in figure 5.10(a). Obtaining this director distribution is easily achieved by spinning the sample. The outer doublet corresponds to a situation in which the *z*-axis is parallel to the magnetic field and the inner doublet is due to the case in which the *x*- or *y*-axis is parallel to the magnetic field. The separation between the outer peaks is twice that of the inner peaks as the ordering perpendicular to the field is half that parallel to the magnetic field. However this only true for very sharp lines, in practice the exact 2:1 ratio is hard to determine.

As the order parameter, and hence the quadrupolar splittings, along the *x*- and *y*-axes are different for a biaxial phase the inner doublet of the 2D powder spectrum has an additional pair of shoulders, as shown in figure 5.10(b). In this case, as with the uniaxial case, it is assumed that the *x*- and *y*-axes are randomly distributed in a plane orthogonal to the magnetic field. However, if we can confine not only the director (*z*-axis) but one of the minor axes, for example the *x*-axis, in a plane containing the magnetic field the spectrum will simplify somewhat and only consist of two pair of doublets representing the different quadrupolar splittings along the *x*- and *z*-axes. Although the production of such a director distribution sounds a non-trivial task, in practice it is easy to achieve by spinning the sample

about an axis orthogonal to the magnetic field above a certain critical speed. For a biaxial phase the separation of the inner doublet will not be half that of the outer doublet as seen for a uniaxial phase. The deviation from this uniaxial case allows us to determine the extent of phase biaxiality, which can be quantified in the following way.

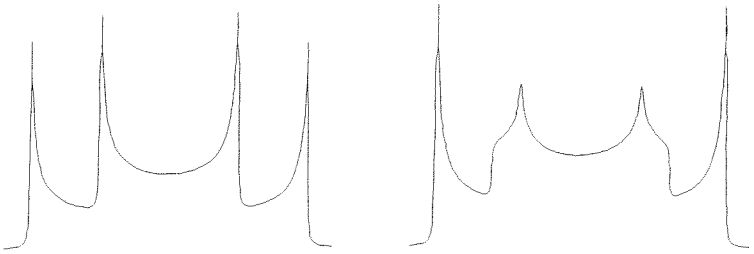

Figure 5.10 : The 2D powder spectrum exhibited by a uniaxial and biaxial phase.

For a uniaxial nematic phase the partially averaged quadrupolar tensor has principal components $\tilde{q}_{zz} \neq \tilde{q}_{xx} = \tilde{q}_{yy}$ where z is parallel to the director and x and y are orthogonal to it. Since the quadrupolar tensor is traceless, that is $\tilde{q}_{xx} + \tilde{q}_{yy} + \tilde{q}_{zz} = 0$, then $\tilde{q}_{zz} = -2\tilde{q}_{xx}$ and so there is only one independent component of this tensor. However, for a biaxial phase the principle components are all different, that is $\tilde{q}_{zz} \neq \tilde{q}_{xx} \neq \tilde{q}_{yy}$ and as the quadrupolar tensor is traceless there are now two independent components, the major component $\tilde{q}_{zz}$ and the difference $\tilde{q}_{xx} - \tilde{q}_{yy}$ which is represented by the dimensionless biaxiality parameter $\tilde{\eta} = (\tilde{q}_{xx} - \tilde{q}_{yy})/\tilde{q}_{zz}$. Therefore, to measure the biaxiality of the phase we need to measure only two of the principle components of the quadrupolar tensor which we have just established is possible. It should be noted that the biaxiality parameter is a pragmatic definition which also depends on the orientation of the C-D bond in a molecule.

For a uniaxial phase the quadrupolar splitting depends only on the angle, β, between the magnetic field and the director such that

$$\Delta\tilde{\nu}(\beta) = \tfrac{3}{2}\tilde{q}_{zz}P_2(\cos\beta), \qquad (3)$$

where the label *zz* indicates the component parallel to the director and $P_2(\cos\beta)$ is the second Legendre polynomial. The positions of the lines in the spectrum are given by

$$\tilde{\nu}(\beta) = \nu_0 \pm \tfrac{3}{4}\tilde{q}_{zz}P_2(\cos\beta), \qquad (4)$$

where ν_0 is the central frequency. To determine the form of the 2D powder spectrum all that is required is to take the sum of spectra from all director orientations with respect to the magnetic field. For a biaxial phase, however, the positions of the line will depend not only on β but also on the biaxiality parameter, and is given by

$$\tilde{\nu}(\beta) = \nu_0 \pm \tfrac{3}{4}\tilde{q}_{zz}[P_2(\cos\beta) + \tfrac{1}{2}\tilde{\eta}\sin^2\beta\cos 2\gamma], \qquad (5)$$

where γ is the angle made to the field by the component $\tilde{q}_{xx} - \tilde{q}_{yy}$ orthogonal to the *z*-axis. Again, to generate a simulated 2D powder spectrum we make cos 2γ = 1 and sum the spectra from all director orientations orthogonal to the spinning axis. Figure 5.11 shows the simulated spectra obtained on varying $\tilde{\eta}$ from 0 to 1, the maximum value [14]. Therefore, by comparing the simulated spectra with the experimental spectra, a measure of the biaxiality of the phase can be obtained.

5.3 Thermotropic Biaxial Nematogens

In this section we will discuss the attempts made to design thermotropic mesogens that exhibit a biaxial nematic phase. The first such example considered was the combination of a disc and a rod reported by Malthete *et al.* [12] shown in figure 5.12.

The identification of the biaxial nematic phase was based on zig-zag disclinations seen running through the schlieren texture observed under a polarising microscope and also on the X-ray diffraction pattern seen. However, the phase sequence reported on cooling from the isotropic phase was I – N_B – N_U and not I – N_U – N_B as predicted by theory [1]. Therefore, in 1994 Shenouda *et al.* [15] resynthesised the material to examine the biaxial nematic phase more closely.

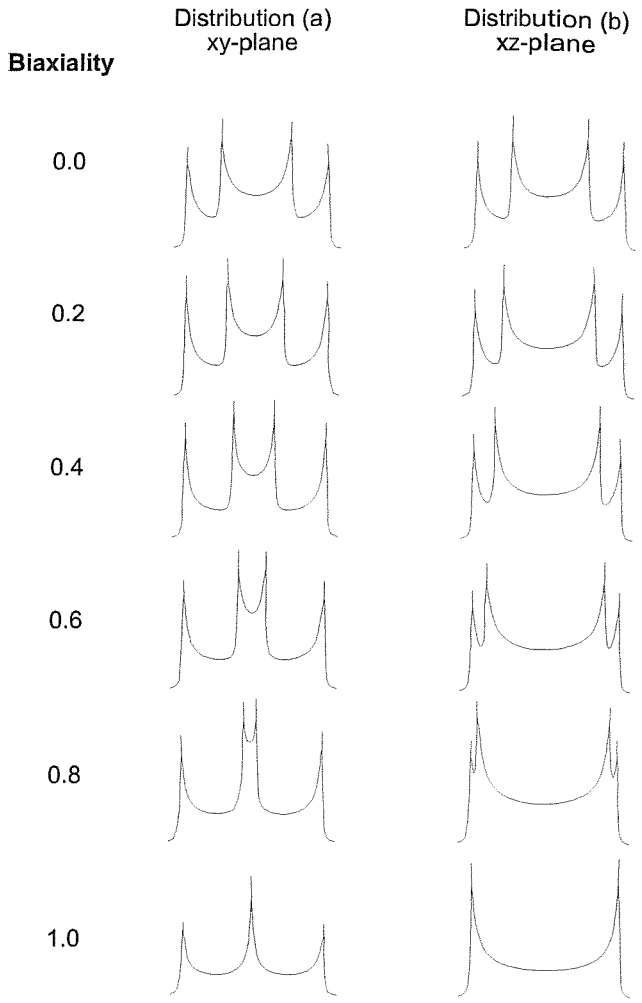

Figure 5.11 : Simulated 2D powder spectra as the biaxiality parameter is varied from 0 to 1.

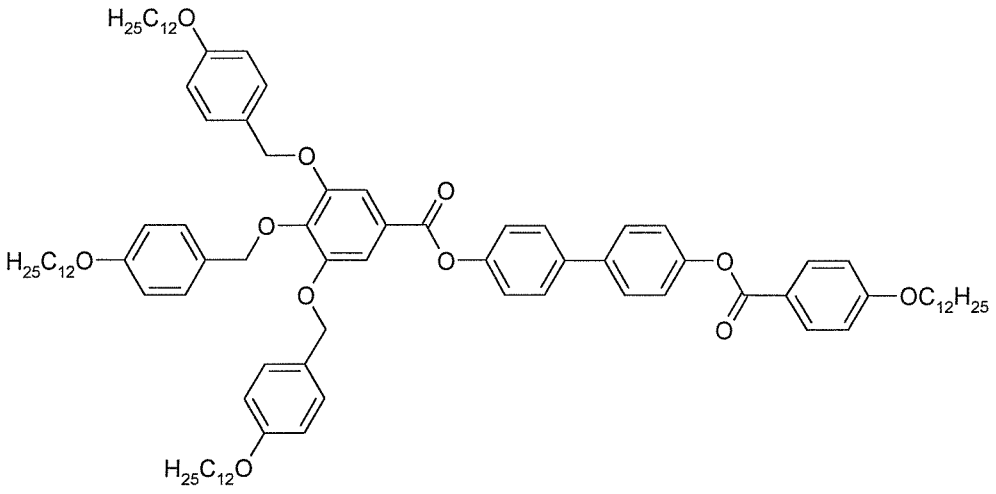

Figure 5.12 : Example of a suggested thermotropic biaxial nematic material prepared by Malthête [12].

X-ray diffraction studies showed that as the phase is cooled from the isotropic liquid in the presence of a magnetic field a uniaxial nematic phase is first observed. Then as cooling is continued cybotactic clusters appear in the nematic phase, with a molecular tilt of ~40°, and subsequently a smectic C phase is formed. The lack of reflections corresponding to three molecular lengths in the X-ray scattering suggested that the nematic phase was uniaxial, although this is not a definite indication of the phase symmetry. The correct phase assignment was later confirmed by Hughes *et al.* [16] using deuterium NMR. The biaxiality parameter was found to be zero within the limits of the experiment for both the specifically deuteriated material and when a small amount of the disc-like hexamethylbenzene-d_{18} was dissolved in the mesogen.

Later, in 1988, Chandrasekhar *et al.* [17,18] reported a monotropic biaxial nematic phase for the copper complex:

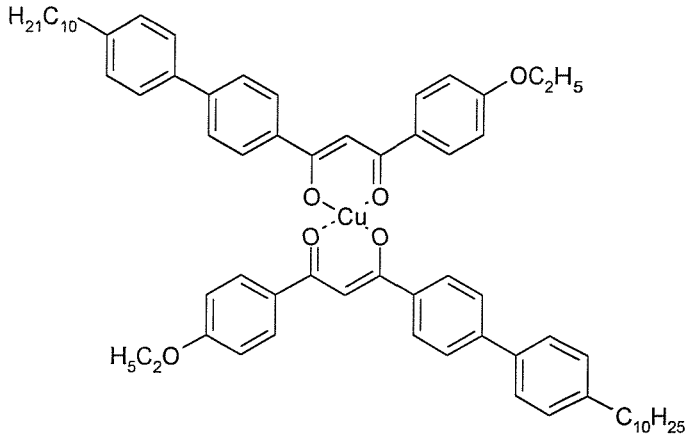

This material underwent a transition directly from the isotropic liquid to the biaxial nematic phase which was identified by conoscopy. However, after a 45° rotation of the microscope stage the malthese cross pattern produced in the extinction position was seen to split into two hyperbolic brushes whose centres remained in close proximity to each other, thus indicating a small optical biaxiality. This small splitting of the hyperbolic brushes may be due to surface effects caused by the microscope slides creating a tilt of the director at the surface and does not compare in size to the large splitting, observed by Yu and Saupe [5], for their lyotropic systems, where the brushes are seen to approach the edges of the microscopic field

of view. It is, therefore, not conclusive that a biaxial nematic phase has been observed. It was thought that due to the paramagentism of the copper ion in the complex it was not possible to carry out any deuterium NMR studies and so determine the symmetry of the phase. However, a deuterium NMR spectrum was obtained and the phase was proved to be uniaxial [19].

Praefcke and his group have claimed also [20], that the discotic materials of the form

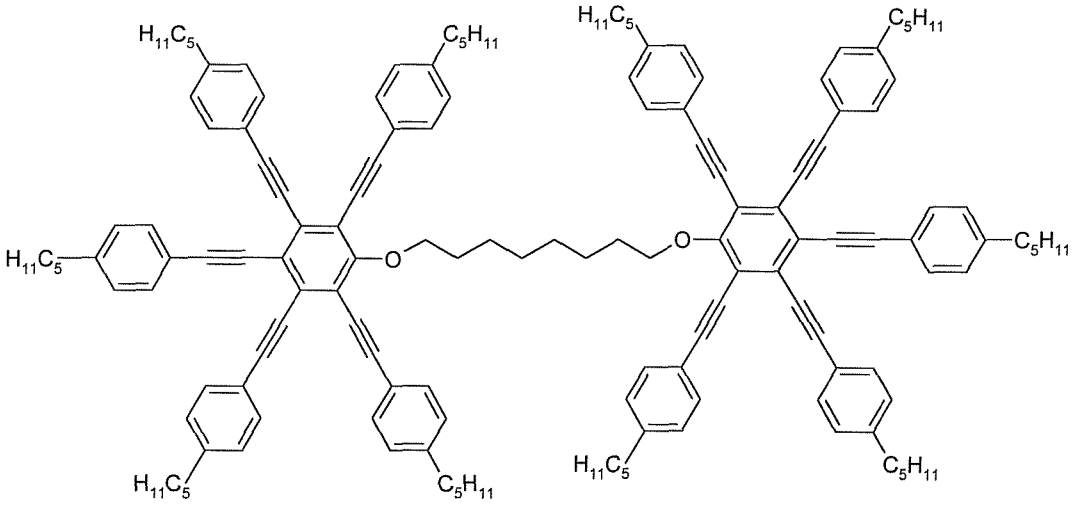

as mentioned in Chapter 2, exhibited biaxial discotic nematic (N_b) phases.

The assignment of these phases was once more based on conoscopic evidence. Like the previous example, when the microscope stage was rotated 45° from the extinction position, the splitting of the hyperbolic brushes was only very small. As the conoscopic effect was unchanged for layers of a different thickness it was inferred that the splitting was not due to any surface effect. The biaxiality of the phase, if any, is therefore only small and not of the order seen in lyotropic systems.

Praefcke *et al.* have also claimed [21,22] that the cinnamic acids:

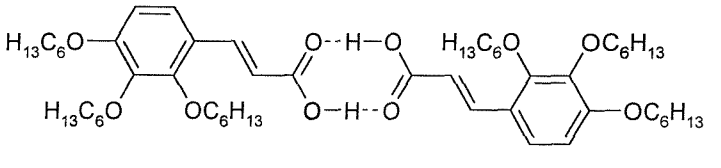

exhibit a biaxial nematic phase. The monomeric materials hydrogen-bond to form dimers that exhibit enantiotropic phases. The symmetry of the nematic phase was assigned using both conoscopy and X-ray diffraction, with the diffraction pattern of an oriented sample showing three diffuse arcs, however this only gives information about the local structure.

To establish the exact nature of the phase exhibited by these cinnamic acids a specifically deuteriated hexyl analogue was prepared, where the deuterons were located in the ethylenic bonds, and the phase investigated using deuterium NMR spectroscopy [23], as outlined in §5.2.6. Comparison of the spectrum obtained by spinning the sample orthogonal to the magnetic field, with simulated spectra, showed that the biaxiality parameter is less than 0.1, which again is small when compared with that for lyotropic biaxial nematic systems.

More recently, a biaxial nematic phase has been reported for the cyclic trimer shown below [24], which it is claimed shows a $N_U - N_B$ phase transition.

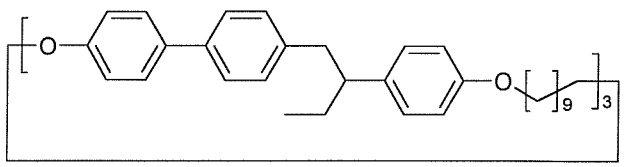

5.4 Quantifying the Biaxiality of Thermotropic Mesogens

Although it can be seen that there is no shortage of materials that have been claimed to exhibit thermotropic biaxial nematic phases there has been no definitive success in forming this elusive phase. The search for such materials may be hindered by the fact that although the molecules appeared to have a high degree of shape biaxiality, the extent of this had not been quantified. Consequently it was not possible to judge how close the materials were to the optimum molecular biaxiality necessary to form a biaxial nematic phase. To address this problem Ferrarini *et al.* [25] used a molecular field approach to estimate the minimum molecular biaxiality for which a biaxial nematic phase might be expected. The phase behaviour was calculated for a system of rigid particles as a function of the molecular biaxiality,

λ, and is shown in figure 5.13. The phase diagram was calculated using the surface tensor model as described by Ferrarini *et al.* [26] and is defined as

$$\lambda = T^{(2,2)} / T^{(2,0)}. \qquad (6)$$

Here, λ is related to the molecular biaxiality for the simplest case of box shaped molecules by

$$\lambda = \frac{\sqrt{3}L(W-B)}{2L(B+W)-2BW}, \qquad (7)$$

where W, B and L are, respectively, the width, breadth and length of the box. The maximum biaxiality occurs when $W^{-1} + L^{-1} = 2B^{-1}$ and then $\lambda = 1/\sqrt{6}$.

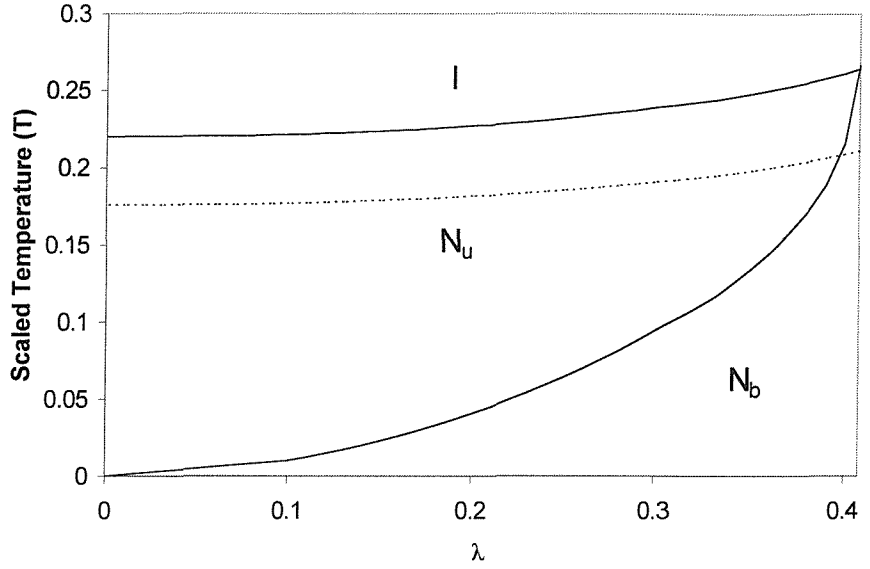

Figure 5.13 : The predicted phase diagram for rigid particles as the biaxiality, λ, is changed. The dashed line corresponds to an assumed freezing point of $0.8T_{NuI}$.

Although this is just a crude approximation of the actual shape of biaxial molecules the phase diagram shows the appearance of a biaxial nematic phase at lower temperatures. The transition temperature for the uniaxial nematic – isotropic transition increases slightly as the biaxiality increases, however the biaxial nematic – uniaxial nematic transition temperature increases faster as λ grows until a point is reached where it is predicted that the isotropic phase will undergo a second order

transition directly to the biaxial nematic phase. This point occurs when $\lambda = 1/\sqrt{6}$, i.e. when the biaxiality of the box is at a maximum.

The phase diagram suggests that, in theory, any compound with λ greater than zero should exhibit a biaxial nematic phase, however in practice this is usually prevented by the uniaxial phase freezing. The dotted line on the phase diagram indicates the freezing point which is assumed to be at a reduced temperature $\tilde{T}/\tilde{T}_{NI}$ of 0.8, which for a nematic – isotropic transition temperature of, say, 400 K corresponds to a nematic range of 80 K. Therefore, for a biaxial nematic phase to be observed the biaxiality has to be very close to the maximum value, and have a very narrow range, i.e. λ needs to be between about 0.39 and 0.41. As a result of this rather tight constraint any molecule that might exhibit a biaxial nematic phase is required to have the geometry of a typical house-brick! As molecules of this shape are not expected to form liquid crystalline phases this no doubt explains the lack of conclusive thermotropic biaxial nematic phases.

However, it has been found that liquid crystalline phases can be formed from biaxial molecules that do not have a lath-like structure. Molecules with a bent, rigid core have been shown to be mesogenic [27,28,29]. These molecules are often referred to somewhat misleadingly as 'banana' shaped molecules. In 1996, Niori *et al.* [30] synthesised the following V-shaped material:

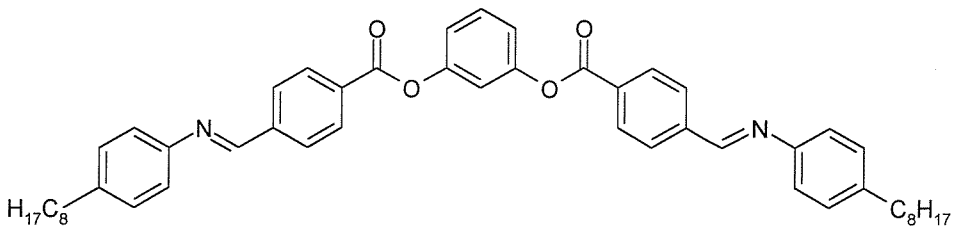

Although this material did not exhibit any nematic phase the material showed two smectic phases. It was proposed, from X-ray and optical microscopic observations, that the higher temperature smectic phase had the structure as shown in figure 5.14(a), with its space group symmetry shown in figure 5.14(b).

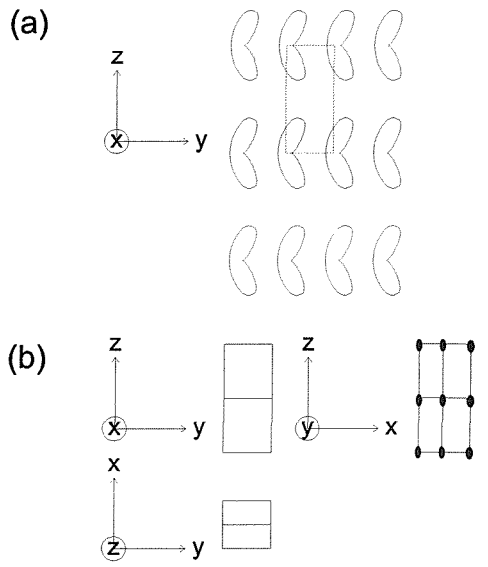

Figure 5.14 : The proposed packing of the V-shaped molecules, prepared by Niori *et al.* [30], in the smectic phase.

It is obvious from figure 5.14 that the layers themselves have biaxiality and that one way of considering the phase is as a biaxial smectic A phase, or even an alternating smectic C phase. It is therefore reasonable to expect that if a biaxial smectic A phase can be formed from biaxial, bent molecules then it may be possible to form a biaxial nematic phase from bent molecules if the biaxiality is large enough and the transition temperatures are not prohibitive.

In the same way that we can quantify the biaxiality of brick-shaped molecules in terms of its dimensions, we should be able to estimate the transition temperatures of bent mesogens, based on the angle between the two mesogenic groups. This would make the design of thermotropic biaxial nematic materials somewhat simpler as it is easier to design a molecule consisting of just two mesogenic groups than a brick shaped molecule where the length, width and breadth need to be considered instead of just the core angle. To do this we need to consider a V-shaped molecule comprising two rigid mesogenic groups connected at an angle, θ, as shown in figure 5.15

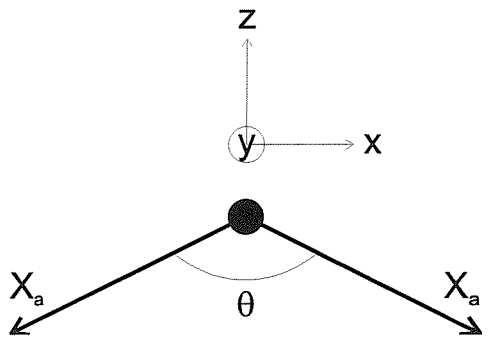

Figure 5.15 : The model used to determine the biaxiality of bent mesogenic materials.

We can define two molecular strength parameters in terms of that for the mesogenic group, X_a, as

$$X_{20} = X_a(1-3\cos\theta)/2, \qquad (8)$$

$$X_{22} = (\tfrac{3}{8})^{\frac{1}{2}} X_a(1+\cos\theta), \qquad (9)$$

where X_{20} and X_{22} are the major and biaxial strength parameters for the V-shaped molecule, respectively, and $X_a = \varepsilon_{aa}\overline{P_2}$, where $\overline{P_2}$ is the order parameter for the mesogenic group and not for the principal axis of the V-shaped molecule. As the biaxiality parameter, λ, is given as the ratio X_{22}/X_{20} then the biaxiality is

$$\lambda = (\tfrac{3}{2})^{\frac{1}{2}}(1+\cos\theta)/(1-3\cos\theta). \qquad (10)$$

In the limit $\theta = 180°$ then X_{22} vanishes and X_{20} is just $2X_a$, which corresponds to a uniaxial molecule, and $\lambda = 0$. At the tetrahedral angle of 109.5°, i.e. $\cos^{-1}(-1/3)$, then $X_{20} = X_a$ and $X_{22} = X_a/\sqrt{6}$. This gives the biaxiality as $1/\sqrt{6}$ which, as we have seen previously, is its maximum value. Now, all that is needed is to reconstruct the phase diagram in figure 5.13 as a function of the angle between the two mesogenic units rather than λ. We also need to scale the temperature with respect to the angle between the two groups and this can be calculated in terms of the transition temperature of a linear molecule using equation (11)

$$\frac{\tilde{T}}{\tilde{T}_{NI}^{(l)}} = \frac{16}{(1-3\cos\theta)^2}, \qquad (11)$$

where $\tilde{T}_{NI}^{(l)}$ is the transition temperature of the linear molecule. Figure 5.16 shows the phase diagram calculated for the V-shaped molecule as θ varies.

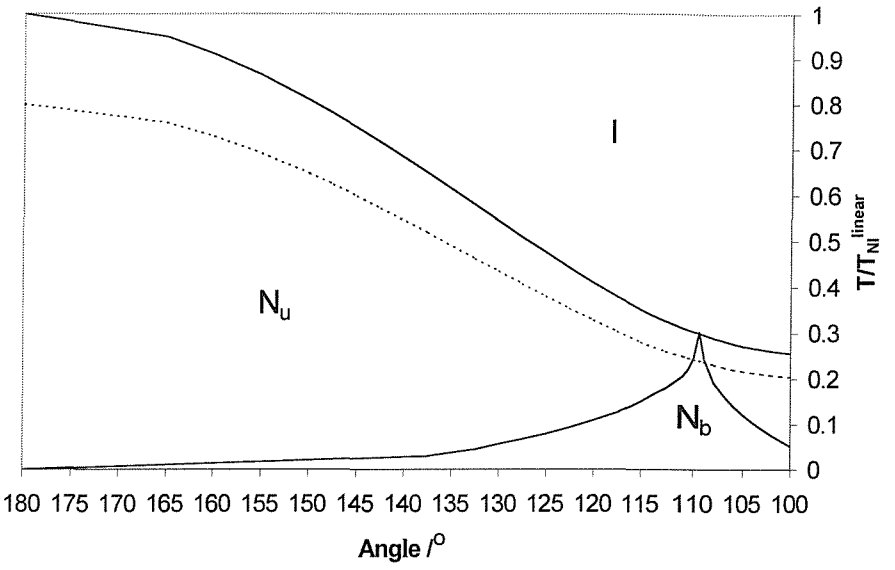

Figure 5.16 : The predicted phase diagram as the angle, θ, between two mesogenic groups is changed, based on the model in figure 5.15. The dashed line corresponds to an assumed freezing point of $0.8T_{NuI}$.

As can be seen the phase diagram is now somewhat different to that seen for box-shaped molecules. As the angle joining the two rigid groups is reduced the uniaxial nematic – isotropic transition temperature falls. This is not too surprising as the prerequisite for liquid crystalline behaviour is for the materials to be linear, and therefore any reduction to this linearity should serve to reduce the transition temperature. However, the uniaxial nematic – biaxial nematic transition temperature shows the expected increase as the angle is reduced until, at the tetrahedral angle of 109.5°, it is predicted that there will be a second-order transition direct from the biaxial nematic phase to the isotropic phase. If we once more assume that the melting point occurs at a reduced temperature, T / T_{NI}, of 0.8 then it appears that a biaxial nematic phase should only exist if the angle between the two mesogenic groups is between about 110° and 108°. Clearly this criteria is as restrictive as that for the box-shaped materials and it would seem that the use of

V-shaped molecules provides as many difficulties in the design of biaxial nematic materials as box-shaped materials.

An alternative approach to determining the phase behaviour of bent molecules is by using the surface tensor model to estimate the biaxiality parameter λ. If we consider the molecule to consist of two square cross-section blocks, of length, L, and breadth, B, joined via a wedge, at an angle, θ, as shown in figure 5.17, we can write expressions for the two components of the interaction tensor, $T^{(2,0)}$ and $T^{(2,2)}$ as such

$$T^{(2,0)} = (2LB - B^2)(1 - 3\cos\theta)/2 \; + \; B^2 \cos(\theta/2)(1 + \sin(\theta/2)), \qquad (12)$$

$$T^{(2,2)} = (3/8)^{1/2}(2LB - B^2)(1 + \cos\theta) \; - \; 2B^2 \cos(\theta/2)(1 - \sin(\theta/2)), \qquad (13)$$

where the first part of each expression is due to the blocks, and the second part of each expression takes into account the wedge shape. If we use equation (6) to determine the biaxiality parameter, λ, and calculate the transition temperature using equation (11) we can once more construct a phase diagram in terms of the angle made between the two blocks again with the temperature scaled with T_{NI} of the linear form. This time, however, we can also vary the length-to-breadth ratio of the two blocks. Figure 5.18 shows the phase diagrams for length-to-breadth ratios of 3:1, 4:1 and 5:1.

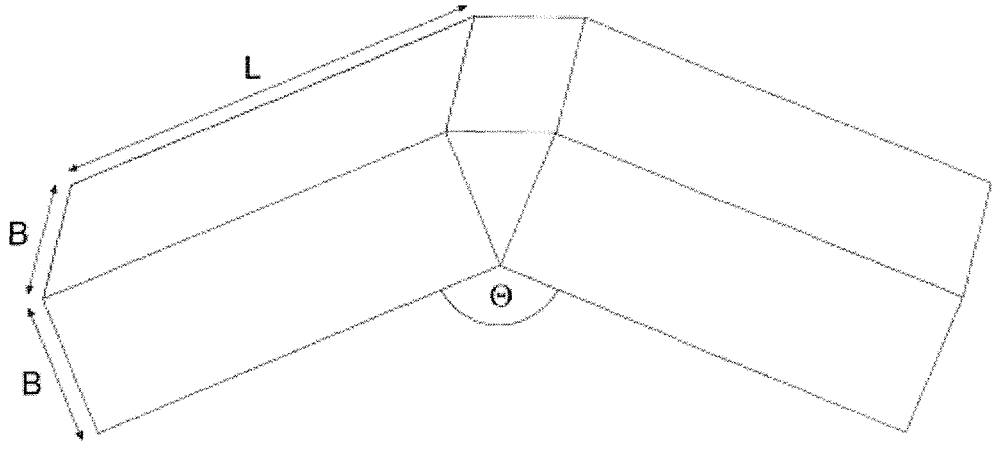

Figure 5.17 : The model used to determine the biaxiality of bent molecules using the surface tensor approach.

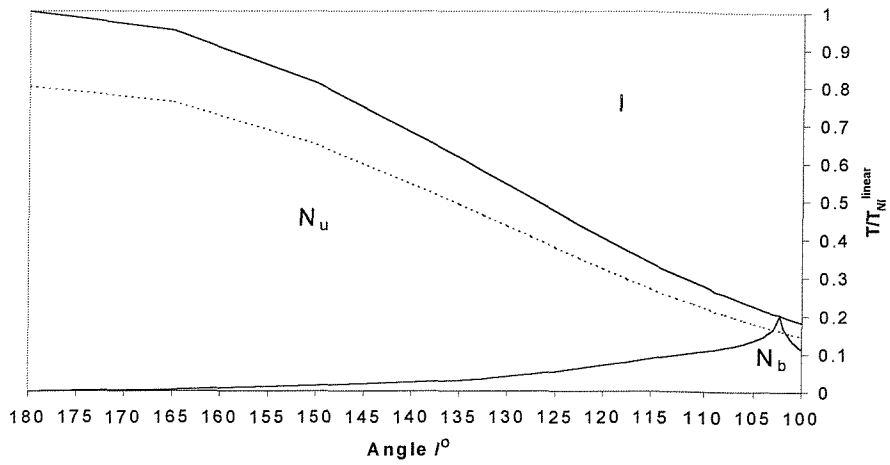

Length-to-breadth ratio = 3:1

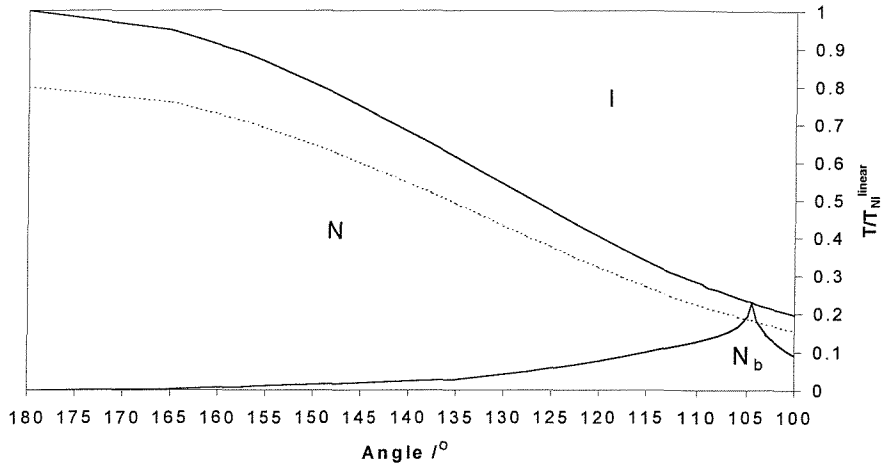

Length-to-breadth ratio = 4:1

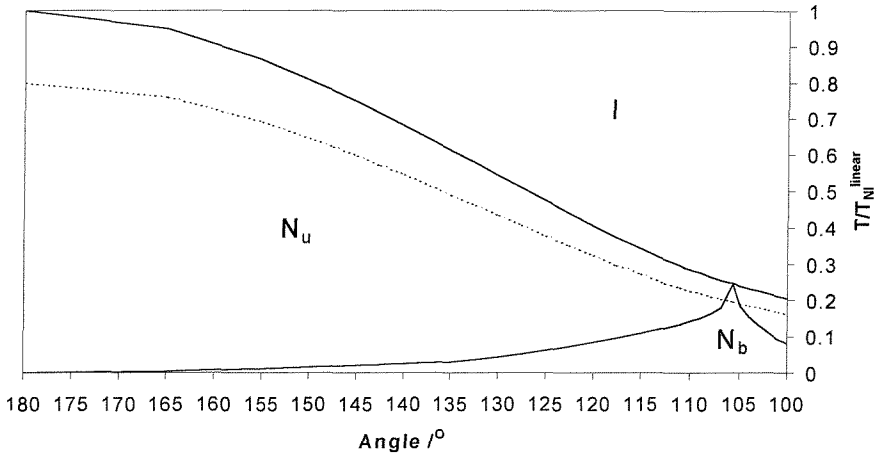

Length-to-breadth ratio = 5:1

Figure 5.18 : The predicted phase diagram as the angle, θ, in the model in figure 5.17 is changed, for different length-to-breadth ratios. The dashed line corresponds to an assumed freezing point of $0.8T_{NuI}$.

Unsurprisingly, the form of the phase diagrams is the same as for the previous model. However, it would appear that the extra wedge-shape serves to move the point at which there is a transition direct from the biaxial nematic to the isotropic phase from the tetrahedral angle to a more acute angle. Conversely, as the length-to-breadth ratio of the blocks is increased this point move back to larger angles. This is because, from equations (12) & (13), as L becomes larger so the terms associated with the wedge-shape become smaller and therefore the angle at which the maximum biaxiality will occur tends to the tetrahedral angle. Also, the reduction in transition temperature as the angle is reduced is greater than the previous model, with the length-to-breadth ratio of 3:1 having the greatest reduction. Once again the dotted line indicates an imaginary melting point of T / T_{NI} of 0.8 and this limits the angle at which a biaxial nematic phase may be observed to a very small range – between about 101° and 103° for a length-to-breadth ratio of 3:1, 104° and 106° for a length-to-breadth ratio of 4:1 and 105° and 107° for a length-to-breadth ratio of 5:1.

5.5 Testing the Theory

For the theory to be useful we should be able to predict the change in the uniaxial nematic phase – isotropic phase transition temperatures, as the angle linking the two mesogenic groups is changed, for real liquid crystals. In this section we will compare a number of series of mesogenic materials where the only difference between the two series are that one contains a linear mesogenic core and the other contains a bent core. Assuming the linking group is a negligible fraction of the total molecule, if the theory holds we would expect that a plot of the transition temperatures of the bent mesogens against the linear mesogens will lie on a straight line. Figure 5.20 shows three plots comparing three different sets of bent and linear mesogens, whose structures are shown in figure 5.19, as the terminal chain lengths increase.

It can be seen that the agreement between the 'bent' and 'linear' transition temperatures in all three cases is good, especially for the thiophene ester vs. phenyl ester. It should be noted that for some of the materials with longer chain lengths the transition to the isotropic is, in fact, from a smectic A phase and not a nematic phase, however this does not seem to have affected the result in any significant

way. The larger scatter seen for the pyrazole vs. terphenyl series may be explained by the fact that it has been suggested that there is a significant amount of hydrogen bonding between the pyrazole rings [31] and this may affect the transition temperatures in an unpredictable manner.

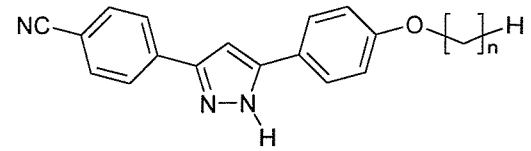

Pyrazine (A)

Bend angle = 154°

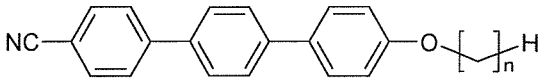

Terphenyl (B)

n = 4 to 12

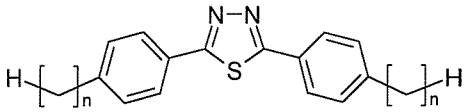

Thiadiazole (C)

Bend angle = 157°

Terphenyl (D)

n = 3 to 8

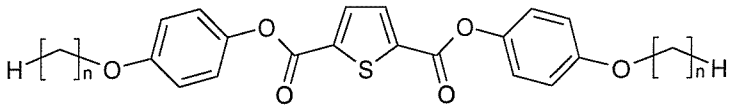

Thiophene ester (E)

Bend angle = 148°

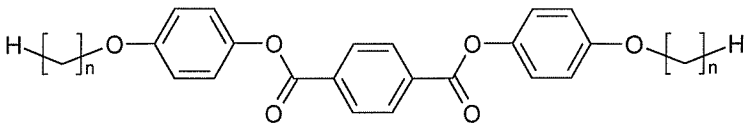

Phenyl ester (F)

n = 1 to 10

Figure 5.19 : The three sets of bent and linear mesogens to test the theory.

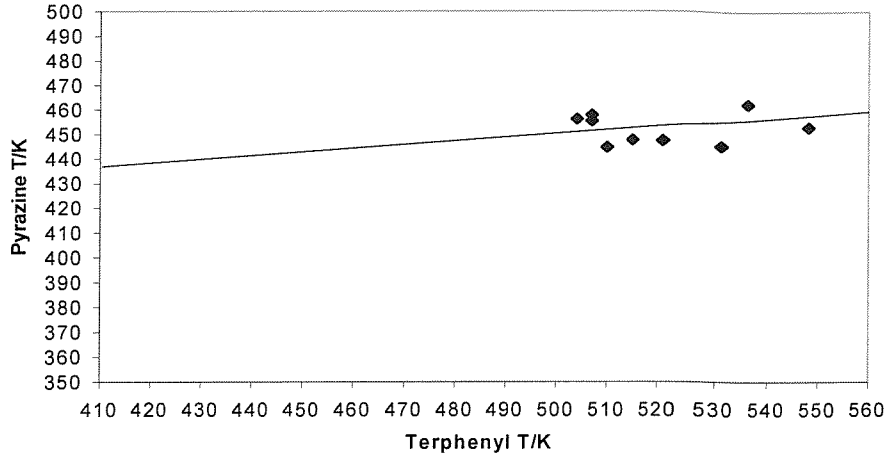

Pyrazine (A) [31] vs. Terphenyl (B) [32]

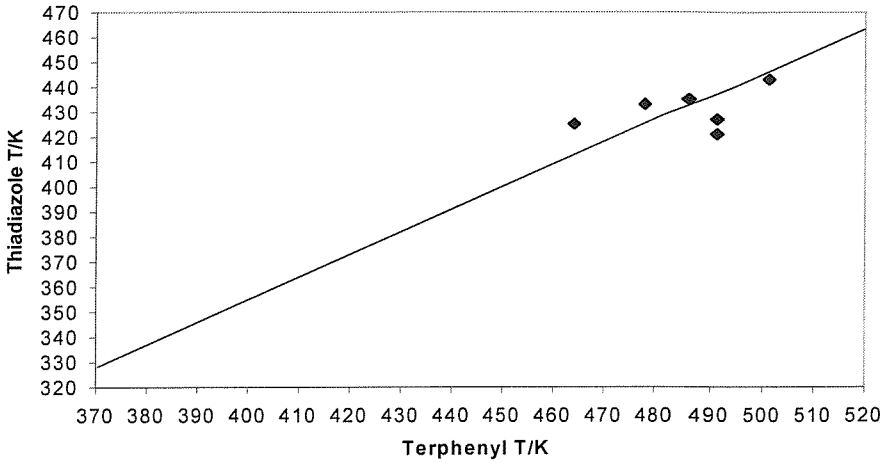

Thiadiazole (C) [35] vs. Terphenyl (D) [35]

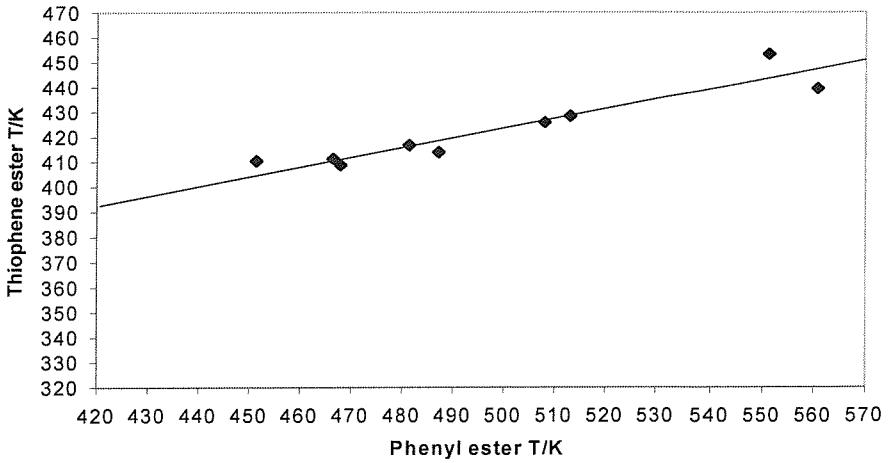

Thiophene ester (E) [27] vs. Phenyl ester (F) [27]

Figure 5.20 : Comparison of the transition temperatures of the linear and bent materials shown in figure 5.19.

Whilst the plots in figure 5.20 give an indication that the change in transition temperatures on going from a linear molecule to a bent molecule remains reasonably consistent, they do not actually tell us whether we are able to predict the transition temperatures by knowing the angle at which the core is bent. Alternatively, by knowing the change in transition temperature we should be able to predict the angle of bend in the molecule. Therefore, tables 5.1, 5.2 and 5.3 list the transition temperatures of the materials used for the plots in figure 5.20 together with the ratio of the bent / linear transition temperatures and the bend angle that the theory predicts. The model we use here is the two mesogenic groups joined at an angle, θ, and not the surface tensor model.

As can be seen the predicted bend angle for each series is quite good. Although there is a small amount of variation throughout each series, with the mean value for the angle being slightly higher than expected, the prediction is surprisingly good, especially for those members of the series with shorter chain lengths. It can also be seen that as the chain lengths are increased the predicted angles increase. This may be a consequence of the flexible alkyl chains effectively trying to straighten out the molecule. As the chains get longer the conformational freedom available to them increases and so it becomes easier to orient themselves to what could be considered as the molecular long axis, i.e. the bend angle is increased, as shown in figure 5.21.

As a stark example of how well the theory seems to predict the transition temperature, or indeed the bend angle, of bent molecules the furan analogue of the methoxy thiophene ester (E) was prepared by Dewar *et al.*[33]. This has a monotropic transition to the nematic phase at 62°C. Using this value it is predicted that the bend angle should be 133°, and we find that the quoted value [34] for furan is in fact 125°. Although the angle predicted is a slight overestimation it would seem that preparing molecules with bent, rigid cores may provide a way of designing thermotropic biaxial nematic liquid crystals. However, the bend angle has to be in a very narrow range and the nematic – isotropic transition temperature of the linear analogue has to be high because of the large reduction in this temperature when the molecule is bent.

n	Transition Temperature /K		Ratio (A/B)	Predicted Angle /°
	Pyrazine (A)	Terphenyl (B)		
4	452.9	548.1	0.826	151.1
5	462.3	536.1	0.862	155.3
6	445.2	531.1	0.838	152.5
7	447.4	521.1	0.859	154.8
8	447.6	515.1	0.869	156.1
9	444.7	510.1	0.872	156.5
10	456.2	504.1	0.905	160.9
11	457.8	507.1	0.903	160.6
12	455.4	507.1	0.898	159.9

n	Transition Temperature /K		Ratio (C/D)	Predicted Angle /°
	Thiadiazole (C)	Terphenyl (D)		
3	501.1	443.1	0.884	158.1
4	491.1	421.1	0.857	154.7
5	486.1	435.1	0.895	159.6
6	491.1	427.1	0.869	156.2
7	478.1	433.1	0.906	161.1
8	464.1	425.1	0.916	162.6

n	Transition Temperature /K		Ratio (E/F)	Predicted Angle /°
	Thiophene (E)	Phenyl ester (F)		
1	560.7	439.3	0.783	146.9
2	551.1	453.2	0.822	150.7
3	513.1	428.3	0.835	152.1
4	508.1	425.8	0.838	152.4
5	487.2	413.8	0.849	153.7
6	481.4	416.7	0.866	155.7
7	467.9	408.8	0.874	156.7
8	466.5	411.3	0.822	157.7
10	451.4	410.4	0.909	161.6

Tables 5.1 (top) [31,32] 5.2 (middle) [35] and 5.3 (bottom) [27]:The predicted angle for the bent mesogens.

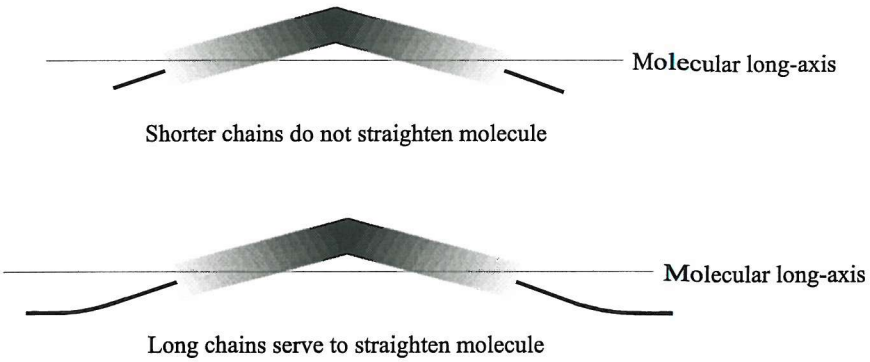

Figure 5.21 : The effect terminal chains have on straightening out the bent mesogens.

5.6 Thermotropic Biaxial Nematic Liquid Crystals

It would appear from the theory outlined in the previous section that to prepare a thermotropic biaxial nematic liquid crystal we need a material that has a linking group that is as close to tetrahedral symmetry as possible. A simple solution is to have two mesogenic moieties linked via a single methylene unit. We therefore prepared a number of methylene linked biphenyl 'dimers' as shown in figure 5.22.

Ideally the terphenyl dimers would seem to be a better choice, as the linear analogues are sexiphenyls which have a high nematic – isotropic transition temperature, but the synthesis of these materials is somewhat more difficult than for the biphenyl dimers. Therefore, by considering the transition temperatures of the linear related quaterphenyls we can get a prediction of the transition temperatures of the bent molecules. The clearing temperatures for short chain quaterphenyls are generally between *ca.* 380° – 400°C [35] which would suggest that the transition temperatures of the tetrahedral molecules (**9**,**11**,**13**) will be in the region of –50°C, and the transition temperature of the ketone (**12**), ignoring the effect that carbonyl group will have, will be around room temperature, although this material may not be bent enough to give a thermotropic biaxial nematic phase. Although these temperatures appear to be rather prohibitive to the formation of a liquid crystalline phase, if the melting points are low also, it may be possible to observe a mesophase.

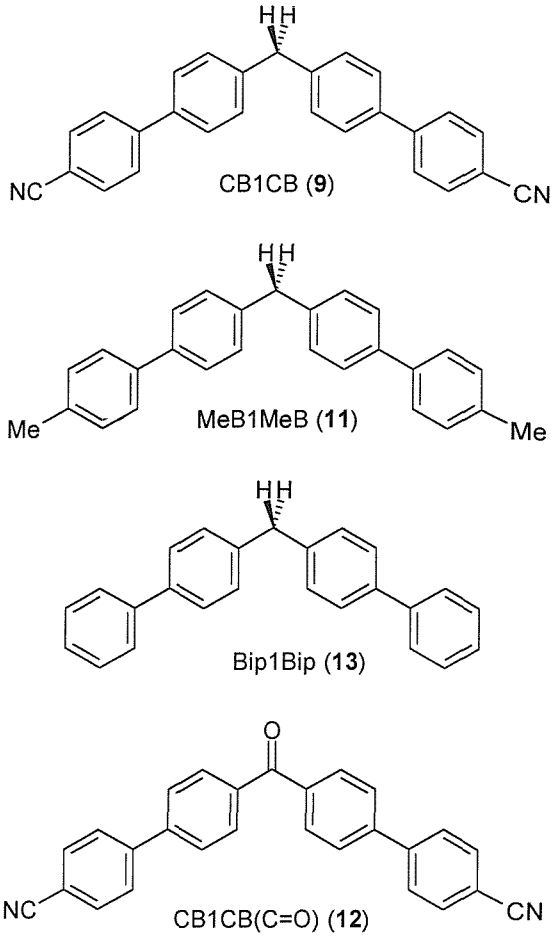

Figure 5.22 : The bent biphenyl 'dimers' we have prepared containing a tetrahedral linking unit and a carbonyl linking unit

However, all the materials had high melting points, as shown in table 5.4, and even supercooling the isotropic liquid by rapid cooling or by cooling small droplets did not reveal any monotropic phases. We have, therefore, determined the virtual transition temperatures, by preparing mixtures of the materials with 4-pentyl-4''-cyanoterphenyl (5CT), as shown in figure 5.23 and table 5.4.

As can be seen all of the tetrahedral materials (**9,11,13**) have virtual transition temperatures well below 0°C, with the methyl substituted biphenyl dimer (**11**) having a virtual transition temperature of –54.6°C which is similar to that predicted by the theory. The scaled transition temperature for the linear 4,4'''-dimethylquaterphenyl is predicted from this to be about 450° which is, in fact, very close to the clearing temperature of 4,4''''-dimethylsexiphenyl, which is 469°C. The one anomaly, however, is the ketone (**12**) which has a virtual transition temperature of 117.5°C. Scaling this temperature for the linear molecule predicts

that 4,4'''-dicyanoquaterphenyl should have a transition temperature of about 680°C which is significantly higher than that seen for other disubstituted quaterphenyls. It appears that the addition of a carbonyl group to the molecule has a significant effect on any mesophase behaviour and may be due to the large dipole associated with this moiety.

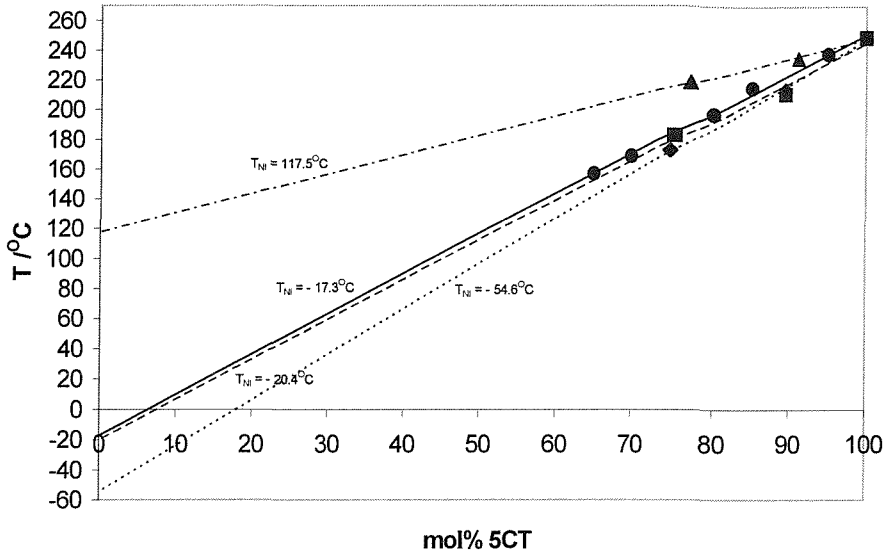

Figure 5.23 : Determination of the virtual transition temperatures of the bent biphenyl 'dimers'.

	Melting point /°C	Virtual T_{NI} /°C
CB1CB (**9**)	215	-17
MeB1MeB (**11**)	189	-55
Bip1Bip (**13**)	157	-20
CB1CB(C=O) (**12**)	197	117

Table 5.4 : The melting points and virtual transition temperatures of the bent biphenyl 'dimers'.

Unfortunately, the very high melting points of these materials prevents us from observing any mesophases and therefore we need a way of reducing them. Generally, the addition of terminal alkyl chains is used to reduce melting points, however we can also increase the number of methylene units between the two mesogenic moieties. Although this approach may appear to move us away from the idea of bent core, if the alkyl chain is taken to be all-trans, for those molecules with

an odd number of carbon atoms in the linking chain there is still a tetrahedral angle between the two moieties. This may still lead to the molecule having a high enough biaxiality to form a thermotropic biaxial nematic phase. The CB*n*CB series, where CB1CB (**9**) is the first member, has been extensively studied [36]. All members of the series with $n > 3$ exhibit an enantiotropic nematic phase, apart from CB5CB which possesses only monotropic phases, with the odd members also having a smectic A phase. In addition to this the entropy change at the nematic – isotropic transition for the odd members of the series is very small even for dimeric materials, with CB5CB having an entropy, $\Delta S/R$, of only 0.12, and CB7CB having an entropy of 0.3. This is significant because it has been predicted [1] that as the molecular biaxiality increases, the isotropic – uniaxial nematic transition weakens until at the maximum biaxiality there is a second order transition from the isotropic to the biaxial nematic phase. Such a low entropy of transition for these materials may indicate that they possess a large degree of biaxiality with a biaxial nematic – uniaxial nematic transition nearby. Therefore we may also expect that the nematic phase may also have some degree of biaxiality. It has also been shown by ESR spectroscopy [37] that the smectic A phase of CB7CB has an unusual structure. It was initially believed that as the smectic phase was cooled the layers began to ripple and that this rippled structure became more pronounced upon further cooling. However, it is apparent that the packing requirements of the molecules are unfavourable and other models have been proposed to explain the unusual ESR spectrum [38]. The results of Niori *et al.* [30] led us to speculate whether the smectic phase of this material may actually be biaxial. Therefore we have prepared CB7CB specifically deuteriated at the α-position:

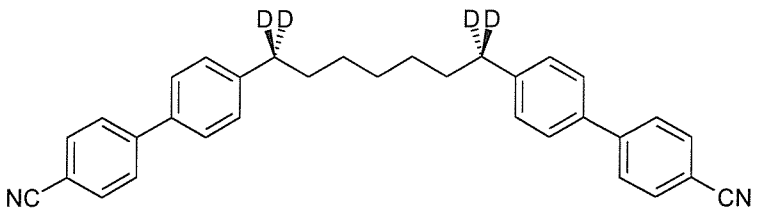

Using deuterium NMR spectroscopy it is hoped the biaxiality of the nematic phase of this material can be assessed, as well as probing the unusual structure of the smectic A phase.

5.7 Deuterium NMR study of CB7CB-d_4

As discussed earlier in this Chapter (§5.2.6), in order to produce the non-uniform distribution of directors that gives the 2D powder spectrum that will allow us to obtain a measure of the biaxiality of the phase, we need to rotate the liquid crystal sample about an axis orthogonal to the magnetic field. This required the use of a specialised NMR probe, as shown in figure 5.24. The probe was built by Dr. B.A.Timimi of the University of Southampton and allows the sample to be spun at rates up to just over 7Hz. The sample tube is held in the centre of the rf coil which is enclosed in a glass jacket through which hot air flows that regulates the temperature. The probe is used with a Bruker MSL 200MHz spectrometer, with a magnetic field of 4.7T.

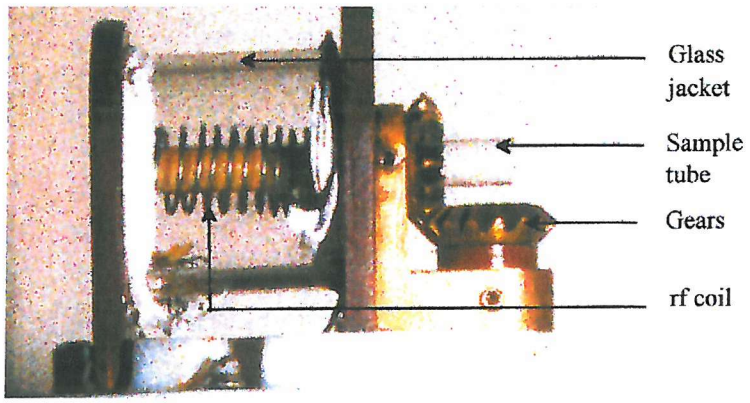

Figure 5.24 : The NMR probe used to spin a liquid crystal sample orthogonal to the magnetic field.

Initially, the sample was held static whilst spectra were accumulated every 2°C on cooling from the isotropic phase until a signal was no longer detectable. A delay of about 15 minutes was allowed between each temperature step to allow for thermal equilibrium to be reached. Figure 5.25 shows spectra at two different temperatures. As can be seen the spectra consist of a single quadrupolar doublet. The first spectrum to form a mesophase occurs at about 116°C, and has a quadrupolar splitting of 31.1kHz, and consists of a pair of sharp peaks with a small peak due to a small amount of residual isotropic phase being present. On continued cooling the quadrupolar splitting increases to a maximum value of about 43.4kHz at a reduced temperature of $T_{NI} - T = 22°C$. However, at this point the spectra become very

noisy and the line widths become large, as seen in figure 5.25b, being as high as 12kHz. In addition there is a large single peak that appears at reduced temperatures of below $T_{NI} - T = 20°C$, where the smectic phase is supercooled below the melting point of the material. Figure 5.26 shows a plot of the quadrupolar splittings as the temperature is reduced. It can be seen that the quadrupolar splitting increases significantly in the nematic phase and there is a change in slope in the splitting at $T_{NI} - T = 16°C$ indicating the transition from the nematic to smectic phase. The jump in quadrupolar splitting is small and may be due to the weak nature of this transition, with the transitional entropy, $\Delta S/R$, being only 0.3.

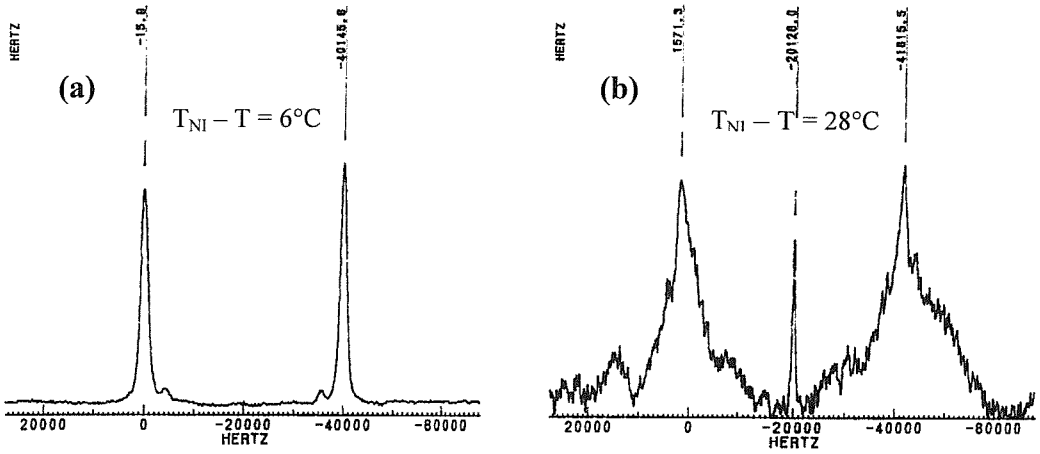

Figure 5.25 : Static deuterium NMR spectra of CB7CB-d_4 in the (a) nematic phase and (b) the smectic phase.

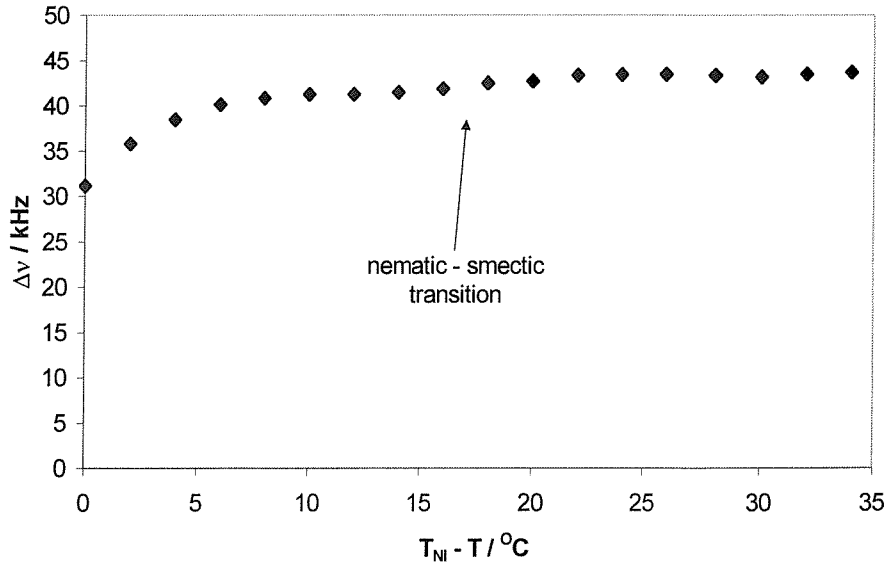

Figure 5.26 : Plot of the quadrupolar splitting for CB7CB-d_4 against the shifted temperature.

To determine the symmetries of the nematic and smectic A phase, the material was cooled from the isotropic phase and held at various temperatures whilst the sample was spun about an axis orthogonal to the magnetic field at various rates. Spectra were obtained at temperatures of $T_{NI} - T = 2, 4, 7, 12$ and $20°C$, with spinning rates of 1.25, 2.5, 3.57, 5, 6.25, 7.14Hz together with a static spectrum. Figure 5.27 shows the spectra that were obtained at two different temperatures, one in the nematic phase and one in the smectic A phase. It was found that for temperatures even down as low as $T_{NI} - T = 20°C$, which is 6°C into the smectic phase, the sample could not be spun fast enough to go above the critical speed, Ω_c, where the non-uniform director distribution will give rise to a 2D powder pattern. However, according to theory and as found experimentally, as the sample is spun the director will be tilted with respect to the magnetic field and this will cause the quadrupolar splitting to be reduced as the spinning speed is increased. This can be seen in figure 5.28, where the quadrupolar splitting at a shifted temperature of $T_{NI} - T = 4°C$ for a static sample is 34.3kHz, whereas at a spinning speed of 7.14Hz the quadrupolar splitting has fallen, but only to 31.4kHz. At lower temperatures, where the sample is now in the smectic A phase, this effect is much more obvious. At $T_{NI} - T = 20°C$, the quadrupolar splitting for a static sample is 42.8kHz, whereas at a spinning speed of 7.14Hz the splitting is now only 29.2kHz. However, at these temperatures as the spinning speed is increased the spectra become significantly noisy and the linewidths become very broad, being around 10kHz for $T_{NI} - T = 20°C$ and a spinning speed of 7.14Hz. At this temperature and spinning speed it can also be seen that there appears to be two outer peaks appearing with a quadrupolar splitting similar to that seen for the static spectrum. This could be an indication that we are approaching the critical speed.

Figure 5.28 shows the variation in quadrupolar splitting as the spinning speed is increased, at different temperatures. The decrease in splitting can be related to the angle the director makes with the magnetic field by

$$\frac{\Delta\tilde{\nu}}{\Delta\tilde{\nu}_0} = \frac{3\cos^2\theta - 1}{2}, \qquad (14)$$

where $\Delta\tilde{\nu}$ is the measured quadrupolar splitting, $\Delta\tilde{\nu}_0$ is the quadrupolar splitting of the static spectrum and θ is the angle the director makes with the magnetic field. Figure 5.29 shows how the director tilt varies with spinning speed. We would expect a 2D powder pattern to appear if the director tilts greater than 45°. It can be seen that at all of the temperatures the director tilt increases fairly regularly with increasing spinning speed. By using

$$\sin 2\theta = \frac{\Omega}{\Omega_c}, \qquad (15)$$

where Ω is the spinning speed, and extrapolating the graph we can determine the critical spinning speed, Ω_c. Figure 5.30 shows the calculated critical speeds for different temperatures. As can be seen the critical speed rises initially from 11.5Hz at $T_{NI} - T = 2°C$ to 13.4Hz at $T_{NI} - T = 4°C$ and then falls steadily as the temperature is decreased until at $T_{NI} - T = 20°C$ the critical speed is only 8.4Hz. This is close to the maximum speed of 7.14Hz that we were able to spin the sample at and could explain the appearance of the shoulders seen in the spectra in figure 5.27b.

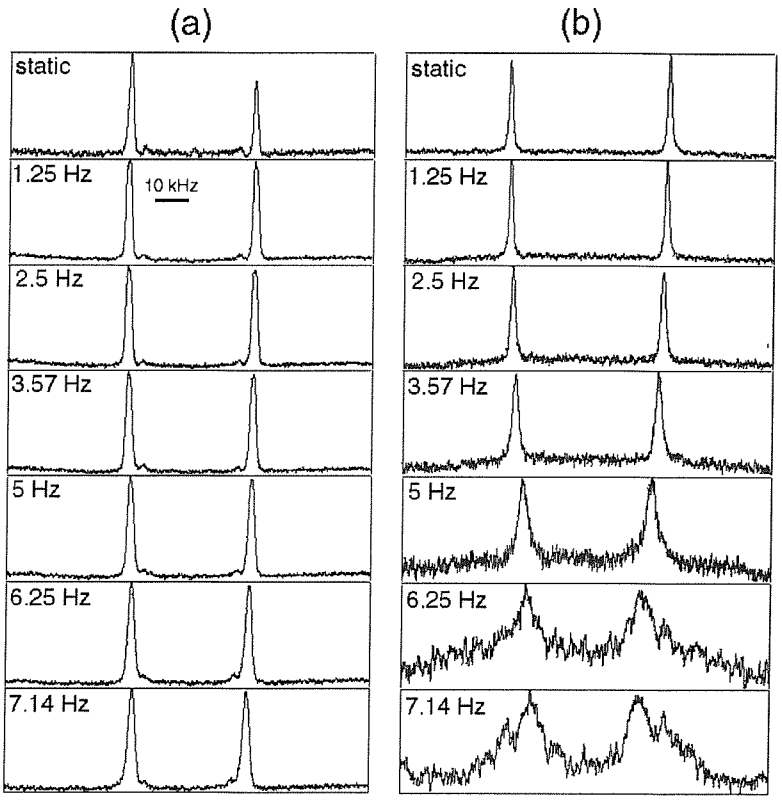

Figure 5.27 : The deuterium NMR spectra for CB7CB-d_4 as the material is spun at different speeds orthogonal to the magnetic field.
(a) $T_{NI} - T = 4°C$ (nematic phase) and (b) $T_{NI} - T = 20°C$ (smectic phase).

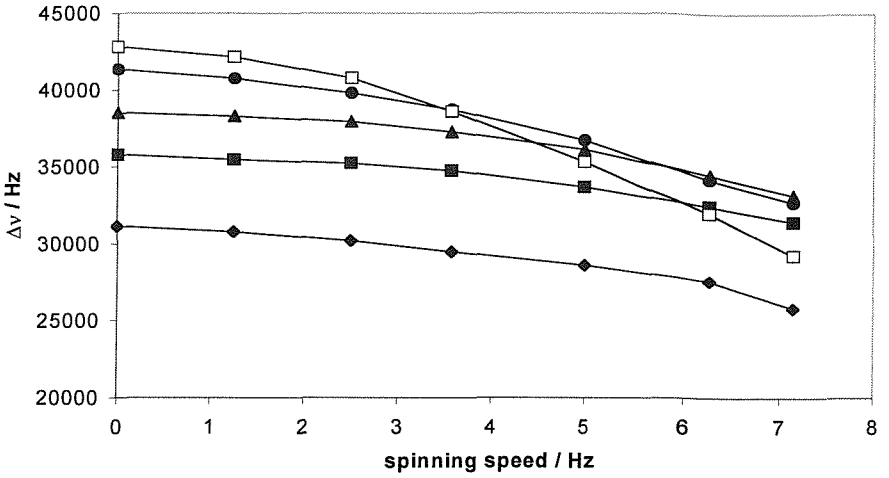

Figure 5.28 : Variation in quadrupolar splitting of CB7CB-d_4 as the temperature is changed. TNI – T: (◆) 2°C, (■) 4°C, (▲) 7°C, (●) 12°C, (□) 20°C.

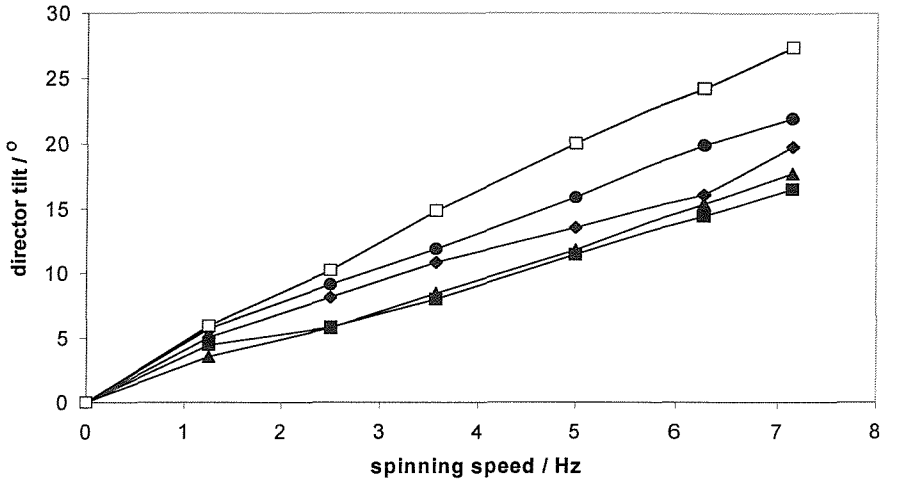

Figure 5.29 : Variation of the director tilt of CB7CB-d_4 as the temperature is changed. TNI – T: (◆) 2°C, (■) 4°C, (▲) 7°C, (●) 12°C, (□) 20°C.

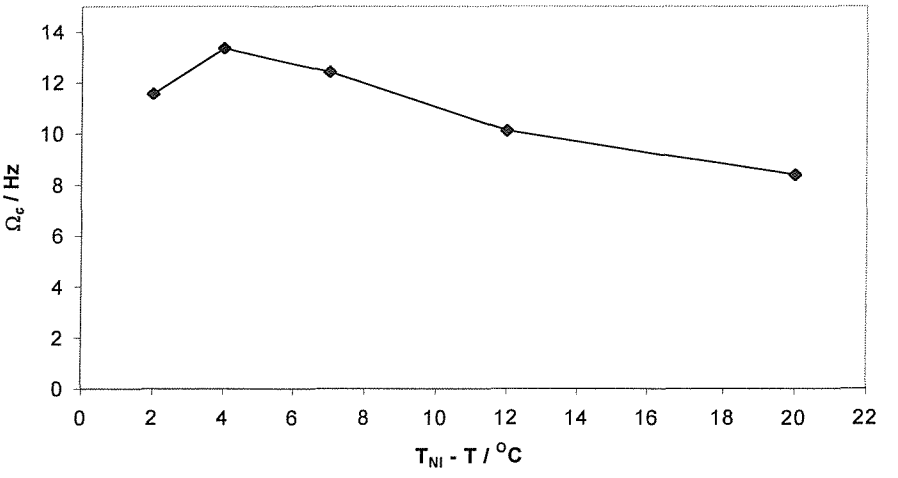

Figure 5.30 : Variation of the critical speed with temperature of CB7CB-d_4.

The critical speed for a liquid crystal can be related to the rotational viscosity of the material by

$$\Omega_c = \frac{\Delta\tilde{\chi}B^2}{2\mu_0\gamma_1}, \qquad (16)$$

where $\Delta\tilde{\chi}$ is the diamagnetic anisotropy of the material, B is the magnetic flux density, μ_0 is the magnetic constant and γ_1 is the rotational viscosity coefficient. When the material stops spinning the magnetic field pulls the director back to being parallel with the field. The time taken for this to occur is known as the relaxation time and is related to

$$\tan\theta_t = \tan\theta_o \exp(-t/\tau), \quad (17)$$

where θ_t is the angle the director makes with the magnetic field at time, t, θ_0 is the angle the director makes with the magnetic field at time, $t = 0$, and τ is given by

$$\tau = \frac{\mu_0\gamma_1}{\Delta\tilde{\chi}B^2}, \qquad (18).$$

By combining equations (16) and (18) we obtain

$$\tau = \frac{1}{2\Omega_c}. \qquad (19)$$

Therefore we can determine the relaxation time of the material being studied if we know the critical speed. It is obvious from equation (18) that the larger the magnetic field the faster the relaxation time, therefore we need to take into account the magnetic field strength of the spectrometer when comparing different materials. As stated previously the field strength of the spectrometer used for this study was 4.7T. At this field the relaxation times are of the order of 50ms. Le Masurier [39] studied the relaxation times of a number of non-symmetric cyanobiphenyl – Schiff base dimers, CBO*n*O.*m*, using ESR spectroscopy, with a field strength of 0.3T. To determine whether our estimation of the critical speeds

for the material are reasonable we can compare the relaxation times for CB7CB with the CBO*n*O.*m*'s. Therefore we need to convert the values obtained at 4.7T to 0.3T. To do this we need to multiply the relaxation times by the ratio of the squares of the two different field strengths. Figure 5.31 shows the relaxation times for CB7CB we would expect for a field strength of 0.3T. As can be seen the relaxation times are of the order of 10s. The results obtained by Le Masurier [39] show that the relaxation times for the non-symmetric dimers range from ~1s at T_{NI} to ~4s as the temperatures are reduced. This suggests that the rotational viscosity of the nematic phase of CB7CB is higher than for the CBO*n*O.*m* dimers or that the anisotropy in the diamagnetic susceptibility is less but further experiments need to be carried out to determine this. However, the relaxation times seen for the smectic A phases of the CBO*n*O.*m* dimers were of the order of minutes or even hours, whereas the relaxation time seen for the smectic A phase of CB7CB is only 14.6s. The smectic A phases of the CBO*n*O.*m* dimers are either intercalated or interdigitated and this leads to the very long relaxation times seen and therefore the smectic A phase of CB7CB is probably a monolayer structure. Whether the bent shape of CB7CB leads to biaxial smectic A phase, as suggested previously for other bent materials [30], is uncertain as unfortunately we were unable to obtain a 2D powder pattern.

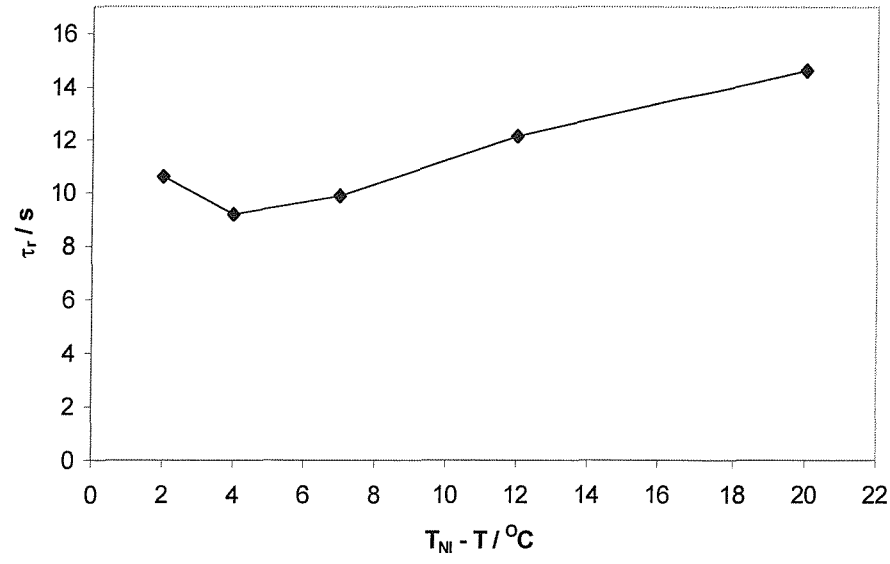

Figure 5.31 : The calculated relaxation times for CB7CB-d_4 at different temperature for a magnetic field strength of 0.3T.

5.8 Conclusions

In trying to understand the structural requirements for the formation of thermotropic biaxial nematic phases we have developed a method of quantifying the biaxiality of mesogenic materials. Ferrarini *et al.* [25] used a molecular field approach to estimate the minimum molecular biaxiality for which a biaxial nematic phase might be expected. It was found that for a thermotropic biaxial nematic phase to be observed the molecules are required to have the geometry similar to that of a house brick. We have developed an alternative approach to the design of thermotropic biaxial nematic materials by considering a V-shaped molecule comprising two rigid mesogenic groups connected at an angle, θ. The resulting phase diagram is somewhat different to that seen for the box-shaped materials, however for a biaxial nematic phase to be formed, the two mesogens need to be joined at an angle of ~109°, which is somewhat restrictive in terms of molecular shape, as the number of linking groups with geometries of ~109° is small.

To test whether our theory was realistic we have compared the transitional behaviour of a number of linear and bent mesogens to determine whether it was possible to predict the nematic – isotropic transition temperature of the bent analogue if we know the transition temperature of the analogous linear material. It was found that the agreement in all cases was reasonably good and so we prepared a number of materials based on biphenyl moieties, linked at angles of 120° and 109°, in an attempt to observe a biaxial nematic phase. Unfortunately none of the materials exhibited mesophases and the virtual transition temperatures suggested T_{NI} was on average ~200°C below the melting transitions. Ideally we need to prepare dimers based on the terphenyl moiety as we would expect the transition temperatures to be somewhat higher as the corresponding sexiphenyls have higher transition temperatures.

Finally, we prepared the cyanobiphenyl dimer CB7CB-d_4 specifically deuteriated at the α-position because, for an all-*trans* conformation of the spacer chain, the material has a bent shape. Also, the entropy associated with the nematic – isotropic transition is low, and it has been predicted [1] that as the molecular biaxiality increases, the nematic – isotropic transition becomes weaker. In addition the

smectic phase exhibited by this materials has an unusual structure and we hoped to probe the nature of both the nematic and smectic phase using deuterium NMR spectroscopy. An aligned sample showed two lines in the spectrum whose quadrupolar splitting increases slightly as the temperature is decreased. Unfortunately, when the sample was spun about an axis orthogonal to the magnetic field we were unable to reach the critical spinning speed to allow the observation of a 2D-powder spectrum, however the field-induced relaxation times we observed were not unreasonable for a nematic phase. Even in the smectic phase we were unable to obtain a 2D-powder spectrum and therefore were unable to ascertain the symmetry of this unusual smectic phase. For future work, to reach the critical spinning speed we need to modify the experimental set-up to allow us to spin the sample faster than about 10Hz.

Although we were unable to observe a thermotropic biaxial nematic phase based on bent mesogens we have explored an alternative approach, which is to use mixtures of disc-like and rod-like molecules. The following Chapter investigates the mesogenic behaviour of the non-symmetric liquid crystal disc-rod dimers.

5.9 References

[1] Freiser, M.J., *Phys. Rev. Lett.*, **24**, 1041, (1970).

[2] Luckhurst, G.R. and Romano, S., *Molec. Phys.*, **40**, 129, (1980).

[3] Allen, M.P., *Liq. Cryst.*, **8**, 499. (1990).

[4] Hashim, R., Luckhurst, G.R., Prata, F. and Romano, S., *Liq. Cryst.*, **15**, 283, (1993).

[5] Yu, L.J. and Saupe, A., *Phys. Rev. Lett.*, **45**, 1000, (1980).

[6] Bartolino, R., Chiaranza, T., Meuti, M. and Compagnoni, R., *Phys. Rev. A.*, **26**, 1116, (1982).

[7] Vasilevskaya, A., Kitaeva, E.L. and Sonin, A.S., *Russ. J. Phys. Chem.*, **64**, 599, (1990).

[8] Oliveira, E.A., Liebert, L. and Figueiredo Neto, A.M., *Liq. Cryst.*, **5**, 1669, (1989).

[9] Nicoletta, F.P., Chidichimo, G., Golemme, A. and Picci, N., *Liq. Cryst.*, **10**, 665, (1991).

[10] Quist, P-O., *Liq. Cryst.*, **18**, 623, (1995).

[11] Galerne, Y. and Liebert, L., *Phys. Rev. Lett.*, **55**, 2449, (1985).

[12] Malthete, J., Liebert, L., Levelut, A.M. and Galerne, Y., *Compt. Rend. Acad. Sci. Paris*, **303**, 1073, (1986).

[13] Chandrasekhar, S., Nair, Geetha.G., Shankar Rao, D.S., Krishna Prasad, S., Praefcke, K. and Blunk, D., *Liq. Cryst.*, **24**, 67, (1998).

[14] Fan, S.M., *PhD. Thesis, University of Southampton*, (1992).

[15] Shenouda, I.G., Shi, Y. and Neubert M.E., *Molec. Cryst. Liq. Cryst.*, **257**, 209, (1994).

[16] Hughes J.R., Kothe, G., Luckhurst, G.R., Malthete, J., Neubert, M.E., Shenouda, I., Timimi, B.A. and Tittelbach, M., *J. Chem. Phys.*, **107**, 9252, (1997).

[17] Chandrasekhar, S., Sadashiva, B.K., Ratna, B.R. and Raja, N.V., *Pramana*, **30**, L491, (1988).

[18] Chandrasekhar, S., Sadashiva, B.K., Ratna, B.R. and Raja, N.V., *Molec. Cryst. Liq. Cryst.*, **165**, 123, (1988).

[19] De Silva, D.S., *Ph.D Thesis, University of Southampton*, (1998).

[20] Preafcke, K., Kohne, B., Singer, D., Demus, D., Pelzl, G. and Diele, S., *Liq. Cryst.*, **7**, 589, (1990).

[21] Praefcke, K, Kohne, B., Gundogan, B., Demus, D., Diele, S. and Pelzl, G., *Mol. Cryst. Liq. Cryst. Lett.*, **7**, 27, (1990).

[22] Preafcke, K., Kohne, B., Gundogan, B., Singer, D., Demus, D., Diele, S., Pelzl, G. and Bakowsky, U., *Mole. Cryst. Liq. Cryst.*, **198**, 393, (1991).

[23] Fan, S.M., Fletcher, I.D., Gundogan, B., Heaton, N.J., Kothe, G., Luckhurst, G.R. and Preafcke, K., *Chem. Phys. Lett.*, **204**, 517, (1993).

[24] Jian-Feng, L., Percec, V., Rosenblatt, C., and Lavrentovich, O.D., *Europhys. Lett.*, **25**, 199, (1994).

[25] Ferrarini, A., Nordio, P.L, Spolaore, E. and Luckhurst, G.R., *J. Chem. Soc. Faraday Trans.*, **91**, 3177, (1995).

[26] Ferrarini, A., Moro, G.J., Nordio, P.L. and Luckhurst, G.R., *Mol. Phys.*, **77**, 1, (1992).

[27] Cai, R. and Samulski, E.T., *Liq. Cryst.*, **9**, 617, (1991).

[28] Seguel, C.G., Borchers, B., Haase, W. and Aguilera, C., *Liq. Cryst.*, **11**, 899, (1992).

[29] Kuboshita, M., Matsunaga, Y. and Miyauchi, T., *Mol. Cryst. Liq. Cryst.*, **264**, 145, (1995).

[30] Niori, T., Sekine, T., Watanabe, J., Furukawa, T. and Takezoe, H., *J. Mater. Chem.*, **6**, 1231, (1996).

[31] Barbera, J., Cativiela, C., Serrano, J.L. and Zurbano, M.M., *Liq. Cryst.*, **11**, 887, (1992).

[32] Wilson, M.J., *PhD. Thesis, University of Southampton*, (1998).

[33] Dewar, M.J.S. and Riddle, R.M., *J. Am. Chem. Soc.*, **97**, 6658, (1975).

[34] *Handbook of Chemistry and Physics*, 79th Edition, page 9-33, CRC Press.

[35] *Flussige Kristalle in Tabellen,* edited by Demus, D., Demus, H. and Zaschke, H.; VEB Deutscher Verlag fur Grundstoffindustrie: Leipzig, (1974).

[36] Barnes, P.J., Douglass, A.G., Heeks, S.K. and Luckhurst, G.R., *Liq. Cryst.*, **13**, 603, (1993).

[37] Imrie, C.T., *Ph.D Thesis, University of Southampton*, (1988).

[38] Dunn, C.J., *Ph.D Thesis, University of Southampton*, (1998).

[39] Le Masurier, P.J., *Ph.D Thesis, University of Southampton*, (1996).

CHAPTER SIX

NON-SYMMETRIC DIMERS CONTAINING DISC-LIKE AND ROD-LIKE MOIETIES

6.1 Introduction

The concept of discotic materials forming liquid crystal phases was discussed briefly in the Introduction (§1.12.3) and explored more fully, in the case of chemically-induced phases, in Chapter 2. In all of the examples presented the materials were monomeric, in other words there is only one mesogenic moiety present in the molecule. This brings us to the question as to whether there are examples of liquid crystal dimers with discotic mesogenic groups, considering the plethora of dimers formed from calamitic mesogens. Naturally we would expect the answer to be yes, and this is indeed the case, examples being the ether linked triphenylene dimer [1]

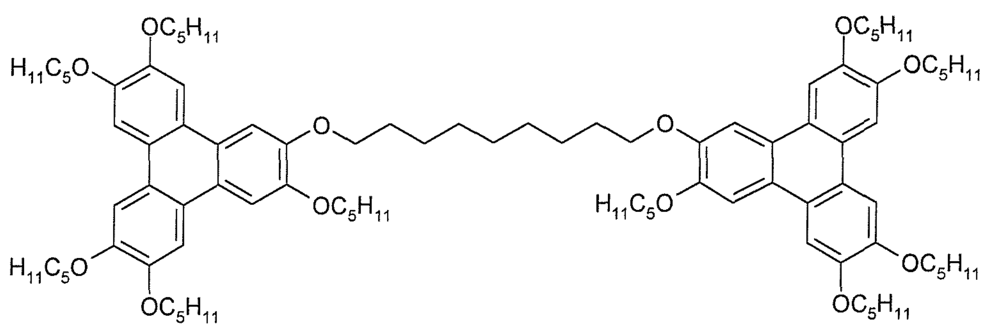

and the ester linked hexa-substituted benzene [2]

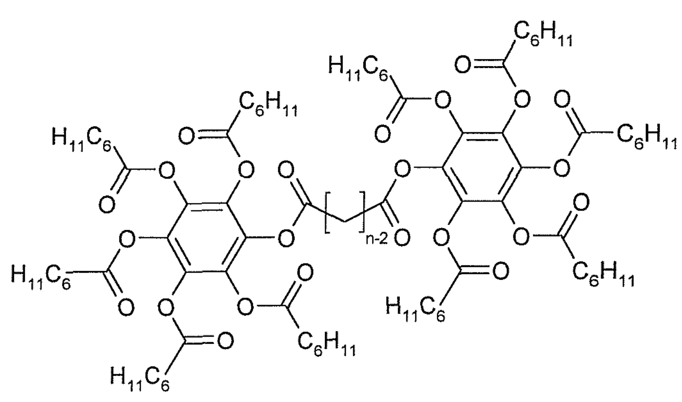

At this point it is worth pointing out that there are also examples of both main-chain [3] and side-chain [4] discotic polymer liquid crystals.

Praefcke *et al.* [5] prepared the symmetric ether-linked dimer based on two large electron rich discotic moieties with the structure

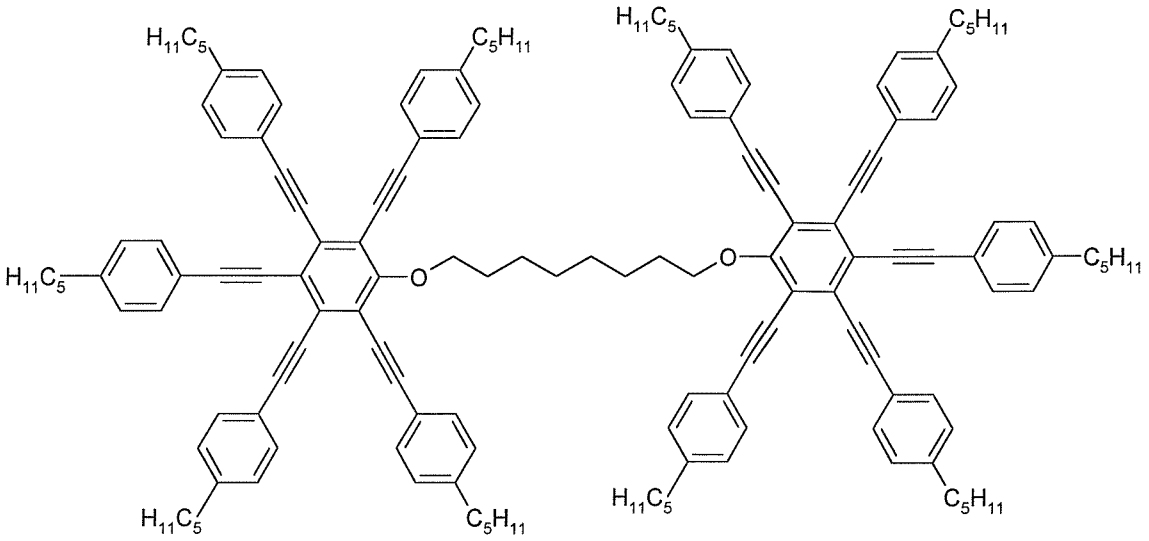

This material is interesting because it was reported, on the basis of conoscopy, that it formed a biaxial nematic (N_b) phase. In fact the existence of biaxial nematic phases has been predicted for mixtures of rod-shaped and disc-shaped molecules [6] and this hypothesis has been supported by computer simulations, of such mixtures [7], where phase separation is prevented, although experimentally the two components phase separate into two uniaxial nematics, one largely composed of rods and the other of discs [8]. This phase separation is also seen for a real mixture of calamitic and discotic mesogens [9]. (A more detailed theoretical and experimental investigation into the biaxial nematic phase was discussed in Chapter 5). One answer to the problem of phase separation would appear to be to link the rod-like and disc-like units together via a flexible spacer. There are at present few examples in the literature of such compounds. Kreuder *et al.* [10] prepared the compounds shown in figure 6.1. When the rod was linked laterally to the discs (figure 6.1a) the material exhibited no mesophase even after extensive supercooling. However, when the discs were attached terminally to the rod (figure 6.1b) an unusual mesophase was formed which was studied by X-ray scattering. This showed that the discs were arranged in columns and the rods were

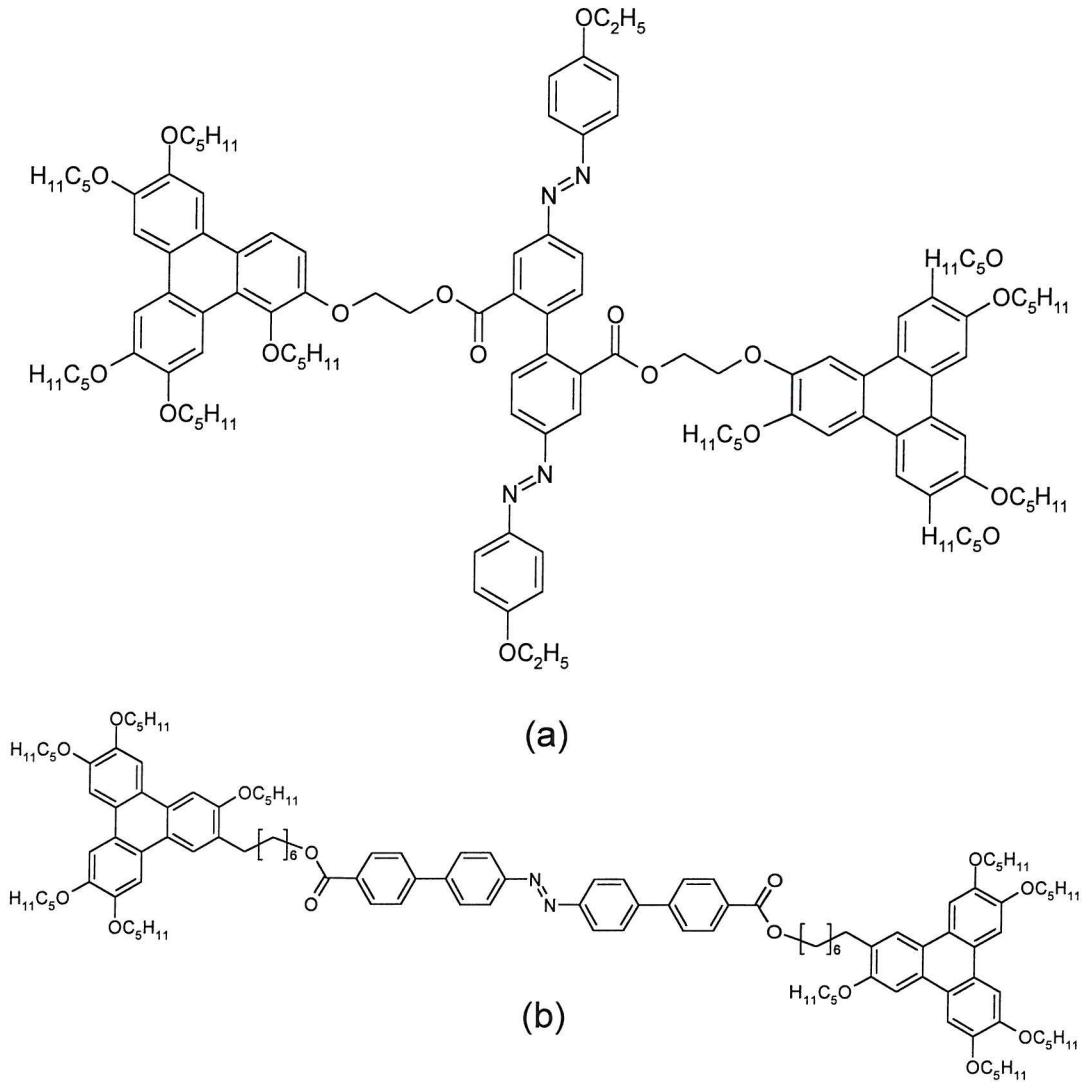

Figure 6.1 : Examples of rod-disc-rod trimers. (a) linked laterally and (b) linked terminally.

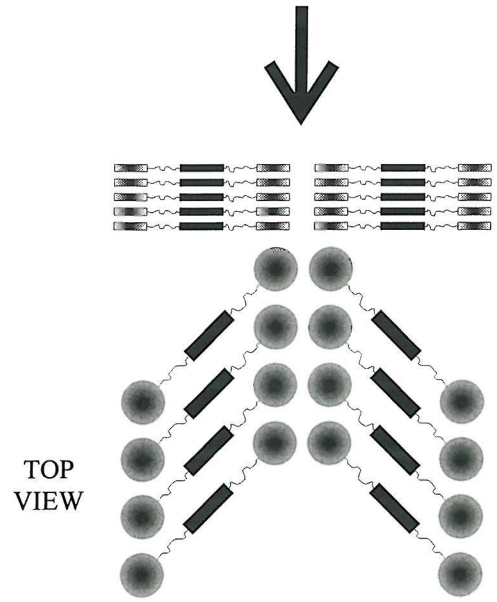

Figure 6.2 : The molecular arrangement of terminally linked trimers shown in figure 6.1(b).

arranged in layers, as shown in figure 6.2. Although a mixture of both rods and discs these two examples are strictly speaking disc-rod-disc trimers.

Fletcher *et al.* [11] prepared a true disc-rod dimer consisting of the disc-like, large, electron rich pentakis(phenylethynyl)benzenes as discussed in Chapter 2 and the rod-like cyanobiphenyls ether linked via a flexible spacer,

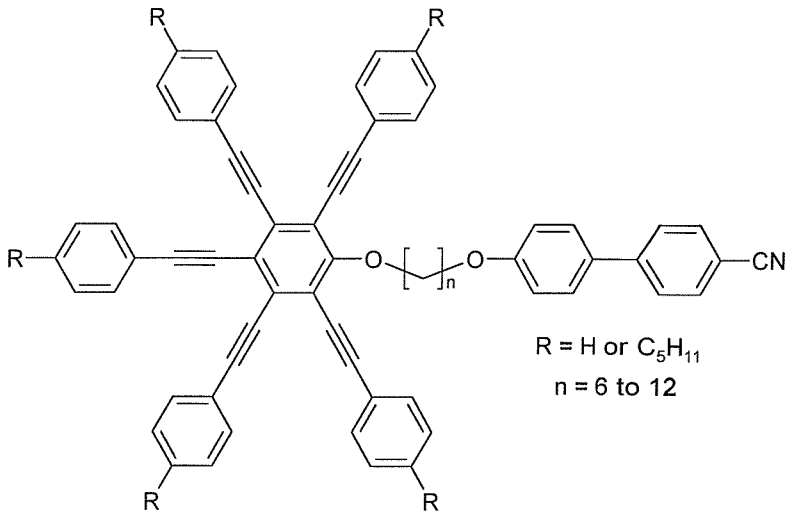

When R = H, the pure compounds displayed no liquid crystal phases; this might have been expected because the monomers studied in Chapter 2 do not. However, even when R = $n$$C_5H_{11}$ the pure dimers still displayed no liquid crystal phases. This is more surprising since the analogous disc-disc dimers, when the spacer chain length is greater than eight, do exhibit a nematic phase [12] and the analogous rod-rod dimers have well-known liquid crystal phases [13]. It has been suggested that the reason for this lack of liquid crystallinity is due to the extreme difficulty these materials have in packing the rod-like and disc-like units simultaneously so that their respective symmetry axes are parallel to a common director. Alternatively, for a biaxial nematic phase the disc-like unit's symmetry axis has to lie parallel to one director and the rod-like unit's symmetry axis parallel to another orthogonal director, however the lack of liquid crystallinity suggest that this does not happen. When both series were mixed with equimolar amounts of 2,4,7-trinitrofluoreneone (TNF), although charge-transfer complexes were formed, as indicated by the appearance of a deep orange-red colour, only monotropic liquid crystal phases were exhibited. This again was surprising considering the behaviour

displayed by the complexes formed by the monomeric discotic materials studied in Chapter 2. What is also apparent, as shown in figure 6.3, is that the nematic to isotropic transitions are below the melting points of the pure materials, so it is not possible to say whether the nematic phase is chemically-induced or a result of the eutectic behaviour of the mixture. These results seem to indicate that there may be large packing incompatibilities when trying to join a disc-like unit to a rod-like unit. This led Wilson [14] to prepare a series of disc-rod dimers where the flexible alkyl spacer and disc-like unit remained constant and the rod-like unit was varied. The structure of these materials is shown in figure 6.4.

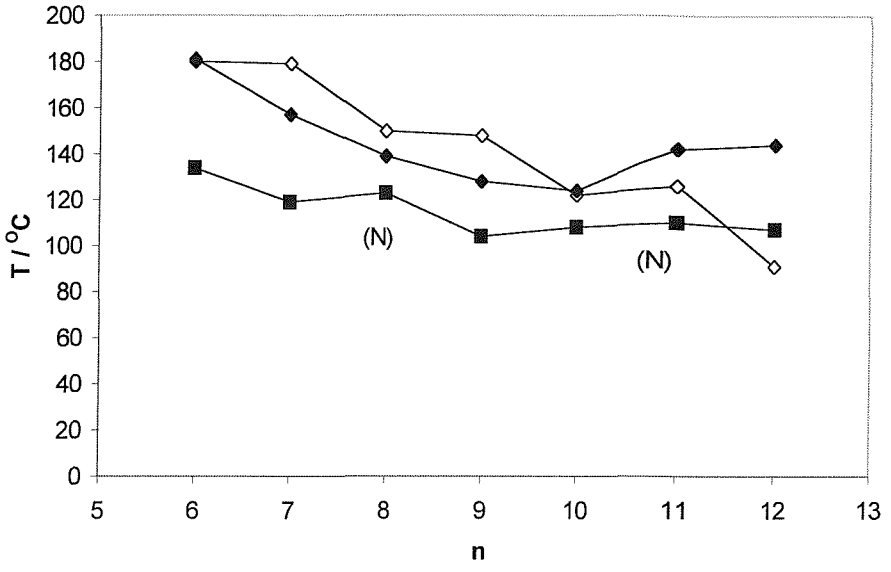

Figure 6.3 : The transitional properties of the α-[(1,2,3,5,6-pentakis(4-phenylethynyl))benzene -4'-oxy]-ω-(4'-cyanobiphenyl-4-yloxy)alkanes as the number of carbon atoms, n, in the alkyl chain is increased.

■ N – I, ◆ Cr – I (equimolar mixture with TNF). ◇ Cr – I (pure material).

Pentakis(phenylethynyl)benzene was chosen as the disc-like unit because a comparison can be made with the dimers prepared by Fletcher [11] and also there is the possibility of phase induction with TNF if the materials are themselves not mesogenic. The rod-like units are basically one or two ring systems with varying length to breadth ratios and varying terminal substituents. The phase behaviour of the pure materials prepared by Wilson [14] produced a number of surprises. Most notable was the existence of enantiotropic phases for two of the materials, those containing a nitrophenyl and biphenyl rod-like unit. This is surprising because these moieties are themselves not mesogenic. There may even be some form of self

phase induction, an example of which was studied by Möller *et al.* [15] on the materials shown below.

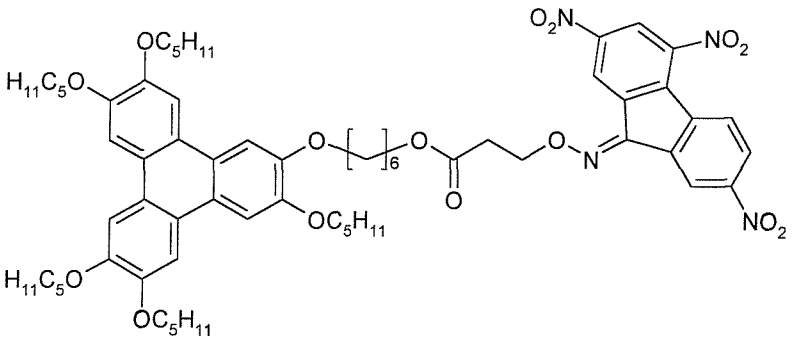

In this example the materials stack into columns of alternating disc-like moiety and TNF moiety. The neighbouring columns are connected along specific directions only and give rise to highly anisotropic structural properties.

The phase behaviour of the 50mol% mixtures of the materials in figure 6.4 with TNF was equally interesting. Unlike the disc-cyanobiphenyl [14] materials, all the compounds, apart from that containing a methoxyphenyl moiety, displayed enantiotropic liquid crystal phases, with two, the phenyl analogue and the nitrostilbene analogue, showing more than one liquid crystal phase. Surprisingly, this seems to suggest that the size, shape and nature of the rod-like unit does not detrimentally affect the molecular organisation as much as the cyanobiphenyl analogues suggest. Although this may seem to be the case, it is well-known that the properties of liquid crystals can be crucially dependent on the length and parity of the flexible spacer chain, however the odd-even alternation seen for the equimolar mixtures of the disc-cyanobiphenyl materials prepared by Fletcher [11] and TNF is only small. To determine the effect of the shape and size of the rod-like unit on the mesophase behaviour of these systems we have synthesised a number of disc-rod dimers with an ether linked flexible alkyl chain containing nine carbon atoms. A number of dimers where the alkyl chain contains ten carbon atoms have also been synthesised for materials where the rod-like unit is different to any of the materials prepared by Wilson [14]. The full range of materials synthesised is shown in figure 6.4.

The C9 alkyl chain was chosen as the flexible spacer because a good comparison can be made to the dimers containing a C10 spacer chain to determine whether odd or even spacers favour mesogenic behaviour. Generally, for calamitic dimers an even spacer chain length is more favourable. Also the dibromononane used in the synthesis is more readily available than dibromoundecane. The rationale behind choosing the various 'rod-like' units was, firstly, to assess the effect subtle changes make to the phases formed, in a similar vein to those studied in Chapter 4. Secondly, the rod-like units were chosen to, hopefully, combine the positive effects seen by Wilson [14] for some of the materials, especially in the choice of the nitrobiphenyl moiety.

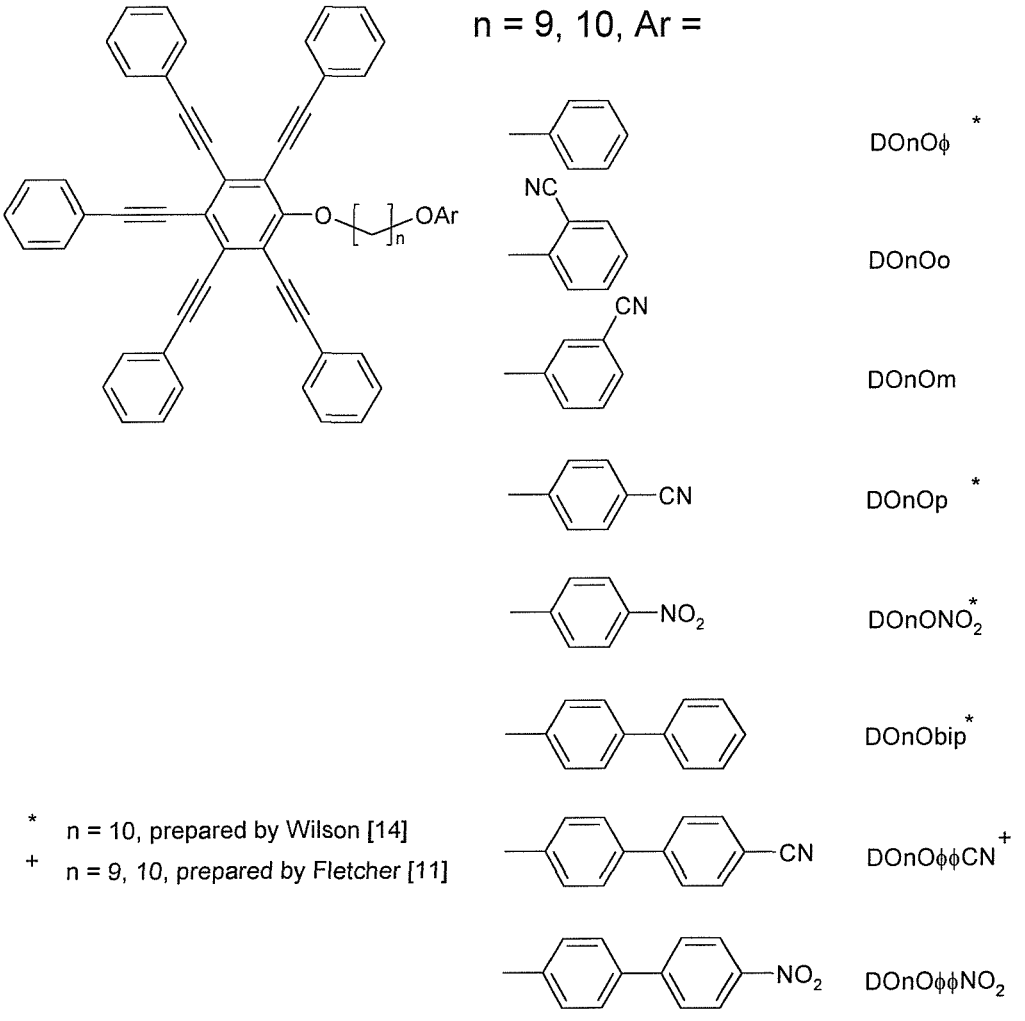

Figure 6.4 : The range of materials studied in this Chapter.

6.2 Results and Discussion

6.2.1 The Pure Materials

Optical microscopy and differential scanning calorimetry (DSC) were used to investigate the transitional behaviour of the pure materials and the data is presented in Table 6.1 and shown in figure 6.5, where the results for those materials prepared by Wilson [14] and Fletcher [11] (indicated with an asterisk) are also included. In contrast to the data presented by Wilson and Fletcher, where the materials appear to melt and crystallise easily, those materials with nine carbon atoms in the alkyl chain spacer show a tendency to form glassy phases on cooling. These glassy phases were identified by the observation of a second order transition, or step in the baseline, on the DSC trace at a temperature well below the melting point of a crystalline sample of the materials; these glass transition temperatures are also listed in table 6.1. When viewed under the microscope the materials cool from a highly mobile isotropic fluid which slowly increases in viscosity until the glass transition, where the phase no longer deforms when subjected to mechanical stress. The values for the melting points were obtained from the observation of crystalline samples upon heating under the microscope. Therefore, unfortunately no entropy values for these transitions are available as only glass transitions were seen on the DSC traces.

As seen by Wilson [14] the dimer containing the biphenyl moiety exhibits a nematic phase. However, unlike the dimer with ten carbon atoms in the alkyl spacer chain, the mesophase for DO9Obip is monotropic. The nematic – isotropic transition for DO9Obip occurs at 57.7°C which is lower than that for DO10Obip, which is 86.6°C. Also, DO9ONO_2 does not exhibit a mesophase unlike DO10ONO_2. For DO9Obip the mesophase has been identified, from microscopy, as a nematic phase from the two and four point singularities observed in the texture. At the nematic – isotropic transition the nematic phase is seen to flash when subjected to mechanical stress. However, as the phase cools towards the glass transition the viscosity increases until the phase no longer flashes, and ultimately the phase cools into a nematic glass. Therefore, although the nematic phase for DO9Obip is monotropic, as it is not observed upon heating a crystalline

n = 9			n = 10		
Material	Mpt /°C	T_g /°C	Material	Mpt /°C	T_g /°C
DO9Oϕ	48	4.8	DO10Oϕ*	100	
DO9Op	82	13.2	DO10Op*	104	
DO9Om	54	5	DO10Om	67	2.9
DO9Oo	50	7.1	DO10Oo	65	3.7
$DO9ONO_2$	101	38.4	$DO10ONO_2$*	82^+	
DO9Obip	97	8.6	DO10Obip*	79^+	
DO9OϕϕCN*	148		DO10OϕϕCN*	122	
$DO9O\phi\phi NO_2$	91	25.3	$DO10O\phi\phi NO_2$	63	28.2

$^+$ crystal – nematic transition.

* Prepared by Wilson [14] and Fletcher [11].

DO9Obip : T_{NI} = 57.7°C

DO10Obip : T_{NI} = 86.6°C

$DO10ONO_2$: T_{NI} = 100.7°C

Table 6.1 : The transition temperatures of the DOnOR materials.

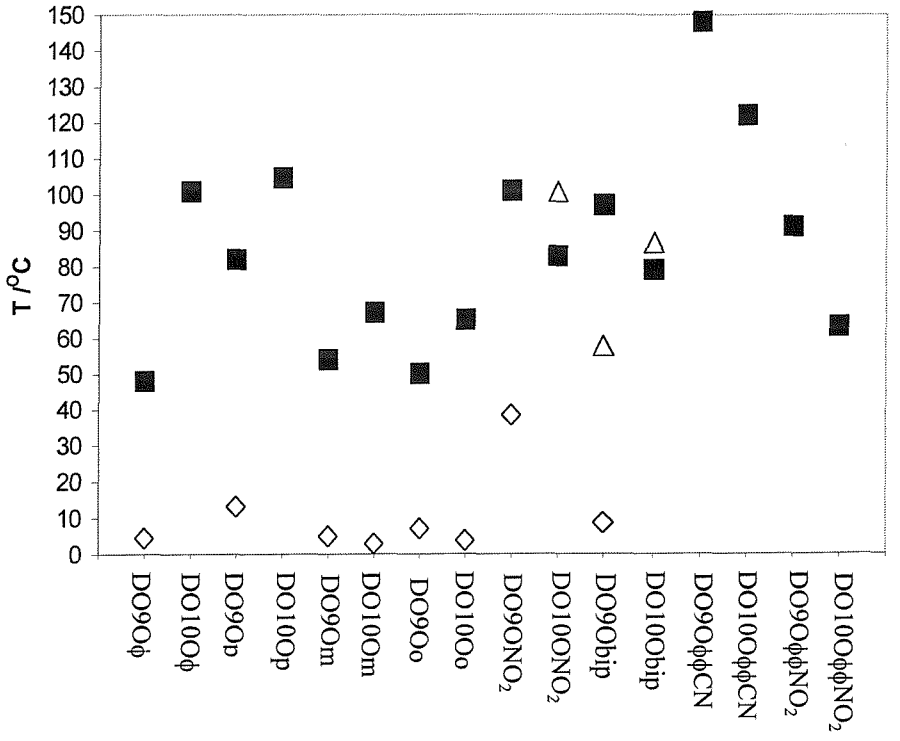

Figure 6.5 : The transition temperatures for the DOnOR materials

■ **Cr – I or N, △ N – I, ◇ T_g.**

sample, when heating from the glassy phase the fluid nematic phase is, naturally, restored and there is the subsequent monotropic transition to the isotropic liquid at T_{NI}. The entropy change at the nematic – isotropic transition for DO9Obip was 0.6 which is higher than that seen by Wilson for the C10 homologues [14], being only 0.24.

Generally, the melting points for the materials can be divided into two different groups. For the C9 homologues with a single ring system for the 'rod-like' moiety the melting points are lower than for the corresponding C10 homologues, except for the p-nitrophenyl homologue. However, for the C9 homologues with a two-ring system for the 'rod-like' moiety the melting points are higher than for the corresponding C10 homologues. Surprisingly, both the C9 and C10 dimers containing a para-substituted cyanophenyl moiety have significantly higher melting points than both the ortho- and meta-substituted cyanophenyl homologues, which have similar melting points.

6.2.2 Mixtures with 2,4,7-Trinitrofluorenone

Equimolar mixtures of the disc-rod dimers with 2,4,7-trinitrofluorenone (TNF) were prepared by mixing solutions of known concentration of the disc-rod dimers in chloroform with a known concentration of TNF, also dissolved in chloroform. A charge-transfer complex was seen to form, characterised by a deep orange-red colour change observed on mixing. The chlorofom was allowed to evaporate and the resulting solid placed under high vacuum (>1 Torr) overnight, to remove the last traces of solvent.

Table 6.2 and figure 6.6 present the results, from DSC studies, for the equimolar mixtures of the disc-rod dimers with TNF, including those materials prepared by Wilson [14] and Fletcher [11] (indicated in both table 6.2 and figure 6.7 with an asterisk). Unsurprisingly, the addition of the highly electron deficient 2,4,7-trinitrofluorenone to these materials, containing the electron rich 'Superdisc' moiety, results in a large change to the mesophase behaviour. As the results in Chapter 2 , and the work by Praefcke *et al.* [16] and Fletcher *et al.* [11] have shown we would expect the formation of stacks of alternating TNF and 'Superdisc' moieties leading to the formation of columnar mesophases. Indeed, all

the materials exhibit enantiotropic mesophases with only those prepared by the Fletcher [11], namely DO9OϕϕCN and DO10ϕϕCN, exhibiting monotropic phases.

	Transition temperatures /°C							
Material	Cr/g		Col		N		I	
DO9Oϕ	•	17.2	•	39.8	•	57.1	•	
DO9Op	•	22.8	•		•	22.9	•	
DO9Om	•	12.7	•		•	27	•	
DO9Oo	•	18.9	•		•	46.1	•	
$DO9ONO_2$	•	22.6	•		•	26.7	•	
DO9Obip	•	21.7	•	37.4	•	55.1	•	
DO9OϕϕCN*	•	128	•		(•	104)	•	
$DO9O\phi\phi NO_2$	•	33.5	•		•	91.9	•	
DO10Oϕ*	•	93.5	•	122.1	•	133.8	•	
DO10Op*	•	96.5	•		•	131.1	•	
DO10Om	•	10.5	•		•	74.1	•	
DO10Oo	•	28.4	•		•	113.8	•	
$DO10ONO_2$*	•	115.6	•		•	127.6	•	
DO10Obip*	•	122.5	•		•	124	•	
DO10OϕϕCN*	•	124	•		(•	108)	•	
$DO10O\phi\phi NO_2$	•	52.3	•		•	64.6	•	

Parentheses indicate a monotropic transition.

* Prepared by Wilson [14] and Fletcher [11].

Table 6.2 : The transition temperatures of equimolar mixtures of the DOnOR materials with TNF.

The nature of the mesophases were, again, determined by polarising optical microscopy. Upon cooling from the isotropic liquid a very fine sanded texture was first seen to emerge and as the phase was slowly annealed the texture was seen to form a fine schlieren texture with very small two and four point singularities, as shown in figure 6.7. For all the materials with nine carbon atoms in the alkyl

spacer, at the liquid crystal to isotropic transition, the phase was seen to flash when subjected to mechanical stress. It was therefore assigned as a nematic phase, and considering the behaviour seen for other 'Superdisc' / TNF mixtures (see Chapter 2) it seems sensible to assume the phase may in fact be a columnar nematic phase, although X-ray diffraction studies are needed to confirm this speculation. As cooling continued the phase became extremely viscous and as a result it no longer flashed when subjected to mechanical stress.

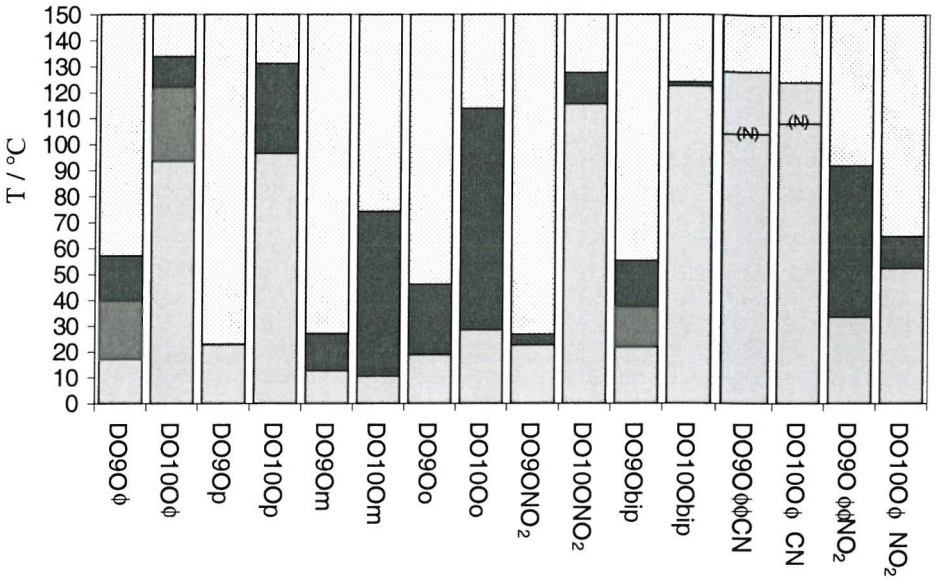

Figure 6.6 : The transition temperatures of equimolar mixtures of the DOnOR materials with TNF. □ isotropic, ■ nematic, ■ Col, ■ glass or crystal.

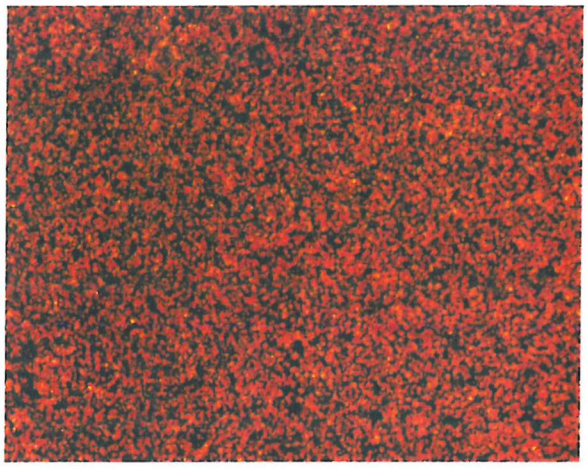

Figure 6.7 : The sanded texture exhibited by DO9Op at 22°C (magnification x500).

As seen in table 6.2 all the materials with nine carbon atoms in the alkyl chain, with the exception of DO9OϕϕCN, have on both heating and cooling either a glass

transition or what appears to be a very weak crystal – nematic transition. For both DO9OpCN and DO9ONO$_2$ the nematic to isotropic transition and the glass transition occur at almost the same temperature. Upon viewing each of these materials under the microscope the isotropic liquid was seen to cool continuously from a highly mobile isotropic fluid into an extremely viscous isotropic fluid. At the nematic – isotropic transition very small birefringent areas began to emerge slowly from the isotropic fluid. Unfortunately at this point the materials turned glassy, characterised by the fact that the phase no longer deforms when mechanical pressure is applied to the cover-slip, and as a result the texture stops developing. Upon heating, just above the glass transition the material is still extremely viscous, however if the temperature is held just below the nematic – isotropic transition the texture slowly emerges as a very fine sanded texture. With further annealing a very fine schlieren texture can be formed, as shown in figure 6.7. This also explains the very weak crystal – nematic transitions seen for DO9Obip and DO9O$\phi\phi$NO$_2$. From microscopic observations as both materials cool, from the nematic phase for DO9O$\phi\phi$NO$_2$ or the Col phase for DO9Obip, the mesophase becomes, once more, extremely viscous. As the materials slowly begin to crystallise the phase goes glassy and crystallisation stops. Upon heating, above the glass transition the materials slowly continue to crystallise but there is subsequently a transition from the crystal to the mesophase. This results in the DSC trace showing a step in the baseline, where the glass transition occurs, accompanied by a small peak, where the small amount of crystalline material melts. As a consequence it is difficult to ascertain the transitional entropies accurately.

Let us now concentrate on the second mesophase, designated Col, formed by DO9Oϕ and DO9Obip. This second mesophase was seen by Wilson [14] for DO10Oϕ, but not for DO10Obip. The absence of the Col phase for DO10Obip may be due to the very small mesophase range of only 1.5°C observed for this material. The widened mesophase range exhibited by DO9Obip probably accounts for the second mesophase being observed. The entropy change, $\Delta S/R$, at the Col – nematic transition for DO9Oϕ is 0.29, and for DO9OBip is 0.32 which is somewhat lower than that observed by Wilson [14], with $\Delta S/R$ for DO10Oϕ being 2.85. It is, however, consistent with the Col$_{ho}$ – nematic columnar transitions seen

for the monomeric 'Superdisc' materials studied in Chapter 2, with the Col_{ho} – nematic transition having an entropy change of 0.21 for C10SD, and would suggest that this phase is a discotic columnar phase. When viewed under the microscope, because of the highly viscous nature of the phases, there appears to be no change in the texture when the materials are cooled from the nematic to the Col_x phase, therefore the only indication of a phase change is the occurrence of a peak on the DSC traces.

It is apparent from figure 6.6 that the nematic – isotropic transition temperatures are significantly lower for those materials with nine carbon atoms in the alkyl chain than for the analogous materials with ten carbon atoms in the alkyl chain, being on average ~50°C lower. The only exception to this is DO9O$\phi\phi$$NO_2$ which has a nematic – isotropic transition temperature of 92°C compared with 65°C for DO10O$\phi\phi$$NO_2$. Also the two dimers containing a cyanobiphenyl moiety have monotropic nematic phases that are only 4°C apart, DO9O$\phi\phi$CN being 104°C and DO10O$\phi\phi$CN being 108°C.

Unlike the melting points of the pure materials, the difference in the transitional properties between the dimers containing ortho-, meta- and para-substituted cyanophenyl moieties is less and appears to show no obvious trend. Apart from the difference in the nematic – isotropic transition temperatures between the C9 and C10 homologues the para-substituted C10 homologue has the highest nematic – isotropic transition temperature of the C10 isomers, being 131.1°C, compared with 113.8°C for DO10Oo and 74.1°C for DO10Om. The para-substituted C9 homologue has the lowest nematic – isotropic transition temperature of the C9 isomers, being 22.9°C, compared with 27°C for DO9Om and 46.1°C for DO9Oo. However, the ortho- and meta-substituted isomers follow the same trend for both the C9 and C10 homologues with the ortho-substituted materials having higher transition temperatures than the meta-substituted materials. This significant odd-even effect will be discussed later.

The entropy change for the nematic – isotropic transitions are presented in table 6.3, together with the transitional entropies of those materials prepared by Wilson

[14] and Fletcher [11] (they are indicated in table 6.3 with an asterisk). As can be seen the transitional entropies for the materials with nine carbon atoms in the alkyl spacer chain are similar to those for materials with ten carbon atoms in the alkyl spacer chain. However, most of the transitional entropies are higher than those determined for the homologous series of α-[(1,2,3,5,6-pentakis(4-phenylethynyl))phenyl-4-oxy]-ω-(4'-cyanobiphenyl-4-yloxy)alkanes [11], of which DO9OϕϕCN and DO10OϕϕCN are two members, with the exception of the C9 and C10 dimers containing a nitrobiphenyl moiety. It was suggested that the low entropy change associated with the nematic – isotropic transition exhibited by the dimers containing a cyanobiphenyl moiety was characteristic of a discotic nematic phase and not a columnar nematic phase, which may be expected to be formed because of the discotic moiety's interaction with TNF, or a nematic phase composed of relatively biaxial units. Whatever the nature of the phase is, it would seem that there is some difficulty in packing the discotic moieties and large rod-like moieties efficiently.

n = 9		n = 10	
Material	$\Delta S_{NI}/R$	Material	$\Delta S_{NI}/R$
DO9Oϕ	0.19	DO10Oϕ*	0.17
DO9Op	0.29	DO10Op*	0.37
DO9Om	0.08	DO10Om	0.19
DO9Oo	0.19	DO10Oo	+
$DO9ONO_2$	0.36	$DO10ONO_2$*	0.29
DO9Obip	0.27	DO10Obip*	0.28
DO9OϕϕCN*	0.16	DO10OϕϕCN*	0.09
$DO9O\phi\phi NO_2$	0.14	$DO10O\phi\phi NO_2$	0.06

+ entropy value unavailable

* Prepared by Wilson [14] and Fletcher [11].

Table 6.3 : The entropy change, ΔS/R, at the nematic – isotropic transition for equimolar mixtures of the DOnOR materials with TNF.

Figure 6.8 shows two possible ways we could pack the disc-like and rod-like units in a nematic phase, depending on how large the rod-like moiety is. If this moiety is large we could expect it to lie between the columns as shown in figure 6.7(a) to

allow the symmetry axes of the disc-like and rod-like moieties to lie parallel with a common director. However, if the rod-like units are small there may be room to accommodate them in a neighbouring column, as shown in figure 6.8(b). This arrangement may lead to the material being highly viscous and eventually forming a glassy phase. Figure 6.9 shows the structures of DO9Obip and DO10Obip. Both structures have been minimised using the MM2 force field in the CambridgeSoft Chem3D Pro modelling package. As established in Chapter 3, the chain protrudes below the plane of the disc and it can be seen that, for an even number of carbon atoms in the alkyl chain, the rod-like unit lies parallel to the plane of the disc, whereas for an odd number of carbon atoms in the alkyl chain the rod-like unit points downwards, away from the plane of the disc. For large rod-like moieties, i.e. biphenyl, cyanobiphenyl and nitrobiphenyl, we would expect the rods to pack in the spaces between the columns and therefore the conformational change needed to align the rod with the symmetry axis of the column for the C9 spacer chain is less than for the C10 spacer. Therefore, we would expect the nematic – isotropic transition temperature and the entropy change to be higher for the C9 homologues than for the C10 homologues, as the conformational change at T_{NI} for the C10 spacer is larger than for the C9 spacer and, apart from the disc-biphenyl dimers, this is indeed the case.

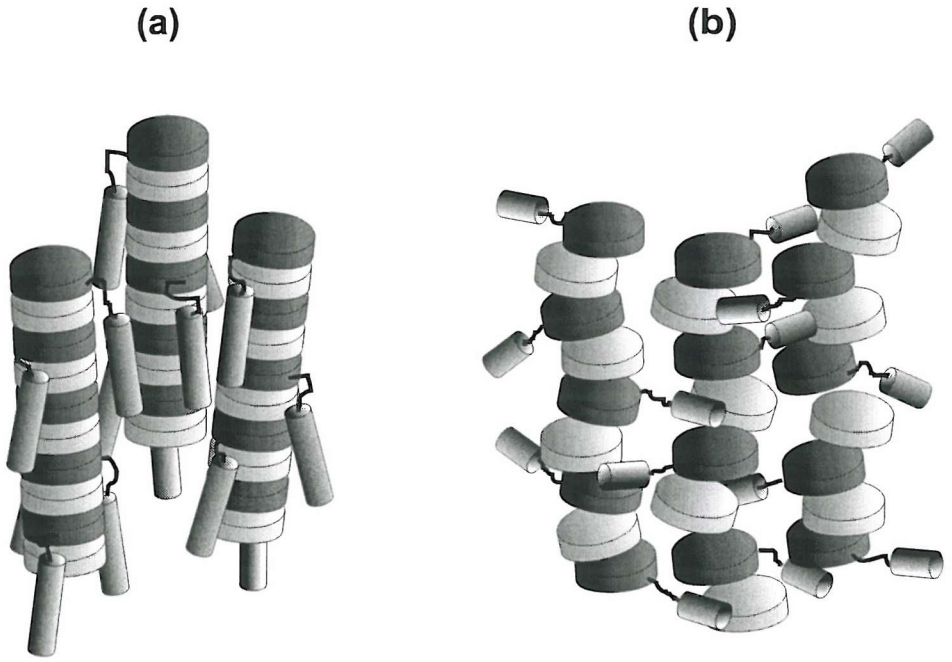

Figure 6.8 : The possible packing of disc-rod dimers (dark discs) and TNF (light discs) Depending on the size of the rod-like unit. (a) large rods and (b) small rods.

For the smaller 'rod-like' units, where it may be that they are incorporated in the neighbouring columns, we would expect the opposite. As shown in figure 6.9 the 'rod-like' units for the C10 homologues are, for an all-*trans* configuration, parallel with the plane of the disc, whereas this is not the case for the C9 homologues. Therefore, at the nematic – isotropic transition there needs to be a large conformational change for the C9 homologues to bring the 'rod-like' group parallel to the plane of the disc, whereas this is not the case for the C10 homologue. Generally, the transitional entropies at the nematic – isotropic transition for the C9 spacer are smaller than for the C10 spacer, however this effect is nowhere near as large as seen for the nematic – isotropic transition temperatures.

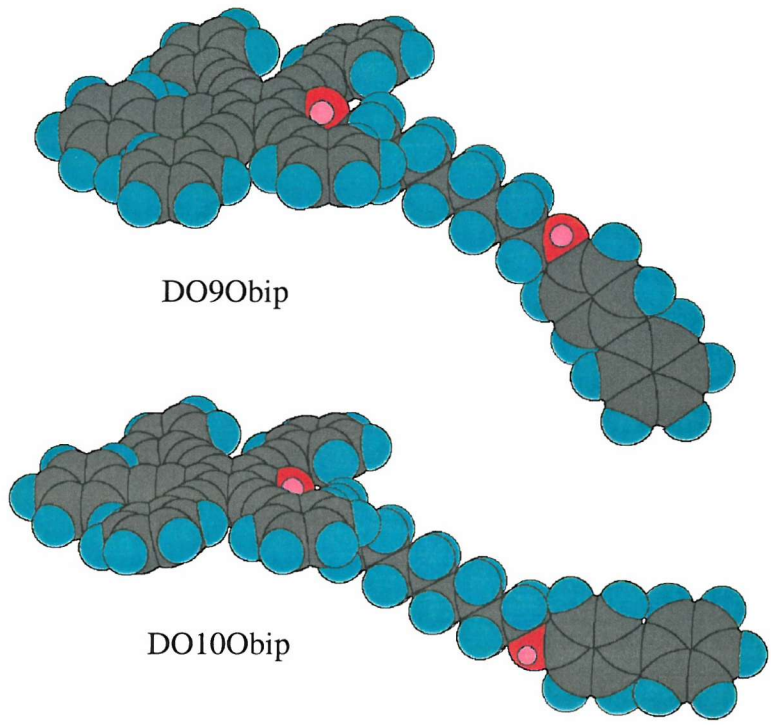

Figure 6.9 : The conformations of a disc-rod dimer, for an all-*trans* configuration of the alkyl spacer, for odd and even homologues.

The transitional entropies of the dimers containing smaller 'rod-like' units are generally larger and more like that of a columnar nematic – isotropic transition which would indicate that the packing incompatibilities are less as would be expected if the dimers pack as shown in figure 6.8(b). This may also explain the existence of the Col phase seen for DO9Oϕ and DO10Oϕ. As was seen in Chapter

2 the monomeric 'Superdiscs' with nine, ten and eleven carbon atoms in the alkyl chain exhibit both a columnar nematic phase and Col_{ho} phase when mixed with equimolar amounts of TNF. If the phenyl ring does not disrupt the packing of the molecules then we could consider the ring as just being part of the alkyl chain and so we may expect similar behaviour to the monomeric 'Superdiscs'. However, the Col phase is also seen for dimers containing a biphenyl moiety which is somewhat larger than a phenyl ring. Both the phenyl and biphenyl moieties do not contain any large electric dipoles, unlike the other rod-like units, which do not exhibit a second mesophase, and therefore these dipoles may disrupt the molecular organisation and so hinder the formation of ordered columnar phases.

6.3 Conclusions

It is apparent from the investigations described here and the work of Wilson [14] and Fletcher [11], together with the results from Chapter 2, that the mesophase behaviour of the pentakis(phenylethynyl)phenyloxyalkyl substituted dimers is critically dependent on the nature of the 'rod-like' moiety and the parity of the alkyl chain. Although almost all of the materials in the pure state are not mesomorphic, as was seen for the CnSD materials in Chapter 2, a mesophase was observed for the dimer containing a biphenyl moiety for both the C9 and C10 spacers. However, although a mesophase was observed by Wilson [14] for $DO10ONO_2$, no mesophase was observed for the C9 homologue.

As we had expected, mixtures of an equimolar amount of TNF with the DOnOR materials form liquid crystalline phases. Although we would anticipate that the interaction between the disc-like unit and TNF to be the dominant feature with respect to mesophase formation the significantly different transition temperatures seen for the C9 homologues when compared to the C10 homologues, especially for the dimers containing single ring terminal groups, suggests that the formation of the molecular stacks is very dependent on the conformation adopted by the terminal group. We have suggested that, depending on the size of the terminal 'rod-like' unit, the alkyl spacer will adopt a conformation that allows these units to be either incorporated within the neighbouring columns or between the molecular stacks. For the smaller 'rod-like' units a spacer chain with an even number of atoms is more favourable for mesophase formation than an odd number of atoms,

whereas for the larger 'rod-like' units an odd number of atoms in the spacer chain would appear to be more favourable. The results presented here, namely the low transition temperatures and transitional entropies exhibited by the C9 homologues with single ring terminal groups when compared to the C10 homologues and the highly viscous nature of the phases, suggest that this speculated arrangement may indeed be correct. This is further supported by the results found for the materials with larger 'rod-like' units. In this case the odd membered homologues generally have higher transition temperatures and entropies than the even membered homologues. However, to determine fully the nature of these phases and the effect the chain parity and terminal moiety has on mesophase behaviour we need to carry out further studies with other spacer chain lengths together with X-ray scattering experiments. Also, to use this approach to form a thermotropic biaxial nematic phase we need to incorporate larger rod-like groups into the dimer, such as the cyanoterphenyl moiety.

6.4 References

[1] Zamir, S., Poupko, R., Luz, Z., Hüser, B., Boeffel, C. and Zimmerman, H., *J. Am. Chem. Soc.*, **116**, 1973, (1994).

[2] Zamir, S., Wachtel, E.J., Zimmerman, H., Dai, S., Spielberg, N., Poupko, R. and Luz, Z., *Liq. Cryst.*, **23**, 689, (1997).

[3] Hermann-Schönherr, O., Wendorff, J.H., Kreuder, W. and Ringsdorf, H., *Makromolek. Chem. Rapid. Commun.*, 7, 97, (1986).

[4] Hüser, B., Pakula, T., Spiess, H.W., *Macromolecules*, **22**, 1960, (1989).

[5] Praefcke, K., Kohne, B., Singer, D., Demus, D., Pelzl, G., Diele, S., *Liq. Cryst.*, 7, 589, (1990).

[6] Alben, R., *J. Chem. Phys.*, **59**, 4299, (1973).

[7] Hashim, R., Luckhurst, G.R., Prata, F. and Romano, S., *Liq. Cryst.*, **15**, 283, (1993).

[8] Tihn, N.H., Destrade, C. and Gasparoux, H., *Phys Lett. A*, **72**, 251, (1979).

[9] Pratibha, R. and Madhusudana, N.V., *Mol. Cryst. Liq. Cryst. Lett.*, **1**, 111, (1985).

[10] Kreuder, W., Ringsdorf, H., Hermann-Schönherr, O. and Wendorff, J.H., *Angew. Chem. Int. Ed. Engl.*, **26**, 1249, (1987).

[11] Fletcher, I.D. and Luckhurst, G.R., *Liq. Cryst.*, **18**, 175, (1995).

[12] Praefcke, K., Kohne, B., Gündogen, B., Singer, D., Demus, D., Diele, D., Pelzl, G. and Bakowsky, U., *Mol. Cryst. Liq. Cryst.*, **198**, 393, (1991).

[13] Emsley, J.W., Luckhurst, G.R., Shilstone, G.N. and Sage, I., *Mol. Cryst. Liq. Cryst. Lett.*, **102**, 223, (1984).

[14] Wilson, M.J., *Ph.D., University of Southampton*, (1998).

[15] Möller, M., Tsukruk, V. and Wendorff, J.H., *Liq. Cryst.*, **12**, 17, (1992).

[16] Praefcke, K., Singer, D., Kohne, B., Ebert, M., Liebmann, A. and Wendorff, J.H., *Liq. Cryst.*, **10**, 147, (1991).

CHAPTER SEVEN

EXPERIMENTAL

All materials used were obtained commercially and used as is, unless otherwise stated.

7.1 Synthesis of the Pentabromophenyl Ethers (1)

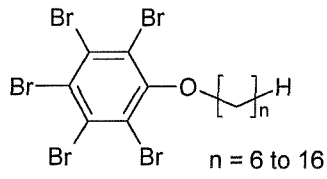

The reaction was carried out according to the method outlined by Praefcke *et al.* [1]. Pentabromophenol (50mmol, 24.42g) was dissolved in dry DMF (100ml). This was then added to a stirred solution of sodium hydride (60mmol, 1.44g) in dry DMF (20ml) in a round bottomed flask fitted with reflux condenser and guard tube. The mixture was stirred at room temperature for 1 hour. The 1-bromoalkane (70mmol) was then added and the mixture was heated at $80^{O}C$ for 26 hours. After cooling, water (50ml) was added and the resulting slurry was extracted with either ether or DCM (4 x 50ml) depending upon the solubility of the product. These organic extracts were combined and washed with water (2 x 50ml), dilute sodium hydroxide solution (50ml) and dilute sodium chloride solution (4 x 50ml). The organic extracts were then dried over anhydrous magnesium sulphate. The solvent was then removed on the rotary evaporator and the solid obtained recrystallised from boiling acetone to yield a white solid.

Pentabromophenyloxyhexane (1a)

Yield 54%

I.R. υ (Nujol) lack of OH peak @ ~3300 cm^{-1} indicates ether, 725 (substituted benzene) cm^{-1}.

^{1}H N.M.R. δ ($CDCl_3$) 0.95 (t, methyl, 3H), 1.2 – 1.5 (m, methylene protons, 4H), 1.55 (p, Ar-O-CH_2-CH_2-$C\underline{H_2}$-, 2H), 1.9 (p, Ar-O-CH_2-$C\underline{H_2}$-, 2H), 4.0 (t, Ar-O-$C\underline{H_2}$-, 2H) ppm.

^{13}C N.M.R. δ ($CDCl_3$) 14.3, 22.8, 26.6, 30.8, 32.1, 73.8, 122.1, 124.8, 128.5, 154.7 ppm.

Pentabromophenyloxyoctane (1b)

Yield 59%

I.R. υ (Nujol) lack of OH peak @ ~3300 cm^{-1} indicates ether, 725 (substituted benzene) cm^{-1}.

^{1}H N.M.R. δ ($CDCl_3$) 0.95 (t, methyl, 3H), 1.2 – 1.5 (m, methylene protons, 8H), 1.55 (p, Ar-O-CH_2-CH_2-$C\underline{H_2}$-, 2H), 1.9 (p, Ar-O-CH_2-$C\underline{H_2}$-, 2H), 4.0 (t, Ar-O-$C\underline{H_2}$-, 2H) ppm.

^{13}C N.M.R. δ ($CDCl_3$) 14.3, 22.8, 26.6, 29.9, 30.8, 32.1, 73.8, 122.1, 124.8, 128.5, 154.7 ppm.

Pentabromophenyloxynonane (1c)

Yield 49%

I.R. υ (Nujol) lack of OH peak @ ~3300 cm^{-1} indicates ether, 725 (substituted benzene) cm^{-1}.

^{1}H N.M.R. δ ($CDCl_3$) 0.95 (t, methyl, 3H), 1.2 – 1.5 (m, methylene protons, 10H), 1.55 (p, Ar-O-CH_2-CH_2-$C\underline{H_2}$-, 2H), 1.9 (p, Ar-O-CH_2-$C\underline{H_2}$-, 2H), 4.0 (t, Ar-O-$C\underline{H_2}$-, 2H) ppm.

^{13}C N.M.R. δ ($CDCl_3$) 14.3, 22.8, 26.6, 29.9, 30.8, 32.1, 73.8, 122.1, 124.8, 128.5, 154.7 ppm..

Pentabromophenyloxydecane (1d)

Yield 58%

I.R. υ (Nujol) lack of OH peak @ ~3300 cm^{-1} indicates ether, 725 (substituted benzene) cm^{-1}.

^{1}H N.M.R. δ ($CDCl_3$) 0.95 (t, methyl, 3H), 1.2 – 1.5 (m, methylene protons, 12H), 1.55 (p, Ar-O-CH_2-CH_2-$C\underline{H_2}$-, 2H), 1.9 (p, Ar-O-CH_2-$C\underline{H_2}$-, 2H), 4.0 (t, Ar-O-$C\underline{H_2}$-, 2H) ppm.

^{13}C N.M.R. δ ($CDCl_3$) 14.3, 22.8, 26.6, 29.9, 30.8, 32.1, 73.8, 122.1, 124.8, 128.5, 154.7 ppm.

Pentabromophenyloxyundecane (1e)

Yield 60%

I.R. υ (Nujol) lack of OH peak @ ~3300 cm^{-1} indicates ether, 725 (substituted benzene) cm^{-1}.

^1H N.M.R. δ ($CDCl_3$) 0.95 (t, methyl, 3H), 1.2 – 1.5 (m, methylene protons, 14H), 1.55 (p, Ar-O-CH_2-CH_2-$C\underline{H_2}$-, 2H), 1.9 (p, Ar-O-CH_2-$C\underline{H_2}$-, 2H), 4.0 (t, Ar-O-$C\underline{H_2}$-, 2H) ppm.

^{13}C N.M.R. δ ($CDCl_3$) 14.3, 22.8, 26.6, 29.9, 30.8, 32.1, 73.8, 122.1, 124.8, 128.5, 154.7 ppm..

Pentabromophenyloxydodecane (1f)

Yield 58%

I.R. υ (Nujol) lack of OH peak @ ~3300 cm^{-1} indicates ether, 725 (substituted benzene) cm^{-1}.

^1H N.M.R. δ ($CDCl_3$) 0.95 (t, methyl, 3H), 1.2 – 1.5 (m, methylene protons, 16H), 1.55 (p, Ar-O-CH_2-CH_2-$C\underline{H_2}$-, 2H), 1.9 (p, Ar-O-CH_2-$C\underline{H_2}$-, 2H), 4.0 (t, Ar-O-$C\underline{H_2}$-, 2H) ppm.

^{13}C N.M.R. δ ($CDCl_3$) 14.3, 22.8, 26.6, 29.9, 30.8, 32.1, 73.8, 122.1, 124.8, 128.5, 154.7 ppm.

Pentabromophenyloxytridecane (1g)

Yield 59%

I.R. υ (Nujol) lack of OH peak @ ~3300 cm^{-1} indicates ether, 725 (substituted benzene) cm^{-1}.

^1H N.M.R. δ ($CDCl_3$) 0.95 (t, methyl, 3H), 1.2 – 1.5 (m, methylene protons, 18H), 1.55 (p, Ar-O-CH_2-CH_2-$C\underline{H_2}$-, 2H), 1.9 (p, Ar-O-CH_2-$C\underline{H_2}$-, 2H), 4.0 (t, Ar-O-$C\underline{H_2}$-, 2H) ppm.

^{13}C N.M.R. δ ($CDCl_3$) 14.3, 22.8, 26.6, 29.9, 30.8, 32.1, 73.8, 122.1, 124.8, 128.5, 154.7 ppm.

Pentabromophenyloxytetradecane (1h)

Yield 68%

I.R. υ (Nujol) lack of OH peak @ ~3300 cm^{-1} indicates ether, 725 (substituted benzene) cm^{-1}.

^{1}H N.M.R. δ ($CDCl_3$) 0.95 (t, methyl, 3H), 1.2 – 1.5 (m, methylene protons, 20H), 1.55 (p, Ar-O-CH_2-CH_2-$C\underline{H_2}$-, 2H), 1.9 (p, Ar-O-CH_2-$C\underline{H_2}$-, 2H), 4.0 (t, Ar-O-$C\underline{H_2}$-, 2H) ppm.

^{13}C N.M.R. δ ($CDCl_3$) 14.3, 22.8, 26.6, 29.9, 30.8, 32.1, 73.8, 122.1, 124.8, 128.5, 154.7 ppm.

Pentabromophenylpentadecane (1i)

Yield 65%

I.R. υ (Nujol) lack of OH peak @ ~3300 cm^{-1} indicates ether, 725 (substituted benzene) cm^{-1}.

^{1}H N.M.R. δ ($CDCl_3$) 0.95 (t, methyl, 3H), 1.2 – 1.5 (m, methylene protons, 22H), 1.55 (p, Ar-O-CH_2-CH_2-$C\underline{H_2}$-, 2H), 1.9 (p, Ar-O-CH_2-$C\underline{H_2}$-, 2H), 4.0 (t, Ar-O-$C\underline{H_2}$-, 2H) ppm.

^{13}C N.M.R. δ ($CDCl_3$) 14.3, 22.8, 26.6, 29.9, 30.8, 32.1, 73.8, 122.1, 124.8, 128.5, 154.7 ppm.

Pentabromophenyloxyhexadecane (1j)

Yield 64%

I.R. υ (Nujol) lack of OH peak @ ~3300 cm^{-1} indicates ether, 725 (substituted benzene) cm^{-1}.

^{1}H N.M.R. δ ($CDCl_3$) 0.95 (t, methyl, 3H), 1.2 – 1.5 (m, methylene protons, 24H), 1.55 (p, Ar-O-CH_2-CH_2-$C\underline{H_2}$-, 2H), 1.9 (p, Ar-O-CH_2-$C\underline{H_2}$-, 2H), 4.0 (t, Ar-O-$C\underline{H_2}$-, 2H) ppm.

^{13}C N.M.R. δ ($CDCl_3$) 14.3, 22.8, 26.6, 29.9, 30.8, 32.1, 73.8, 122.1, 124.8, 128.5, 154.7 ppm.

7.2 Synthesis of the Pentakis(phenylethynyl)phenyloxyalkanes (CnSD) (2)

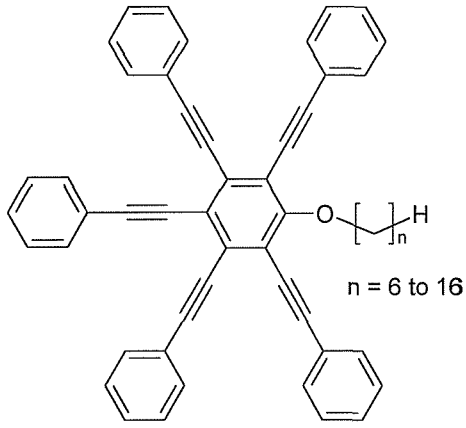

The reaction was carried out according to the method outlined by Praefcke *et al.* [1]. The pentabromophenyl ethers (**1a – 1j**) (1mmol), phenylacetylene (10mmol), bis(triphenylphosphine) palladium (II) chloride (50mg), copper iodide (50mg) and triphenylphosphine (100mg) were dissolved in degassed (N_2/1 hour) triethylamine (50ml). This was then refluxed under nitrogen for between 18 and 48 hours. After this time the reaction mixture was dissolved in DCM (50ml) and washed with dilute hydrochloric acid (CARE!) (2 x 50ml) and water (2 x 50 ml). The organic extract was then dried over anhydrous magnesium sulphate and the solvent removed on the rotary evaporator. The solid obtained was recrystallised several times from boiling acetone to yield a yellow solid.

Pentakis(phenylethynyl)phenyloxyhexane (C6SD) (2a)

Yield 59%

^{1}H N.M.R. δ ($CDCl_3$) 0.85 (t, methyl, 3H), 1.05 – 1.6 (m, methylene protons, 4H), 1.9 (p, Ar-O-CH_2-$C\underline{H_2}$-, 2H), 4.3 (t, Ar-O-$C\underline{H_2}$-), 7.4 (m, aromatic protons ortho to acetylene, 10H), 7.65 (m, other aromatic protons, 15H) ppm.

^{13}C N.M.R. δ ($CDCl_3$) 14.3, 22.8, 26.6, 30.8, 32.1, 75.1, 84.6, 97.4, 120.4, 123.4, 124.2, 128.6, 129.0, 131.8, 131.9, 160.7 ppm.

Pentakis(phenylethynyl)phenyloxyoctane (C8SD) (2b)

Yield 63%

^{1}H N.M.R. δ ($CDCl_3$) 0.85 (t, methyl, 3H), 1.05 – 1.6 (m, methylene protons, 8H), 1.9 (p, Ar-O-CH_2-$C\underline{H_2}$-, 2H), 4.3 (t, Ar-O-$C\underline{H_2}$-), 7.4 (m, aromatic protons ortho to acetylene, 10H), 7.65 (m, other aromatic protons, 15H) ppm.

^{13}C N.M.R. δ ($CDCl_3$) 14.3, 22.8, 26.6, 29.9, 30.8, 32.1, 75.1, 84.6, 97.4, 120.4, 123.4, 124.2, 128.6, 129.0, 131.8, 131.9, 160.7 ppm.

Pentakis(phenylethynyl)phenyloxynonane (C9SD) (2c)

Yield 48%

^{1}H N.M.R. δ ($CDCl_3$) 0.85 (t, methyl, 3H), 1.05 – 1.6 (m, methylene protons, 10H), 1.9 (p, Ar-O-CH_2-$C\underline{H_2}$-, 2H), 4.3 (t, Ar-O-$C\underline{H_2}$-), 7.4 (m, aromatic protons ortho to acetylene, 10H), 7.65 (m, other aromatic protons, 15H) ppm.

^{13}C N.M.R. δ ($CDCl_3$) 14.3, 22.8, 26.6, 29.9, 30.8, 32.1, 75.1, 84.6, 97.4, 120.4, 123.4, 124.2, 128.6, 129.0, 131.8, 131.9, 160.7 ppm.

Pentakis(phenylethynyl)phenyloxydecane (C10SD) (2d)

Yield 52%

^{1}H N.M.R. δ ($CDCl_3$) 0.85 (t, methyl, 3H), 1.05 – 1.6 (m, methylene protons, 12H), 1.9 (p, Ar-O-CH_2-$C\underline{H_2}$-, 2H), 4.3 (t, Ar-O-$C\underline{H_2}$-), 7.4 (m, aromatic protons ortho to acetylene, 10H), 7.65 (m, other aromatic protons, 15H) ppm.

^{13}C N.M.R. δ ($CDCl_3$) 14.3, 22.8, 26.6, 29.9, 30.8, 32.1, 75.1, 84.6, 97.4, 120.4, 123.4, 124.2, 128.6, 129.0, 131.8, 131.9, 160.7 ppm.

Pentakis(phenylethynyl)phenyloxyundecane (C11SD) (2e)

Yield 59%

^{1}H N.M.R. δ ($CDCl_3$) 0.85 (t, methyl, 3H), 1.05 – 1.6 (m, methylene protons, 14H), 1.9 (p, Ar-O-CH_2-$C\underline{H_2}$-, 2H), 4.3 (t, Ar-O-$C\underline{H_2}$-), 7.4 (m, aromatic protons ortho to acetylene, 10H), 7.65 (m, other aromatic protons, 15H) ppm.

^{13}C N.M.R. δ ($CDCl_3$) 14.3, 22.8, 26.6, 29.9, 30.8, 32.1, 75.1, 84.6, 97.4, 120.4, 123.4, 124.2, 128.6, 129.0, 131.8, 131.9, 160.7 ppm.

Pentakis(phenylethynyl)phenyloxydodecane (C12SD) (2f)

Yield 51%

^{1}H N.M.R. δ ($CDCl_3$) 0.85 (t, methyl, 3H), 1.05 – 1.6 (m, methylene protons, 16H), 1.9 (p, Ar-O-CH_2-$C\underline{H_2}$-, 2H), 4.3 (t, Ar-O-$C\underline{H_2}$-), 7.4 (m, aromatic protons ortho to acetylene, 10H), 7.65 (m, other aromatic protons, 15H) ppm.

^{13}C N.M.R. δ ($CDCl_3$) 14.3, 22.8, 26.6, 29.9, 30.8, 32.1, 75.1, 84.6, 97.4, 120.4, 123.4, 124.2, 128.6, 129.0, 131.8, 131.9, 160.7 ppm.

Pentakis(phenylethynyl)phenyloxytridecane (C13SD) (2g)

Yield 45%

^{1}H N.M.R. δ ($CDCl_3$) 0.85 (t, methyl, 3H), 1.05 – 1.6 (m, methylene protons, 18H), 1.9 (p, Ar-O-CH_2-$C\underline{H_2}$-, 2H), 4.3 (t, Ar-O-$C\underline{H_2}$-), 7.4 (m, aromatic protons ortho to acetylene, 10H), 7.65 (m, other aromatic protons, 15H) ppm.

^{13}C N.M.R. δ ($CDCl_3$) 14.3, 22.8, 26.6, 29.9, 30.8, 32.1, 75.1, 84.6, 97.4, 120.4, 123.4, 124.2, 128.6, 129.0, 131.8, 131.9, 160.7 ppm.

Pentakis(phenylethynyl)phenyloxytetradecane (C14SD) (2h)

Yield 57%

^{1}H N.M.R. δ ($CDCl_3$) 0.85 (t, methyl, 3H), 1.05 – 1.6 (m, methylene protons, 20H), 1.9 (p, Ar-O-CH_2-$C\underline{H_2}$-, 2H), 4.3 (t, Ar-O-$C\underline{H_2}$-), 7.4 (m, aromatic protons ortho to acetylene, 10H), 7.65 (m, other aromatic protons, 15H) ppm.

^{13}C N.M.R. δ ($CDCl_3$) 14.3, 22.8, 26.6, 29.9, 30.8, 32.1, 75.1, 84.6, 97.4, 120.4, 123.4, 124.2, 128.6, 129.0, 131.8, 131.9, 160.7 ppm.

Pentakis(phenylethynyl)phenyloxypentadecane (C15SD) (2i)

Yield 55%

^{1}H N.M.R. δ ($CDCl_3$) 0.85 (t, methyl, 3H), 1.05 – 1.6 (m, methylene protons, 22H), 1.9 (p, Ar-O-CH_2-$C\underline{H_2}$-, 2H), 4.3 (t, Ar-O-$C\underline{H_2}$-), 7.4 (m, aromatic protons ortho to acetylene, 10H), 7.65 (m, other aromatic protons, 15H) ppm.

^{13}C N.M.R. δ ($CDCl_3$) 14.3, 22.8, 26.6, 29.9, 30.8, 32.1, 75.1, 84.6, 97.4, 120.4, 123.4, 124.2, 128.6, 129.0, 131.8, 131.9, 160.7 ppm.

Pentakis(phenylethynyl)phenyloxyhexadecane (C16SD) (2j)

Yield 62%

^{1}H N.M.R. δ ($CDCl_3$) 0.85 (t, methyl, 3H), 1.05 – 1.6 (m, methylene protons, 24H), 1.9 (p, Ar-O-CH_2-$C\underline{H_2}$-, 2H), 4.3 (t, Ar-O-$C\underline{H_2}$-), 7.4 (m, aromatic protons ortho to acetylene, 10H), 7.65 (m, other aromatic protons, 15H) ppm.

^{13}C N.M.R. δ ($CDCl_3$) 14.3, 22.8, 26.6, 29.9, 30.8, 32.1, 75.1, 84.6, 97.4, 120.4, 123.4, 124.2, 128.6, 129.0, 131.8, 131.9, 160.7 ppm.

7.3 Synthesis of 1-decanol-d_2 (3)

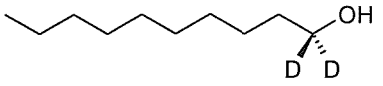

Aluminium (III) chloride (0.2mol, 26.6g) was slowly dissolved in dry ether (200ml) and this was then added dropwise to a mixture of lithium aluminium deuteride (0.12mol, 5.04g) in dry ether (80ml) under nitrogen. Ethyl caprate (0.04mol, 8g) was dissolved in dry chloroform (100ml) and then added dropwise to the reducing mixture. This was then stirred for 3 hours at room temperature under nitrogen after which time concentrated hydrochloric acid (115ml) was added carefully followed by water (150ml). The mixed was then extracted with DCM and the organic extracts combined and dried over anhydrous magnesium sulphate. The solvent was then removed on the rotary evaporator to yield a pale brown liquid. This was distilled under reduced pressure to leave a clear liquid.

Yield 95%

I.R. υ (liquid film) 3300cm^{-1}, (s, O-H str).

^{1}H N.M.R. δ ($CDCl_3$) 0.9 (t, methyl, 3H), 1.2 – 1.5 (m, methylene protons, 14H), 1.65 (p, HO-CH_2-$C\underline{H_2}$-, 2H) ppm. No peak at 3.6ppm indicates presence of deuterium at α-position.

^{13}C N.M.R. δ ($CDCl_3$) 14.0, 22.9, 26.2, 29.6, 29.8, 29.9, 32.2, 32.9, 62.0 ppm.

7.4 Synthesis of 1-bromodecane-d_2 (4)

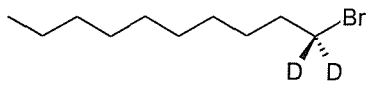

The reaction was carried out using a previously described method [2]. A mixture of 1-decanol-d_2 (**3**) (0.0625mol, 10g) and purified red phosphorus (0.52g) was vigorously stirred at ~250^{O}C. Bromine (1.8ml) was added dropwise ensuring a controlled reaction. The mixture was then cooled and ether added (50ml). The excess phosphorus was filtered off and the ethereal solution was washed with water (4 x 50ml) and dried over anhydrous potassium carbonate. The solvent was then removed on the rotary evaporator to afford a brown liquid. This was then distilled under reduced pressure to yield a clear liquid.

Yield 74%

^{1}H N.M.R. δ ($CDCl_3$) 0.9 (t, methyl, 3H), 1.2 – 1.5 (m, methylene protons, 14H), 1.85 (p, Br-CH_2-$C\underline{H_2}$-, 2H) ppm. No peak at 3.4ppm indicates presence of deuterium at α-position.

^{13}C N.M.R. δ ($CDCl_3$) 14.1, 22.7, 28.2, 28.8, 29.3, 29.5, 32.9, 33.5 ppm.

7.5 Synthesis of 1-pentabromophenyloxydecane-1-d_2 (5)

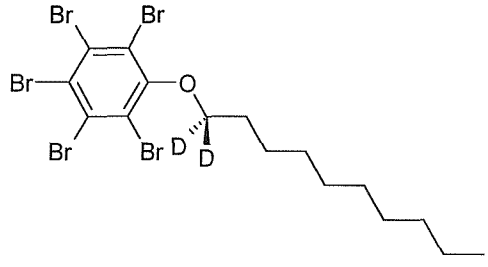

The reaction was carried out according to the method outlined by Praefcke *et al.* [1]. Pentabromophenol (25mmol, 12.21g) was dissolved in dry DMF (50ml). This was then added to a stirred solution of sodium hydride (30mmol) in dry DMF (10ml) in a round bottomed flask fitted with reflux condenser and guard tube. The mixture was stirred at room temperature for 1 hour. The 1-bromodecane-1-d_2

(25mmol, 5.58g) was then added and the mixture was heated at 80°C for 26 hours. After cooling, water (50ml) was added and the resulting slurry was extracted with either ether or DCM (4 x 50ml) depending upon the solubility of the product. These organic extracts were combined and washed with water (2 x 50ml), dilute sodium hydroxide solution (50ml) and dilute sodium chloride solution (4 x 50ml). The organic extracts were then dried over anhydrous magnesium sulphate. The solvent was then removed on the rotary evaporator and the solid obtained recrystallised from boiling acetone to yield a white solid.

Yield 51%

I.R. υ (Nujol) lack of OH peak @ ~3300 cm^{-1} indicates ether, 725 (substituted benzene) cm^{-1}.

^{1}H N.M.R. δ ($CDCl_3$) 0.95 (t, methyl, 3H), 1.2 – 1.5 (m, methylene protons, 12H), 1.55 (p, Ar-O-CH_2-CH_2-$C\underline{H_2}$-, 2H), 1.9 (p, Ar-O-CH_2-$C\underline{H_2}$-, 2H), lack of peak @ 4.0 (t, Ar-O-$C\underline{H_2}$-, 2H) ppm indicates the presence of deuterium.

^{13}C N.M.R. δ ($CDCl_3$) 14.3, 22.8, 26.6, 29.9, 30.8, 32.1, 73.8, 122.1, 124.8, 128.5, 154.7 ppm.

7.6 Synthesis of 1-[pentakis(phenylethynyl)phenyloxy]decane-1-d_2 (C10SDD2) (6)

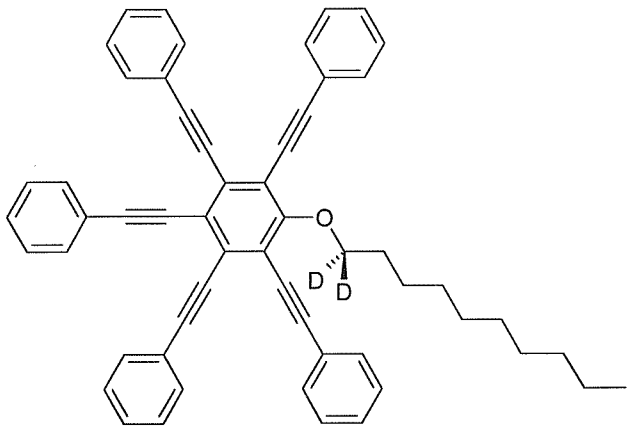

The reaction was carried out according to the method outlined by Praefcke *et al.* [1]. 1-pentabromophenyloxydecane-1-d_2 (5mmol, 3.15g), phenylacetylene (50mmol, 5.1g), bis(triphenylphosphine) palladium (II) chloride (100mg), copper iodide (100mg) and triphenylphosphine (200mg) were dissolved in degassed (N_2/1

hour) triethylamine (50ml). This was then refluxed under nitrogen for between 18 and 48 hours. After this time the reaction mixture was dissolved in DCM (100ml) and washed with dilute hydrochloric acid (CARE!) (2 x 100ml) and water (2 x 100 ml). The organic extract was then dried over anhydrous magnesium sulphate and the solvent removed on the rotary evaporator. The solid obtained was recrystallised several times from boiling acetone to yield a yellow solid.

Yield 67%

^{1}H N.M.R. δ ($CDCl_3$) 0.85 (t, methyl, 3H), 1.05 – 1.6 (m, methylene protons, 4H), 1.9 (p, Ar-O-CH_2-$C\underline{H_2}$-, 2H), lack of peak @ 4.3 (t, Ar-O-$C\underline{H_2}$-) indicates the presence of deuterium, 7.1 – 7.6 (m, aromatic protons, 25H) ppm.

^{13}C N.M.R. δ ($CDCl_3$) 14.3, 22.8, 26.6, 29.9, 30.8, 32.1, 75.1, 84.6, 97.4, 120.4, 123.4, 124.2, 128.6, 129.0, 131.8, 131.9, 160.7 ppm.

7.7 Synthesis of Bis(4-bromophenylyl)methane (7)

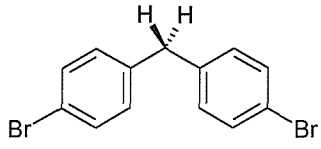

Aluminium (III) chloride (125mmol, 16.66g) was slowly dissolved in ether (100ml). This was added slowly to a stirred suspension of lithium aluminium hydride (75mmol, 2.85g) in ether (50ml) under nitrogen. 4,4'-dibromo benzophenone (25mmol, 8.5g) was dissolved in dry chloroform and this was added dropwise to the reducing mixture. This was then stirred for 3 hours at room temperature. After this time concentrated hydrochloric acid (75ml) was added carefully, followed by water (100ml). This was then extracted with DCM and the organic extracts were combined and dried over anhydrous magnesium sulphate. The solvent was then removed on the rotary evaporator and the product recrystallised from ethanol to yield a white solid.

Yield 93%

^{1}H N.M.R. δ ($CDCl_3$) 4.1 (s, methylene protons, 2H), 7.04 (d, phenyl 2-H, 4H), 7.41 (d, phenyl 3-H, 4H) ppm.

^{13}C N.M.R. δ ($CDCl_3$) 41.4, 120.4, 130.7, 131.8, 139.5 ppm.

7.8 Synthesis of 4-benzonitrile boronic acid (8)

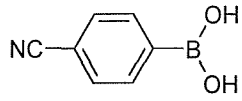

4-bromobenzonitrile (20mmol, 3.64g) was dissolved in dry THF (100ml) and cooled to -78^{O}C in a three-necked round bottomed flask, fitted with a dropping funnel and a thermometer, under nitrogen. To this was added 2.5M n-butyllithium in hexanes (20mmol, 8ml) as fast as possible without causing a temperature rise and stirred at –78^{O}C for 15 minutes. Trimethylborate (30mmol, 3.12g, 2.3ml) was then added as fast as possible without a temperature rise and the mixture allowed to warm to room temperature overnight. Dilute hydrochloric acid (15%) was then added until the mixture was acidic to universal indicator paper and the mixture was extracted with DCM (4 x 50ml). The organic extracts were combined and washed with water (2 x 100ml) and then dried over anhydrous magnesium sulphate. The solvent was then removed on the rotary evaporator to yield a white waxy solid.

Yield 78%

IR υ (Nujol) 825 (p-substituted aromatic), 930 (B-C str), 1365 (B-O str), 2225 (nitrile str) cm^{-1}.

7.9 Synthesis of Bis(4-cyanobiphenylyl)methane (CB1CB) (9)

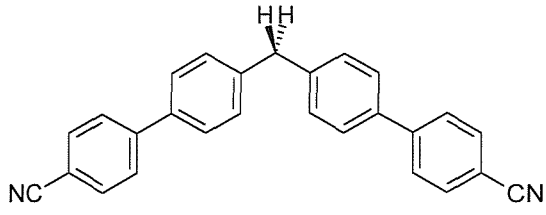

Bis(4-bromophenyl)methane (**7**) (2mmol, 0.65g) and 4-benzonitrile boronic acid (**8**) (5mmol, 0.74g) were dissolved in freshly distilled DME (20ml) in a two-necked round bottomed flask, fitted with a reflux condenser, and stirred under nitrogen. 2M sodium carbonate solution (10ml) was added followed by a catalytic amount of tetrakis(triphenylphosphine) palladium (0) (50mg). This was then heated under reflux for 2 - 3 days. After the reaction was complete the aqueous layer was separated and extracted with DCM (4 x 50ml). The organic extracts were then combined, dried over anhydrous magnesium sulphate and the solvent removed on a rotary evaporator. The crude solid was then purified by column chromatography (Silica gel 60 / 3:1 toluene:hexane) and recrystallised from a mixture of ethanol and toluene to yield a white fluffy solid.

Yield 42%

^{1}H N.M.R. δ ($CDCl_3$) 4.1 (s, methylene protons, 2H), 7.32 (d, biphenyl 2'-H, 4H), 7.6 (d, biphenyl 3'-H, 4H), 7.77 (unres. d, biphenyl 2-H, 4H), 7.81 (unres. d, biphenyl 3-H, 4H) ppm.

^{13}C N.M.R δ ($CDCl_3$) 41.4, 112.1, 118.8, 127.2, 127.4, 128.0, 132.5, 139.3, 140.3, 144.1 ppm.

7.10 Synthesis of 4-toluene boronic acid (10)

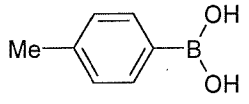

Synthetic procedure as for 4-cyanophenyl boronic acid

Yield 65%

IR υ (Nujol) 825 (p-substituted aromatic), 930 (B-C str), 1365 (B-O str), 2225 (nitrile str) cm^{-1}.

7.11 Synthesis of Bis(4-methylbiphenylyl)methane (MeB1MeB) (11)

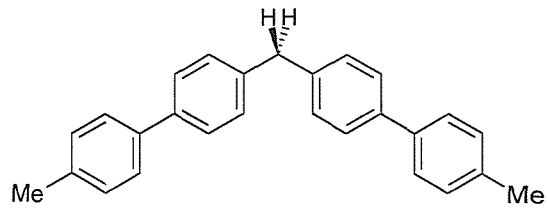

Carried out according to the method outlined by Suzuki *et al.* [3]. Bis(4-bromophenyl)methane (**7**) (2mmol, 0.65g) and 4-toluene boronic acid (**10**) (5mmol, 0.68 g) were dissolved in freshly distilled DME (20ml) in a two-necked round bottomed flask, fitted with a reflux condenser, and stirred under nitrogen. 2M sodium carbonate solution (10ml) was added followed by a catalytic amount of tetrakis(triphenylphosphine) palladium (0) (50mg). This was then heated under reflux for 2 - 3 days. After this time the aqueous layer was separated and extracted with DCM (4 x 50ml). The organic extracts were then combined, dried over anhydrous magnesium sulphate and the solvent removed on a rotary evaporator. The crude solid was then purified by column chromatography (Silica gel 60 / 3:1 toluene:hexane) and recrystallised from a mixture of ethanol and toluene to yield a white solid.

Yield 58%

^{1}H N.M.R. δ ($CDCl_3$) 2.4 (s, methyl protons, 6H), 4.1 (s, methylene protons, 2H), 7.26 (d, biphenyl 3-H, 2H), 7.31 (d, biphenyl 2'-H, 2H), 7.49 (d, biphenyl 3'-H, 2H), 7.54 (d, biphenyl 2-H, 2H) ppm.

^{13}C N.M.R. δ ($CDCl_3$) 21.3, 41.4, 127.0, 127.2, 129.4, 129.6, 137.0, 138.3, 139.4, 140.0 ppm.

7.12 Synthesis of Bis(4-cyanobiphenylyl)ketone (CB1CB(C=O)) (12)

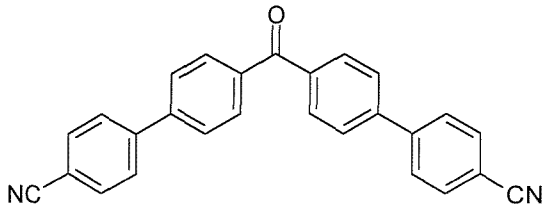

Carried out according to the method outlined by Suzuki *et al.* [3]. Dibromobenzophenone (5mmol, 1.7g) and 4-benzonitrile boronic acid (**8**) (12.5mmol, 1.83g) were dissolved in freshly distilled DME (50ml) in a two-necked round bottomed flask, fitted with reflux condenser, and stirred under nitrogen. 2M sodium carbonate solution (25ml) was added followed by a catalytic amount of tetrakis(triphenylphosphine) palladium (0) (100mg). This was then heated under reflux for 2 - 3 days. After this time the aqueous layer was separated and extracted with DCM (4 x 100ml). The organic extracts were then combined, dried over anhydrous magnesium sulphate and the solvent removed on a rotary evaporator. The crude solid was then purified by column chromatography (Silica gel 60 / 3:1 toluene:hexane) and recrystallised from a mixture of ethanol and toluene to yield a white solid.

Yield 42%

^{1}H N.M.R. δ ($CDCl_3$) 7.75 (d, biphenyl 3'-H, 4H), 7.77 (unres. d, biphenyl 2-H, 4H), 7.81 (unres. d, biphenyl 3-H, 4H), 7.97 (d, biphenyl 2'-H, 4H) ppm.

^{13}C N.M.R. δ ($CDCl_3$) 112.1, 118.8, 127.5, 128.1, 131.0, 133.0, 137.4, 143.3, 144.4, 195.8 ppm.

7.13 Synthesis of Bis(4-biphenylyl)methane (Bip1Bip) (13)

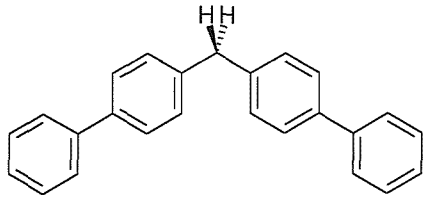

Biphenyl (0.2mol, 30.84g) and chloral hydrate (0.1mol, 16.54g) were stirred mechanically and heated to 50°C. Sulphuric acid (100ml) was added dropwise and the mixture heated to 70°C for 2 hours. After this time the mixture was cooled and poured onto ice. The resulting solid was filtered and the aqueous layer extracted with diethyl ether (4 x 100ml). The organic extracts were combined, dried over magnesium sulphate and the solvent removed on a rotary evaporator. The solid intermediate was recrystallised from acetone. Potassium hydroxide (52.5g) was

dissolved in water (52.5ml) and added to diethylene glycol (420ml). The water was removed by distillation and the solution cooled to 100°C. The intermediate was added and the mixture heated at reflux for 3 hours. The mixture was then cooled and poured onto ice and left to stand overnight. The resulting solid was filtered and the aqueous layer extracted with ether (4 x 100ml). The organic extracts were combined, dried over magnesium sulphate and the solvent removed on a rotary evaporator. The combined products were recrystallised once from acetone and once from ethanol to yield a pale yellow solid.

Yield 52%

^{1}H N.M.R. δ ($CDCl_3$) 4.1 (s, methylene protons, 2H), 7.27 – 7.37 (m, biphenyl 4-H & 2'-H, 6H), 7.45 (t, biphenyl 3-H, 4H), 7.56 (d, biphenyl 2-H, 4H), 7.6 (d, biphenyl 3'-H, 4H) ppm.

^{13}C N.M.R. δ ($CDCl_3$) 41.4, 127.2, 127.3, 127.4, 128.9, 129.5, 139.3, 140.3, 141.1 ppm.

7.14 Synthesis of the α-(4-cyanobiphenyloxy)-ω-bromoalkanes (14)

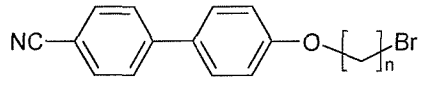

n = 3 to 12

Carried out according to the method outlined by Crivello *et el.* [4] 4-hydroxycyanobiphenyl (5mmol, 0.97g) and potassium carbonate (50mmol, 6.7g) in AnalaR acetone (50ml) were stirred at reflux in a quickfit-conical flask fitted with reflux condenser and guard tube for 1 hour. After this time the α,ω-dibromoalkane (50mmol) was added and the mixture was stirred at reflux for 2 – 3 days. The mixture was then cooled and water (100ml) was added. This was then extracted with DCM (4 x 50ml), the organic extracts combined, dried over anhydrous magnesium sulphate and the solvent removed on the rotary evaporator to yield a crude mix of the required product and excess α,ω-dibromoalkane. The excess α,ω-dibromoalkane was then removed under vacuum on the Kugelrohr and the crude product remaining was poured into petroleum ether. The precipitated α-

(4-cyanobiphenyloxy)-ω-bromoalkane is then filtered and recrystallised from ethanol to yield a white solid.

1-(4-cyanobiphenyloxy)-3-bromopropane (14a)

Yield 86%

^{1}H N.M.R. δ ($CDCl_3$) 2.35 (apparent p, Br-CH_2-$C\underline{H}_2$-CH_2-OAr, 2H), 3.65 (t, Br-$C\underline{H}_2$-R), 4.20 (t, ArO-$C\underline{H}_2$-Br), 7.02 (d, biphenyl 2-$\underline{H}$, 2H), 7.55 (d, biphenyl 3-$\underline{H}$, 2H), 7.67 (d, biphenyl 2'-$\underline{H}$, 2H), 7.72 (d, biphenyl 3'-$\underline{H}$, 2H) ppm.

^{13}C N.M.R. δ ($CDCl_3$) 30.1, 32.4, 65.6, 110.3, 115.3, 119.2, 127.2, 128.6, 131.8, 132.7, 145.4, 159.5 ppm.

1-(4-cyanobiphenyloxy)-4-bromobutane (14b)

Yield 82%

^{1}H N.M.R. δ ($CDCl_3$) 1.85 (d of t, Br-CH_2-$C\underline{H}_2$-R, 2H), 2.05 (d of t, ArO-CH_2-$C\underline{H}_2$-R, 2H), 3.45 (t, Br-$C\underline{H}_2$-R, 2H), 4.10 (t, ArO-$C\underline{H}_2$-R, 2H), 7.02 (d, biphenyl 2-$\underline{H}$, 2H), 7.55 (d, biphenyl 3-$\underline{H}$, 2H), 7.67 (d, biphenyl 2'-$\underline{H}$, 2H), 7.72 (d, biphenyl 3'-$\underline{H}$, 2H) ppm.

^{13}C N.M.R. δ ($CDCl_3$) 28.6, 30.1, 32.6, 67.3, 110.3, 115.3, 119.2, 127.2, 128.6, 131.8, 132.7, 145.4, 159.5 ppm.

1-(4-cyanobiphenyloxy)-5-bromopentane (14c)

Yield 72%

^{1}H N.M.R. δ ($CDCl_3$) 1.45 (m, methylene protons, 2H), 1.85 (d of t, Br-CH_2-$C\underline{H}_2$-R, 2H), 2.05 (d of t, ArO-CH_2-$C\underline{H}_2$-R, 2H), 3.45 (t, Br-$C\underline{H}_2$-R, 2H), 4.10 (t, ArO-$C\underline{H}_2$-R, 2H), 7.02 (d, biphenyl 2-$\underline{H}$, 2H), 7.55 (d, biphenyl 3-$\underline{H}$, 2H), 7.67 (d, biphenyl 2'-$\underline{H}$, 2H), 7.72 (d, biphenyl 3'-$\underline{H}$, 2H) ppm.

^{13}C N.M.R. δ ($CDCl_3$) 25.0, 28.6, 32.6, 33.8, 67.8, 110.3, 115.3, 119.2, 127.2, 128.6, 131.8, 132.7, 145.4, 159.5 ppm.

1-(4-cyanobiphenyloxy)-6-bromohexane (14d)

Yield 91%

^{1}H N.M.R. δ ($CDCl_3$) 1.2 – 1.5 (m, methylene protons, 4H), 1.85 (d of t, Br-CH_2-$C\underline{H}_2$-R, 2H), 2.05 (d of t, ArO-CH_2-$C\underline{H}_2$-R, 2H), 3.45 (t, Br-$C\underline{H}_2$-R, 2H), 4.10 (t,

ArO-C$\underline{H_2}$-R, 2H), 7.02 (d, biphenyl 2-$\underline{H}$, 2H), 7.55 (d, biphenyl 3-$\underline{H}$, 2H), 7.67 (d, biphenyl 2'-$\underline{H}$, 2H), 7.72 (d, biphenyl 3'-$\underline{H}$, 2H) ppm.

^{13}C N.M.R. δ ($CDCl_3$) 25.8, 28.4, 29.4, 32.9, 34.1, 68.2, 110.3, 115.3, 119.2, 127.2, 128.6, 131.8, 132.7, 145.4, 159.5 ppm.

1-(4-cyanobiphenyloxy)-7-bromoheptane (14e)

Yield 88%

^{1}H N.M.R. δ ($CDCl_3$) 1.2 – 1.5 (m, methylene protons, 6H), 1.85 (d of t, Br-CH_2-C$\underline{H_2}$-R, 2H), 2.05 (d of t, ArO-CH_2-C$\underline{H_2}$-R, 2H), 3.45 (t, Br-C$\underline{H_2}$-R, 2H), 4.10 (t, ArO-C$\underline{H_2}$-R, 2H), 7.02 (d, biphenyl 2-$\underline{H}$, 2H), 7.55 (d, biphenyl 3-$\underline{H}$, 2H), 7.67 (d, biphenyl 2'-$\underline{H}$, 2H), 7.72 (d, biphenyl 3'-$\underline{H}$, 2H) ppm.

^{13}C N.M.R. δ ($CDCl_3$) 26.1, 28.2, 28.7, 29.3, 32.9, 34.1, 68.1, 110.3, 115.3, 119.2, 127.2, 128.6, 131.8, 132.7, 145.4, 159.5 ppm.

1-(4-cyanobiphenyloxy)-8-bromooctane (14f)

Yield 89%

^{1}H N.M.R. δ ($CDCl_3$) 1.2 – 1.5 (m, methylene protons, 8H), 1.85 (d of t, Br-CH_2-C$\underline{H_2}$-R, 2H), 2.05 (d of t, ArO-CH_2-C$\underline{H_2}$-R, 2H), 3.45 (t, Br-C$\underline{H_2}$-R, 2H), 4.10 (t, ArO-C$\underline{H_2}$-R, 2H), 7.02 (d, biphenyl 2-$\underline{H}$, 2H), 7.55 (d, biphenyl 3-$\underline{H}$, 2H), 7.67 (d, biphenyl 2'-$\underline{H}$, 2H), 7.72 (d, biphenyl 3'-$\underline{H}$, 2H) ppm.

^{13}C N.M.R. δ ($CDCl_3$) 26.1, 28.2, 28.8, 29.3, 32.9, 34.1, 68.1110.3, 115.3, 119.2, 127.2, 128.6, 131.8, 132.7, 145.4, 159.5 ppm.

1-(4-cyanobiphenyloxy)-9-bromononane (14g)

Yield 80%

^{1}H N.M.R. δ ($CDCl_3$) 1.2 – 1.5 (m, methylene protons, 10H), 1.85 (d of t, Br-CH_2-C$\underline{H_2}$-R, 2H), 2.05 (d of t, ArO-CH_2-C$\underline{H_2}$-R, 2H), 3.45 (t, Br-C$\underline{H_2}$-R, 2H), 4.10 (t, ArO-C$\underline{H_2}$-R, 2H), 7.02 (d, biphenyl 2-$\underline{H}$, 2H), 7.55 (d, biphenyl 3-$\underline{H}$, 2H), 7.67 (d, biphenyl 2'-$\underline{H}$, 2H), 7.72 (d, biphenyl 3'-$\underline{H}$, 2H) ppm.

^{13}C N.M.R. δ ($CDCl_3$) 26.1, 28.3, 28.9, 29.5, 29.7, 30.0, 32.9, 34.2, 68.1, 110.3, 115.3, 119.2, 127.2, 128.6, 131.8, 132.7, 145.4, 159.5 ppm.

1-(4-cyanobiphenyloxy)-10-bromodecane (14h)

Yield 90%

^{1}H N.M.R. δ ($CDCl_3$) 1.2 – 1.5 (m, methylene protons, 12H), 1.85 (d of t, Br-CH_2-$C\underline{H_2}$-R, 2H), 2.05 (d of t, ArO-CH_2-$C\underline{H_2}$-R, 2H), 3.45 (t, Br-$C\underline{H_2}$-R, 2H), 4.10 (t, ArO-$C\underline{H_2}$-R, 2H), 7.02 (d, biphenyl 2-$\underline{H}$, 2H), 7.55 (d, biphenyl 3-$\underline{H}$, 2H), 7.67 (d, biphenyl 2'-$\underline{H}$, 2H), 7.72 (d, biphenyl 3'-$\underline{H}$, 2H) ppm.

^{13}C N.M.R. δ ($CDCl_3$) 26.1, 28.3, 28.9, 29.5, 29.7, 30.0, 32.9, 34.2, 68.1, 110.3, 115.3, 119.2, 127.2, 128.6, 131.8, 132.7, 145.4, 159.5 ppm.

1-(4-cyanobiphenyloxy)-11-bromoundecane (14i)

Yield 69%

^{1}H N.M.R. δ ($CDCl_3$) 1.2 – 1.5 (m, methylene protons, 14H), 1.85 (d of t, Br-CH_2-$C\underline{H_2}$-R, 2H), 2.05 (d of t, ArO-CH_2-$C\underline{H_2}$-R, 2H), 3.45 (t, Br-$C\underline{H_2}$-R, 2H), 4.10 (t, ArO-$C\underline{H_2}$-R, 2H), 7.02 (d, biphenyl 2-$\underline{H}$, 2H), 7.55 (d, biphenyl 3-$\underline{H}$, 2H), 7.67 (d, biphenyl 2'-$\underline{H}$, 2H), 7.72 (d, biphenyl 3'-$\underline{H}$, 2H) ppm.

^{13}C N.M.R. δ ($CDCl_3$) 26.1, 28.3, 28.9, 29.5, 29.7, 30.0, 32.9, 34.2, 68.1, 110.3, 115.3, 119.2, 127.2, 128.6, 131.8, 132.7, 145.4, 159.5 ppm.

1-(4-cyanobiphenyloxy)-12-bromododecane (14j)

Yield 65%

^{1}H N.M.R. δ ($CDCl_3$) 1.2 – 1.5 (m, methylene protons, 16H), 1.85 (d of t, Br-CH_2-$C\underline{H_2}$-R, 2H), 2.05 (d of t, ArO-CH_2-$C\underline{H_2}$-R, 2H), 3.45 (t, Br-$C\underline{H_2}$-R, 2H), 4.10 (t, ArO-$C\underline{H_2}$-R, 2H), 7.02 (d, biphenyl 2-$\underline{H}$, 2H), 7.55 (d, biphenyl 3-$\underline{H}$, 2H), 7.67 (d, biphenyl 2'-$\underline{H}$, 2H), 7.72 (d, biphenyl 3'-$\underline{H}$, 2H) ppm.

^{13}C N.M.R. δ ($CDCl_3$) 26.1, 28.3, 28.9, 29.5, 29.7, 30.0, 32.9, 34.2, 68.1, 110.3, 115.3, 119.2, 127.2, 128.6, 131.8, 132.7, 145.4, 159.5 ppm.

7.15 Synthesis of the α-(4-cyanobiphenyloxy)-ω-(2-cyanophenyloxy)alkanes (CBOnO2CP) (15)

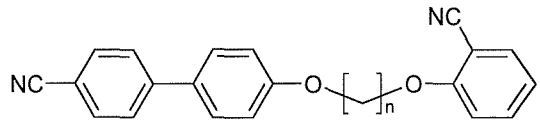

n = 3 to 12

2-cyanophenol (1mmol, 0.12g) and potassium carbonate (10mmol, 1.38g) in AnalaR acetone (50ml) are stirred at reflux in a quickfit conical flask fitted with reflux condenser and guard tube for 1 hour. After this time the α-(4-cyanobiphenyloxy)-ω-bromoalkane was added and the mixture stirred at reflux for 2 – 3 days. The mixture was then cooled and water (50ml) was added. This was then extracted with DCM (4 x 50ml), the organic extracts combined, dried over anhydrous magnesium sulphate and the solvent removed on the rotary evaporator. The crude product was then purified by column chromatography (Silica gel 60 / DCM) and recrystallised from a mixture of ethanol and toluene to afford a white solid.

1-(4-cyanobiphenyloxy)-3-(2-cyanophenyloxy)propane (CBO3O2CP) (15a)

Yield 12%

I.R. υ (Nujol) lack of OH peak @ ~3300 cm^{-1} indicates ether, 2225 (nitrile str) 830 (p-substituted benzene) 725 (o-substituted benzene) cm^{-1}.

^{1}H N.M.R. δ ($CDCl_3$) 2.35 (apparent p, Br-CH_2-$C\underline{H}_2$-CH_2-OAr, 2H), 3.65 (t, Br-$C\underline{H}_2$-R), 4.20 (t, ArO-$C\underline{H}_2$-Br), 7.02 (d, biphenyl 2-H, 2H), 7.55 (d, biphenyl 3-H, 2H), 7.67 (d, biphenyl 2'-H, 2H), 7.72 (d, biphenyl 3'-H, 2H), 7.54 (d, phenyl 3-H, 1H), 7.01 (d of d, phenyl 4-H, 1H), 7.46 (d of d, phenyl 5-H, 1H), 6.98 (d, phenyl 6-H, 1H) ppm.

^{13}C N.M.R. δ ($CDCl_3$) 29.5, 65.1, 66.1, 102.1, 112.3, 115.2, 120.7, 121.3, 127.2, 128.5, 132.6, 132.7, 133.9, 134.4, 145.1, 159.1, 161.0 ppm.

1-(4-cyanobiphenyloxy)-4-(2-cyanophenyloxy)butane (CBO4O2CP) (15b)

Yield 31%

I.R. υ (Nujol) lack of OH peak @ ~3300 cm^{-1} indicates ether, 2225 (nitrile str) 830 (p-substituted benzene) 725 (o-substituted benzene) cm^{-1}.

^1H N.M.R. δ ($CDCl_3$) 2.05 (d of t, 2 x ArO-CH_2-$C\underline{H}_2$-R, 4H), 4.10 (d of t, 2 x ArO-$C\underline{H}_2$-R, 4H), 7.02 (d, biphenyl 2-H, 2H), 7.55 (d, biphenyl 3-H, 2H), 7.67 (d, biphenyl 2'-H, 2H), 7.72 (d, biphenyl 3'-H, 2H), 7.54 (d, phenyl 3-H, 1H), 7.01 (d of d, phenyl 4-H, 1H), 7.46 (d of d, phenyl 5-H, 1H), 6.98 (d, phenyl 6-H, 1H) ppm.

^{13}C N.M.R. δ ($CDCl_3$) 26.0, 67.5, 68.5, 102.1, 112.3, 115.2, 120.7, 121.3, 127.2, 128.5, 132.6, 132.7, 133.9, 134.4, 145.1, 159.1, 161.0 ppm.

1-(4-cyanobiphenyloxy)-5-(2-cyanophenyloxy)pentane (CBO5O2CP) (15c)

Yield 58%

I.R. υ (Nujol) lack of OH peak @ ~3300 cm^{-1} indicates ether, 2225 (nitrile str) 830 (p-substituted benzene) 725 (o-substituted benzene) cm^{-1}.

^1H N.M.R. δ ($CDCl_3$) 1.45 (m, methylene protons, 2H), 2.05 (d of t, 2 x ArO-CH_2-$C\underline{H}_2$-R, 4H), 4.10 (d of t, 2 x ArO-$C\underline{H}_2$-R, 4H), 7.02 (d, biphenyl 2-H, 2H), 7.55 (d, biphenyl 3-H, 2H), 7.67 (d, biphenyl 2'-H, 2H), 7.72 (d, biphenyl 3'-H, 2H), 7.54 (d, phenyl 3-H, 1H), 7.01 (d of d, phenyl 4-H, 1H), 7.46 (d of d, phenyl 5-H, 1H), 6.98 (d, phenyl 6-H, 1H) ppm.

^{13}C N.M.R. δ ($CDCl_3$) 21.3, 29.3, 67.9, 68.9, 102.1, 112.3, 115.2, 120.7, 121.3, 127.2, 128.5, 132.6, 132.7, 133.9, 134.4, 145.1, 159.1, 161.0 ppm.

1-(4-cyanobiphenyloxy)-6-(2-cyanophenyloxy)hexane (CBO6O2CP) (15d)

Yield 63%

I.R. υ (Nujol) lack of OH peak @ ~3300 cm^{-1} indicates ether, 2225 (nitrile str) 830 (p-substituted benzene) 725 (o-substituted benzene) cm^{-1}.

^1H N.M.R. δ ($CDCl_3$) 1.2 – 1.5 (m, methylene protons, 4H), 2.05 (d of t, 2 x ArO-CH_2-$C\underline{H}_2$-R, 4H), 4.10 (d of t, 2 x ArO-$C\underline{H}_2$-R, 4H), 7.02 (d, biphenyl 2-H, 2H), 7.55 (d, biphenyl 3-H, 2H), 7.67 (d, biphenyl 2'-H, 2H), 7.72 (d, biphenyl 3'-H, 2H), 7.54 (d, phenyl 3-H, 1H), 7.01 (d of d, phenyl 4-H, 1H), 7.46 (d of d, phenyl 5-H, 1H), 6.98 (d, phenyl 6-H, 1H) ppm.

^{13}C N.M.R. δ ($CDCl_3$) 21.3, 29.6, 67.9, 68.9, 102.1, 112.3, 115.2, 120.7, 121.3, 127.2, 128.5, 132.6, 132.7, 133.9, 134.4, 145.1, 159.1, 161.0 ppm.

1-(4-cyanobiphenyloxy)-7-(2-cyanophenyloxy)heptane (CBO7O2CP) (15e)

Yield 43%

I.R. υ (Nujol) lack of OH peak @ ~3300 cm^{-1} indicates ether, 2225 (nitrile str) 830 (p-substituted benzene) 725 (o-substituted benzene) cm^{-1}.

^1H N.M.R. δ ($CDCl_3$) 1.2 – 1.5 (m, methylene protons, 6H), 2.05 (d of t, 2 x ArO-CH_2-$C\underline{H}_2$-R, 4H), 4.10 (d of t, 2 x ArO-$C\underline{H}_2$-R, 4H), 7.02 (d, biphenyl 2-H, 2H), 7.55 (d, biphenyl 3-H, 2H), 7.67 (d, biphenyl 2'-H, 2H), 7.72 (d, biphenyl 3'-H, 2H), 7.54 (d, phenyl 3-H, 1H), 7.01 (d of d, phenyl 4-H, 1H), 7.46 (d of d, phenyl 5-H, 1H), 6.98 (d, phenyl 6-H, 1H) ppm.

^{13}C N.M.R. δ ($CDCl_3$) 26.6, 29.4, 67.5, 68.5, 102.1, 112.3, 115.2, 120.7, 121.3, 127.2, 128.5, 132.6, 132.7, 133.9, 134.4, 145.1, 159.1, 161.0 ppm.

1-(4-cyanobiphenyloxy)-8-(2-cyanophenyloxy)octane (CBO8O2CP) (15f)

Yield 64%

I.R. υ (Nujol) lack of OH peak @ ~3300 cm^{-1} indicates ether, 2225 (nitrile str) 830 (p-substituted benzene) 725 (o-substituted benzene) cm^{-1}.

^1H N.M.R. δ ($CDCl_3$) 1.2 – 1.5 (m, methylene protons, 8H), 2.05 (d of t, 2 x ArO-CH_2-$C\underline{H}_2$-R, 4H), 4.10 (d of t, 2 x ArO-$C\underline{H}_2$-R, 4H), 7.02 (d, biphenyl 2-H, 2H), 7.55 (d, biphenyl 3-H, 2H), 7.67 (d, biphenyl 2'-H, 2H), 7.72 (d, biphenyl 3'-H, 2H), 7.54 (d, phenyl 3-H, 1H), 7.01 (d of d, phenyl 4-H, 1H), 7.46 (d of d, phenyl 5-H, 1H), 6.98 (d, phenyl 6-H, 1H) ppm.

^{13}C N.M.R. δ ($CDCl_3$) 26.6, 29.4, 67.5, 68.5, 102.1, 112.3, 115.2, 120.7, 121.3, 127.2, 128.5, 132.6, 132.7, 133.9, 134.4, 145.1, 159.1, 161.0 ppm.

1-(4-cyanobiphenyloxy)-9-(2-cyanophenyloxy)nonane (CBO9O2CP) (15g)

Yield 74%

I.R. υ (Nujol) lack of OH peak @ ~3300 cm^{-1} indicates ether, 2225 (nitrile str) 830 (p-substituted benzene) 725 (o-substituted benzene) cm^{-1}.

^1H N.M.R. δ ($CDCl_3$) 1.2 – 1.5 (m, methylene protons, 10H), 2.05 (d of t, 2 x ArO-CH_2-$C\underline{H}_2$-R, 4H), 4.10 (d of t, 2 x ArO-$C\underline{H}_2$-R, 4H), 7.02 (d, biphenyl 2-H, 2H),

7.55 (d, biphenyl 3-H, 2H), 7.67 (d, biphenyl 2'-H, 2H), 7.72 (d, biphenyl 3'-H, 2H), 7.54 (d, phenyl 3-H, 1H), 7.01 (d of d, phenyl 4-H, 1H), 7.46 (d of d, phenyl 5-H, 1H), 6.98 (d, phenyl 6-H, 1H) ppm.

^{13}C N.M.R. δ ($CDCl_3$) 26.6, 29.4, 67.5, 68.5, 102.1, 112.3, 115.2, 120.7, 121.3, 127.2, 128.5, 132.6, 132.7, 133.9, 134.4, 145.1, 159.1, 161.0 ppm.

1-(4-cyanobiphenyloxy)-10-(2-cyanophenyloxy)decane (CBO10O2CP) (15h)

Yield 41%

I.R. υ (Nujol) lack of OH peak @ ~3300 cm^{-1} indicates ether, 2225 (nitrile str) 830 (p-substituted benzene) 725 (o-substituted benzene) cm^{-1}.

^{1}H N.M.R. δ ($CDCl_3$) 1.2 – 1.5 (m, methylene protons, 12H), 2.05 (d of t, 2 x ArO-CH_2-CH_2-R, 4H), 4.10 (d of t, 2 x ArO-CH_2-R, 4H), 7.02 (d, biphenyl 2-H, 2H), 7.55 (d, biphenyl 3-H, 2H), 7.67 (d, biphenyl 2'-H, 2H), 7.72 (d, biphenyl 3'-H, 2H), 7.54 (d, phenyl 3-H, 1H), 7.01 (d of d, phenyl 4-H, 1H), 7.46 (d of d, phenyl 5-H, 1H), 6.98 (d, phenyl 6-H, 1H) ppm.

^{13}C N.M.R. δ ($CDCl_3$) 26.6, 29.4, 67.5, 68.5, 102.1, 112.3, 115.2, 120.7, 121.3, 127.2, 128.5, 132.6, 132.7, 133.9, 134.4, 145.1, 159.1, 161.0 ppm.

1-(4-cyanobiphenyloxy)-11-(2-cyanophenyloxy)undecane (CBO11O2CP) (15i)

Yield 67%

I.R. υ (Nujol) lack of OH peak @ ~3300 cm^{-1} indicates ether, 2225 (nitrile str) 830 (p-substituted benzene) 725 (o-substituted benzene) cm^{-1}.

^{1}H N.M.R. δ ($CDCl_3$) 1.2 – 1.5 (m, methylene protons, 14H), 2.05 (d of t, 2 x ArO-CH_2-CH_2-R, 4H), 4.10 (d of t, 2 x ArO-CH_2-R, 4H), 7.02 (d, biphenyl 2-H, 2H), 7.55 (d, biphenyl 3-H, 2H), 7.67 (d, biphenyl 2'-H, 2H), 7.72 (d, biphenyl 3'-H, 2H), 7.54 (d, phenyl 3-H, 1H), 7.01 (d of d, phenyl 4-H, 1H), 7.46 (d of d, phenyl 5-H, 1H), 6.98 (d, phenyl 6-H, 1H) ppm.

^{13}C N.M.R. δ ($CDCl_3$) 26.6, 29.4, 67.5, 68.5, 102.1, 112.3, 115.2, 120.7, 121.3, 127.2, 128.5, 132.6, 132.7, 133.9, 134.4, 145.1, 159.1, 161.0 ppm.

1-(4-cyanobiphenyloxy)-12-(2-cyanophenyloxy)dodecane (CBO12O2CP) (15j)

Yield 67%

I.R. υ (Nujol) lack of OH peak @ ~3300 cm^{-1} indicates ether, 2225 (nitrile str) 830 (p-substituted benzene) 725 (o-substituted benzene) cm^{-1}.

^{1}H N.M.R. δ ($CDCl_3$) 1.2 – 1.5 (m, methylene protons, 16H), 2.05 (d of t, 2 x ArO-CH_2-$C\underline{H}_2$-R, 4H), 4.10 (d of t, 2 x ArO-$C\underline{H}_2$-R, 4H), 7.02 (d, biphenyl 2-H, 2H), 7.55 (d, biphenyl 3-H, 2H), 7.67 (d, biphenyl 2'-H, 2H), 7.72 (d, biphenyl 3'-H, 2H), 7.54 (d, phenyl 3-H, 1H), 7.01 (d of d, phenyl 4-H, 1H), 7.46 (d of d, phenyl 5-H, 1H), 6.98 (d, phenyl 6-H, 1H) ppm.

^{13}C N.M.R. δ ($CDCl_3$) 26.6, 29.4, 67.5, 68.5, 102.1, 112.3, 115.2, 120.7, 121.3, 127.2, 128.5, 132.6, 132.7, 133.9, 134.4, 145.1, 159.1, 161.0 ppm.

7.16 Synthesis of the α-(4-cyanobiphenyloxy)-ω-(3-cyanophenyloxy)alkanes (CBOnO3CP) (16)

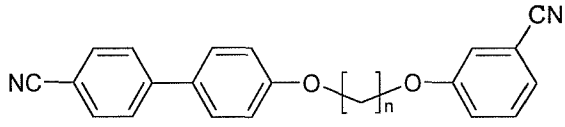

n = 3 to 12

3-cyanophenol (1mmol, 0.12g) and potassium carbonate (10mmol, 1.38g) in AnalaR acetone (50ml) are stirred at reflux in a quickfit conical flask fitted with reflux condenser and guard tube for 1 hour. After this time the α-(4-cyanobiphenyloxy)-ω-bromoalkane was added and the mixture stirred at reflux for 2 – 3 days. The mixture was then cooled and water (50ml) was added. This was then extracted with DCM (4 x 50ml), the organic extracts combined, dried over anhydrous magnesium sulphate and the solvent removed on the rotary evaporator. The crude product was then purified by column chromatography (Silica gel 60 / DCM) and recrystallised from a mixture of ethanol and toluene to afford a white solid.

1-(4-cyanobiphenyloxy)-3-(3-cyanophenyloxy)propane (CBO3O3CP) (16a)

Yield 80%

I.R. υ (Nujol) lack of OH peak @ ~3300 cm^{-1} indicates ether, 2225 (nitrile str) 830 (p-substituted benzene) 790, 710 (m-substituted benzene) cm^{-1}.

^1H N.M.R. δ ($CDCl_3$) 2.05 (d of t, ArO-CH_2-$C\underline{H}_2$-CH_2-OAr, 2H), 4.10 (d of t, 2 x ArO-$C\underline{H}_2$-R, 4H), 7.02 (d, biphenyl 2-H, 2H), 7.55 (d, biphenyl 3-H, 2H), 7.67 (d, biphenyl 2'-H, 2H), 7.72 (d, biphenyl 3'-H, 2H), 7.15 (s, phenyl 2-H, 1H), 7.23 (d, phenyl 4-H, 1H), 7.37 (apparent t, phenyl 5-H, 1H), 7.12 (d, phenyl 6-H, 1H) ppm.

^{13}C N.M.R. δ ($CDCl_3$) 29.5, 65.8, 66.1, 112.3, 113.7, 115.2, 117.5, 119.9, 121.3, 124.6, 127.2, 128.5, 130.5, 132.7, 133.9, 145.1, 159.1, 159.9 ppm.

1-(4-cyanobiphenyloxy)-4-(3-cyanophenyloxy)butane (CBO4O3CP) (16b)

Yield 52%

I.R. υ (Nujol) lack of OH peak @ ~3300 cm^{-1} indicates ether, 2225 (nitrile str) 830 (p-substituted benzene) 790, 710 (m-substituted benzene) cm^{-1}.

^1H N.M.R. δ ($CDCl_3$) 2.05 (d of t, 2 x ArO-CH_2-$C\underline{H}_2$-R, 4H), 4.10 (d of t, 2 x ArO-$C\underline{H}_2$-R, 4H), 7.02 (d, biphenyl 2-H, 2H), 7.55 (d, biphenyl 3-H, 2H), 7.67 (d, biphenyl 2'-H, 2H), 7.72 (d, biphenyl 3'-H, 2H), 7.15 (s, phenyl 2-H, 1H), 7.23 (d, phenyl 4-H, 1H), 7.37 (apparent t, phenyl 5-H, 1H), 7.12 (d, phenyl 6-H, 1H) ppm.

^{13}C N.M.R. δ ($CDCl_3$) 26.0, 68.2, 68.5, 112.3, 113.7, 115.2, 117.5, 119.9, 121.3, 124.6, 127.2, 128.5, 130.5, 132.7, 133.9, 145.1, 159.1, 159.9 ppm.

1-(4-cyanobiphenyloxy)-5-(3-cyanophenyloxy)pentane (CBO5O3CP) (16c)

Yield 49%

I.R. υ (Nujol) lack of OH peak @ ~3300 cm^{-1} indicates ether, 2225 (nitrile str) 830 (p-substituted benzene) 790, 710 (m-substituted benzene) cm^{-1}.

^1H N.M.R. δ ($CDCl_3$) 1.45 (m, methylene protons, 2H), 2.05 (d of t, 2 x ArO-CH_2-$C\underline{H}_2$-R, 4H), 4.10 (d of t, 2 x ArO-$C\underline{H}_2$-R, 4H), 7.02 (d, biphenyl 2-H, 2H), 7.55 (d, biphenyl 3-H, 2H), 7.67 (d, biphenyl 2'-H, 2H), 7.72 (d, biphenyl 3'-H, 2H), 7.15 (s, phenyl 2-H, 1H), 7.23 (d, phenyl 4-H, 1H), 7.37 (apparent t, phenyl 5-H, 1H), 7.12 (d, phenyl 6-H, 1H) ppm.

^{13}C N.M.R. δ ($CDCl_3$) 21.3, 29.3, 68.6, 68.9, 112.3, 113.7, 115.2, 117.5, 119.9, 121.3, 124.6, 127.2, 128.5, 130.5, 132.7, 133.9, 145.1, 159.1, 159.9 ppm.

1-(4-cyanobiphenyloxy)-6-(3-cyanophenyloxy)hexane (CBO6O3CP) (16d)

Yield 61%

I.R. υ (Nujol) lack of OH peak @ ~3300 cm^{-1} indicates ether, 2225 (nitrile str) 830 (p-substituted benzene) 790, 710 (m-substituted benzene) cm^{-1}.

^{1}H N.M.R. δ ($CDCl_3$) 1.2 – 1.5 (m, methylene protons, 4H), 2.05 (d of t, 2 x ArO-CH_2-C$\underline{H}_2$-R, 4H), 4.10 (d of t, 2 x ArO-C$\underline{H}_2$-R, 4H), 7.02 (d, biphenyl 2-$\underline{H}$, 2H), 7.55 (d, biphenyl 3-$\underline{H}$, 2H), 7.67 (d, biphenyl 2'-$\underline{H}$, 2H), 7.72 (d, biphenyl 3'-$\underline{H}$, 2H), 7.15 (s, phenyl 2-$\underline{H}$, 1H), 7.23 (d, phenyl 4-$\underline{H}$, 1H), 7.37 (apparent t, phenyl 5-$\underline{H}$, 1H), 7.12 (d, phenyl 6-$\underline{H}$, 1H) ppm.

^{13}C N.M.R. δ ($CDCl_3$) 21.3, 29.6, 68.6, 68.9, 112.3, 113.7, 115.2, 117.5, 119.9, 121.3, 124.6, 127.2, 128.5, 130.5, 132.7, 133.9, 145.1, 159.1, 159.9 ppm.

1-(4-cyanobiphenyloxy)-7-(3-cyanophenyloxy)heptane (CBO7O3CP) (16e)

Yield 31%

I.R. υ (Nujol) lack of OH peak @ ~3300 cm^{-1} indicates ether, 2225 (nitrile str) 830 (p-substituted benzene) 790, 710 (m-substituted benzene) cm^{-1}.

^{1}H N.M.R. δ ($CDCl_3$) 1.2 – 1.5 (m, methylene protons, 6H), 2.05 (d of t, 2 x ArO-CH_2-C$\underline{H}_2$-R, 4H), 4.10 (d of t, 2 x ArO-C$\underline{H}_2$-R, 4H), 7.02 (d, biphenyl 2-$\underline{H}$, 2H), 7.55 (d, biphenyl 3-$\underline{H}$, 2H), 7.67 (d, biphenyl 2'-$\underline{H}$, 2H), 7.72 (d, biphenyl 3'-$\underline{H}$, 2H), 7.15 (s, phenyl 2-$\underline{H}$, 1H), 7.23 (d, phenyl 4-$\underline{H}$, 1H), 7.37 (apparent t, phenyl 5-$\underline{H}$, 1H), 7.12 (d, phenyl 6-$\underline{H}$, 1H) ppm.

^{13}C N.M.R. δ ($CDCl_3$) 26.6, 29.4, 68.2, 68.5, 112.3, 113.7, 115.2, 117.5, 119.9, 121.3, 124.6, 127.2, 128.5, 130.5, 132.7, 133.9, 145.1, 159.1, 159.9 ppm.

1-(4-cyanobiphenyloxy)-8-(3-cyanophenyloxy)octane (CBO8O3CP) (16f)

Yield 64%

I.R. υ (Nujol) lack of OH peak @ ~3300 cm^{-1} indicates ether, 2225 (nitrile str) 830 (p-substituted benzene) 790, 710 (m-substituted benzene) cm^{-1}.

^{1}H N.M.R. δ ($CDCl_3$) 1.2 – 1.5 (m, methylene protons, 8H), 2.05 (d of t, 2 x ArO-CH_2-C$\underline{H}_2$-R, 4H), 4.10 (d of t, 2 x ArO-C$\underline{H}_2$-R, 4H), 7.02 (d, biphenyl 2-$\underline{H}$, 2H),

7.55 (d, biphenyl 3-H, 2H), 7.67 (d, biphenyl 2'-H, 2H), 7.72 (d, biphenyl 3'-H, 2H), 7.15 (s, phenyl 2-H, 1H), 7.23 (d, phenyl 4-H, 1H), 7.37 (apparent t, phenyl 5-H, 1H), 7.12 (d, phenyl 6-H, 1H) ppm.

^{13}C N.M.R. δ ($CDCl_3$) 26.6, 29.4, 68.2, 68.5, 112.3, 113.7, 115.2, 117.5, 119.9, 121.3, 124.6, 127.2, 128.5, 130.5, 132.7, 133.9, 145.1, 159.1, 159.9 ppm.

1-(4-cyanobiphenyloxy)-9-(3-cyanophenyloxy)nonane (CBO9O3CP) (16g)

Yield 71%

I.R. υ (Nujol) lack of OH peak @ ~3300 cm^{-1} indicates ether, 2225 (nitrile str) 830 (p-substituted benzene) 790, 710 (m-substituted benzene) cm^{-1}.

^{1}H N.M.R. δ ($CDCl_3$) 1.2 – 1.5 (m, methylene protons, 10H), 2.05 (d of t, 2 x ArO-CH_2-CH_2-R, 4H), 4.10 (d of t, 2 x ArO-CH_2-R, 4H), 7.02 (d, biphenyl 2-H, 2H), 7.55 (d, biphenyl 3-H, 2H), 7.67 (d, biphenyl 2'-H, 2H), 7.72 (d, biphenyl 3'-H, 2H), 7.15 (s, phenyl 2-H, 1H), 7.23 (d, phenyl 4-H, 1H), 7.37 (apparent t, phenyl 5-H, 1H), 7.12 (d, phenyl 6-H, 1H) ppm.

^{13}C N.M.R. δ ($CDCl_3$) 26.6, 29.4, 68.2, 68.5, 112.3, 113.7, 115.2, 117.5, 119.9, 121.3, 124.6, 127.2, 128.5, 130.5, 132.7, 133.9, 145.1, 159.1, 159.9 ppm.

1-(4-cyanobiphenyloxy)-10-(3-cyanophenyloxy)decane (CBO10O3CP) (16h)

Yield 67%

I.R. υ (Nujol) lack of OH peak @ ~3300 cm^{-1} indicates ether, 2225 (nitrile str) 830 (p-substituted benzene) 790, 710 (m-substituted benzene) cm^{-1}.

^{1}H N.M.R. δ ($CDCl_3$) 1.2 – 1.5 (m, methylene protons, 12H), 2.05 (d of t, 2 x ArO-CH_2-CH_2-R, 4H), 4.10 (d of t, 2 x ArO-CH_2-R, 4H), 7.02 (d, biphenyl 2-H, 2H), 7.55 (d, biphenyl 3-H, 2H), 7.67 (d, biphenyl 2'-H, 2H), 7.72 (d, biphenyl 3'-H, 2H), 7.15 (s, phenyl 2-H, 1H), 7.23 (d, phenyl 4-H, 1H), 7.37 (apparent t, phenyl 5-H, 1H), 7.12 (d, phenyl 6-H, 1H) ppm.

^{13}C N.M.R. δ ($CDCl_3$) 26.6, 29.4, 68.2, 68.5, 112.3, 113.7, 115.2, 117.5, 119.9, 121.3, 124.6, 127.2, 128.5, 130.5, 132.7, 133.9, 145.1, 159.1, 159.9 ppm.

1-(4-cyanobiphenyloxy)-11-(3-cyanophenyloxy)undecane (CBO11O3CP) (16i)

Yield 60%

I.R. υ (Nujol) lack of OH peak @ ~3300 cm^{-1} indicates ether, 2225 (nitrile str) 830 (p-substituted benzene) 790, 710 (m-substituted benzene) cm^{-1}.

^1H N.M.R. δ ($CDCl_3$) 1.2 – 1.5 (m, methylene protons, 14H), 2.05 (d of t, 2 x ArO-CH_2-$C\underline{H}_2$-R, 4H), 4.10 (d of t, 2 x ArO-$C\underline{H}_2$-R, 4H), 7.02 (d, biphenyl 2-H, 2H), 7.55 (d, biphenyl 3-H, 2H), 7.67 (d, biphenyl 2'-H, 2H), 7.72 (d, biphenyl 3'-H, 2H), 7.15 (s, phenyl 2-H, 1H), 7.23 (d, phenyl 4-H, 1H), 7.37 (apparent t, phenyl 5-H, 1H), 7.12 (d, phenyl 6-H, 1H) ppm.

^{13}C N.M.R. δ ($CDCl_3$) 26.6, 29.4, 68.2, 68.5, 112.3, 113.7, 115.2, 117.5, 119.9, 121.3, 124.6, 127.2, 128.5, 130.5, 132.7, 133.9, 145.1, 159.1, 159.9 ppm.

1-(4-cyanobiphenyloxy)-12-(3-cyanophenyloxy)dodecane (CBO12O3CP) (16j)

Yield 52%

I.R. υ (Nujol) lack of OH peak @ ~3300 cm^{-1} indicates ether, 2225 (nitrile str) 830 (p-substituted benzene) 790, 710 (m-substituted benzene) cm^{-1}.

^1H N.M.R. δ ($CDCl_3$) 1.2 – 1.5 (m, methylene protons, 16H), 2.05 (d of t, 2 x ArO-CH_2-$C\underline{H}_2$-R, 4H), 4.10 (d of t, 2 x ArO-$C\underline{H}_2$-R, 4H), 7.02 (d, biphenyl 2-H, 2H), 7.55 (d, biphenyl 3-H, 2H), 7.67 (d, biphenyl 2'-H, 2H), 7.72 (d, biphenyl 3'-H, 2H), 7.15 (s, phenyl 2-H, 1H), 7.23 (d, phenyl 4-H, 1H), 7.37 (apparent t, phenyl 5-H, 1H), 7.12 (d, phenyl 6-H, 1H) ppm.

^{13}C N.M.R. δ ($CDCl_3$) 26.6, 29.4, 68.2, 68.5, 112.3, 113.7, 115.2, 117.5, 119.9, 121.3, 124.6, 127.2, 128.5, 130.5, 132.7, 133.9, 145.1, 159.1, 159.9 ppm.

7.17 Synthesis of α-bromo-ω-(4-bromobiphenyl-4'-yloxy)alkanes (17)

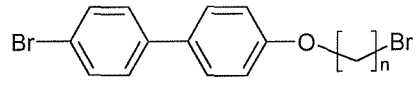

n = 3 to 12

Carried out according to the method outlined by Crivello *et al.* [4]. 4-bromo-4'-hyroxybiphenyl (10mmol, 2.49g) and potassium carbonate (0.1mol, 13.4g) in AnalaR acetone (100ml) are stirred at reflux in a quickfit conical flask fitted with

reflux condenser and guard tube for 1 hour. After this time the α,ω-dibromoalkane was added and the mixture stirred at reflux for 2 – 3 days. The mixture was then cooled and water (200ml) was added. This was then extracted with DCM (4 x 50ml), the organic extracts combined, dried over anhydrous magnesium sulphate and the solvent removed on the rotary evaporator to yield a crude mix of the required product and excess α,ω-dibromoalkane. The excess α,ω-dibromoalkane was then removed under vacuum on the Kugelrohr and the crude product remaining was poured into petroleum ether. The precipitated α-bromo-ω-(4-bromobiphenyl-4'-yloxy)alkane is then filtered and recrystallised from ethanol to yield a white solid.

1-bromo-3-(4-bromobiphenyl-4'-yloxy)propane (17a)

Yield 67%

^{1}H N.M.R. δ ($CDCl_3$) 2.35 (apparent p, Br-CH_2-$C\underline{H_2}$-CH_2-OAr, 2H), 3.65 (t, Br-$C\underline{H_2}$-R), 4.20 (t, ArO-$C\underline{H_2}$-Br), 6.96 (d, biphenyl 2-$\underline{H}$, 2H), 7.44 (d, biphenyl 2'-$\underline{H}$, 2H), 7.50 (d, biphenyl 3-$\underline{H}$, 2H), 7.55 (d, biphenyl 3'-$\underline{H}$, 2H) ppm.

^{13}C N.M.R. δ ($CDCl_3$) 30.1, 32.4, 65.6, 115.0, 120.8, 128.1, 128.4, 131.9, 132.4, 139.9, 159.1 ppm.

1-bromo-4-(4-bromobiphenyl-4'-yloxy)butane (17b)

Yield 72%

^{1}H N.M.R. δ ($CDCl_3$) 1.85 (d of t, Br-CH_2-$C\underline{H_2}$-R, 2H), 2.05 (d of t, ArO-CH_2-$C\underline{H_2}$-R, 2H), 3.45 (t, Br-$C\underline{H_2}$-R, 2H), 4.10 (t, ArO-$C\underline{H_2}$-R, 2H), 6.96 (d, biphenyl 2-$\underline{H}$, 2H), 7.44 (d, biphenyl 2'-$\underline{H}$, 2H), 7.50 (d, biphenyl 3-$\underline{H}$, 2H), 7.55 (d, biphenyl 3'-$\underline{H}$, 2H) ppm.

^{13}C N.M.R. δ ($CDCl_3$) 28.6, 30.1, 32.6, 67.3, 115.0, 120.8, 128.1, 128.4, 131.9, 132.4, 139.9, 159.1 ppm.

1-bromo-5-(4-bromobiphenyl-4'-yloxy)pentane (17c)

Yield 63%

^{1}H N.M.R. δ ($CDCl_3$) 1.45 (m, methylene protons, 2H), 1.85 (d of t, Br-CH_2-$C\underline{H_2}$-R, 2H), 2.05 (d of t, ArO-CH_2-$C\underline{H_2}$-R, 2H), 3.45 (t, Br-$C\underline{H_2}$-R, 2H), 4.10 (t, ArO-

$C\underline{H_2}$-R, 2H), 6.96 (d, biphenyl 2-H, 2H), 7.44 (d, biphenyl 2'-H, 2H), 7.50 (d, biphenyl 3-H, 2H), 7.55 (d, biphenyl 3'-H, 2H) ppm.

^{13}C N.M.R. δ ($CDCl_3$) 25.0, 28.6, 32.6, 33.8, 67.8, 115.0, 120.8, 128.1, 128.4, 131.9, 132.4, 139.9, 159.1 ppm.

1-bromo-6-(4-bromobiphenyl-4'-yloxy)hexane (17d)

Yield 88%

^1H N.M.R. δ ($CDCl_3$) 1.2 – 1.5 (m, methylene protons, 4H), 1.85 (d of t, Br-CH_2-$C\underline{H_2}$-R, 2H), 2.05 (d of t, ArO-CH_2-$C\underline{H_2}$-R, 2H), 3.45 (t, Br-$C\underline{H_2}$-R, 2H), 4.10 (t, ArO-$C\underline{H_2}$-R, 2H), 6.96 (d, biphenyl 2-H, 2H), 7.44 (d, biphenyl 2'-H, 2H), 7.50 (d, biphenyl 3-H, 2H), 7.55 (d, biphenyl 3'-H, 2H) ppm.

^{13}C N.M.R. δ ($CDCl_3$) 25.8, 28.4, 29.4, 32.9, 34.1, 68.2, 115.0, 120.8, 128.1, 128.4, 131.9, 132.4, 139.9, 159.1 ppm.

1-bromo-7-(4-bromobiphenyl-4'-yloxy)heptane (17e)

Yield 85%

^1H N.M.R. δ ($CDCl_3$) 1.2 – 1.5 (m, methylene protons, 6H), 1.85 (d of t, Br-CH_2-$C\underline{H_2}$-R, 2H), 2.05 (d of t, ArO-CH_2-$C\underline{H_2}$-R, 2H), 3.45 (t, Br-$C\underline{H_2}$-R, 2H), 4.10 (t, ArO-$C\underline{H_2}$-R, 2H), 6.96 (d, biphenyl 2-H, 2H), 7.44 (d, biphenyl 2'-H, 2H), 7.50 (d, biphenyl 3-H, 2H), 7.55 (d, biphenyl 3'-H, 2H) ppm.

^{13}C N.M.R. δ ($CDCl_3$) 26.1, 28.2, 28.7, 29.3, 32.9, 34.1, 68.1, 115.0, 120.8, 128.1, 128.4, 131.9, 132.4, 139.9, 159.1 ppm.

1-bromo-8-(4-bromobiphenyl-4'-yloxy)octane (17f)

Yield 81%

^1H N.M.R. δ ($CDCl_3$) 1.2 – 1.5 (m, methylene protons, 8H), 1.85 (d of t, Br-CH_2-$C\underline{H_2}$-R, 2H), 2.05 (d of t, ArO-CH_2-$C\underline{H_2}$-R, 2H), 3.45 (t, Br-$C\underline{H_2}$-R, 2H), 4.10 (t, ArO-$C\underline{H_2}$-R, 2H), 6.96 (d, biphenyl 2-H, 2H), 7.44 (d, biphenyl 2'-H, 2H), 7.50 (d, biphenyl 3-H, 2H), 7.55 (d, biphenyl 3'-H, 2H) ppm.

^{13}C N.M.R. δ ($CDCl_3$) 26.1, 28.2, 28.8, 29.3, 32.9, 34.1, 68.1, 115.0, 120.8, 128.1, 128.4, 131.9, 132.4, 139.9, 159.1 ppm.

1-bromo-9-(4-bromobiphenyl-4'-yloxy)nonane (17g)

Yield 82%

^{1}H N.M.R. δ ($CDCl_3$) 1.2 – 1.5 (m, methylene protons, 10H), 1.85 (d of t, Br-CH_2-$C\underline{H_2}$-R, 2H), 2.05 (d of t, ArO-CH_2-$C\underline{H_2}$-R, 2H), 3.45 (t, Br-$C\underline{H_2}$-R, 2H), 4.10 (t, ArO-$C\underline{H_2}$-R, 2H), 6.96 (d, biphenyl 2-$\underline{H}$, 2H), 7.44 (d, biphenyl 2'-$\underline{H}$, 2H), 7.50 (d, biphenyl 3-$\underline{H}$, 2H), 7.55 (d, biphenyl 3'-$\underline{H}$, 2H) ppm.

^{13}C N.M.R. δ ($CDCl_3$) 26.1, 28.3, 28.9, 29.5, 29.7, 30.0, 32.9, 34.2, 68.1, 115.0, 120.8, 128.1, 128.4, 131.9, 132.4, 139.9, 159.1 ppm.

1-bromo-10-(4-bromobiphenyl-4'-yloxy)decane (17h)

Yield 70%

^{1}H N.M.R. δ ($CDCl_3$) 1.2 – 1.5 (m, methylene protons, 12H), 1.85 (d of t, Br-CH_2-$C\underline{H_2}$-R, 2H), 2.05 (d of t, ArO-CH_2-$C\underline{H_2}$-R, 2H), 3.45 (t, Br-$C\underline{H_2}$-R, 2H), 4.10 (t, ArO-$C\underline{H_2}$-R, 2H), 6.96 (d, biphenyl 2-$\underline{H}$, 2H), 7.44 (d, biphenyl 2'-$\underline{H}$, 2H), 7.50 (d, biphenyl 3-$\underline{H}$, 2H), 7.55 (d, biphenyl 3'-$\underline{H}$, 2H) ppm.

^{13}C N.M.R. δ ($CDCl_3$) 26.1, 28.3, 28.9, 29.5, 29.7, 30.0, 32.9, 34.2, 68.1, 115.0, 120.8, 128.1, 128.4, 131.9, 132.4, 139.9, 159.1 ppm.

1-bromo-11-(4-bromobiphenyl-4'-yloxy)undecane (17i)

Yield 73%

^{1}H N.M.R. δ ($CDCl_3$) 1.2 – 1.5 (m, methylene protons, 14H), 1.85 (d of t, Br-CH_2-$C\underline{H_2}$-R, 2H), 2.05 (d of t, ArO-CH_2-$C\underline{H_2}$-R, 2H), 3.45 (t, Br-$C\underline{H_2}$-R, 2H), 4.10 (t, ArO-$C\underline{H_2}$-R, 2H), 6.96 (d, biphenyl 2-$\underline{H}$, 2H), 7.44 (d, biphenyl 2'-$\underline{H}$, 2H), 7.50 (d, biphenyl 3-$\underline{H}$, 2H), 7.55 (d, biphenyl 3'-$\underline{H}$, 2H) ppm.

^{13}C N.M.R. δ ($CDCl_3$) 26.1, 28.3, 28.9, 29.5, 29.7, 30.0, 32.9, 34.2, 68.1, 115.0, 120.8, 128.1, 128.4, 131.9, 132.4, 139.9, 159.1 ppm.

1-bromo-12-(4-bromobiphenyl-4'-yloxy)dodecane (17j)

Yield 81%

^{1}H N.M.R. δ ($CDCl_3$) 1.2 – 1.5 (m, methylene protons, 16H), 1.85 (d of t, Br-CH_2-$C\underline{H_2}$-R, 2H), 2.05 (d of t, ArO-CH_2-$C\underline{H_2}$-R, 2H), 3.45 (t, Br-$C\underline{H_2}$-R, 2H), 4.10 (t, ArO-$C\underline{H_2}$-R, 2H), 6.96 (d, biphenyl 2-$\underline{H}$, 2H), 7.44 (d, biphenyl 2'-$\underline{H}$, 2H), 7.50 (d, biphenyl 3-$\underline{H}$, 2H), 7.55 (d, biphenyl 3'-$\underline{H}$, 2H) ppm.

^{13}C N.M.R. δ ($CDCl_3$) 26.1, 28.3, 28.9, 29.5, 29.7, 30.0, 32.9, 34.2, 68.1, 115.0, 120.8, 128.1, 128.4, 131.9, 132.4, 139.9, 159.1 ppm.

7.18 Synthesis of α-bromo-ω-(4-cyanoterphenyl-4''-yloxy)alkanes (18)

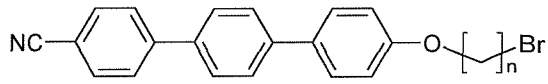

n = 3 to 12

Carried out according to the method outline by Suzuki *et al.* [3]. The α-bromo-ω-(4-bromobiphenyl-4'-yloxy)alkane (5mmol) and 4-benzonitrile boronic acid (**8**) (7.5mmol, 1.1g) were dissolved in freshly distilled DME (20ml) in a two-necked round bottomed flask, fitted with a reflux condenser, and stirred under nitrogen. 2M sodium carbonate solution (10ml) was added followed by a catalytic amount of tetrakis(triphenylphosphine) palladium (0) (50mg). This was then heated under reflux for 2 - 3 days. After the reaction was complete the aqueous layer was separated and extracted with DCM (4 x 50ml). The organic extracts were then combined, dried over anhydrous magnesium sulphate and the solvent removed on a rotary evaporator. The crude solid was then purified by column chromatography (Silica gel 60 / DCM) and recrystallised from a mixture of ethanol and toluene to yield a white fluffy solid.

1-bromo-3-(4-cyanoterphenyl-4''-yloxy)propane (18a)

Yield 61%

^{1}H N.M.R. δ ($CDCl_3$) 2.35 (apparent p, Br-CH_2-$C\underline{H_2}$-CH_2-OAr, 2H), 3.65 (t, Br-$C\underline{H_2}$-R), 4.20 (t, ArO-$C\underline{H_2}$-Br), 7.01 (d, terphenyl 2-$\underline{H}$, 2H), 7.58 (d, terphenyl 3-$\underline{H}$, 2H), 7.67 (apparent s, terphenyl 2'-$\underline{H}$ & 3'-$\underline{H}$, 4H), 7.75 (apparent s, terphenyl 2''-$\underline{H}$ & 3''-$\underline{H}$, 4H) ppm.

^{13}C N.M.R. δ ($CDCl_3$) 30.1, 32.4, 65.6, 110.9, 115.1, 119.1, 127.4, 127.6, 127.7, 128.3, 132.7, 141.3, 145.2, 145.3 ppm.

1-bromo-4-(4-cyanoterphenyl-4''-yloxy)butane (18b)

Yield 67%

^{1}H N.M.R. δ ($CDCl_3$) 1.85 (d of t, Br-CH_2-$C\underline{H}_2$-R, 2H), 2.05 (d of t, ArO-CH_2-$C\underline{H}_2$-R, 2H), 3.45 (t, Br-$C\underline{H}_2$-R, 2H), 4.10 (t, ArO-$C\underline{H}_2$-R, 2H), 7.01 (d, terphenyl 2-H, 2H), 7.58 (d, terphenyl 3-H, 2H), 7.67 (apparent s, terphenyl 2'-H & 3'-H, 4H), 7.75 (apparent s, terphenyl 2''-H & 3''-H, 4H) ppm.

^{13}C N.M.R. δ ($CDCl_3$) 28.6, 30.1, 32.6, 67.3, 110.9, 115.1, 119.1, 127.4, 127.6, 127.7, 128.3, 132.7, 141.3, 145.2, 145.3 ppm.

1-bromo-5-(4-cyanoterphenyl-4''-yloxy)pentane (18c)

Yield 55%

^{1}H N.M.R. δ ($CDCl_3$) 1.45 (m, methylene protons, 2H), 1.85 (d of t, Br-CH_2-$C\underline{H}_2$-R, 2H), 2.05 (d of t, ArO-CH_2-$C\underline{H}_2$-R, 2H), 3.45 (t, Br-$C\underline{H}_2$-R, 2H), 4.10 (t, ArO-$C\underline{H}_2$-R, 2H), 7.01 (d, terphenyl 2-H, 2H), 7.58 (d, terphenyl 3-H, 2H), 7.67 (apparent s, terphenyl 2'-H & 3'-H, 4H), 7.75 (apparent s, terphenyl 2''-H & 3''-H, 4H) ppm.

^{13}C N.M.R. δ ($CDCl_3$) 25.0, 28.6, 32.6, 33.8, 67.8, 110.9, 115.1, 119.1, 127.4, 127.6, 127.7, 128.3, 132.7, 141.3, 145.2, 145.3 ppm.

1-bromo-6-(4-cyanoterphenyl-4''-yloxy)hexane (18d)

Yield 61%

^{1}H N.M.R. δ ($CDCl_3$) 1.2 – 1.5 (m, methylene protons, 4H), 1.85 (d of t, Br-CH_2-$C\underline{H}_2$-R, 2H), 2.05 (d of t, ArO-CH_2-$C\underline{H}_2$-R, 2H), 3.45 (t, Br-$C\underline{H}_2$-R, 2H), 4.10 (t, ArO-$C\underline{H}_2$-R, 2H), 7.01 (d, terphenyl 2-H, 2H), 7.58 (d, terphenyl 3-H, 2H), 7.67 (apparent s, terphenyl 2'-H & 3'-H, 4H), 7.75 (apparent s, terphenyl 2''-H & 3''-H, 4H) ppm.

^{13}C N.M.R. δ ($CDCl_3$) 25.8, 28.4, 29.4, 32.9, 34.1, 68.2, 110.9, 115.1, 119.1, 127.4, 127.6, 127.7, 128.3, 132.7, 141.3, 145.2, 145.3 ppm.

1-bromo-7-(4-cyanoterphenyl-4''-yloxy)heptane (18e)

Yield 61%

^{1}H N.M.R. δ ($CDCl_3$) 1.2 – 1.5 (m, methylene protons, 6H), 1.85 (d of t, Br-CH_2-$C\underline{H}_2$-R, 2H), 2.05 (d of t, ArO-CH_2-$C\underline{H}_2$-R, 2H), 3.45 (t, Br-$C\underline{H}_2$-R, 2H), 4.10 (t,

ArO-C$\underline{H_2}$-R, 2H), 7.01 (d, terphenyl 2-$\underline{H}$, 2H), 7.58 (d, terphenyl 3-$\underline{H}$, 2H), 7.67 (apparent s, terphenyl 2'-$\underline{H}$ & 3'-$\underline{H}$, 4H), 7.75 (apparent s, terphenyl 2''-$\underline{H}$ & 3''-$\underline{H}$, 4H) ppm.

^{13}C N.M.R. δ ($CDCl_3$) 26.1, 28.2, 28.7, 29.3, 32.9, 34.1, 68.1, 110.9, 115.1, 119.1, 127.4, 127.6, 127.7, 128.3, 132.7, 141.3, 145.2, 145.3 ppm.

1-bromo-8-(4-cyanoterphenyl-4''-yloxy)octane (18f)

Yield 62%

^{1}H N.M.R. δ ($CDCl_3$) 1.2 – 1.5 (m, methylene protons, 8H), 1.85 (d of t, Br-CH_2-C$\underline{H_2}$-R, 2H), 2.05 (d of t, ArO-CH_2-C$\underline{H_2}$-R, 2H), 3.45 (t, Br-C$\underline{H_2}$-R, 2H), 4.10 (t, ArO-C$\underline{H_2}$-R, 2H), 7.01 (d, terphenyl 2-$\underline{H}$, 2H), 7.58 (d, terphenyl 3-$\underline{H}$, 2H), 7.67 (apparent s, terphenyl 2'-$\underline{H}$ & 3'-$\underline{H}$, 4H), 7.75 (apparent s, terphenyl 2''-$\underline{H}$ & 3''-$\underline{H}$, 4H) ppm.

^{13}C N.M.R. δ ($CDCl_3$) 26.1, 28.2, 28.8, 29.3, 32.9, 34.1, 68.1, 110.9, 115.1, 119.1, 127.4, 127.6, 127.7, 128.3, 132.7, 141.3, 145.2, 145.3 ppm.

1-bromo-9-(4-cyanoterphenyl-4''-yloxy)nonane (18g)

Yield 53%

^{1}H N.M.R. δ ($CDCl_3$) 1.2 – 1.5 (m, methylene protons, 10H), 1.85 (d of t, Br-CH_2-C$\underline{H_2}$-R, 2H), 2.05 (d of t, ArO-CH_2-C$\underline{H_2}$-R, 2H), 3.45 (t, Br-C$\underline{H_2}$-R, 2H), 4.10 (t, ArO-C$\underline{H_2}$-R, 2H), 7.01 (d, terphenyl 2-$\underline{H}$, 2H), 7.58 (d, terphenyl 3-$\underline{H}$, 2H), 7.67 (apparent s, terphenyl 2'-$\underline{H}$ & 3'-$\underline{H}$, 4H), 7.75 (apparent s, terphenyl 2''-$\underline{H}$ & 3''-$\underline{H}$, 4H) ppm.

^{13}C N.M.R. δ ($CDCl_3$) 26.1, 28.3, 28.9, 29.5, 29.7, 30.0, 32.9, 34.2, 68.1, 110.9, 115.1, 119.1, 127.4, 127.6, 127.7, 128.3, 132.7, 141.3, 145.2, 145.3 ppm.

1-bromo-10-(4-cyanoterphenyl-4''-yloxy)decane (18h)

Yield 57%

^{1}H N.M.R. δ ($CDCl_3$) 1.2 – 1.5 (m, methylene protons, 12H), 1.85 (d of t, Br-CH_2-C$\underline{H_2}$-R, 2H), 2.05 (d of t, ArO-CH_2-C$\underline{H_2}$-R, 2H), 3.45 (t, Br-C$\underline{H_2}$-R, 2H), 4.10 (t, ArO-C$\underline{H_2}$-R, 2H), 7.01 (d, terphenyl 2-$\underline{H}$, 2H), 7.58 (d, terphenyl 3-$\underline{H}$, 2H), 7.67 (apparent s, terphenyl 2'-$\underline{H}$ & 3'-$\underline{H}$, 4H), 7.75 (apparent s, terphenyl 2''-$\underline{H}$ & 3''-$\underline{H}$, 4H) ppm.

^{13}C N.M.R. δ ($CDCl_3$) 26.1, 28.3, 28.9, 29.5, 29.7, 30.0, 32.9, 34.2, 68.1, 110.9, 115.1, 119.1, 127.4, 127.6, 127.7, 128.3, 132.7, 141.3, 145.2, 145.3 ppm.

1-bromo-11-(4-cyanoterphenyl-4''-yloxy)undecane (18i)

Yield 58%

^{1}H N.M.R. δ ($CDCl_3$) 1.2 – 1.5 (m, methylene protons, 14H), 1.85 (d of t, Br-CH_2-$C\underline{H_2}$-R, 2H), 2.05 (d of t, ArO-CH_2-$C\underline{H_2}$-R, 2H), 3.45 (t, Br-$C\underline{H_2}$-R, 2H), 4.10 (t, ArO-$C\underline{H_2}$-R, 2H), 7.01 (d, terphenyl 2-H, 2H), 7.58 (d, terphenyl 3-H, 2H), 7.67 (apparent s, terphenyl 2'-H & 3'-H, 4H), 7.75 (apparent s, terphenyl 2''-H & 3''-H, 4H) ppm.

^{13}C N.M.R. δ ($CDCl_3$) 26.1, 28.3, 28.9, 29.5, 29.7, 30.0, 32.9, 34.2, 68.1, 110.9, 115.1, 119.1, 127.4, 127.6, 127.7, 128.3, 132.7, 141.3, 145.2, 145.3 ppm.

1-bromo-12-(4-cyanoterphenyl-4''-yloxy)dodecane (18j)

Yield 62%

^{1}H N.M.R. δ ($CDCl_3$) 1.2 – 1.5 (m, methylene protons, 16H), 1.85 (d of t, Br-CH_2-$C\underline{H_2}$-R, 2H), 2.05 (d of t, ArO-CH_2-$C\underline{H_2}$-R, 2H), 3.45 (t, Br-$C\underline{H_2}$-R, 2H), 4.10 (t, ArO-$C\underline{H_2}$-R, 2H), 7.01 (d, terphenyl 2-H, 2H), 7.58 (d, terphenyl 3-H, 2H), 7.67 (apparent s, terphenyl 2'-H & 3'-H, 4H), 7.75 (apparent s, terphenyl 2''-H & 3''-H, 4H) ppm.

^{13}C N.M.R. δ ($CDCl_3$) 26.1, 28.3, 28.9, 29.5, 29.7, 30.0, 32.9, 34.2, 68.1, 110.9, 115.1, 119.1, 127.4, 127.6, 127.7, 128.3, 132.7, 141.3, 145.2, 145.3 ppm.

7.19 Synthesis of the α-(4-cyanoterphenyloxy)-ω-(2-cyanophenyloxy)alkanes (CTOnO2CP) (19)

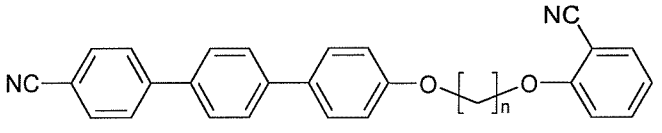

n = 3 to 12

2-cyanophenol (1mmol, 0.12g) and potassium carbonate (10mmol, 1.38g) in AnalaR acetone (50ml) are stirred at reflux in a quickfit conical flask fitted with

reflux condenser and guard tube for 1 hour. After this time the α-(4-cyanoterphenyloxy)-ω-bromoalkane was added and the mixture stirred at reflux for 2 – 3 days. The mixture was then cooled and water (50ml) was added. This was then extracted with DCM (4 x 50ml), the organic extracts combined, dried over anhydrous magnesium sulphate and the solvent removed on the rotary evaporator. The crude product was then purified by column chromatography (Silica gel 60 / DCM) and recrystallised from a mixture of ethanol and toluene to afford a white solid.

1-(4-cyanobterphenyloxy)-3-(2-cyanophenyloxy)propane (CTO3O2CP) (19a)

Yield 53%

I.R. υ (Nujol) lack of OH peak @ ~3300 cm^{-1} indicates ether, 2225 (nitrile str) 830 (p-substituted benzene) 725 (o-substituted benzene) cm^{-1}.

^{1}H N.M.R. δ ($CDCl_3$) 2.05 (d of t, ArO-CH_2-$C\underline{H}_2$-CH_2-OAr, 2H), 4.10 (d of t, 2 x ArO-$C\underline{H}_2$-R, 4H), 7.01 (d, terphenyl 2-H, 2H), 7.58 (d, terphenyl 3-H, 2H), 7.67 (apparent s, terphenyl 2'-H & 3'-H, 4H), 7.75 (apparent s, terphenyl 2''-H & 3''-H, 4H), 7.54 (d, phenyl 3-H, 1H), 7.01 (d of d, phenyl 4-H, 1H), 7.46 (d of d, phenyl 5-H, 1H), 6.98 (d, phenyl 6-H, 1H) ppm.

^{13}C N.M.R. δ ($CDCl_3$) 29.5, 65.1, 66.1, 102.1, 111.1, 114.9, 115.2, 120.7, 127.3, 127.5, 127.6, 128.1, 132.4, 132.6, 134.4, 141.2, 145.8, 159.1, 161.0 ppm.

1-(4-cyanoterphenyloxy)-4-(2-cyanophenyloxy)butane (CTO4O2CP) (19b)

Yield 75%

I.R. υ (Nujol) lack of OH peak @ ~3300 cm^{-1} indicates ether, 2225 (nitrile str) 830 (p-substituted benzene) 725 (o-substituted benzene) cm^{-1}.

^{1}H N.M.R. δ ($CDCl_3$) 2.05 (d of t, 2 x ArO-CH_2-$C\underline{H}_2$-R, 4H), 4.10 (d of t, 2 x ArO-$C\underline{H}_2$-R, 4H), 7.01 (d, terphenyl 2-H, 2H), 7.58 (d, terphenyl 3-H, 2H), 7.67 (apparent s, terphenyl 2'-H & 3'-H, 4H), 7.75 (apparent s, terphenyl 2''-H & 3''-H, 4H), 7.54 (d, phenyl 3-H, 1H), 7.01 (d of d, phenyl 4-H, 1H), 7.46 (d of d, phenyl 5-H, 1H), 6.98 (d, phenyl 6-H, 1H) ppm.

^{13}C N.M.R. δ ($CDCl_3$) 26.0, 67.5, 68.5, 102.1, 111.1, 114.9, 115.2, 120.7, 127.3, 127.5, 127.6, 128.1, 132.4, 132.6, 134.4, 141.2, 145.8, 159.1, 161.0 ppm.

1-(4-cyanoterphenyloxy)-5-(2-cyanophenyloxy)pentane (CTO5O2CP) (19c)

Yield 90%

I.R. υ (Nujol) lack of OH peak @ ~3300 cm^{-1} indicates ether, 2225 (nitrile str) 830 (p-substituted benzene) 725 (o-substituted benzene) cm^{-1}.

^{1}H N.M.R. δ ($CDCl_3$) 1.45 (m, methylene protons, 2H), 2.05 (d of t, 2 x ArO-CH_2-$C\underline{H}_2$-R, 4H), 4.10 (d of t, 2 x ArO-$C\underline{H}_2$-R, 4H), 7.01 (d, terphenyl 2-H, 2H), 7.58 (d, terphenyl 3-H, 2H), 7.67 (apparent s, terphenyl 2'-H & 3'-H, 4H), 7.75 (apparent s, terphenyl 2''-H & 3''-H, 4H), 7.54 (d, phenyl 3-H, 1H), 7.01 (d of d, phenyl 4-H, 1H), 7.46 (d of d, phenyl 5-H, 1H), 6.98 (d, phenyl 6-H, 1H) ppm.

^{13}C N.M.R. δ ($CDCl_3$) 21.3, 29.3, 67.9, 68.9, 102.1, 111.1, 114.9, 115.2, 120.7, 127.3, 127.5, 127.6, 128.1, 132.4, 132.6, 134.4, 141.2, 145.8, 159.1, 161.0 ppm.

1-(4-cyanoterphenyloxy)-6-(2-cyanophenyloxy)hexane (CTO6O2CP) (19d)

Yield 26%

I.R. υ (Nujol) lack of OH peak @ ~3300 cm^{-1} indicates ether, 2225 (nitrile str) 830 (p-substituted benzene) 725 (o-substituted benzene) cm^{-1}.

^{1}H N.M.R. δ ($CDCl_3$) 1.2 – 1.5 (m, methylene protons, 4H), 2.05 (d of t, 2 x ArO-CH_2-$C\underline{H}_2$-R, 4H), 4.10 (d of t, 2 x ArO-$C\underline{H}_2$-R, 4H), 7.01 (d, terphenyl 2-H, 2H), 7.58 (d, terphenyl 3-H, 2H), 7.67 (apparent s, terphenyl 2'-H & 3'-H, 4H), 7.75 (apparent s, terphenyl 2''-H & 3''-H, 4H), 7.54 (d, phenyl 3-H, 1H), 7.01 (d of d, phenyl 4-H, 1H), 7.46 (d of d, phenyl 5-H, 1H), 6.98 (d, phenyl 6-H, 1H) ppm.

^{13}C N.M.R. δ ($CDCl_3$) 21.3, 29.6, 67.9, 68.9, 102.1, 111.1, 114.9, 115.2, 120.7, 127.3, 127.5, 127.6, 128.1, 132.4, 132.6, 134.4, 141.2, 145.8, 159.1, 161.0 ppm.

1-(4-cyanoterphenyloxy)-7-(2-cyanophenyloxy)heptane (CTO7O2CP) (19e)

Yield 29%

I.R. υ (Nujol) lack of OH peak @ ~3300 cm^{-1} indicates ether, 2225 (nitrile str) 830 (p-substituted benzene) 725 (o-substituted benzene) cm^{-1}.

^{1}H N.M.R. δ ($CDCl_3$) 1.2 – 1.5 (m, methylene protons, 6H), 2.05 (d of t, 2 x ArO-CH_2-$C\underline{H}_2$-R, 4H), 4.10 (d of t, 2 x ArO-$C\underline{H}_2$-R, 4H), 7.01 (d, terphenyl 2-H, 2H), 7.58 (d, terphenyl 3-H, 2H), 7.67 (apparent s, terphenyl 2'-H & 3'-H, 4H), 7.75 (apparent s, terphenyl 2''-H & 3''-H, 4H), 7.54 (d, phenyl 3-H, 1H), 7.01 (d of d, phenyl 4-H, 1H), 7.46 (d of d, phenyl 5-H, 1H), 6.98 (d, phenyl 6-H, 1H) ppm.

^{13}C N.M.R. δ ($CDCl_3$) 26.6, 29.4, 67.5, 68.5, 102.1, 111.1, 114.9, 115.2, 120.7, 127.3, 127.5, 127.6, 128.1, 132.4, 132.6, 134.4, 141.2, 145.8, 159.1, 161.0 ppm.

1-(4-cyanoterphenyloxy)-8-(2-cyanophenyloxy)octane (CTO8O2CP) (19f)

Yield 52%

I.R. υ (Nujol) lack of OH peak @ ~3300 cm^{-1} indicates ether, 2225 (nitrile str) 830 (p-substituted benzene) 725 (o-substituted benzene) cm^{-1}.

^{1}H N.M.R. δ ($CDCl_3$) 1.2 – 1.5 (m, methylene protons, 8H), 2.05 (d of t, 2 x ArO-CH_2-C$\underline{H}_2$-R, 4H), 4.10 (d of t, 2 x ArO-C$\underline{H}_2$-R, 4H), 7.01 (d, terphenyl 2-$\underline{H}$, 2H), 7.58 (d, terphenyl 3-$\underline{H}$, 2H), 7.67 (apparent s, terphenyl 2'-$\underline{H}$ & 3'-$\underline{H}$, 4H), 7.75 (apparent s, terphenyl 2''-$\underline{H}$ & 3''-$\underline{H}$, 4H), 7.54 (d, phenyl 3-$\underline{H}$, 1H), 7.01 (d of d, phenyl 4-$\underline{H}$, 1H), 7.46 (d of d, phenyl 5-$\underline{H}$, 1H), 6.98 (d, phenyl 6-$\underline{H}$, 1H) ppm.

^{13}C N.M.R. δ ($CDCl_3$) 26.6, 29.4, 67.5, 68.5, 102.1, 111.1, 114.9, 115.2, 120.7, 127.3, 127.5, 127.6, 128.1, 132.4, 132.6, 134.4, 141.2, 145.8, 159.1, 161.0 ppm.

1-(4-cyanoterphenyloxy)-9-(2-cyanophenyloxy)nonane (CTO9O2CP) (19g)

Yield 85%

I.R. υ (Nujol) lack of OH peak @ ~3300 cm^{-1} indicates ether, 2225 (nitrile str) 830 (p-substituted benzene) 725 (o-substituted benzene) cm^{-1}.

^{1}H N.M.R. δ ($CDCl_3$) 1.2 – 1.5 (m, methylene protons, 10H), 2.05 (d of t, 2 x ArO-CH_2-C$\underline{H}_2$-R, 4H), 4.10 (d of t, 2 x ArO-C$\underline{H}_2$-R, 4H), 7.01 (d, terphenyl 2-$\underline{H}$, 2H), 7.58 (d, terphenyl 3-$\underline{H}$, 2H), 7.67 (apparent s, terphenyl 2'-$\underline{H}$ & 3'-$\underline{H}$, 4H), 7.75 (apparent s, terphenyl 2''-$\underline{H}$ & 3''-$\underline{H}$, 4H), 7.54 (d, phenyl 3-$\underline{H}$, 1H), 7.01 (d of d, phenyl 4-$\underline{H}$, 1H), 7.46 (d of d, phenyl 5-$\underline{H}$, 1H), 6.98 (d, phenyl 6-$\underline{H}$, 1H) ppm.

^{13}C N.M.R. δ ($CDCl_3$) 26.6, 29.4, 67.5, 68.5, 102.1, 111.1, 114.9, 115.2, 120.7, 127.3, 127.5, 127.6, 128.1, 132.4, 132.6, 134.4, 141.2, 145.8, 159.1, 161.0 ppm.

1-(4-cyanoterphenyloxy)-10-(2-cyanophenyloxy)decane (CTO10O2CP) (19h)

Yield 86%

I.R. υ (Nujol) lack of OH peak @ ~3300 cm^{-1} indicates ether, 2225 (nitrile str) 830 (p-substituted benzene) 725 (o-substituted benzene) cm^{-1}.

^{1}H N.M.R. δ ($CDCl_3$) 1.2 – 1.5 (m, methylene protons, 12H), 2.05 (d of t, 2 x ArO-CH_2-C$\underline{H}_2$-R, 4H), 4.10 (d of t, 2 x ArO-C$\underline{H}_2$-R, 4H), 7.01 (d, terphenyl 2-$\underline{H}$, 2H),

7.58 (d, terphenyl 3-H, 2H), 7.67 (apparent s, terphenyl 2'-H & 3'-H, 4H), 7.75 (apparent s, terphenyl 2''-H & 3''-H, 4H), 7.54 (d, phenyl 3-H, 1H), 7.01 (d of d, phenyl 4-H, 1H), 7.46 (d of d, phenyl 5-H, 1H), 6.98 (d, phenyl 6-H, 1H) ppm.
^{13}C N.M.R. δ ($CDCl_3$) 26.6, 29.4, 67.5, 68.5, 102.1, 111.1, 114.9, 115.2, 120.7, 127.3, 127.5, 127.6, 128.1, 132.4, 132.6, 134.4, 141.2, 145.8, 159.1, 161.0 ppm.

1-(4-cyanoterphenyloxy)-11-(2-cyanophenyloxy)undecane (CTO11O2CP)(19i)
Yield 84%
I.R. υ (Nujol) lack of OH peak @ ~3300 cm^{-1} indicates ether, 2225 (nitrile str) 830 (p-substituted benzene) 725 (o-substituted benzene) cm^{-1}.
^{1}H N.M.R. δ ($CDCl_3$) 1.2 – 1.5 (m, methylene protons, 14H), 2.05 (d of t, 2 x ArO-CH_2-CH_2-R, 4H), 4.10 (d of t, 2 x ArO-CH_2-R, 4H), 7.01 (d, terphenyl 2-H, 2H), 7.58 (d, terphenyl 3-H, 2H), 7.67 (apparent s, terphenyl 2'-H & 3'-H, 4H), 7.75 (apparent s, terphenyl 2''-H & 3''-H, 4H), 7.54 (d, phenyl 3-H, 1H), 7.01 (d of d, phenyl 4-H, 1H), 7.46 (d of d, phenyl 5-H, 1H), 6.98 (d, phenyl 6-H, 1H) ppm.
^{13}C N.M.R. δ ($CDCl_3$) 26.6, 29.4, 67.5, 68.5, 102.1, 111.1, 114.9, 115.2, 120.7, 127.3, 127.5, 127.6, 128.1, 132.4, 132.6, 134.4, 141.2, 145.8, 159.1, 161.0 ppm.

1-(4-cyanoterphenyloxy)-12-(2-cyanophenyloxy)dodecane (CTO12O2CP)(19j)
Yield 55%
I.R. υ (Nujol) lack of OH peak @ ~3300 cm^{-1} indicates ether, 2225 (nitrile str) 830 (p-substituted benzene) 725 (o-substituted benzene) cm^{-1}.
^{1}H N.M.R. δ ($CDCl_3$) 1.2 – 1.5 (m, methylene protons, 16H), 2.05 (d of t, 2 x ArO-CH_2-CH_2-R, 4H), 4.10 (d of t, 2 x ArO-CH_2-R, 4H), 7.01 (d, terphenyl 2-H, 2H), 7.58 (d, terphenyl 3-H, 2H), 7.67 (apparent s, terphenyl 2'-H & 3'-H, 4H), 7.75 (apparent s, terphenyl 2''-H & 3''-H, 4H), 7.54 (d, phenyl 3-H, 1H), 7.01 (d of d, phenyl 4-H, 1H), 7.46 (d of d, phenyl 5-H, 1H), 6.98 (d, phenyl 6-H, 1H) ppm.
^{13}C N.M.R. δ ($CDCl_3$) 26.6, 29.4, 67.5, 68.5, 102.1, 111.1, 114.9, 115.2, 120.7, 127.3, 127.5, 127.6, 128.1, 132.4, 132.6, 134.4, 141.2, 145.8, 159.1, 161.0 ppm.

7.20 Synthesis of the α-(4-cyanoterphenyloxy)-ω-(3-cyanophenyloxy)alkanes (CTOnO3CP) (20)

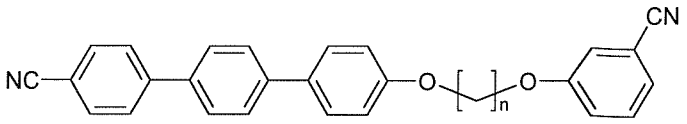

n = 3 to 12

3-cyanophenol (1mmol, 0.12g) and potassium carbonate (10mmol, 1.38g) in AnalaR acetone (50ml) are stirred at reflux in a quickfit conical flask fitted with reflux condenser and guard tube for 1 hour. After this time the α-(4-cyanoterphenyloxy)-ω-bromoalkane was added and the mixture stirred at reflux for 2 – 3 days. The mixture was then cooled and water (50ml) was added. This was then extracted with DCM (4 x 50ml), the organic extracts combined, dried over anhydrous magnesium sulphate and the solvent removed on the rotary evaporator. The crude product was then purified by column chromatography (Silica gel 60 / DCM) and recrystallised from a mixture of ethanol and toluene to afford a white solid.

1-(4-cyanobterphenyloxy)-3-(3-cyanophenyloxy)propane (CTO3O3CP) (20a)

Yield 80%

I.R. υ (Nujol) lack of OH peak @ ~3300 cm^{-1} indicates ether, 2225 (nitrile str) 830 (p-substituted benzene) 790, 710 (m-substituted benzene) cm^{-1}.

^{1}H N.M.R. δ ($CDCl_3$) 2.05 (d of t, ArO-CH_2-$C\underline{H}_2$-CH_2-OAr, 2H), 4.10 (d of t, 2 x ArO-$C\underline{H}_2$-R, 4H), 7.01 (d, terphenyl 2-H, 2H), 7.58 (d, terphenyl 3-H, 2H), 7.67 (apparent s, terphenyl 2'-H & 3'-H, 4H), 7.75 (apparent s, terphenyl 2''-H & 3''-H, 4H), 7.15 (s, phenyl 2-H, 1H), 7.23 (d, phenyl 4-H, 1H), 7.37 (apparent t, phenyl 5-H, 1H), 7.12 (d, phenyl 6-H, 1H) ppm.

^{13}C N.M.R. δ ($CDCl_3$) 29.5, 65.8, 66.1, 111.1, 113.1, 114.9, 117.3, 119.8, 124.3, 127.3, 127.5, 127.6, 128.1, 130.3, 132.4, 132.6, 141.2, 145.8, 159.1, 159.6 ppm.

1-(4-cyanoterphenyloxy)-4-(3-cyanophenyloxy)butane (CTO4O3CP) (20b)

Yield 75%

I.R. υ (Nujol) lack of OH peak @ ~3300 cm^{-1} indicates ether, 2225 (nitrile str) 830 (p-substituted benzene) 790, 710 (m-substituted benzene) cm^{-1}.

^1H N.M.R. δ ($CDCl_3$) 2.05 (d of t, 2 x ArO-CH_2-$C\underline{H}_2$-R, 4H), 4.10 (d of t, 2 x ArO-$C\underline{H}_2$-R, 4H), 7.01 (d, terphenyl 2-H, 2H), 7.58 (d, terphenyl 3-H, 2H), 7.67 (apparent s, terphenyl 2'-H & 3'-H, 4H), 7.75 (apparent s, terphenyl 2''-H & 3''-H, 4H), 7.15 (s, phenyl 2-H, 1H), 7.23 (d, phenyl 4-H, 1H), 7.37 (apparent t, phenyl 5-H, 1H), 7.12 (d, phenyl 6-H, 1H) ppm.

^{13}C N.M.R. δ ($CDCl_3$) 26.0, 68.2, 68.5, 111.1, 113.1, 114.9, 117.3, 119.8, 124.3, 127.3, 127.5, 127.6, 128.1, 130.3, 132.4, 132.6, 141.2, 145.8, 159.1, 159.6 ppm.

1-(4-cyanoterphenyloxy)-5-(3-cyanophenyloxy)pentane (CTO5O3CP) (20c)

Yield 87%

I.R. υ (Nujol) lack of OH peak @ ~3300 cm^{-1} indicates ether, 2225 (nitrile str) 830 (p-substituted benzene) 790, 710 (m-substituted benzene) cm^{-1}.

^1H N.M.R. δ ($CDCl_3$) 1.45 (m, methylene protons, 2H), 2.05 (d of t, 2 x ArO-CH_2-$C\underline{H}_2$-R, 4H), 4.10 (d of t, 2 x ArO-$C\underline{H}_2$-R, 4H), 7.01 (d, terphenyl 2-H, 2H), 7.58 (d, terphenyl 3-H, 2H), 7.67 (apparent s, terphenyl 2'-H & 3'-H, 4H), 7.75 (apparent s, terphenyl 2''-H & 3''-H, 4H), 7.15 (s, phenyl 2-H, 1H), 7.23 (d, phenyl 4-H, 1H), 7.37 (apparent t, phenyl 5-H, 1H), 7.12 (d, phenyl 6-H, 1H) ppm.

^{13}C N.M.R. δ ($CDCl_3$) 21.3, 29.3, 68.6, 68.9, 111.1, 113.1, 114.9, 117.3, 119.8, 124.3, 127.3, 127.5, 127.6, 128.1, 130.3, 132.4, 132.6, 141.2, 145.8, 159.1, 159.6 ppm.

1-(4-cyanoterphenyloxy)-6-(3-cyanophenyloxy)hexane (CTO6O3CP) (20d)

Yield 35%

I.R. υ (Nujol) lack of OH peak @ ~3300 cm^{-1} indicates ether, 2225 (nitrile str) 830 (p-substituted benzene) 790, 710 (m-substituted benzene) cm^{-1}.

^1H N.M.R. δ ($CDCl_3$) 1.2 – 1.5 (m, methylene protons, 4H), 2.05 (d of t, 2 x ArO-CH_2-$C\underline{H}_2$-R, 4H), 4.10 (d of t, 2 x ArO-$C\underline{H}_2$-R, 4H), 7.01 (d, terphenyl 2-H, 2H), 7.58 (d, terphenyl 3-H, 2H), 7.67 (apparent s, terphenyl 2'-H & 3'-H, 4H), 7.75

(apparent s, terphenyl 2''-H & 3''-H, 4H), 7.15 (s, phenyl 2-H, 1H), 7.23 (d, phenyl 4-H, 1H), 7.37 (apparent t, phenyl 5-H, 1H), 7.12 (d, phenyl 6-H, 1H) ppm.
^{13}C N.M.R. δ ($CDCl_3$) 21.3, 29.6, 68.6, 68.9, 111.1, 113.1, 114.9, 117.3, 119.8, 124.3, 127.3, 127.5, 127.6, 128.1, 130.3, 132.4, 132.6, 141.2, 145.8, 159.1, 159.6 ppm.

1-(4-cyanoterphenyloxy)-7-(3-cyanophenyloxy)heptane (CTO7O3CP) (20e)
Yield 26%
I.R. υ (Nujol) lack of OH peak @ ~3300 cm^{-1} indicates ether, 2225 (nitrile str) 830 (p-substituted benzene) 790, 710 (m-substituted benzene) cm^{-1}.
^{1}H N.M.R. δ ($CDCl_3$) 1.2 – 1.5 (m, methylene protons, 6H), 2.05 (d of t, 2 x ArO-CH_2-CH_2-R, 4H), 4.10 (d of t, 2 x ArO-CH_2-R, 4H), 7.01 (d, terphenyl 2-H, 2H), 7.58 (d, terphenyl 3-H, 2H), 7.67 (apparent s, terphenyl 2'-H & 3'-H, 4H), 7.75 (apparent s, terphenyl 2''-H & 3''-H, 4H), 7.15 (s, phenyl 2-H, 1H), 7.23 (d, phenyl 4-H, 1H), 7.37 (apparent t, phenyl 5-H, 1H), 7.12 (d, phenyl 6-H, 1H) ppm.
^{13}C N.M.R. δ ($CDCl_3$) 26.6, 29.4, 68.2, 68.5, 111.1, 113.1, 114.9, 117.3, 119.8, 124.3, 127.3, 127.5, 127.6, 128.1, 130.3, 132.4, 132.6, 141.2, 145.8, 159.1, 159.6 ppm.

1-(4-cyanoterphenyloxy)-8-(3-cyanophenyloxy)octane (CTO8O3CP) (20f)
Yield 64%
I.R. υ (Nujol) lack of OH peak @ ~3300 cm^{-1} indicates ether, 2225 (nitrile str) 830 (p-substituted benzene) 790, 710 (m-substituted benzene) cm^{-1}.
^{1}H N.M.R. δ ($CDCl_3$) 1.2 – 1.5 (m, methylene protons, 8H), 2.05 (d of t, 2 x ArO-CH_2-CH_2-R, 4H), 4.10 (d of t, 2 x ArO-CH_2-R, 4H), 7.01 (d, terphenyl 2-H, 2H), 7.58 (d, terphenyl 3-H, 2H), 7.67 (apparent s, terphenyl 2'-H & 3'-H, 4H), 7.75 (apparent s, terphenyl 2''-H & 3''-H, 4H), 7.15 (s, phenyl 2-H, 1H), 7.23 (d, phenyl 4-H, 1H), 7.37 (apparent t, phenyl 5-H, 1H), 7.12 (d, phenyl 6-H, 1H) ppm.
^{13}C N.M.R. δ ($CDCl_3$) 26.6, 29.4, 68.2, 68.5, 111.1, 113.1, 114.9, 117.3, 119.8, 124.3, 127.3, 127.5, 127.6, 128.1, 130.3, 132.4, 132.6, 141.2, 145.8, 159.1, 159.6 ppm.

1-(4-cyanoterphenyloxy)-9-(3-cyanophenyloxy)nonane (CTO9O3CP) (20g)

Yield 88%

I.R. υ (Nujol) lack of OH peak @ ~3300 cm^{-1} indicates ether, 2225 (nitrile str) 830 (p-substituted benzene) 790, 710 (m-substituted benzene) cm^{-1}.

^{1}H N.M.R. δ ($CDCl_3$) 1.2 – 1.5 (m, methylene protons, 10H), 2.05 (d of t, 2 x ArO-CH_2-$C\underline{H}_2$-R, 4H), 4.10 (d of t, 2 x ArO-$C\underline{H}_2$-R, 4H), 7.01 (d, terphenyl 2-H, 2H), 7.58 (d, terphenyl 3-H, 2H), 7.67 (apparent s, terphenyl 2'-H & 3'-H, 4H), 7.75 (apparent s, terphenyl 2''-H & 3''-H, 4H), 7.15 (s, phenyl 2-H, 1H), 7.23 (d, phenyl 4-H, 1H), 7.37 (apparent t, phenyl 5-H, 1H), 7.12 (d, phenyl 6-H, 1H) ppm.

^{13}C N.M.R. δ ($CDCl_3$) 26.6, 29.4, 68.2, 68.5, 111.1, 113.1, 114.9, 117.3, 119.8, 124.3, 127.3, 127.5, 127.6, 128.1, 130.3, 132.4, 132.6, 141.2, 145.8, 159.1, 159.6 ppm.

1-(4-cyanoterphenyloxy)-10-(3-cyanophenyloxy)decane (CTO10O3CP) (20h)

Yield 86%

I.R. υ (Nujol) lack of OH peak @ ~3300 cm^{-1} indicates ether, 2225 (nitrile str) 830 (p-substituted benzene) 790, 710 (m-substituted benzene) cm^{-1}.

^{1}H N.M.R. δ ($CDCl_3$) 1.2 – 1.5 (m, methylene protons, 12H), 2.05 (d of t, 2 x ArO-CH_2-$C\underline{H}_2$-R, 4H), 4.10 (d of t, 2 x ArO-$C\underline{H}_2$-R, 4H), 7.01 (d, terphenyl 2-H, 2H), 7.58 (d, terphenyl 3-H, 2H), 7.67 (apparent s, terphenyl 2'-H & 3'-H, 4H), 7.75 (apparent s, terphenyl 2''-H & 3''-H, 4H), 7.15 (s, phenyl 2-H, 1H), 7.23 (d, phenyl 4-H, 1H), 7.37 (apparent t, phenyl 5-H, 1H), 7.12 (d, phenyl 6-H, 1H) ppm.

^{13}C N.M.R. δ ($CDCl_3$) 26.6, 29.4, 68.2, 68.5, 111.1, 113.1, 114.9, 117.3, 119.8, 124.3, 127.3, 127.5, 127.6, 128.1, 130.3, 132.4, 132.6, 141.2, 145.8, 159.1, 159.6 ppm.

1-(4-cyanoterphenyloxy)-11-(3-cyanophenyloxy)undecane (CTO11O3CP)(20i)

Yield 20%

I.R. υ (Nujol) lack of OH peak @ ~3300 cm^{-1} indicates ether, 2225 (nitrile str) 830 (p-substituted benzene) 790, 710 (m-substituted benzene) cm^{-1}.

^{1}H N.M.R. δ ($CDCl_3$) 1.2 – 1.5 (m, methylene protons, 14H), 2.05 (d of t, 2 x ArO-CH_2-$C\underline{H}_2$-R, 4H), 4.10 (d of t, 2 x ArO-$C\underline{H}_2$-R, 4H), 7.01 (d, terphenyl 2-H, 2H), 7.58 (d, terphenyl 3-H, 2H), 7.67 (apparent s, terphenyl 2'-H & 3'-H, 4H), 7.75

(apparent s, terphenyl 2''-H & 3''-H, 4H), 7.15 (s, phenyl 2-H, 1H), 7.23 (d, phenyl 4-H, 1H), 7.37 (apparent t, phenyl 5-H, 1H), 7.12 (d, phenyl 6-H, 1H) ppm. ^{13}C N.M.R. δ ($CDCl_3$) 26.6, 29.4, 68.2, 68.5, 111.1, 113.1, 114.9, 117.3, 119.8, 124.3, 127.3, 127.5, 127.6, 128.1, 130.3, 132.4, 132.6, 141.2, 145.8, 159.1, 159.6 ppm.

1-(4-cyanoterphenyloxy)-12-(3-cyanophenyloxy)dodecane (CTO12O3CP)(20j)

Yield 56%

I.R. υ (Nujol) lack of OH peak @ ~3300 cm^{-1} indicates ether, 2225 (nitrile str) 830 (p-substituted benzene) 790, 710 (m-substituted benzene) cm^{-1}.

^{1}H N.M.R. δ ($CDCl_3$) 1.2 – 1.5 (m, methylene protons, 16H), 2.05 (d of t, 2 x ArO-CH_2-CH_2-R, 4H), 4.10 (d of t, 2 x ArO-CH_2-R, 4H), 7.01 (d, terphenyl 2-H, 2H), 7.58 (d, terphenyl 3-H, 2H), 7.67 (apparent s, terphenyl 2'-H & 3'-H, 4H), 7.75 (apparent s, terphenyl 2''-H & 3''-H, 4H), 7.15 (s, phenyl 2-H, 1H), 7.23 (d, phenyl 4-H, 1H), 7.37 (apparent t, phenyl 5-H, 1H), 7.12 (d, phenyl 6-H, 1H) ppm. ^{13}C N.M.R. δ ($CDCl_3$) 26.6, 29.4, 68.2, 68.5, 111.1, 113.1, 114.9, 117.3, 119.8, 124.3, 127.3, 127.5, 127.6, 128.1, 130.3, 132.4, 132.6, 141.2, 145.8, 159.1, 159.6 ppm.

7.21 Synthesis of the α-(pentabromophenyloxy)-ω-bromoalkane (21)

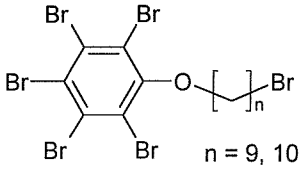

The reaction was carried out according to the method outlined by Praefcke *et al.* [1]. Pentabromophenol (50mmol, 24.42g) was dissolved in dry DMF (100ml). This was then added to a stirred solution of sodium hydride (60mmol, 1.44g) in dry DMF (20ml) in a round bottomed flask fitted with reflux condenser and guard tube. The mixture was stirred at room temperature for 1 hour. The α,ω-dibromoalkane (0.5mol) was then added and the mixture was heated at 80^{O}C for 26 hours. After cooling water (100ml) was added and the resulting slurry was extracted with either ether or DCM (4 x 50ml) depending upon the solubility of the

product. These organic extracts were combined and washed with water (2 x 50ml), dilute sodium hydroxide solution (50ml) and diluted sodium chloride solution (4 x 50ml). The organic extracts were then dried over anhydrous magnesium sulphate. The solvent was then removed on the rotary evaporator and the excess α,ω-dibromoalkane was removed on the rotary evaporator. The product was then recrystallised from acetone to yield a white solid.

1-(pentabromophenyloxy)-9-bromononane (21a)

Yield 52%

I.R. υ (Nujol) lack of OH peak @ ~3300 cm^{-1} indicates ether, 725 (substituted benzene) cm^{-1}.

^{1}H N.M.R. δ ($CDCl_3$) 1.2 – 1.5 (m, methylene protons, 10H), 1.85 (apparent quintet, ArO-CH_2-$C\underline{H_2}$-R & R-$C\underline{H_2}$-CH_2-Br, 4H), 3.4 (t, Br-$C\underline{H_2}$-R, 2H), 4.0 (t, ArO-$C\underline{H_2}$-R, 2H) ppm.

^{13}C N.M.R. δ ($CDCl_3$) 25.9, 28.3, 28.8, 29.5, 30.0, 30.2, 32.9, 34.2, 73.8, 116.3, 125.6, 130.8, 154.8 ppm.

1-(pentabromophenyloxy)-10-bromodecane (21b)

Yield 68%

I.R. υ (Nujol) lack of OH peak @ ~3300 cm^{-1} indicates ether, 725 (substituted benzene) cm^{-1}.

^{1}H N.M.R. δ ($CDCl_3$) 1.2 – 1.5 (m, methylene protons, 12H), 1.85 (apparent quintet, ArO-CH_2-$C\underline{H_2}$-R & R-$C\underline{H_2}$-CH_2-Br, 4H), 3.4 (t, Br-$C\underline{H_2}$-R, 2H), 4.0 (t, ArO-$C\underline{H_2}$-R, 2H) ppm.

^{13}C N.M.R. δ ($CDCl_3$) 25.9, 28.3, 28.8, 29.5, 30.0, 30.2, 32.9, 34.2, 73.8, 116.3, 125.6, 130.8, 154.8 ppm.

7.22 Synthesis of 4-biphenyl benzoate (22)

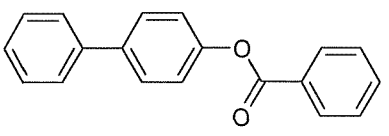

To a stirred solution of 4-biphenol (50mmol, 8.5g) in pyridine (100ml), in a three necked flask fitted with reflux condenser and guard tube, benzoyl chloride (55mmol, 7.73g) was added dropwise. A white precipitate was seen to form. After the addition of the acetyl chloride the mixture was stirred at room temperature for 1 hour. After this time the precipitate was filtered and recrystallised from ethanol to yield white crystals.

Yield 93%

^{1}H N.M.R. δ ($CDCl_3$) 7.56 (apparent t, biphenyl 3'-H, 2H), 7.6 – 7.75 (m, biphenyl 3-H, 2'-H & 4'-H, 7H), 7.32 (d, biphenyl 2-H, 2H), 8.25 (d, benzoate 2-H, 2H), 7.48 (apparent t, benzoate 3-H, 2H) 7.4 (d, benzoate 4-H, 1H) ppm.

^{13}C N.M.R. δ ($CDCl_3$) 122.2, 127.3, 127.5, 128.4, 128.8, 129.0, 129.7, 130.4, 133.8, 139.2, 140.6, 150.5, 165.4 ppm.

7.23 Synthesis of 4'-nitro-4-biphenyl benzoate (23)

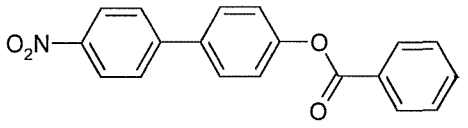

To a stirred solution of 4-biphenylyl benzoate (**22**) (30mmols, 8.22g), in glacial acetic acid, in a three necked round bottomed flask fitted with reflux condenser and guard tube, (100ml) at 85°C, fuming nitric acid (2g) was added dropwise, ensuring no temperature rise. As the last few drops of nitric acid were added 4'-nitro-4-biphenyl benzoate began to separate from the solution. After cooling to room temperature the solution was filtered and the solid collected washed with water and then methanol. The impure solid was then recrystallised from boiling acetic acid to yield a pale yellow crystalline solid.

Yield 52%

^{1}H N.M.R. δ ($CDCl_3$) 7.28 (d, biphenyl 2-H, 2H), 7.64 (d, biphenyl 3-H, 2H), 7.68 (d, biphenyl 2'-H, 2H), 8.15 (d, biphenyl 3'-H, 2H), 8.25 (d, benzoate 2-H, 2H), 7.48 (apparent t, benzoate 3-H, 2H) 7.6 (d, benzoate 4-H, 1H) ppm.

^{13}C N.M.R. δ ($CDCl_3$) 122.7, 124.3, 127.9, 128.7, 128.8, 129.3, 130.4, 134.0, 136.7, 147.1, 147.8, 151.8, 165.4 ppm.

7.24 Synthesis of 4-hydroxy-4'-nitrobiphenyl (23)

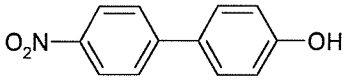

A suspension of 4'-nitro-4-biphenyl benzoate (**23**) (10mmol, 3.19g) in ethanol (200ml), in a quickfit conical flask, was heated at reflux and hydrolysed by careful addition of potassium hydroxide solution (10ml 2M soln). The mixture immediately turned deep red and was heated for a furthur 15 minutes. After cooling to room temperature the potassium salt of 4-hydroxy-4'-nitrobiphenyl separated out and the solution was filtered. The collected solid was then dissolved in the minimum volume of hot water and acidified. The 4-hydroxy-4'-nitrobiphenyl precipitated out, was collected by filtration and recrystallised from ethanol to yield a bright yellow solid.

Yield 86%

^{1}H N.M.R. δ ($CDCl_3$) 3.0 (s, phenol proton, 1H), 7.0 (d, biphenyl 2-H, 2H), 7.65 (d, biphenyl 3-H, 2H), 7.87 (d, biphenyl 2'-H, 2H), 8.25 (d, biphenyl 3'-H, 2H) ppm.

^{13}C N.M.R. δ ($CDCl_3$) 116.7, 124.6, 127.5, 129.4, 130.3, 147.1, 148.0, 159.3 ppm.

7.25 Synthesis of the α-(pentabromophenyloxy)-ω-(aryloxy)alkanes (25)

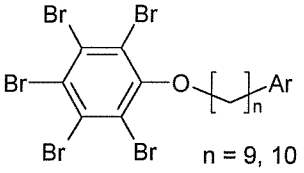

The aryl alcohol (2mmol) and potassium carbonate (20mmol, 2.76g) in AnalaR acetone (50ml) are stirred at reflux in a quickfit conical flask fitted with reflux condenser and guard tube for 1 hour. After this time the α-(pentabromophenyloxy)-ω-bromoalkane was added and the mixture stirred at

reflux for 2 – 3 days. The mixture was then cooled and water (50ml) was added. This was then extracted with DCM (4 x 50ml), the organic extracts combined, dried over anhydrous magnesium sulphate and the solvent removed on the rotary evaporator. The crude product was then purified by column chromatography (Silica gel 60 / DCM) and recrystallised from a mixture of ethanol and toluene to afford a white solid.

1-(pentabromophenyloxy)-9-(phen-4-yloxy)nonane (25a)

Yield 62%

I.R. υ (Nujol) lack of OH peak @ ~3300 cm^{-1} indicates ether, 725 (substituted benzene) cm^{-1}.

^{1}H N.M.R. δ ($CDCl_3$) 1.2 – 1.5 (m, methylene protons, 10H), 1.85 (t, $Ar(Br_5)O$-CH_2-$C\underline{H_2}$-R, 2H), 2.05 (t, ArO-CH_2-$C\underline{H_2}$-R, 2H), 4.0 (t, $Ar(Br_5)O$-$C\underline{H_2}$-R, 2H), 4.10 (t, ArO-$C\underline{H_2}$-R, 2H), 6.85 (apparent q, phenyl 2,4,6-$\underline{H}$, 3H), 7.18 (apparent t, phenyl 3,5-$\underline{H}$, 2H) ppm.

^{13}C N.M.R. δ ($CDCl_3$) 26.6, 29.4, 68.5, 71.2, 113.7, 116.3, 120.6, 125.6, 129.4, 130.8, 154.8 158.7 ppm.

1-(pentabromophenyloxy)-9-(2-cyanophen-4-yloxy)nonane (25b)

Yield 72%

I.R. υ (Nujol) lack of OH peak @ ~3300 cm^{-1} indicates ether, 2225 (nitrile str) 830 (p-substituted benzene) 725 (o-substituted benzene) cm^{-1}.

^{1}H N.M.R. δ ($CDCl_3$) 1.2 – 1.5 (m, methylene protons, 10H), 1.85 (t, $Ar(Br_5)O$-CH_2-$C\underline{H_2}$-R, 2H), 2.05 (t, ArO-CH_2-$C\underline{H_2}$-R, 2H), 4.0 (t, $Ar(Br_5)O$-$C\underline{H_2}$-R, 2H), 4.10 (t, ArO-$C\underline{H_2}$-R, 2H), 7.54 (d, phenyl 3-$\underline{H}$, 1H), 7.01 (d of d, phenyl 4-$\underline{H}$, 1H), 7.46 (d of d, phenyl 5-$\underline{H}$, 1H), 6.98 (d, phenyl 6-$\underline{H}$, 1H) ppm.

^{13}C N.M.R. δ ($CDCl_3$) 26.6, 29.4, 68.5, 71.2, 102.1, 112.3, 115.2, 116.3, 120.7, 125.6, 130.8, 132.6, 134.4, 154.8 161.0 ppm.

1-(pentabromophenyloxy)-9-(3-cyanophen-4-yloxy)nonane (25c)

Yield 65%

I.R. υ (Nujol) lack of OH peak @ ~3300 cm^{-1} indicates ether, 2225 (nitrile str) 830 (p-substituted benzene) 725 (o-substituted benzene) cm^{-1}.

^{1}H N.M.R. δ ($CDCl_3$) 1.2 – 1.5 (m, methylene protons, 10H), 1.85 (t, Ar(Br_5)O-CH_2-C$\underline{H_2}$-R, 2H), 2.05 (t, ArO-CH_2-C$\underline{H_2}$-R, 2H), 4.0 (t, Ar(Br_5)O-C$\underline{H_2}$-R, 2H), 4.10 (t, ArO-C$\underline{H_2}$-R, 2H), 7.15 (s, phenyl 2-$\underline{H}$, 1H), 7.23 (d, phenyl 4-$\underline{H}$, 1H), 7.37 (apparent t, phenyl 5-$\underline{H}$, 1H), 7.12 (d, phenyl 6-$\underline{H}$, 1H) ppm.

^{13}C N.M.R. δ ($CDCl_3$) 26.6, 29.4, 68.5, 71.2, 113.7, 115.2, 116.3, 117.5, 119.9, 124.6, 125.6, 130.5, 130.8, 154.8 159.9 ppm.

1-(pentabromophenyloxy)-9-(4-cyanophen-4-yloxy)nonane (25d)

Yield 81%

I.R. υ (Nujol) lack of OH peak @ ~3300 cm^{-1} indicates ether, 2225 (nitrile str) 830 (p-substituted benzene) 725 (o-substituted benzene) cm^{-1}.

^{1}H N.M.R. δ ($CDCl_3$) 1.2 – 1.5 (m, methylene protons, 10H), 1.85 (t, Ar(Br_5)O-CH_2-C$\underline{H_2}$-R, 2H), 2.05 (t, ArO-CH_2-C$\underline{H_2}$-R, 2H), 4.0 (t, Ar(Br_5)O-C$\underline{H_2}$-R, 2H), 4.10 (t, ArO-C$\underline{H_2}$-R, 2H), 6.95 (d, phenyl 2,4-$\underline{H}$, 2H), 7.55 (d, phenyl 3,5-$\underline{H}$, 2H) ppm.

^{13}C N.M.R. δ ($CDCl_3$) 26.6, 29.4, 68.5, 71.2, 100.5, 114.5, 116.3, 125.6, 130.8, 134.1, 154.8, 163.0 ppm.

1-(pentabromophenyloxy)-9-(biphenyl-4-yloxy)nonane (25e)

Yield 85%

I.R. υ (Nujol) lack of OH peak @ ~3300 cm^{-1} indicates ether, 725 (substituted benzene) cm^{-1}.

^{1}H N.M.R. δ ($CDCl_3$) 1.2 – 1.5 (m, methylene protons, 10H), 1.85 (t, Ar(Br_5)O-CH_2-C$\underline{H_2}$-R, 2H), 2.05 (t, ArO-CH_2-C$\underline{H_2}$-R, 2H), 4.0 (t, Ar(Br_5)O-C$\underline{H_2}$-R, 2H), 4.10 (t, ArO-C$\underline{H_2}$-R, 2H), 6.95 (d, biphenyl 2,6-$\underline{H}$, 2H), 7.35 – 7.5 (m, biphenyl 3',4',5'-$\underline{H}$, 3H), 7.62, (d, biphenyl 2',6'-$\underline{H}$, 2H), 8.2 (d, biphenyl 3,5-$\underline{H}$, 2H) ppm.

^{13}C N.M.R. δ ($CDCl_3$) 26.6, 29.4, 68.5, 71.2, 115.3, 116.3, 125.6, 127.2, 127.8, 128.3, 130.8, 131.4, 132.9, 146.6, 154.8 159.9 ppm.

1-(pentabromophenyloxy)-9-(4-nitrophen-4-yloxy)nonane (25f)

Yield 68%

I.R. υ (Nujol) lack of OH peak @ ~3300 cm^{-1} indicates ether, 725 (substituted benzene) cm^{-1}.

^{1}H N.M.R. δ ($CDCl_3$) 1.2 – 1.5 (m, methylene protons, 10H), 1.85 (t, Ar(Br_5)O-CH_2-C$\underline{H_2}$-R, 2H), 2.05 (t, ArO-CH_2-C$\underline{H_2}$-R, 2H), 4.0 (t, Ar(Br_5)O-C$\underline{H_2}$-R, 2H), 4.10 (t, ArO-C$\underline{H_2}$-R, 2H), 6.92 (d, phenyl 2,6-$\underline{H}$, 2H), 8.2 (d, phenyl 3,5-$\underline{H}$, 2H) ppm.

^{13}C N.M.R. δ ($CDCl_3$) 26.6, 29.4, 68.5, 71.2, 114.6, 116.3, 124.1, 125.6, 130.8, 140.0, 154.8 164.7 ppm.

1-(pentabromophenyloxy)-9-(4-nitrobiphenyl-4-yloxy)nonane (25g)

Yield 74%

I.R. υ (Nujol) lack of OH peak @ ~3300 cm^{-1} indicates ether, 725 (substituted benzene) cm^{-1}.

^{1}H N.M.R. δ ($CDCl_3$) 1.2 – 1.5 (m, methylene protons, 10H), 1.85 (t, Ar(Br_5)O-CH_2-C$\underline{H_2}$-R, 2H), 2.05 (t, ArO-CH_2-C$\underline{H_2}$-R, 2H), 4.0 (t, Ar(Br_5)O-C$\underline{H_2}$-R, 2H), 4.10 (t, ArO-C$\underline{H_2}$-R, 2H), 7.0 (d, biphneyl 2,6-$\underline{H}$, 2H), 7.65 (d, biphenyl 3,5-$\underline{H}$, 2H), 7.72 (d, biphenyl 2',6'-$\underline{H}$, 2H), 8.35 (d, biphenyl 3',5'-$\underline{H}$, 2H) ppm.

^{13}C N.M.R. δ ($CDCl_3$) 26.6, 29.4, 68.5, 71.2, 114.4, 116.3, 124.1, 125.6, 128.2, 128.3, 130.8, 133.4, 140.0, 147.5, 154.8 157.7 ppm.

1-(pentabromophenyloxy)-10-(2-cyanophen-4-yloxy)decane (25h)

Yield 83%

I.R. υ (Nujol) lack of OH peak @ ~3300 cm^{-1} indicates ether, 2225 (nitrile str) 830 (p-substituted benzene) 725 (o-substituted benzene) cm^{-1}.

^{1}H N.M.R. δ ($CDCl_3$) 1.2 – 1.5 (m, methylene protons, 12H), 1.85 (t, Ar(Br_5)O-CH_2-C$\underline{H_2}$-R, 2H), 2.05 (t, ArO-CH_2-C$\underline{H_2}$-R, 2H), 4.0 (t, Ar(Br_5)O-C$\underline{H_2}$-R, 2H), 4.10 (t, ArO-C$\underline{H_2}$-R, 2H), 7.54 (d, phenyl 3-$\underline{H}$, 1H), 7.01 (d of d, phenyl 4-$\underline{H}$, 1H), 7.46 (d of d, phenyl 5-$\underline{H}$, 1H), 6.98 (d, phenyl 6-$\underline{H}$, 1H) ppm.

^{13}C N.M.R. δ ($CDCl_3$) 26.6, 29.4, 68.5, 71.2, 102.1, 112.3, 115.2, 116.3, 120.7, 125.6, 130.8, 132.6, 134.4, 154.8 161.0 ppm.

1-(pentabromophenyloxy)-10-(3-cyanophen-4-yloxy)decane (25i)

Yield 79%

I.R. υ (Nujol) lack of OH peak @ ~3300 cm^{-1} indicates ether, 2225 (nitrile str) 830 (p-substituted benzene) 725 (o-substituted benzene) cm^{-1}.

^{1}H N.M.R. δ ($CDCl_3$) 1.2 – 1.5 (m, methylene protons, 12H), 1.85 (t, Ar(Br_5)O-CH_2-C$\underline{H_2}$-R, 2H), 2.05 (t, ArO-CH_2-C$\underline{H_2}$-R, 2H), 4.0 (t, Ar(Br_5)O-C$\underline{H_2}$-R, 2H), 4.10 (t, ArO-C$\underline{H_2}$-R, 2H), 7.15 (s, phenyl 2-$\underline{H}$, 1H), 7.23 (d, phenyl 4-$\underline{H}$, 1H), 7.37 (apparent t, phenyl 5-$\underline{H}$, 1H), 7.12 (d, phenyl 6-$\underline{H}$, 1H) ppm.

^{13}C N.M.R. δ ($CDCl_3$) 26.6, 29.4, 68.5, 71.2, 113.7, 115.2, 116.3, 117.5, 119.9, 124.6, 125.6, 130.5, 130.8, 154.8 159.9 ppm.

1-(pentabromophenyloxy)-10-(4-nitrobiphenyl-4-yloxy)decane (25j)

Yield 81%

I.R. υ (Nujol) lack of OH peak @ ~3300 cm^{-1} indicates ether, 725 (substituted benzene) cm^{-1}.

^{1}H N.M.R. δ ($CDCl_3$) 1.2 – 1.5 (m, methylene protons, 12H), 1.85 (t, Ar(Br_5)O-CH_2-C$\underline{H_2}$-R, 2H), 2.05 (t, ArO-CH_2-C$\underline{H_2}$-R, 2H), 4.0 (t, Ar(Br_5)O-C$\underline{H_2}$-R, 2H), 4.10 (t, ArO-C$\underline{H_2}$-R, 2H), 7.0 (d, biphneyl 2,6-$\underline{H}$, 2H), 7.65 (d, biphenyl 3,5-$\underline{H}$, 2H), 7.72 (d, biphenyl 2',6'-$\underline{H}$, 2H), 8.35 (d, biphenyl 3',5'-$\underline{H}$, 2H) ppm.

^{13}C N.M.R. δ ($CDCl_3$) 26.6, 29.4, 68.5, 71.2, 114.4, 116.3, 124.1, 125.6, 128.2, 128.3, 130.8, 133.4, 140.0, 147.5, 154.8 157.7 ppm.

7.26 Synthesis of the α-[1,2,3,5,6-pentakis(phenylethynyl)phen-4-yloxy)-ω-(aryloxy)alkanes (26)

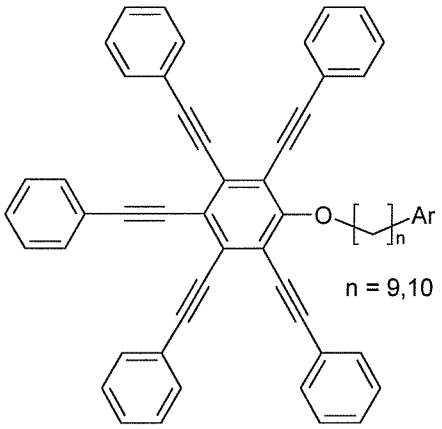

The reaction was carried out according to the method outlined by Praefcke *et al.* [1]. The α-(pentabromophenyloxy)-ω-(aryloxy)alkanes (**25**) (1mmol), phenylacetylene (10mmol), bis(triphenylphosphine) palladium (II) chloride

(50mg), copper iodide (50mg) and triphenylphosphine (100mg) were dissolved in degassed (N_2/1 hour) triethylamine (50ml). This was then refluxed under nitrogen for between 18 and 48 hours. After this time the reaction mixture was dissolved in DCM (50ml) and washed with dilute hydrochloric acid (CARE!) (2 x 50ml) and water (2 x 50 ml). The organic extract was then dried over anhydrous magnesium sulphate and the solvent removed on the rotary evaporator. The crude product was then purified by column chromatography (Silica gel 60 / DCM) and was recrystallised several times from boiling acetone to yield and yellow solid.

1-[1,2,3,5,6-pentakis(phenylethynyl)phen-4-yloxy)-9-(phen-4-yloxy)nonane (26a)

Yield 54%

^{1}H N.M.R. δ ($CDCl_3$) 1.2 – 1.5 (m, methylene protons, 10H), 1.95 (t, Ar(Ar_5)O-CH_2-$C\underline{H}_2$-R, 2H), 2.05 (t, ArO-CH_2-$C\underline{H}_2$-R, 2H), 4.4 (t, Ar(Ar_5)O-$C\underline{H}_2$-R, 2H), 4.10 (t, ArO-$C\underline{H}_2$-R, 2H), 7.4 (m, aromatic protons ortho to acetylene, 10H), 7.65 (m, other aromatic protons, 15H), 6.85 (apparent q, phenyl 2,4,6-H, 3H), 7.18 (apparent t, phenyl 3,5-H, 2H) ppm.

^{13}C N.M.R. δ ($CDCl_3$) 26.6, 29.4, 68.5, 75.1, 84.6, 97.4, 113.8, 120.4, 120.6, 123.4, 124.2, 128.6, 129.0, 129.4, 131.8, 131.9, 158.7, 160.7 ppm.

1-[1,2,3,5,6-pentakis(phenylethynyl)phen-4-yloxy)-9-(2-cyanophen-4-yloxy)nonane (26b)

Yield 35%

^{1}H N.M.R. δ ($CDCl_3$) 1.2 – 1.5 (m, methylene protons, 10H), 1.95 (t, Ar(Ar_5)O-CH_2-$C\underline{H}_2$-R, 2H), 2.05 (t, ArO-CH_2-$C\underline{H}_2$-R, 2H), 4.4 (t, Ar(Ar_5)O-$C\underline{H}_2$-R, 2H), 4.10 (t, ArO-$C\underline{H}_2$-R, 2H), 7.4 (m, aromatic protons ortho to acetylene & phenyl 5-H, 11H), 7.65 (m, other aromatic protons, 15H), 7.54 (d, phenyl 3-H, 1H), 7.01 (d of d, phenyl 4-H, 1H), 6.98 (d, phenyl 6-H, 1H) ppm.

^{13}C N.M.R. δ ($CDCl_3$) 26.6, 29.4, 68.5, 75.1, 84.6, 97.4, 102.1, 112.3, 115.2, 120.4, 120.7, 123.4, 124.2, 128.6, 129.0, 131.8, 131.9, 132.6, 134.4, 160.7, 161.0 ppm.

1-[1,2,3,5,6-pentakis(phenylethynyl)phen-4-yloxy)-9-(3-cyanophen-4-yloxy)nonane (26c)

Yield 62%

^{1}H N.M.R. δ ($CDCl_3$) 1.2 – 1.5 (m, methylene protons, 10H), 1.95 (t, $Ar(Ar_5)O-CH_2-C\underline{H}_2-R$, 2H), 2.05 (t, $ArO-CH_2-C\underline{H}_2-R$, 2H), 4.4 (t, $Ar(Ar_5)O-C\underline{H}_2-R$, 2H), 4.10 (t, $ArO-C\underline{H}_2-R$, 2H), 7.4 (m, aromatic protons ortho to acetylene & phenyl 5-H, 11H), 7.65 (m, other aromatic protons, 15H), 7.15 (s, phenyl 2-H, 1H), 7.23 (d, phenyl 4-H, 1H), 7.12 (d, phenyl 6-H, 1H) ppm.

^{13}C N.M.R. δ ($CDCl_3$) 26.6, 29.4, 68.5, 75.1, 84.6, 97.4, 113.7, 115.2, 117.5, 119.9, 120.4, 123.4, 124.2, 124.6, 128.6, 129.0, 130.5, 131.8, 131.9, 159.9, 160.7 ppm.

1-[1,2,3,5,6-pentakis(phenylethynyl)phen-4-yloxy)-9-(4-cyanophen-4-yloxy)nonane (26d)

Yield 50%

^{1}H N.M.R. δ ($CDCl_3$) 1.2 – 1.5 (m, methylene protons, 10H), 1.95 (t, $Ar(Ar_5)O-CH_2-C\underline{H}_2-R$, 2H), 2.05 (t, $ArO-CH_2-C\underline{H}_2-R$, 2H), 4.4 (t, $Ar(Ar_5)O-C\underline{H}_2-R$, 2H), 4.10 (t, $ArO-C\underline{H}_2-R$, 2H), 7.4 (m, aromatic protons ortho to acetylene, 10H), 7.65 (m, other aromatic protons & phenyl 3,5-H, 17H), 6.95 (d, phenyl 2,4-H, 2H) ppm.

^{13}C N.M.R. δ ($CDCl_3$) 26.6, 29.4, 68.5, 75.1, 84.6, 97.4, 100.5, 114.5, 120.4, 123.4, 124.2, 128.6, 129.0, 131.8, 131.9, 134.1, 160.7 163.0 ppm.

1-[1,2,3,5,6-pentakis(phenylethynyl)phen-4-yloxy)-9-(biphenyl-4-yloxy)nonane (26e)

Yield 53%

^{1}H N.M.R. δ ($CDCl_3$) 1.2 – 1.5 (m, methylene protons, 10H), 1.95 (t, $Ar(Ar_5)O-CH_2-C\underline{H}_2-R$, 2H), 2.05 (t, $ArO-CH_2-C\underline{H}_2-R$, 2H), 4.4 (t, $Ar(Ar_5)O-C\underline{H}_2-R$, 2H), 4.10 (t, $ArO-C\underline{H}_2-R$, 2H), 7.4 (m, aromatic protons ortho to acetylene & biphenyl 3',4',5'-H,13H), 7.65 (m, other aromatic protons & biphenyl 2',6'-H, 17H), 6.95 (d, biphenyl 2,6-H, 2H), 8.2 (d, biphenyl 3,5-H, 2H) ppm.

^{13}C N.M.R. δ ($CDCl_3$) 26.6, 29.4, 68.5, 75.1, 84.6, 97.4, 115.3, 120.4, 123.4, 124.2, 127.2, 127.8, 128.3, 128.6, 129.0, 131.4, 131.8, 131.9, 132.9, 146.6, 159.9, 160.7 ppm.

1-[1,2,3,5,6-pentakis(phenylethynyl)phen-4-yloxy)-9-(4-nitrophen-4-yloxy)nonane (26f)

Yield 44%

^{1}H N.M.R. δ ($CDCl_3$) 1.2 – 1.5 (m, methylene protons, 10H), 1.95 (t, $Ar(Ar_5)O$-CH_2-$C\underline{H_2}$-R, 2H), 2.05 (t, ArO-CH_2-$C\underline{H_2}$-R, 2H), 4.4 (t, $Ar(Ar_5)O$-$C\underline{H_2}$-R, 2H), 4.10 (t, ArO-$C\underline{H_2}$-R, 2H), 7.4 (m, aromatic protons ortho to acetylene, 10H), 7.65 (m, other aromatic protons, 15H), 6.92 (d, phenyl 2,6-H, 2H), 8.2 (d, phenyl 3,5-H, 2H) ppm.

^{13}C N.M.R. δ ($CDCl_3$) 26.6, 29.4, 68.5, 75.1, 84.6, 97.4, 114.6, 120.4, 123.4, 124.1, 124.2, 128.6, 129.0, 131.8, 131.9, 140.0, 160.7 164.7 ppm.

1-[1,2,3,5,6-pentakis(phenylethynyl)phen-4-yloxy)-9-(4-nitrobiphenyl-4-yloxy)nonane (26g)

Yield 39%

^{1}H N.M.R. δ ($CDCl_3$) 1.2 – 1.5 (m, methylene protons, 10H), 1.95 (t, $Ar(Ar_5)O$-CH_2-$C\underline{H_2}$-R, 2H), 2.05 (t, ArO-CH_2-$C\underline{H_2}$-R, 2H), 4.4 (t, $Ar(Ar_5)O$-$C\underline{H_2}$-R, 2H), 4.10 (t, ArO-$C\underline{H_2}$-R, 2H), 7.4 (m, aromatic protons ortho to acetylene, 10H), 7.65 (m, other aromatic protons & biphenyl 3,5-H, 17H), 7.0 (d, biphenyl 2,6-H, 2H), 7.72 (d, biphenyl 2',6'-H, 2H), 8.35 (d, biphenyl 3',5'-H, 2H) ppm.

^{13}C N.M.R. δ ($CDCl_3$) 26.6, 29.4, 68.5, 75.1, 84.6, 97.4, 114.3, 120.4, 123.4, 124.1, 124.2, 128.2, 128.3, 128.6, 129.0, 131.8, 131.9, 133.4, 140.0, 147.5, 157.7, 160.7 ppm.

1-[1,2,3,5,6-pentakis(phenylethynyl)phen-4-yloxy)-10-(2-cyanophen-4-yloxy)decane (26h)

Yield 47%

^{1}H N.M.R. δ ($CDCl_3$) 1.2 – 1.5 (m, methylene protons, 12H), 1.95 (t, $Ar(Ar_5)O$-CH_2-$C\underline{H_2}$-R, 2H), 2.05 (t, ArO-CH_2-$C\underline{H_2}$-R, 2H), 4.4 (t, $Ar(Ar_5)O$-$C\underline{H_2}$-R, 2H), 4.10 (t, ArO-$C\underline{H_2}$-R, 2H), 7.4 (m, aromatic protons ortho to acetylene & phenyl 5-H, 11H), 7.65 (m, other aromatic protons, 15H), 7.54 (d, phenyl 3-H, 1H), 7.01 (d of d, phenyl 4-H, 1H), 6.98 (d, phenyl 6-H, 1H) ppm.

^{13}C N.M.R. δ ($CDCl_3$) 26.6, 29.4, 68.5, 75.1, 84.6, 97.4, 102.1, 112.3, 115.2, 120.4, 120.7, 123.4, 124.2, 128.6, 129.0, 131.8, 131.9, 132.6, 134.4, 160.7, 161.0 ppm.

1-[1,2,3,5,6-pentakis(phenylethynyl)phen-4-yloxy)-10-(3-cyanophen-4-yloxy)decane (26i)

Yield 21%

^{1}H N.M.R. δ ($CDCl_3$) 1.2 – 1.5 (m, methylene protons, 12H), 1.95 (t, $Ar(Ar_5)O$-CH_2-$C\underline{H}_2$-R, 2H), 2.05 (t, ArO-CH_2-$C\underline{H}_2$-R, 2H), 4.4 (t, $Ar(Ar_5)O$-$C\underline{H}_2$-R, 2H), 4.10 (t, ArO-$C\underline{H}_2$-R, 2H), 7.4 (m, aromatic protons ortho to acetylene & phenyl 5-H,11H), 7.65 (m, other aromatic protons, 15H), 7.15 (s, phenyl 2-H, 1H), 7.23 (d, phenyl 4-H, 1H), 7.12 (d, phenyl 6-H, 1H) ppm.

^{13}C N.M.R. δ ($CDCl_3$) 26.6, 29.4, 68.5, 75.1, 84.6, 97.4, 113.7, 115.2, 117.5, 119.9, 120.4, 123.4, 124.2, 124.6, 128.6, 129.0, 130.5, 131.8, 131.9, 159.9, 160.7 ppm.

1-[1,2,3,5,6-pentakis(phenylethynyl)phen-4-yloxy)-10-(4-nitrobiphenyl-4-yloxy)decane (26j)

Yield 41%

^{1}H N.M.R. δ ($CDCl_3$) 1.2 – 1.5 (m, methylene protons, 12H), 1.95 (t, $Ar(Ar_5)O$-CH_2-$C\underline{H}_2$-R, 2H), 2.05 (t, ArO-CH_2-$C\underline{H}_2$-R, 2H), 4.4 (t, $Ar(Ar_5)O$-$C\underline{H}_2$-R, 2H), 4.10 (t, ArO-$C\underline{H}_2$-R, 2H), 7.4 (m, aromatic protons ortho to acetylene, 10H), 7.65 (m, other aromatic protons & biphenyl 3,5-H, 17H), 7.0 (d, biphneyl 2,6-H, 2H), 7.72 (d, biphenyl 2',6'-H, 2H), 8.35 (d, biphenyl 3',5'-H, 2H) ppm.

^{13}C N.M.R. δ ($CDCl_3$) 26.6, 29.4, 68.5, 75.1, 84.6, 97.4, 114.3, 120.4, 123.4, 124.1, 124.2, 128.2, 128.3, 128.6, 129.0, 131.8, 131.9, 133.4, 140.0, 147.5, 157.7, 160.7 ppm.

7.27 References

[1] Praefcke, K., Singer, D., Kohne, B., Ebert, M., Liebmann, A. and Wendorff, J.H., *Liq. Cryst.*, **10**, 147, (1991).

[2] *Vogel's Textbook of Practical Organic Chemistry*, 5th edition, edited by Furniss, B.S., Hannaford, A.J., Smith, P.W.G. and Tatchell, A.R.; Longman, (1995).

[3] Suzuki, A., Miyaura, N. and Yanagi, T., *Synth. Commun.*, **11**, 513, (1981).

[4] Crivello, J.V., Deptolla, M. and Ringsdorff, H., *Liq. Cryst.*, **3**, 235, (1988).

APPENDIX

Abbreviations used in this Thesis.

Ar	Aryl
Bpt	Boiling point
d	Doublet
DCM	Dichloromethane
DME	Ethylene glycol dimethyl ether
DMF	*N*,*N*-dimethylformamide
Ether	Diethyl ether
I.R.	Infra-red spectroscopy
m	Multiplet
Mpt	Melting point
N.M.R.	Nuclear magnetic resonance spectroscopy
p	Quintet
q	Quartet
t	Triplet
THF	Tetrahydrofuran